Permanent-Magnet Synchronous Motors and Associated Power Electronics for Direct-Drive Vehicle Propulsion

by

John Ofori-Tenkorang

S.B., Massachusetts Institute of Technology (1989)
S.M., Massachusetts Institute of Technology (1993)
E.E., Massachusetts Institute of Technology (1993)

Submitted to the Department of Electrical Engineering and Computer Science
in partial fulfillment of the requirements for the degree of

Doctor of Science

at the

MASSACHUSETTS INSTITUTE OF TECHNOLOGY

September 1996

Author .....
Department of Electrical Engineering and Computer Science
September 11th, 1996

Certified by .....
Jeffrey H. Lang
Professor of Electrical Engineering and Computer Science
Thesis Supervisor

Accepted by .....
Frederic R. Morgenthaler
Chairman, Departmental Committee on Graduate Students

Permanent-Magnet Synchronous Motors and Associated Power Electronics for Direct-Drive Vehicle Propulsion

by

John Ofori-Tenkorang

Submitted to the Department of Electrical Engineering and Computer Science
on September 11th, 1996, in partial fulfillment of the
requirements for the degree of
Doctor of Science

Abstract

The quest for improved air quality in urban areas and improved automobile fuel efficiency has rekindled interest in the development of all-electric and hybrid vehicles. The lack of an economical low-weight on-board energy storage medium with high power and energy density remains a major obstacle to the commercialization of electric vehicles. Problems with energy storage notwithstanding, the efficiency of the powertrain can be improved and its complexity reduced by employing a direct-drive wheel motor propulsion system. By integrating the drive motor with the wheel, one can eliminate transaxles, differentials, clutches and reduction gears, thus simplifying the mechanical design of the vehicle. With wheel motors, losses deriving from the mechanical transmission and the drive line are eliminated, thereby yielding significant improvements in the efficiency of the drive system from battery to wheel. This thesis develops such a drive system.

The availability of high-energy Neodymium-Iron-Boron magnets, coupled with the emergence of high-power, fast-switching, third generation IGBTs make a highly-efficient low-weight direct-drive powertrain possible. A 20 hp high-torque, low-weight, permanent-magnet synchronous wheel motor and the associated power electronics was designed, fabricated and experimentally evaluated. The motor fits in a 19-inch wheel and produces 450 Nm of peak torque from 0 to 325 rpm, with constant power operation up to a maximum speed of 1300 rpm. A 4:1 speed range is achieved with a bi-directional boost converter in the dc link of a 3-phase PWM voltage source inverter. The active mass of the resulting motor is 25.1 kg, and the total efficiency from traction power source to wheel is approximately 85% over the Federal Urban Drive Schedule and 92% over the Federal Highway Drive Schedule.

Finally this thesis answers the question of when to use a Halbach magnet array in the design of permanent-magnet synchronous motors. We conclude that for applications that preclude the use of a magnetic rotor backing, such as high-speed energy-storage flywheels, a Halbach array produces higher torque per volume of magnet material than a conventional array. With a permeable rotor backing, a conventional array produces higher torque per magnet volume in the regime of thin magnets. As the magnet thickness increases, a Halbach array offers superior performance.

Thesis Supervisor: Jeffrey H. Lang
Title: Professor of Electrical Engineering and Computer Science

Acknowledgments

Funding for this work was provided by Ford Motor Company under subcontract number 47-2-RN0095. I would like to thank Mr. Brad Bates and Mr. Allan Gale, both at Ford Motor Company, for funding this project and for the several valuable discussions.

At MIT, I would like to thank my thesis supervisor, Professor Jeff Lang, for his patience, guidance and support hroughout this work. I have learned a lot from Jeff over the past 3 years, and working with him was great fun. I thank Professors Jim Kirtley, David Trumper and John Kassakian for serving as readers for this thesis.

Several people have been of great help during the experimental phase of this thesis. My thanks go to Wayne Ryan at MIT for machining the inverter parts and helping with the construction of the inverter and to Tracy Clark and Dave Otten for helping me decode some of the obscure inner workings of the MC68HC16Z1 microprocessor. Much thanks to Deron Jackson and Professor Steven Leeb for letting me borrow test equipment and ad hoc electronic parts when I couldn't afford to wait for a purchase order to go through. Thanks to Wayne Hagman an Vivian Mizuno for helping me repair my inverter when an IGBT decided to go up in smokes on a Friday night! Thanks to Carol Choi for helping with the drawing of circuit schematics.

I thank my colleagues and friends at LEES, Khurram Afridi, Dave Perreault, Mark Thompson, Brian Perreault, Robert Selders, Mary Tolikas, Kamakshi Srinivasan, Jeff Chapman, Ahmed Mitwalli, Julio Castrillon-Candas, Vahe Caliskan, Jama Mohammed, Jesko Hagee, and ... (the list goes on) for making this Lab a fun place study.

The prototype wheel motor presented in this thesis was built and tested at the Superior Electric Company (SECO) in Bristol, CT. Several people at SECO have been of tremendous help for which I am very grateful. My first thanks go to Dr. Marty Kaplan, Vice President of Engineering at SECO, for supervising the motor construction project. I thank Dr. Peter Senak designing the apparatus needed to wind the motor and providing me with all the necessary support needed to wind the motor and get it running. Thanks to Tom Corlozzi for setting up the Powerstat and rectifier set that was used as the dc power source to the inverter, and to Willis Dudley for his help with setting up the thermocouple readers. I thank Dick Connors for designing the mechanical parts needed to assemble the motor and Lee Faucher for machining all the parts and assembling the motor. Thanks to Joe Levesque, Ron Strid and Art Johnson for helping with mounting of the motor on the dynamometer. Special thanks to Jim Burns for setting up the dynamometer and bringing me up to speed on how to operate the dyno. Thanks to Lane Woodland for all his help including lending me a laptop so that I could edit my thesis in my hotel room while watching Atlanta '96 on CNN. Thanks to Mark Rollins, Charlie Bald, and Mark Beaulieau for all their help and making me feel at home at SECO.

Back to MIT where I have spent 11 years (whew!) as a student, I would like to thank some very special people. If I were asked to name a mentor during my tenure at MIT, it would be Professor John G. Kassakian. I first met John during my first semester, sophomore year at MIT when he taught me 6.002 (Circuits and Electronics, for the non-MIT types).

John has always believed in me, given me great advice and most importantly *opportunity*, for which I am extremely grateful for. Other professors who have also taken special interest in my education, professional growth and personal well-being at MIT are Professors Markus Zahn, Leonard Gould and Robert Kingston (my undergraduate academic advisor). To them I extend my profound gratitude.

Like they say ... all work and no play ..., you know what I mean! Eleven years in Boston wouldn't have been any fun without great friends like Albert Essiam, Mike Owu, Mawuli Tse, Evelyn Anim, Gillian Brown, Madeline Jeune, Elizabeth N. Ngonzi, Khaitsa Wasiyo, Kofi Fynn, Kamel Addo, the late John A. Selormey '97 and many others whose names I haven't mentioned. A big thanks to all my African brothers and sisters in the Africans Association at MIT and African-American brothers and sisters in the BGSA for all the good times we have shared.

Finally I would like to thank Dr. & Mrs. Clarence G. Williams for being my parents away from home.

To my mother and my father,

for the huge sacrifices they made,

so that I may get an education!

Contents

List of Figures

List of Tables

Chapter 1

Introduction

1.1 Background

Electric vehicles (EVs) have existed since the late 1800s, and were a dominant means of transportation in the early 1900s [1, 2]. In the late 1920s to early 1930s battery-powered EVs, with their limited energy storage capability and hence limited range, were displaced by the internal-combustion-engine vehicles (ICEVs), and therefore EVs ceased to be a competitive means of transportation.

The increased cost of petroleum during the oil crisis in the early 1970s and concern for national energy security brought attention to electric and hybrid vehicles as a potentially cost-competitive alternative means of transportation. In the United States for example, the Electric and Hybrid Vehicle Research, Development and Demonstration Act of 1976 was passed by the U.S. Department of Energy (DOE), and was amended in 1978 to provide funding for research and development projects for EVs. A few all-electric test vehicles including the first and second generation Electric TransaXel (ETX-I/II), and the ETV-I/II, were developed under the DOE electric and hybrid vehicles program [2]. Outside the United States, many prototype EVs were developed. Some efforts in Japan, Hong Kong, and Europe are documented in [3], [4], and [5] respectively.

To date EVs have not been able to displace ICE vehicles for a number of reasons including the higher energy density and lower cost of petroleum compared to that of electrochemical batteries, and the ease and flexibility of re-fuelling ICE vehicles. Current EV

batteries are expensive and slow to charge, and an extensive battery charging infrastructure comparable to gasoline filling stations for ICE vehicles has yet to be developed. Furthermore, the high price of current EVs coupled with their limited range, lower acceleration and lower attainable top-speed makes the EV an unattractive choice in comparison to their rival ICE vehicles. Even for short trips such as intra-city driving and short-distance commuting where range is not an issue, these expensive EVs have to compete against older ICE vehicles that are usually acquired at lower cost. Thus EVs remain a tough sell to the public at large.

However, in October 1990, the California Air Resources Board (CARB) introduced legislation aimed at reducing urban atmospheric pollution. This legislation, which mandates that 2% of all the cars and light trucks sold by 1998 in the state of California be zero-emission vehicles (ZEVs) at the tailpipe rekindled interest in the development of battery-powered EVs. The CARB sales quota for ZEVs is scheduled to rise to 10% by 2003 (see Figure 1-1). One year after the CARB legislation was passed, nine other states in the northeast, including Massachusetts, New York and the District of Columbia voted to adopt the CARB regulations. It is estimated that the mandated sales for ZEVs in the United Staes will be about 300,000 by the turn of the century [6]. ZEVs have therefore moved from the research phase to the development of production prototypes by Ford, General Motors, and Chrysler, as well as other small EV companies, such as U.S. Electricar in California and Solectria Corporation in Massachusetts, who retrofit ICE vehicles with electric motors. Examples of the current state-of-the-art EVs include the Ford Ecostar, GM Impact, Chrysler G-Van and TEVan in the United States, and the BMW-E1/E2, Nissan FEV and Tepco Iza in Europe and Japan, respectively.

Unfortunately, as the year 1998 rapidly approaches, U.S. Automakers have yet to find an affordable traction battery that can give ZEVs a sufficient range to make them an attractive choice for the general consumer. Recognizing this problem, CARB in July 1995 proposed to amend its mandated ZEV quota to include a new class of vehicles called equivalent zero-emission vehicles (EZEVs). These EZEVs are allowed to have up to only 10% of the emission of ultralow-emission vehicles (ULEVs) which are to be introduced in 1997. The rational is that, EZEVs would produce no more nitrogen oxides (NO_x) and non-methane organic gases (NMOG) than would the electric power plants in the California South Coast

Emission standards set by the California Air Resources Board (CARB)

Category	Emission Level (g/mi)		
	NMOG	NO_x	CO
Transitional Low-Emission Vehicle	0.125	0.4	3.4
Low-Emission Vehicle	0.075	0.2	3.4
Ultra-Low Emission Vehicle	0.040	0.2	1.7
Zero-Emission Vehicle	0.00	0.00	0.00

NMOG *Non-Methane Organic Gases* NO_x *Nitrogen Oxides*

CO *Carbon Monoxide*

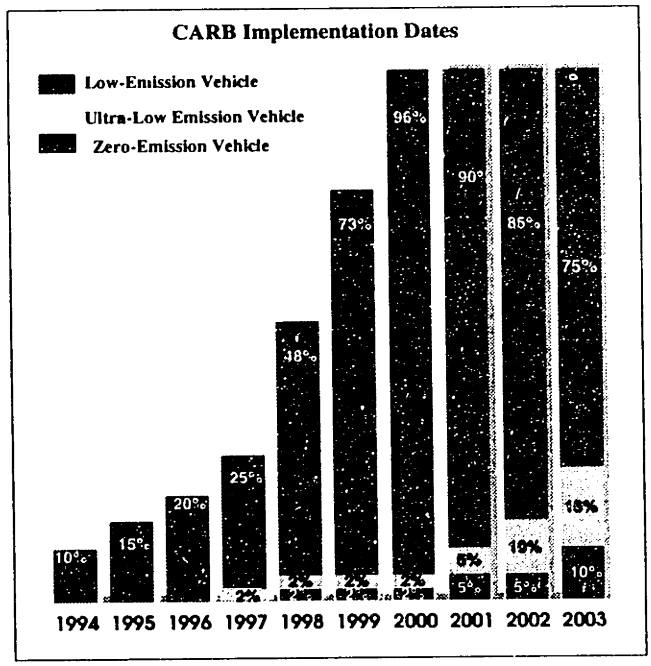

Source: Electric Transportation Coalition

Figure 1-1: CARB mandated emission standards.

Air Basin in charging battery-powered ZEVs. The provision for *some* tailpipe emissions allow for hybrid vehicles, which permit the vehicle to be propelled by a combination of an efficient heat engine and an electric motor, to qualify as EZEVs. These hybrid vehicles would also earn partial ZEV credit depending on their all-electric range and other safeguards designed into the vehicle to preserve its EZEV status such as prevention of the use of the heat engine to charge the battery or power accessories in the all-electric mode [7].

Adding to the momentum to develop EVs as a competitive means of transportation in the United States is the Partnership for a New Generation of Vehicles (PNGV) initiative, launched by President Clinton and Vice President Gore with the Chief Executive Officers

of the Big Three U.S. Automakers on September 29, 1993. The PNGV initiative is aimed at developing technologies that would strengthen U.S. competitiveness in the world automotive market. To this end, the U.S. government and the U.S. Council of Automotive Research (USCAR) have launched development efforts to develop a mid-size family sedan that would achieve up to three times the fuel efficiency of today's comparable vehicle such as the 1994 Chrysler Concorde, Ford Taurus and Chevrolet Lumina [8]. This new vehicle, dubbed the Supercar, aims at achieving 80 miles per gallon of gasoline and meeting ULEV emission levels of 0.125 gal/mile of hydrocarbons (HC), 1.7 g/mile of carbon monoxide (CO) and 0.2 g/mile of nitrogen oxides (NO_x) at 100,000 miles while complying with other Clean Air Act requirements. These requirements make the all-electric or hybrid vehicle a strong candidate for the future car. In evaluating the fuel efficiency of the EV, one gallon of gasoline is considered equivalent to 114,132 BTUs (33.4 kWh) which, after processing through a typical power plant that is 40% efficient results in 13 kWh of available energy. Thus, the EV must achieve the formidable energy efficiency of at least 0.16 kWh/mile in order to meet the PNGV fuel efficiency target. Note that this energy efficiency is for the powertrain alone and does not include the energy required to run the so called "hotel loads" in the vehicle, such as the air-conditioning, passenger compartment heaters, window defrosters etc. Current prototype EVs achieve a powertrain efficiency of about 0.32 kWh/mile.

1.2 Technological Challenges

Many technological innovations still remain to be achieved in order to improve the performance of EVs. First on the list is obviously the development of high-capacity low-weight traction batteries or other forms of on-board energy storage for extended driving range. The next is the development of a more energy-efficient, high-performance powertrain.

1.2.1 Energy Storage

One of the major challenges facing EV development is the lack of a high-energy and high-power density on-board energy storage medium. This lack of adequate energy storage severely limits the range of all-electric vehicles, powered by electrochemical batteries today,

to about 100 miles per charge [9]. For EVs to gain wide public acceptance, significant progress must be made in this domain.

Assuming a total mileage of about 150,000 miles over a vehicle lifetime, and a range of about 150 miles per charge, the traction battery must survive about 1000 charge-discharge cycles. According to the U.S. Advanced Battery Consortium, EV batteries will need to achieve a specific energy of about 200 Wh/kg at C/3 [1]discharge rate, a specific power of 400 W/kg (80% depth of discharge per 30 seconds), a recharge time of 3 to 6 hours, a battery lifetime of about 10 years and cost less than $100 per kWh [9].

Lead-acid has been the battery technology of choice in many EV prototype vehicles such as the GM Impact because it is a low-cost, commercially available and a proven battery technology. However, these batteries suffer from low specific energy and specific power of about 35 Wh/kg and 120 W/kg respectively, low life-cycle of approximately 750 cycles, and high recharge times of about 8-12 hours [10]. Sodium-Sulphur (NaS) battery technology, pioneered by Ford Motor Company, has also found widespread use in prototype EVs, including the Ford Ecostar and BMW-E1/E2, and is considered to be a very promising battery technology due to its high specific energy and specific power. NaS batteries today achieve about 81 Wh/kg and 152 W/kg, with a theoretical projection for energy storage targeted at 150 Wh/kg. Their recharge time of 6-8 hours is significantly lower than that of Lead-acid, however, this high operating temperatures of about 350 - 380°C pose safety problems. Additionally, they have a low life cycle of only 592 cycles [13]. Nickel-based batteries, such as Nickel-Cadmium, Nickel-Iron, Nickel-Zinc, Nickel-Metal-Hydride also have high energy densities and high peak powers but are very costly. Among the Nickel-based batteries, Nickel-Metal-Hydride has shown the most potential. Ovonic Battery Company has achieved a specific energy density of 95 Wh/kg with Nickel-Metal-Hydride technology and there are talks of a joint venture between Toyota Motor Corporation and Matsushita Electric Industrial Company to develop, produce and market Nickel-Metal-Hydride batteries. Thus Nickel-Metal-Hydride batteries may be the EV battery of choice in the mid-term. Although Nickel-Cadmium is a proven battery technology, it's toxic nature disqualifies it as being a contender for a viable EV battery. Lithium-based batteries are

[1]C/3 discharge rate: the current that would discharge a fully charged battery in 3 hours

also considered to have great potential due to their high energy densities and short recharge times. In fact, Lithium-Aluminum/Iron-Disulfide batteries boast of a recharge time of "minutes" but are currently only experimental. In the long term, Lithium-polymer batteries with a specific energy density of four to five times that of contemporary lead-acid batteries are expected to be produced for $100 per kWh, according to the U.S. Advanced Battery Consortium.

Although it is not easy to predict which battery technology will eventually emerge as a winner, the metrics of a winner are well established, namely high energy and power densities, short recharge times, long cycle life, environmental friendliness and, of course, low cost. Other forms of energy storage including fuel cells, ultracapacitors, and electromechanical flywheels are also being researched [30]. Containment for on-board storage of hydrogen is currently a big issue for fuel cells. Commercially available ultracapacitors today have a low specific energy density of about 1-2 Wh/kg and need significant improvement in this domain. Prototype flywheel systems with installed specific energy and power densities of 5 Wh/kg and 375 W/kg have been demonstrated in transit buses, however, significant work remains to be done to increase specific energy density, provide lightweight containment, simplify overall system integration and reduce cost [8].

1.2.2 Current EV Powertrains

EV powertrains can be broadly classified into two categories: all-electric and hybrid powertrains. All-electric vehicles derive all of their propulsion power from an electric motor whereas a hybrid vehicle can accept power from a combination of two sources, typically an electric motor and an internal combustion engine.

The hybrid electric vehicle (HEV) concept is also not a new one. In fact, U.S. patent records show that hybrids have existed since the early 1900s [12]. With hybrids, the availability of an alternative source of propulsion energy, other than an electrochemical battery, helps to increase the range of the vehicle and control emissions at the same time since the auxiliary ICE can be operated at its most efficient point. Thus, if the CARB-proposed EZEV category that accommodates hybrid vehicles is implemented, a near term

goal of an EV that can offer competitive performance to an ICE vehicle while meeting strict emission levels may be achieved. A disadvantage of hybrid powertrains, though, is the added cost and complexity deriving from the addition of the second prime mover.

The EV industry has not as yet adopted a particular type of motor drive as a standard and a great deal of experimentation still continues. Electric powertrains can employ a single (or multiple) high-speed central motor(s) with mechanical reduction gears or direct-drive wheel motors. There are also a host of motor technologies to choose from such as induction, switched-reluctance, wound-field and permanent-magnet. The GM-Impact, Nissan FEV and Ford Ecostar, for example, use three-phase induction motors with reduction gears. The G-Van and TEVan use series wound dc motors while the BMW-E1, ETX-II and Tepco IZA use permanent-magnet motors [9, 11]. Different forms of mechanical integration and packaging abound such as the integration of reduction gears and planetary differentials into a single transaxle as in the Ford Ecostar.

1.3 Towards a more Efficient Electric Powertrain

Permanent-magnet (PM) motors, despite their potentially catastrophic failure modes, are gaining popularity in traction drives due to the low weight and high efficiencies that these motors offer. The use of a single high-speed central motor with mechanical transmission offer advantages in weight and cost reduction of the motors and simplicity in vehicle control, since only one motor needs to be controlled. However, one suffers about 10-15% losses in mechanical transmissions (Figure 1-2), and the mechanical linkages from the central motor-drive to wheels increase the part count and the complexity of the powertrain.

Figure 1-2 show the losses from battery to wheel in a typical electric vehicle during motoring. Significant simplicity in the mechanical design and packaging of the electric vehicle can be obtained by integrating the drive motor into the wheel as shown in Figure 1-3, and thereby eliminating the need for shafts, transaxles, differentials, clutches and reduction gears. The resulting powertrain can be more efficient, as the losses from the mechanical transmission are completely eliminated, and the vehicle is easier to assemble and manufacture due to the reduction in mechanical part count. In the EV driven by

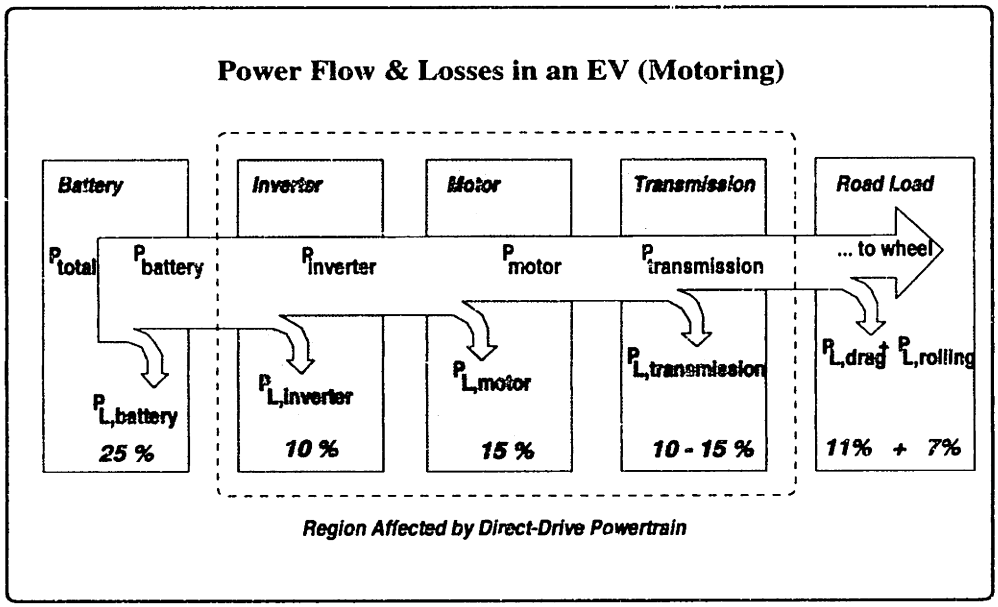

Figure 1-2: Losses in an EV powertrain during motoring.

wheel motors, the rated torque is equally distributed among the drive wheels. Each of the traction motors has its own independent drive and each can be controlled electronically to yield the torque-speed characteristics of a motor-gearbox combination. A differential is implemented electronically by commanding the same torque at different wheels rotating at different speeds. Full starting torque can be applied directly at the wheel and the motors can be controlled to yield a smoother drive at low speeds. Furthermore, auxiliary hydraulic actuators for traction control such as antilock braking systems can be eliminated since these functions can be implemented electronically.

Of all the prototype EVs cited in Section 1.1, only the Tepco IZA is advertised to have used a wheel motor arrangement, but little data on the powertrain performance and cost savings derived from such a wheel motor arrangement is available in the open literature.

A wheel motor based traction system, however, poses the unique challenge of designing a high-torque, low-mass motor, in the restricted mechanical envelope offered by the hub of a wheel, that would operate efficiently over the wide speed range of the vehicle. The low motor mass is needed to reduce the unsprung weight of the vehicle, as this weight affects vehicle suspension design and hence ride quality. The motor must operate in a dirty and harsh environment characterized by a wide range of ambient temperatures, and large shock and vibration forces. Induction motors are ill-suited for this application due to the difficulty

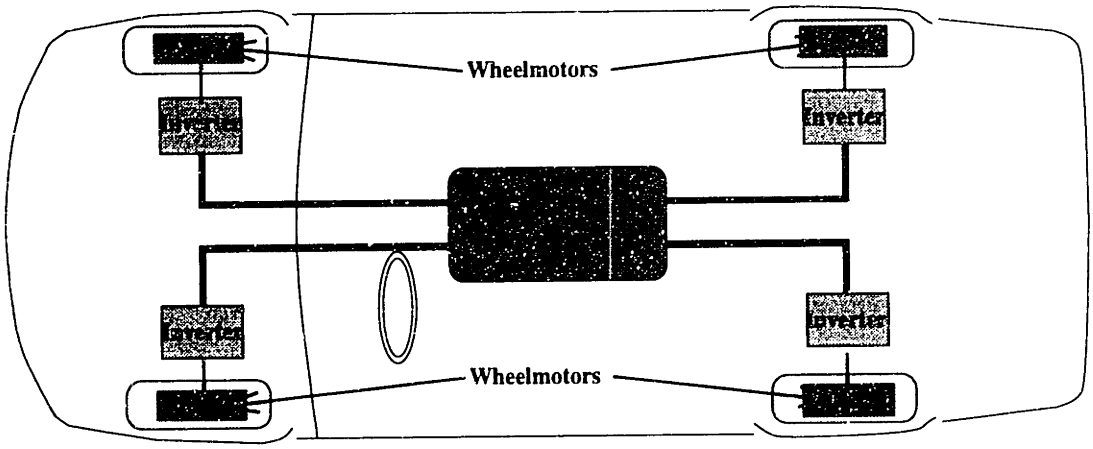

(a) All-electric vehicle with wheel motors.

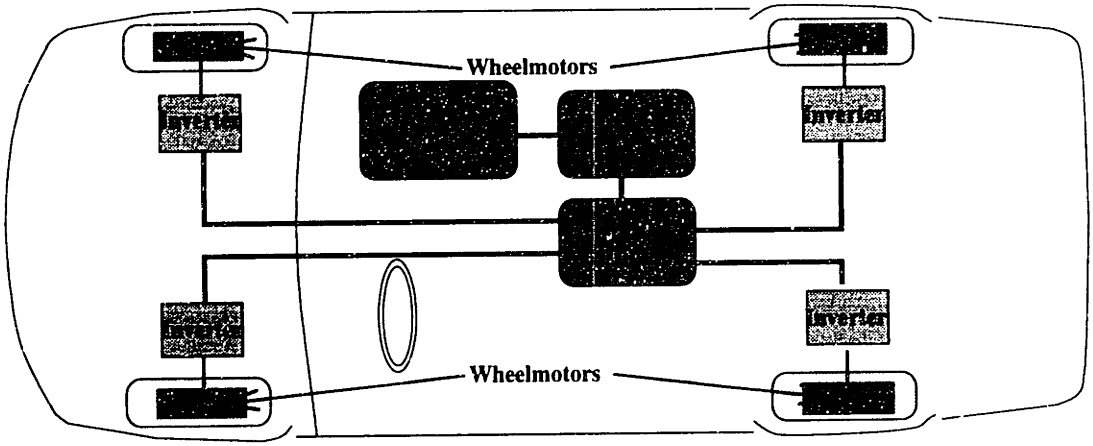

(b) Series hybrid electric vehicle with wheel motors.

Figure 1-3: Four-wheel-drive all-electric and hybrid powertrain with wheel motors.

of removing heat from the rotor, which is a rotating member. Switched-reluctance motors require a very small airgap to produce high torques and hence raise a survivability issue with regard to their ability to withstand the vibration forces at the wheel; their high level of acoustic noise notwithstanding. Permanent-magnet synchronous motors (PMSMs) do not suffer from the above disadvantages since there are no significant rotor losses and large airgaps are possible. In view of the foregoing concerns about other motor technologies, our studies in this thesis were restricted to PMSMs as they do not suffer from the above deficiencies.

1.4 Enabling Technologies

Improvements in the performance of conventional EV powertrains that use induction motors, over the last decade, have mainly been in the area of drive and control electronics. The availability of high-power, fast-switching, and low-loss semiconductor devices, coupled with super-fast microprocessors and floating point digital signal processors (DSPs) have allowed for better waveform synthesis and control for induction motor drives. The story for PM powertrains is a bit more extensive. Here, in addition to the above improvements in drive and control electronics, the availability of new high-energy permanent magnet materials have also stimulated a number of novel PMSM designs [14, 15]. Despite these significant improvements in technical performance, device and material costs still remain high and a major breakthrough in cost reduction is still needed to drive down the cost of EV powertrains.

1.4.1 Permanent Magnets

Figure 1-4 shows the demagnetization curves for current commercially available PM materials. Until the early 1970s, the only permanent magnets that were available to PM motor designers were Alnico and Ceramic Ferrites. Then came along rare-earth magnet materials such as Samarium Cobalt (Sm-Co) in the 70s followed by Neodymium-Iron-Boron (Nd-Fe-B) in the early 80s.

Nd-Fe-B magnets lead in terms of energy product, remanent flux density and coercive force. Commercially available Nd-Fe-B magnets have energy products that range from 27-42 MGOe (215 - 334 kJ/m^3) and improvements are still being made in this area towards the projected theoretical maximum energy product of 64 MGOe (509 kJ/m^3) [19]. These magnets are finding increasing use in old applications such as voice coil motors for computer disk drives, high-performance small-sized synchronous and stepper motors, as well as new applications that include Magnetic Resonance Imaging (MRI) systems, undulators or electron wigglers for the production of high quality synchrotron radiation, eddy-current retarder brakes for large motor vehicles such as trucks and busses, as well as EV propulsion motors. The main disadvantages of Nd-Fe-B magnets are their relatively high temperature

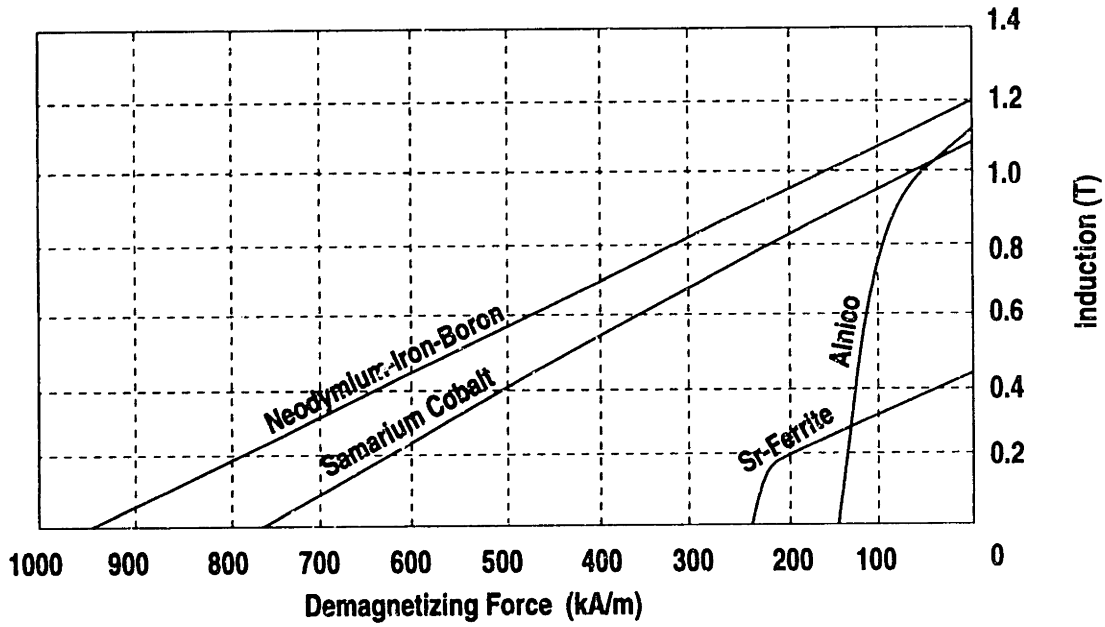

Figure 1-4: Demagnetization characteristics of typical PM materials.

dependence of remanent flux and coercive force as shown in Figure 1-5, and their poor resistance to corrosion. The corrosion problem is often solved by employing one of a host of proven coating technologies including, ion vapor deposition of aluminum and/or chromate coating of 7-19 μm thickness, electrodeposition of an epoxy coating of 20-30 μm and electroplating the magnets with about 10-20 μm of nickel. Magnet manufacturers are also producing new grades of Nd-Dy-Fe-Co-B-Mo sintered magnets with improved temperature stability [16, 19]. Sm-Co, the predecessor to Nd-Fe-B, does not suffer from the corrosion and temperature problems described above, but is about 2-3 times as expensive as Nd-Fe-B. Current bulk prices for Nd-Fe-B on the U.S. market are about \$80 - \$100 USD per lb, and there are reports that magnets with similar performance (but less professional finishing) to that obtainable on the U.S. market, can be obtained from the Tsinghua University in China [18].

1.4.2 Power Semiconductor Switches

The Insulated Gate Bipolar Transistor (IGBT) is gradually becoming the power semiconductor switch of choice in EV drives. The IGBT combines the desirable high voltage and current switching capabilities of the bipolar transistor as well as the high input impedance

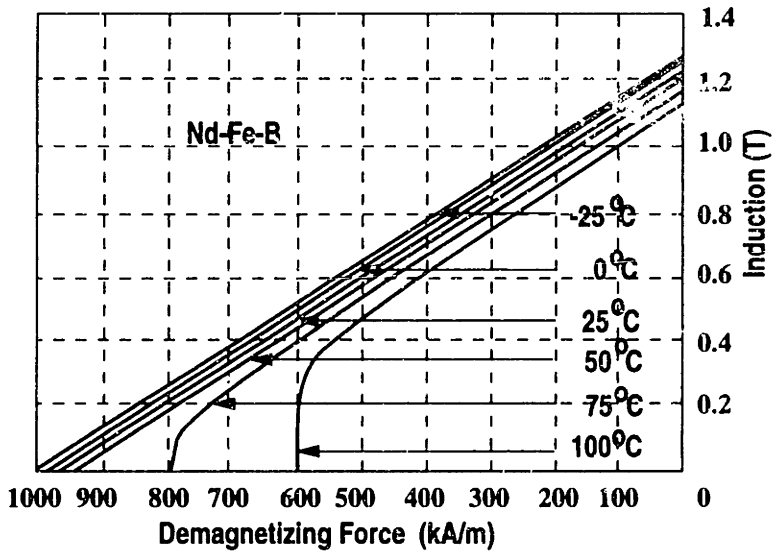

Figure 1-5: Effect of temperature on the demagnetization characteristics of Nd-Fe-B magnets.

and fast switching speed of the Metal-Oxide-Semiconductor Field-Effect Transistor. Its square safe operating area reduces its snubbing requirements in hard-switched inverters. With switching times of less than a microsecond, third generation IGBTs are capable of PWM operation up to 20 kHz, thus lowering ripple current filtration requirements and acoustic noise. Design and development of high-power variable-speed drives have been further simplified with the introduction of Intelligent Power Modules (Intellimods^{TM}) by Powerex, in alliance with Mitsubishi Electric [20]. These Intellimods^{TM} integrate gate drives and other protection circuitry with third-generation IGBTs and soft recovery anti-parallel diodes in one module, simplifying the interface of the power switches to inverter control circuitry. Intellimods^{TM} are currently available as singles, duals (two IGBTs connected in a half-bridge configuration), or six-packs (six IGBTs connected as three half bridges on a common bus). The rated current of these devices range from 10 A to 600 A with a rated collector-to-emitter voltage of 600 V or 1200 V, thus making them appropriate for the design of multi-kiloWatt inverters. Intellimods^{TM} with rated collector-to-emitter voltage of 1500 V are about to be introduced.

1.5 Thesis Objectives and Contributions

This thesis seeks to accomplish three major objectives. The first objective is to develop, for the first time, a prototype 15 kW (20 hp) high-performance direct-drive PM wheel motor, novel IGBT-based power-electronic inverter and a microprocessor controller for the propulsion of a battery-powered or hybrid mid-size family sedan. The motor employs Nd-Fe-B magnets, is capable of producing a constant torque of 450 Nm up to 325 rpm, and 15 kW of constant power up to a top speed of 1300 rpm. The active mass of the motor is only 25 kg, compared to the competition which has a mass of 53 kg [21]. The motor-inverter combination has been tested on a dynamometer in a laboratory environment and the drive efficiencies from battery to wheel are estimated at 85 % and 92 % over the Federal Urban Drive Schedule (FUDS) and the Federal Highway Drive Schedule (FHDS) respectively.

To arrive at an economical motor design that uses a minimum amount of surface-mounted magnets, a detailed study of the torque production characteristics of a new class of surface-mounted PM motors called Halbach motors, which to date have not been widely used in the electric machines community, was performed. The motivation for this study was driven by the search for novel electromechanical arrangements with the high torque densities (i.e. low mass) and high efficiencies required by an EV wheel motor. Through this endeavor, we gain a quantitative and intuitive understanding of the operation of this class of PM machines and outlined their merits vis a vis conventional surface-mounted motors. We have been able to answer the question as to when and why one should consider using a Halbach magnet arrangement in the design of PMSMs. We learn that a slotted stator with square-wave windings and a conventional surface-mounted rotor magnet arrangement, where magnetization vector rotates 180° from one rotor pole to the next, yields a more economic wheel motor than a slotless stator with Halbach magnets.

The third objective is to develop a novel power-electronic inverter that is particularly suited for PMSMs with a high torque constant, and hence high back-emf constant, that require wide-speed-range operation. This novel inverter topology consists of standard three-phase voltage source inverter, modified to include a bidirectional boost converter in its dc link. This topology allows PMSMs to be designed for wide speed range operation

without the need to introduce rotor saliency in the motor. Efficient extended speed range operation without field-weakening or phase advance, which carry the penalties of reduced efficiency and increased torque ripple, is made possible. For an IGBT inverter operation from a fixed dc bus, the conduction losses are reduces if the output power is delivered at a high voltage and hence low current since the on-state voltages of the IGBT and its antiparallel diode are fairly constant with current. Furthermore, high voltage, low-current inverters have fewer electrolytic dc bus filter capacitors, smaller current-related voltage overshoots, less conduction losses and hence smaller heatsinks, smaller conductors and high efficiency. Since the semiconductor switches are rated to withstand the highest motor back-emf, catastrophic failure modes that will result in large currents injected by the motor into the traction battery are avoided.

1.6 Thesis Organization

Recognizing that the ability to reduce the no-load losses in a traction motor is key towards motor efficiency maximization over both Urban and City drive cycles, Chapter 2 sets out to explore and compare the troque production characteristics of slotless Halbach slotless conventional surface-mounted PMSMs and their suitability for application in a wheel motor powertrain, since slotless motors have significantly lower no-load losses compared to their slotted counterparts. Unfortunately we learn that, to produce the high torques necessary for a direct-drive wheel motor, slotless machines require a substantial amount of high-energy Nd-Fe-B magnets, thus making the resulting motors uneconomical. Chapter 3 therefore deals with the design of a slotted motor which can produce the high torques necessary with reduced magnet mass. The magnet arrangement is of the conventional type since with reduced magnet mass and a permeable rotor backing, the conventional magnet arrangement is preferred.

In seeking to increase the efficiency of the power-electronic inverter, achieve a wide-speed-range for motor operation without inefficient flux-weakening, and also prevent the catastrophic failure modes associated with inverter reset, Chapter 4 examines the benefits of driving the motor with a novel high-voltage/low-current inverter, compared to a low-

voltage/high-current inverter. In Chapter 5, we design the inverter and the microprocessor controller for the wheel motor designed in Chapter 3.

The prototype wheel motor and inverter are built and tested in Chapter 6. The motor has a back-emf constant of 7.26 V/rad-s. An efficiency map under the low-speed region of the torque-speed envelope is provided.

Finally, Chapter 7 presents a brief summary of the ground covered in this thesis and conclusions drawn from this experience, and it lays out the roadmap for future work.

Chapter 2

Torque Production in Slotless Halbach and Conventional Permanent-Magnet Motors: A Comparative Analysis

2.1 Introduction

The elimination of intermediate gearing in direct-drive applications requires the drive motor to produce the total load torque electromagnetically. High torques in an electric motor can be achieved by increasing the magnetic loading, electric loading and force lever arm. Volume constraints and rotor inertia often limit the maximum lever arm of the motor and the electric loading is limited by the maximum power dissipation in the armature windings as well as the coercive force of the rotor magnet material, since one has to guard against demagnetization of the rotor magnets. The magnetic loading is also limited by saturation of the rotor and stator back iron and losses in the stator back iron. If expensive magnet materials such as Nd-Fe-B or Sm-Co are to be used for high-performance, low-weight machines, then magnet cost and hence the volume or mass of magnet material becomes a constraint for economical designs.

The choice of rotor magnet arrangement is an important initial step in the design of permanent-magnet synchronous motors. Numerous rotor magnet configurations, such as

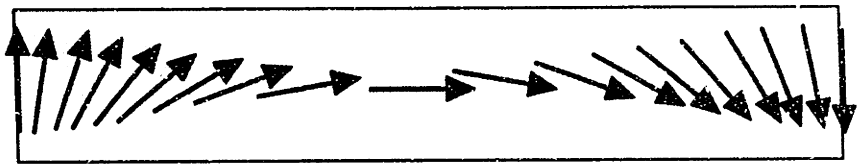

(a) Ideal Halbach array

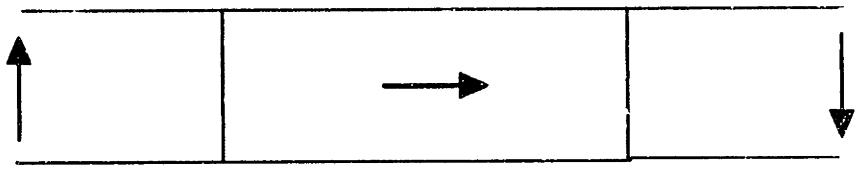

(b) Discrete Halbach array

Figure 2-1: Magnetization pattern in continuous and discrete Halbach arrays.

buried (interior) tangential, radial and inclined magnets exist in addition to their commonly used surface-mounted counterparts, and their relative merits have been compared in [22, 23] using finite-element simulations. The Halbach permanent-magnet arrangement, named after its inventor Klaus Halbach, has traditionally been used to produce harmonically pure magnetic fields for undulators or electron wigglers for particle accelerators, free electron laser systems, and synchrotron radiators [24] - [28]. Recently the Halbach array is finding use in electric machines including linear motors for wafer transport, high-speed energy storage flywheels and direct-drive wheel motors for electric vehicle propulsion [29, 30, 31].

The ideal Halbach magnet arrangement is one whose magnetization rotates continuously in a sinusoidal fashion as schematically shown in Figure 2-1(a). Since a continuously rotating magnetization is difficult to achieve in practice, the ideal array is often approximated with discrete sets of magnets. In [32], Marinescu et al. compared the airgap flux of a discrete Halbach array where the magnetization vector rotates 60° (3 magnet segments per pole) and 45° (4 magnet segments per pole) between magnet pieces to that of a conventional radially-magnetized surface-mounted arrangement. The results in [32] showed that the multipolar Halbach array is capable of producing higher peak airgap flux and hence machine torque.

To date, the general question of when and why one should use a Halbach rotor in the design of electric machines has not been addressed. In this chapter we study and compare

the torque production capability of Halbach and conventional rotor magnet arrangements on a slotless armature. Furthermore, to simplify the fabrication of the rotor magnet array it is useful to consider a Halbach array which consists of only radial and azimuthal magnetizations, where the magnetization vector rotates 90° between magnet pieces as shown in Figure 2-1(b). Such a rotor arrangement is easier to manufacture since in applications with high number of pole-pairs and large rotor diameter, such as a wheel motor, the radial and azimuthal magnets can be cut out of the same magnetized block.

Figure 2-2 shows a gray-scale representation of the proportion of time the drive motor spends at the operating points underneath its normalized torque-speed curve under the FUDS and the FHDS [38]. Darker shades in the Figure represent more frequent operation. Our motivation for studying a slotless armature stems from noting from Figure 2-2 that the ability of the EV propulsion motor to produce low torques efficiently is key in efficiency maximization over both the city and highway drive cycles, as shown by the shaded areas in Figure 2-2. Slotless motors are desirable in this respect since the stator teeth, which often carry high flux densities that contribute significantly to the no-load motor losses, are eliminated. The armature conductors in a slotless machine however, are not shielded by the stator teeth and hence can exhibit significant eddy-current losses. The eddy-current loss, fortunately, is proportional to the fourth power of the diameter of the armature conductors and hence can be significantly reduced by reducing the strand size of the conductors, with the lowest strand size set by manufacturing constraints[33]. The conductors must be properly transposed so that each strand experiences the same average magnetic field. Thus the armature windings are often made out of Litz wire. With a slotless armature, rotor pole-face losses associated with stator slot harmonics are also eliminated, as well as torque ripple associated with magnet cogging which can be troublesome at low vehicle speeds. EV drives notwithstanding, slotless motors are becoming serious candidates for high speed applications such as machine tools and generators, and also in other applications where low cogging torque is necessary, such as direct drive servo positioning, and have been the subject of many recent papers [34] - [37]. In studying the Halbach and conventional arrangement for the rotor magnets, our goal is to determine which of the two magnet arrangements produces the highest torque per mass of magnet material used, subject to the same armature

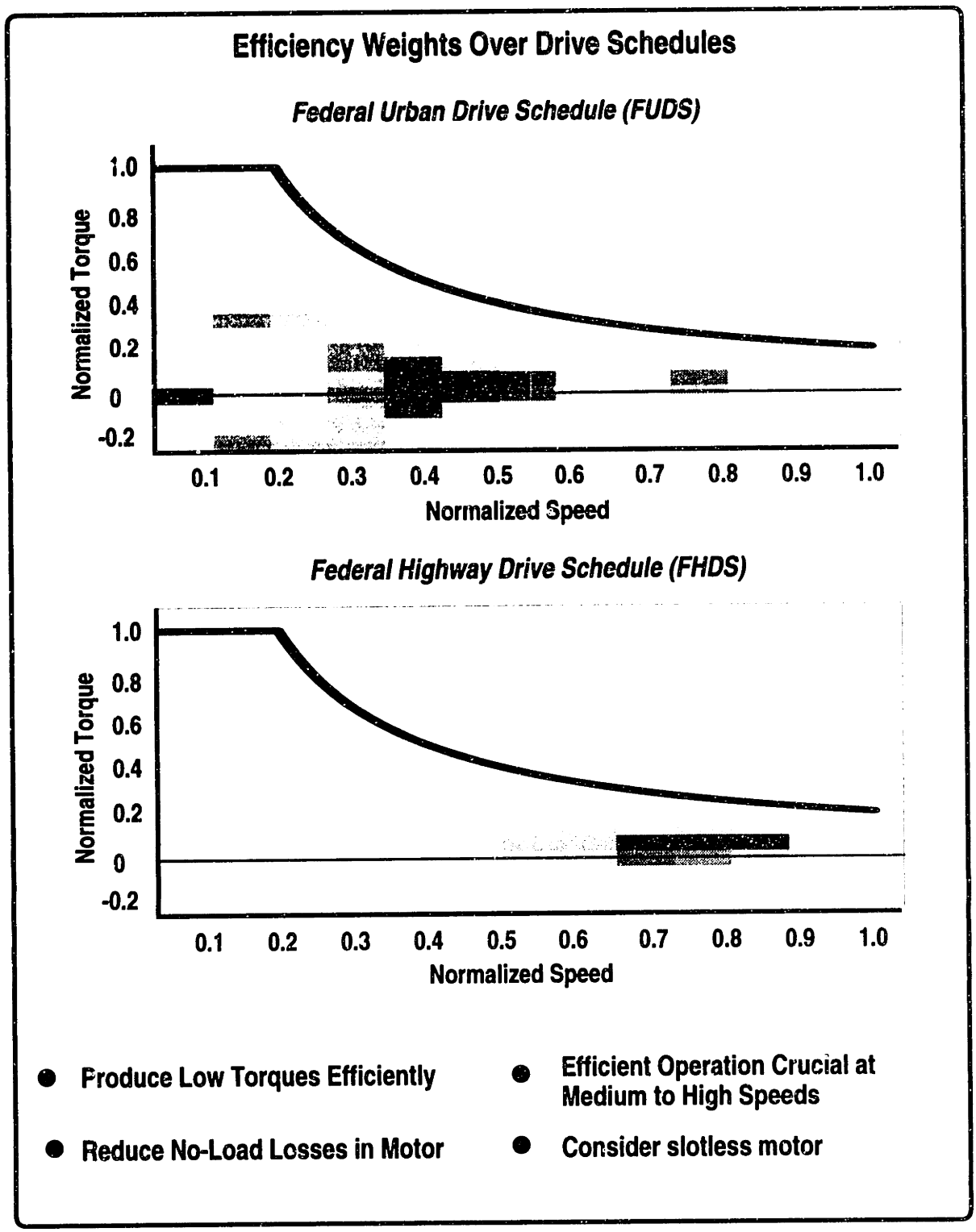

Figure 2-2: Motor operating points under Urban and Highway Drive Schedules.

current excitation. We also seek to determine regions of operation where each magnet arrangement performs best, in terms of peak torque per magnet mass, thus aiding the motor designer to choose appropriately between the two magnet arrays. We study the two cases where the rotor backing is made of a highly-permeable material such as magnetic steel or a non-magnetic material such as synthetic fibers for mechanical reasons [30]. The volume of magnets as well as the power dissipation in the armature windings are kept the same for each study.

We find that in machines with a permeable rotor backing, the conventional arrangement produces a higher torque up to a certain magnet thickness after which the Halbach arrangement excels. For machines without a permeable rotor backing, the Halbach arrangement always produces higher torque. We develop simple intuitive explanations, in terms of magnetic charges, that explain this result, and enable one to predict the torque production capability of these machines without resorting to somewhat cumbersome mathematics.

2.2 The Halbach Array: An Intuitive Understanding of Spatial Flux Distribution

The Halbach array has traditionally been used to produce harmonically pure magnetic fields for use in undulators and electron wigglers. It has been shown in [29] that for the ideal Halbach array, the magnetic field intensity vanishes on one side of the array, and for a square block array such as the one shown in Figure 2-3(d), the spatial fundamental field is canceled on one side of the array while the field intensity on the other side enhanced by $\sqrt{2}$.

In this section we present an intuitive model that explains the "one-sidedness" of discrete Halbach arrays. For this purpose, it is useful to think of magnet blocks as being composed of paired magnetic charges. Magnetic fields emanate from positive magnetic charges and terminate on negative charges. Furthermore, field lines from positive charges terminate on the closest "free" negative charge. With these simple rules, the field lines from the conventional magnet array are constructed, as shown in Figure 2-3(a).

The field lines from the Halbach array are constructed via superposition. We first

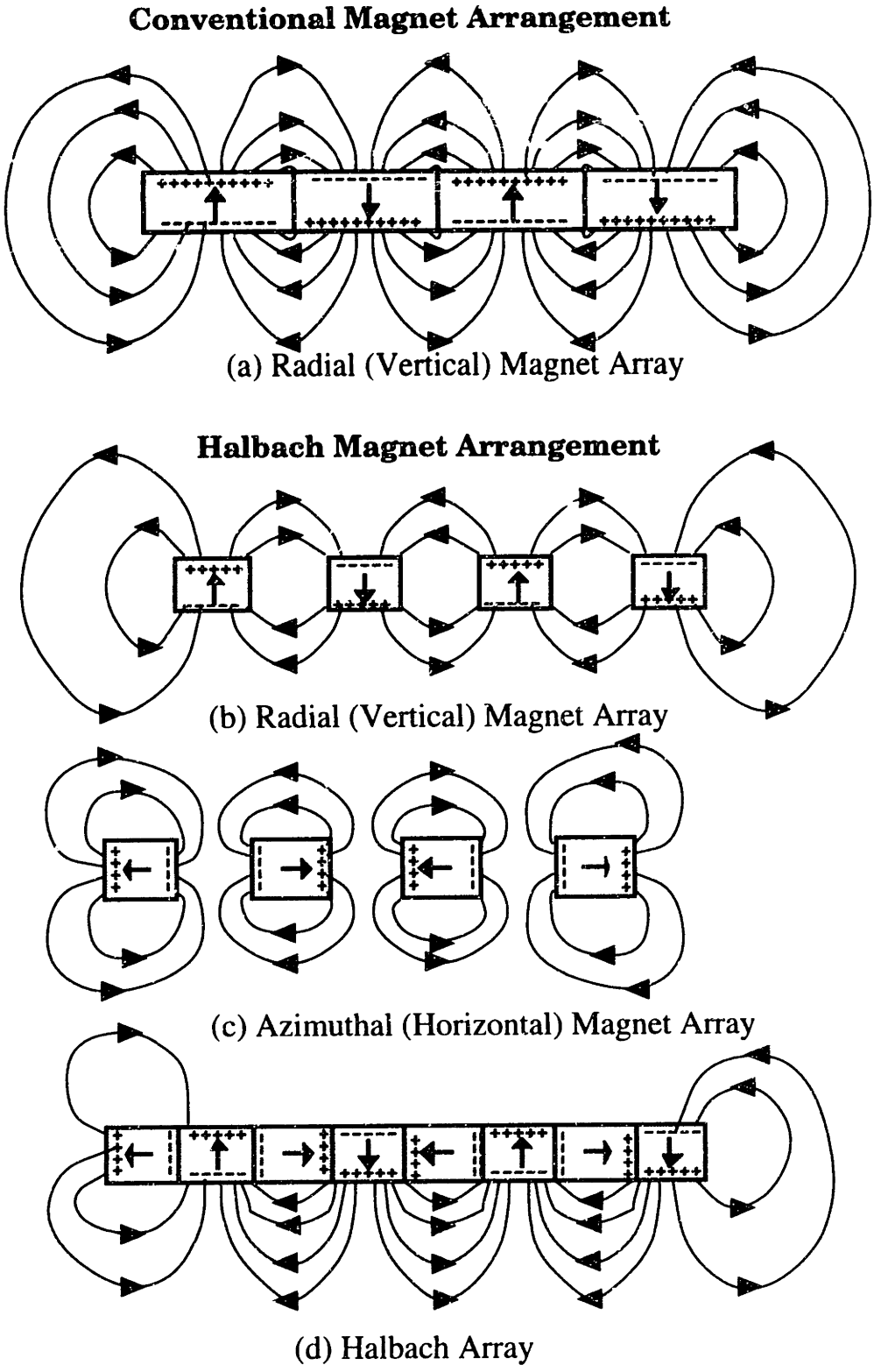

Figure 2-3: Intuitive illustration of flux distribution in conventional and Halbach magnet arrays.

separate the magnet blocks into a radial (vertical for a linear motor) array and an azimuthal (horizontal for a linear motor) array as shown in Figure 2-3(b) and (c). By applying the simple rules outlined above, one can construct the field lines for the individual arrays as shown in Figure 2-3(d). The spatial flux distribution of the combined array is the sum of the flux distributions for the individual arrays. Note that there is field cancellation on one side of the array while the fields on the other side of the array reinforce. Which side of the array the cancellation takes place depends on the direction of rotation of the magnets. Figure 2-4 shows a finite-element simulation of the magnetic flux distribution of a conventional and Halbach magnet arrangement for a 10 pole-pair cylindrical rotor, using the 2-D finite-element analysis program QuickField[1]. The rotor backing is non-magnetic in both simulations. The flux distribution in Figure 2-4(b) shows the one-sidedness of the Halbach arrangement vis-a-vis that of the conventional arrangement in Figure 2-4(a).

2.3 Torque Computation

In this section, we study the torque production characteristics of conventional and Halbach arrays with and without a permeable rotor backing. The armature used for this comparison is slotless, due to its desirable attributes of low no-load losses and absence of magnet cogging. The winding consists of a three -phase set wound in a square-wave fashion, of which two phases out of three are excited at a time with rectangular currents. We have explored various winding placement patterns and numbers of phases, under the constraint of fixed ohmic power dissipation in the armature and have learned that a 3-phase square-wave excitation with only two phases on at a time yields high torque while keeping the inverter simple and the cost of the semiconductor switches under control. In this study, the outer diameter of the motor is held constant at its maximum value (as dictated by the application) and our objective in optimization is therefore to determine, for a given volume of magnets, which configuration of rotor magnets produces the highest torque per ohmic power dissipated in the armature windings. The machine torque is computed by integrating the product of the

[1]QuickField is a registered trade mark of *Tera Analysis Company*, 17114 Bircher Street, Granada Hills, CA 91344

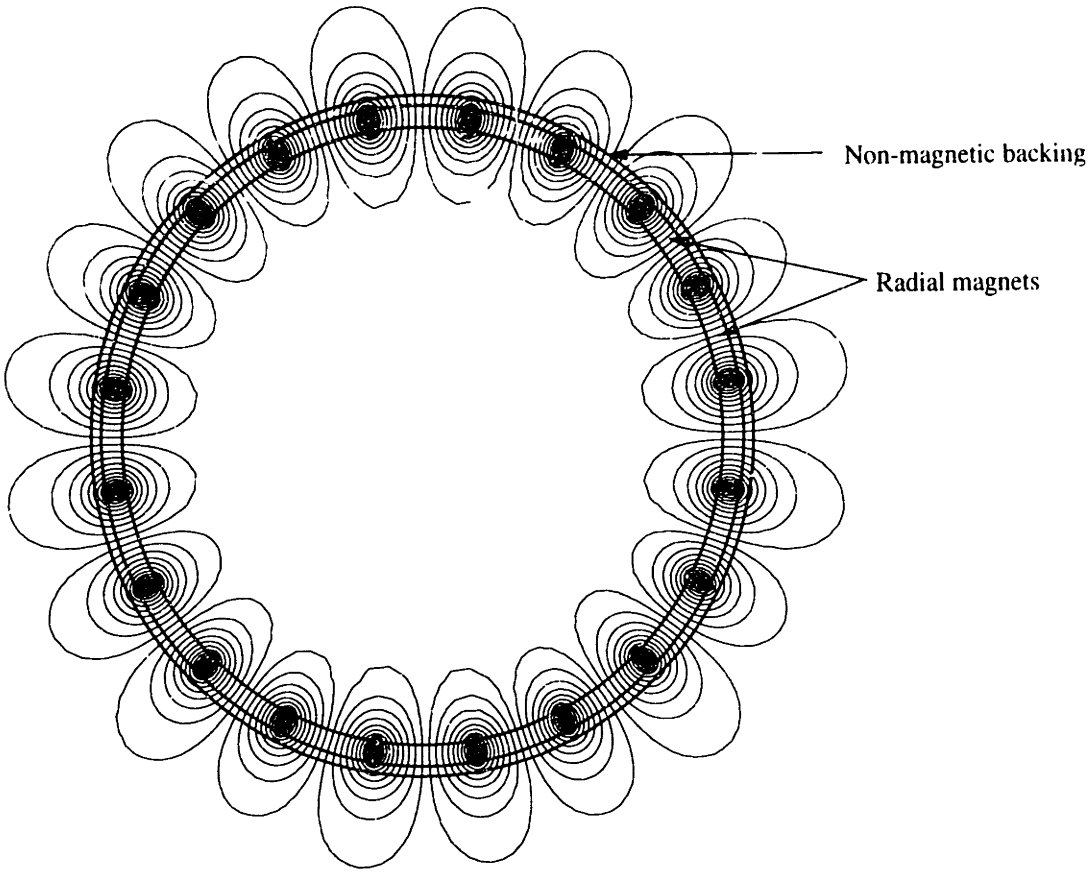

(a) Conventional Magnet Arrangement on Non-Magnetic Backing

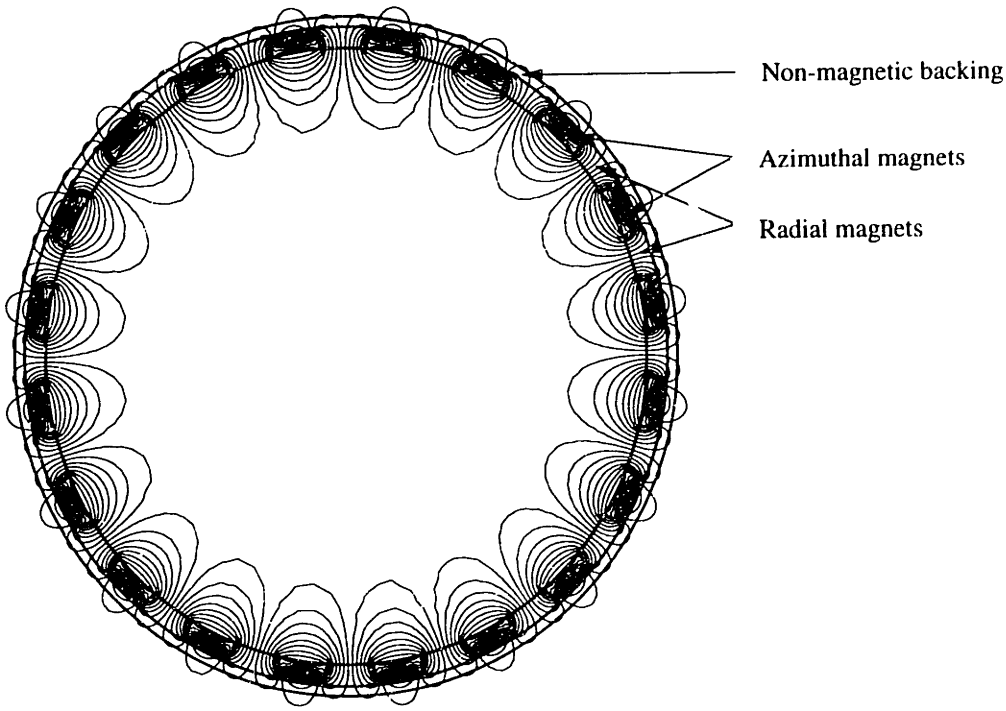

(b) Halbach Magnet Arrangement on Non-Magnetic Backing

Figure 2-4: Finite element simulation of flux distributions of conventional and Halbach magnet arrangements.

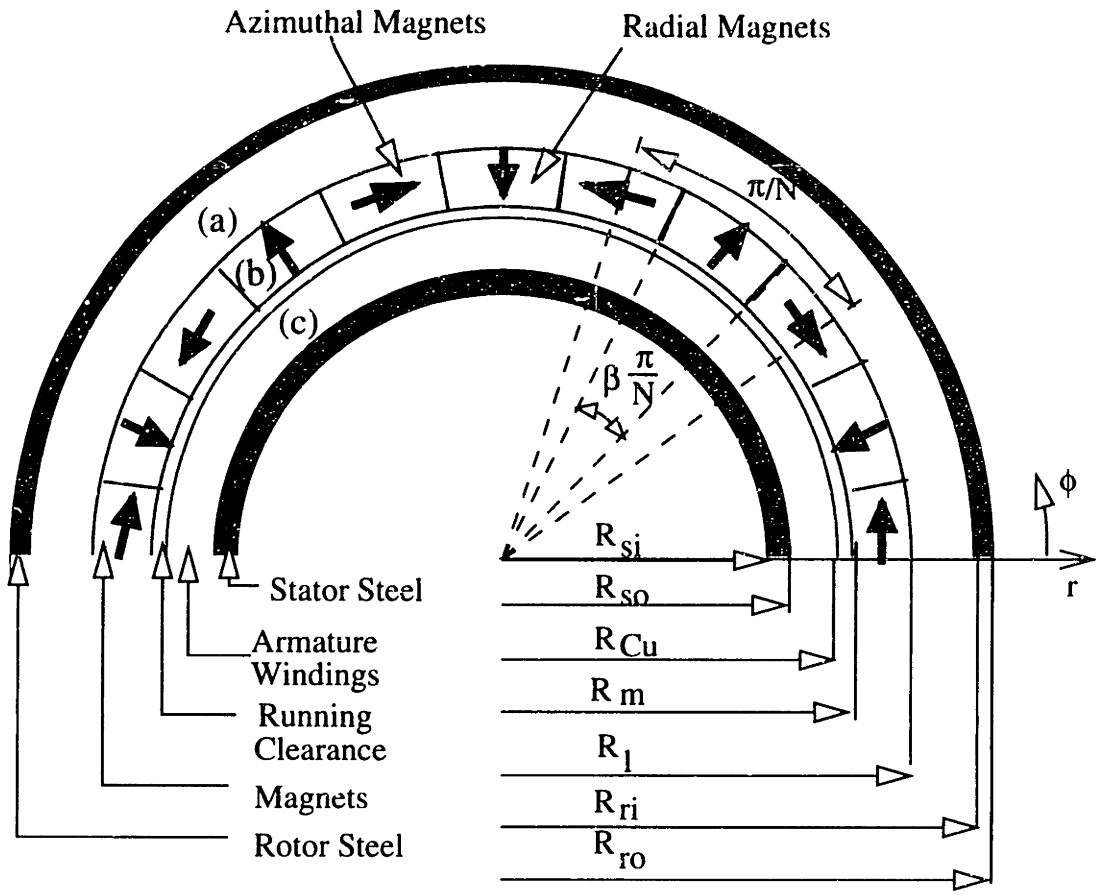

Figure 2-5: Analytical model of generalized magnetic circuit.

radial no-load magnetic flux and the armature current density over the volume occupied by the armature conductors. For the torque computation, we assume that the coercive force of the magnets is large enough to avoid demagnetization.

2.3.1 Two-Dimensional Analytical No-Load Magnetic Field Computations

Figure 2-5 shows a cross-section of the magnetic circuit of the motor to be analyzed, where we have ignored end fringing effects by making the structure infinitely long into the figure. This generalized magnetic circuit can be used to analyze the no-load magnetic field density distribution for both Halbach and conventional motors, with and without a permeable rotor backing. To analyze designs without a permeable rotor back-iron, the dimensions R_{ri}

and R_{ro} are set to infinity. For designs with permeable rotor backing, R_{ri} is set to R_1. The parameter β represents the ratio of the pole arc of the radial magnets to the pole pitch. Thus by varying β from zero to one, the full range of Halbach rotor designs with various pole-arc to pole-pitch ratios can be studied. For example, $\beta = 1$ corresponds to a conventional design with full-pitch magnets since this value of β leaves no room for the azimuthal magnets. On the other hand, $\beta = 0$ corresponds to a rotor magnet arrangement with only azimuthal magnetization. As will be seen later on in this Chapter, we shall compare the torque comparison of Halbach and conventional magnets arrays under the constraint of fixed magnet mass. A parameter δ will be introduced, which can be used to turn off the azimuthal magnetization to permit non full-pitch conventional magnet arrays to be studied. For Halbach designs $\delta = 1$, and for conventional designs, $\delta = 0$. For $\delta = 1$, the resulting Halbach magnet arrangement corresponds to that shown in Figure 2-5, and for $\delta = 0$, the resulting conventional arrangement corresponds to that shown in Figure 2-5 with the azimuthal magnet segments removed.

In our magnetic circuit analysis, the recoil permeability, μ_r, of the magnets is assumed to be unity; an assumption which is not bad for rare-earth magnets such as Nd-Fe-B ($\mu_r = 1.05$) or Sm-Co ($\mu_r = 1.02$). We are interested in computing the magnetic flux density in the armature windings in order to compute torque. This region occupied by the armature conductors, together with the running clearance constitute region (c) in Figure 2-5. The magnetic field intensity in the magnets (region (b)) is needed to assess possible demagnetization of the azimuthal magnets. In our analyses, it will be assumed that the sizes of all permeable back-iron are adequately chosen such that infinite permeability can be assumed and magnetic saturation can be ignored.

A. Representation of magnetic field sources

The radially-oriented magnets are assumed to be radially magnetized with a magnetization vector given by $\mathbf{M}_{rad} = M_0 R_m / r \, \hat{\mathbf{r}}$, and the magnetization vector for the azimuthal magnets is given by $\mathbf{M}_{az} = M_0 R_m / r \, \hat{\phi}$, where M_0 is the maximum magnetization and is related to

the remanent flux density B_{r0} by $M_0 = B_{r0}/\mu_0$[2]. The remanent flux B_{r0} has a negative temperature coefficient and is related to the magnet temperature in °C by T_{mag} by the equation

$$B_{r0}(T_{mag}) = B_{r20}\left[1 - \frac{0.11(T_{mag} - 20)}{100}\right] \tag{2.1}$$

where B_{r20} is the magnet remanent flux at 20°C. The assumption of radial (instead of parallel) magnetization simplifies greatly our analysis, and does not detract from the generality of our results since for machines with high numbers of pole-pairs, the difference between the flux distributions for radial and parallel magnets is practically negligible [39].

The magnetic flux distributions in the three regions ((a), (b), and (c)) are determined via superposition. We first solve for the fields from the radial magnets and add them to those from the azimuthal magnets. The magnetization vectors for the radial and azimuthal magnets can be written in terms of their Fourier components as

$$\mathbf{M}_{rad} = \sum_{k\ odd}^{\infty} \frac{R_m}{r}\frac{4M_0}{k\pi} \cdot (-1)^{\frac{k-1}{2}} \sin k\beta\pi \cdot \sin kN\phi\ \hat{\mathbf{r}} \tag{2.2}$$

$$\mathbf{M}_{az} = \sum_{k\ odd}^{\infty} \frac{R_m}{r}\frac{4M_0\delta}{k\pi} \cdot (-1)^{\frac{k-1}{2}} \cos k\beta\pi \cdot \cos kN\phi\ \hat{\phi} \tag{2.3}$$

where k is the harmonic number and N is the number of pole pairs. The parameter δ is set to unity for the Halbach arrangement and zero to turn off the azimuthal magnetization for the conventional arrangement. Notice that the divergence of each of the Fourier components of $\mathbf{M}_{rad}$ is zero, therefore the magnetic field in all three regions (a), (b), and (c) are governed by Laplace's Equation, for the radially-oriented magnets. For the azimuthal magnets, the Fourier components of the magnetization vector are not divergence-free even though the total magnetization vector $\mathbf{M}_{az}$ has no divergence. Therefore the solution for the magnetic field intensity in the magnets (region (b)) contains a particular solution from Poisson's Equation, in addition to a Laplacian homogeneous solution which is used to satisfy the boundary conditions.

[2]Vector quantities are represented with bold typeface throughout this thesis.

B. Boundary conditions

We solve for the magnetic fields via use of a scalar potential ψ which obeys Laplace's Equation $\nabla^2\psi = 0$ in cylindrical coordinates. The magnetic field intensity is given by $\mathbf{H} = -\nabla\psi$. The permeabilities of the stator and rotor steel, when present, are assumed to be infinite for ease of illustration in this thesis. At the boundaries $r = R_{ri}$ and $r = R_{so}$, the corresponding scalar potentials $\psi_{(a)}$ and $\psi_{(c)}$ vanish due to the infinite permeability of the steels. At the boundaries $r = R_1$ and $r = R_m$, we require the tangential magnetic field H^ϕ and the radial component of the magnetic flux density B^r to be continuous, noting that within the magnets, the magnetic flux density $\mathbf{B} = \mu_0(\mathbf{H} + \mathbf{M})$. It is also useful to note that continuity of H^ϕ at a boundary is equivalent to the scalar potential ψ being continuous at that boundary.

C. Solutions

The general solutions for the magnetic scalar potentials in the three regions are of the form

$$\psi_{(a),rad} = \sum_{k\ odd}^{\infty} C1_{rad}\left[\left(\frac{r}{R_{ri}}\right)^{kN} - \left(\frac{R_{ri}}{r}\right)^{kN}\right]\cdot \sin kN\phi \tag{2.4}$$

$$\psi_{(b),rad} = \sum_{k\ odd}^{\infty} \left[C2_{rad}r^{kN} - C3_{rad}r^{-kN}\right]\cdot \sin kN\phi \tag{2.5}$$

$$\psi_{(c),rad} = \sum_{k\ odd}^{\infty} C4_{rad}\left[\left(\frac{r}{R_{so}}\right)^{kN} - \left(\frac{R_{so}}{r}\right)^{kN}\right]\cdot \sin kN\phi \tag{2.6}$$

for the radially-oriented magnets and

$$\psi_{(a),az} = \sum_{k\ odd}^{\infty} C1_{az}\left[\left(\frac{r}{R_{ri}}\right)^{kN} - \left(\frac{R_{ri}}{r}\right)^{kN}\right]\cdot \sin kN\phi \tag{2.7}$$

$$\psi_{(b),az} = \sum_{k\ odd}^{\infty} \left[\frac{M_{az}R_m}{kN} + C2_{az}r^{kN} - C3_{az}r^{-kN}\right]\cdot \sin kN\phi \tag{2.8}$$

$$\psi_{(c),az} = \sum_{k\ odd}^{\infty} C4_{az}\left[\left(\frac{r}{R_{so}}\right)^{kN} - \left(\frac{R_{so}}{r}\right)^{kN}\right]\cdot \sin kN\phi \tag{2.9}$$

for the azimuthally-oriented magnets. Note that the solutions for $\psi_{(a)}$ and $\psi_{(c)}$ are chosen such that they vanish at $r = R_{ri}$ and $r = R_{so}$ respectively, and that the first term in Equation 2.8 is the particular solution. The equations that must be solved in view of the the boundary

conditions outlined in the previous section are:

$$\psi_{(a),rad}\Big|_{r=R_1} = \psi_{(b),rad}\Big|_{r=R_1} \tag{2.10}$$

$$\psi_{(a),az}\Big|_{r=R_1} = \psi_{(b),az}\Big|_{r=R_1} \tag{2.11}$$

$$\psi_{(b),rad}\Big|_{r=R_m} = \psi_{(c),rad}\Big|_{r=R_m} \tag{2.12}$$

$$\psi_{(b),az}\Big|_{r=R_m} = \psi_{(c),az}\Big|_{r=R_m} \tag{2.13}$$

$$B^r_{(a),rad}\Big|_{r=R_1} = B^r_{(b),rad}\Big|_{r=R_1} \tag{2.14}$$

$$B^r_{(a),az}\Big|_{r=R_1} = B^r_{(b),az}\Big|_{r=R_1} \tag{2.15}$$

$$B^r_{(b),rad}\Big|_{r=R_m} = B^r_{(c),rad}\Big|_{r=R_m} \tag{2.16}$$

$$B^r_{(b),az}\Big|_{r=R_m} = B^r_{(c),az}\Big|_{r=R_m} \quad . \tag{2.17}$$

Solving Equations (2.10) - (2.17) for the arbitrary constants $C1_{rad}$ - $C4_{rad}$, and $C1_{az}$ - $C4_{az}$, via the symbolic manipulation package Maple V[3] yield

$$C1_{rad} = \frac{M_{rad}R_m R_{ri}^{kN}}{2kN\left(R_{ri}^{2kN} - R_{so}^{2kN}\right)} \cdot \left(R_1^{kN} - R_{so}^{2kN}R_1^{-kN} - R_m^{kN} + R_{so}^{2kN}R_m^{-kN}\right) \tag{2.18}$$

$$C2_{rad} = \frac{M_{rad}R_m}{2kN\left(R_{ri}^{2kN} - R_{so}^{2kN}\right)} \cdot \left(R_1^{kN} - R_m^{kN} + R_{so}^{2kN}R_m^{-kN} - R_{ri}^{2kN}R_1^{-kN}\right) \tag{2.19}$$

$$C3_{rad} = \frac{M_{rad}R_m}{2kN\left(R_{ri}^{2kN} - R_{so}^{2kN}\right)} \cdot \left(R_{so}^{2kN}R_{ri}^{2kN}R_M^{-kN} - R_{ri}^{2kN}R_{so}^{2kN}R_1^{-kN} - R_{ri}^{2kN}R_M^{kN} + R_{so}^{2kN}R_1^{kN}\right) \tag{2.20}$$

$$C4_{rad} = \frac{M_{rad}R_m R_{so}^{kN}}{2kN\left(R_{so}^{2kN} - R_{ri}^{2kN}\right)} \cdot \left(R_m^{kN} - R_1^{kN} + R_{ri}^{2kN}R_m^{-kN} - R_{ri}^{2kN}R_1^{-kN}\right) \tag{2.21}$$

$$C1_{az} = \frac{M_{az}R_m R_{ri}^{kN}}{2kN\left(R_{ri}^{2kN} - R_{so}^{2kN}\right)} \cdot \left(-R_{so}^{2kN}R_1^{-kN} + R_m^{kN} - R_1^{kN} + R_{so}^{2kN}R_m^{-kN}\right) \tag{2.22}$$

$$C2_{az} = \frac{M_{az}R_m}{2kN\left(R_{ri}^{2kN} - R_{so}^{2kN}\right)} \cdot \left(R_m^{kN} - R_1^{kN} - R_{ri}^{2kN}R_1^{-kN} + R_{so}^{2kN}R_m^{-kN}\right) \tag{2.23}$$

$$C3_{az} = \frac{M_{az}R_m}{2kN\left(R_{ri}^{2kN} - R_{so}^{2kN}\right)} \cdot \left(R_{ri}^{2kN}R_{so}^{2kN}R_m^{-kN} - R_{so}^{2kN}R_1^{kN} - R_{ri}^{2kN}R_{so}^{2kN}R_1^{-kN} + R_{ri}^{2kN}R_m^{kN}\right) \tag{2.24}$$

[3]Source code for computation of unknown constants is attached in Appendix D.1. Maple V is a registered trademark of Waterloo Maple Inc, 450 Phillip St., Waterloo, ON, Canada, N2L5J5.

$$C4_{az} = \frac{M_{az} R_m R_{so}^{kN}}{2kN\left(R_{ri}^{2kN} - R_{so}^{2kN}\right)} \cdot \left(R_{ri}^{2kN} R_m^{-kN} + R_m^{kN} - R_1^{kN} - R_{ri}^{2kN} R_1^{-kN}\right) \quad (2.25)$$

where

$$M_{az} = \frac{4M_0\delta}{k\pi} \cdot (-1)^{\frac{k-1}{2}} \cos k\beta\pi \quad (2.26)$$

and

$$M_{rad} = \frac{4M_0}{k\pi} \cdot (-1)^{\frac{k-1}{2}} \sin k\beta\pi \quad . \quad (2.27)$$

The total magnetic scalar potential in each region is the sum of the contributions from the radial and azimuthal magnetizations and are therefore given by

$$\psi_{(a),tot} = \psi_{(a),rad} + \psi_{(a),az} \quad (2.28)$$

$$\psi_{(b),tot} = \psi_{(b),rad} + \psi_{(b),az} \quad (2.29)$$

$$\psi_{(c),tot} = \psi_{(c),rad} + \psi_{(c),az} \quad . \quad (2.30)$$

The airgap magnetic flux density $\mathbf{B}_{ag}$, which is used to compute machine torque, is given by

$$\mathbf{B}_{ag} = -\mu_0 \nabla \psi_{(c),tot} \quad . \quad (2.31)$$

D. Torque production under fixed magnet volume

For a fair comparison of the torque production capability of Halbach and conventional magnet arrays, we need to fix the volume (and hence the mass and cost) of the magnets used in each design. Thus, given an outer radius R_1 for the magnet array, the inner radius R_m can be calculated as

$$R_m = \sqrt{R_1^2 - \frac{M_{mag}}{\pi \rho_{mag} l_{mag} (\beta + \delta(1-\beta))}} \quad (2.32)$$

where ρ_{mag} is the magnet density, M_{mag} is the magnet mass, and l_{mag} is the magnet length. Remember that $\delta = 1$ for Halbach designs and $\delta = 0$ for conventional designs. For a given armature current excitation, the peak motor torque within a commutation interval **T** is computed by integrating the product of the radial component of the no-load airgap magnetic

flux density B_{ag}^{r} and the armature current density over the volume occupied by the armature conductors as

$$\mathbf{T} = -2NW_{eff} \int_{R_{so}}^{R_{Cu}} \int_{\frac{\pi}{6N}}^{\frac{5\pi}{6N}} J_0 \cdot B_{ag}^{r}\, r^2 d\phi dr\, \hat{\phi} \tag{2.33}$$

where J_0 is the armature current density, $B_{ag,r}$ is the radial component of the no-load magnetic flux density as defined in Equation 2.31, W_{eff} is the effective length of the motor, which is the stack length reduced by a fringing factor, and R_{so} and R_{Cu} refer to the inner and outer radii of the annulus formed by the armature windings, as shown in Figure 2-5. The expression in Equation 2.33 is computed using Maple V. Note that this torque expression is a function of the magnet mass, the magnet pole-arc to pole-pitch ratio β, the thickness of copper $(R_{Cu} - R_{so})$, and the Halbach/conventional parameter δ.

To illustrate the torque production characteristics of slotless Halbach and conventional motors, we consider the design of a slotless motor for a possible direct-drive wheel motor application. The outer diameter of the magnets, R_1, is fixed to 19.6 cm and the active length of the motor W_{eff} is 6 cm, such that the motor can fit in the hub of a 19-inch wheel. The ohmic (I^2R) power dissipated in the armature windings is fixed to 2.5 kW and a copper packing factor of 0.7 is assumed. The motor has 10 pole-pairs and a running clearance of 0.625 mm (25 mils) exists between the magnets and the armature windings. The remanent flux of the magnets at 20°C is 1.2 T, and the magnet temperature is 110°C, reducing the remanent flux to 1.08 T.

Figure 2-6 shows the radial and tangential components of the the airgap flux density within the armature windings for both the conventional and Halbach arrangements. For these plots, the magnet mass is 16 kg, the pole-arc to pole-pitch ratio β is 0.75, and winding thickness $(R_{Cu} - R_{so})$ is set to 2 cm to highlight the decay of the airgap flux. Both rotor and stator backings are magnetic with infinite permeability, and the extent of the plots is one pole-pair in the azimuthal direction. First, note that the *tangential* flux is *zero* at outer periphery of the stator (R_{so}) as expected from the infinitely permeable stator. Secondly, the fields decay away from the magnets with the higher harmonics decaying faster, as expected from Laplace's Equation. These observations serve as a check of the correctness of the analytic solutions. The interesting observations to be made from these figures are that

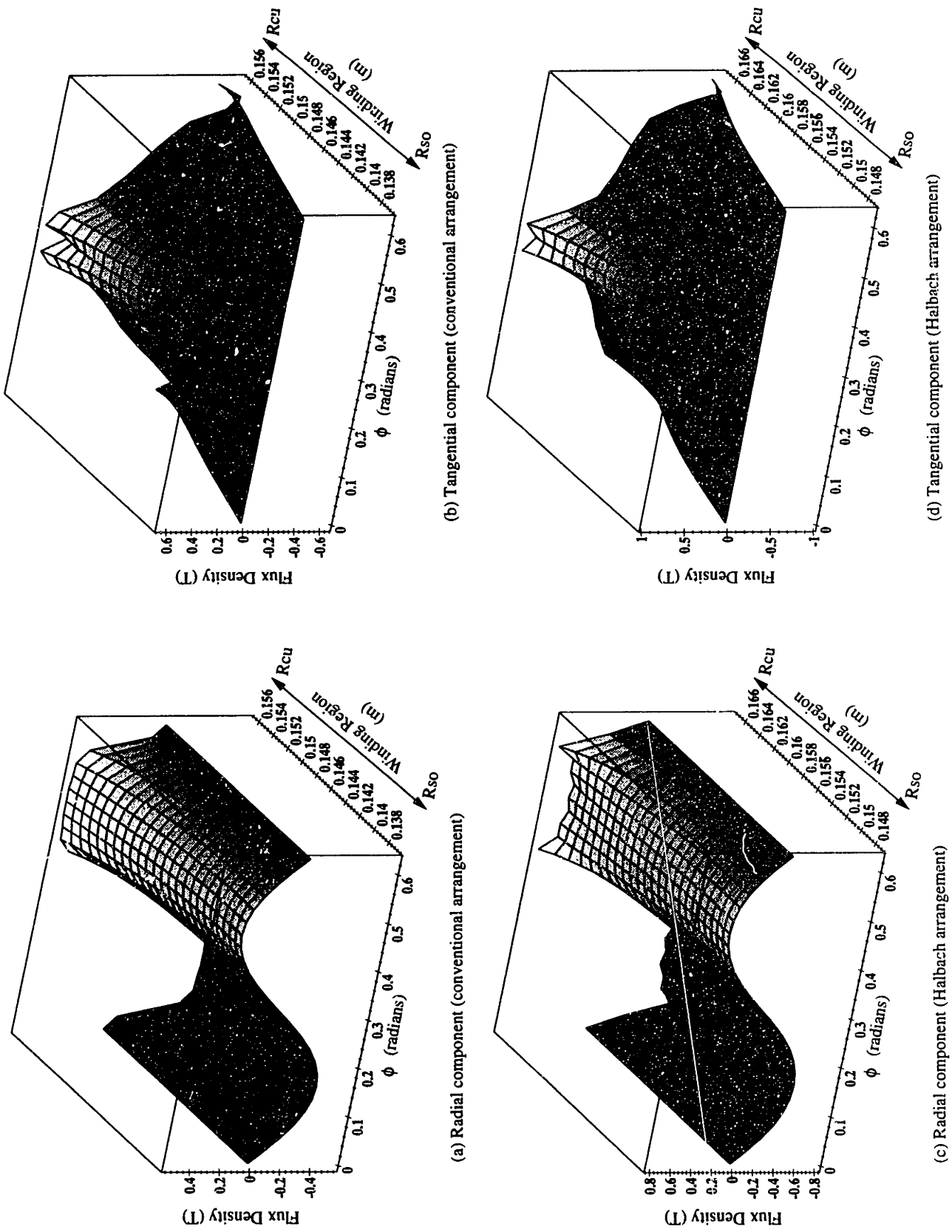

Figure 2-6: Radial and tangential flux distribution within armature windings for conventional and Halbach arrangements.

the field strength for the Halbach array is higher than that of the conventional array, and furthermore, that some high peaks exist in the radial field distribution of the Halbach array at the areas where the azimuthal magnets abut the radial magnets. The existence of these high peaks may suggest that one should put the armature windings in the area underneath the peaks. However these peaks decay rapidly and in both the Halbach and conventional arrangements higher torques are produced when the windings are placed underneath the center of the pole; thus producing torque from the peak of the fundamental component of the rotor's magnetic field.

2.4 Results

2.4.1 Slotless Armature: Optimal Thickness of Windings

One interesting characteristic of slotless motors is the existence of an optimal thickness of armature windings to produce maximum torque per ohmic power dissipated in the armature windings. The existence of this optimal winding thickness can be understood by considering the variation of the airgap magnetic flux density and the current density in the armature windings as the winding thickness is varied. Figure 2-7(a) shows the variation of the current density in the armature windings with the thickness of the windings under the constraint of constant ohmic power dissipation in the armature. For fixed I^2R dissipation, the allowable current density decreases with the winding thickness. Plotted in Figure 2-7(b) is the torque per current density in the windings, which is the integral of the radial component of the no-load airgap magnetic flux density over the volume occupied by the armature conductors. With zero winding thickness, the torque per current density is zero since the integration is over zero volume. The product of the two plots which represents the peak motor torque within a commutation interval is shown in Figure 2-7(c). This figure indicates that for illustrative design under consideration, the optimal thickness of armature windings is 0.8 cm. Above this thickness of copper, the available torque degrades gradually and the excess copper adds unnecessarily to the weight and cost of the motor. Furthermore, if the armature windings are to be cooled by circulating coolant fluid at the inner surface to the stator

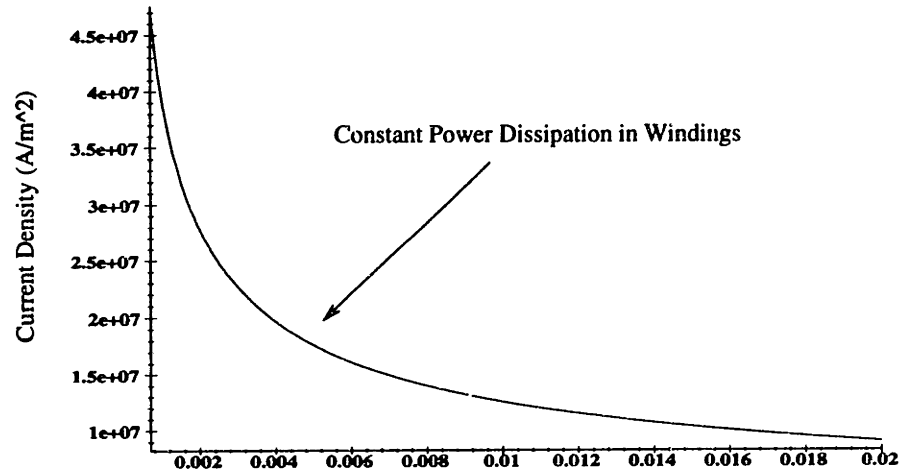

(a) Current density in windings under constant power dissipation

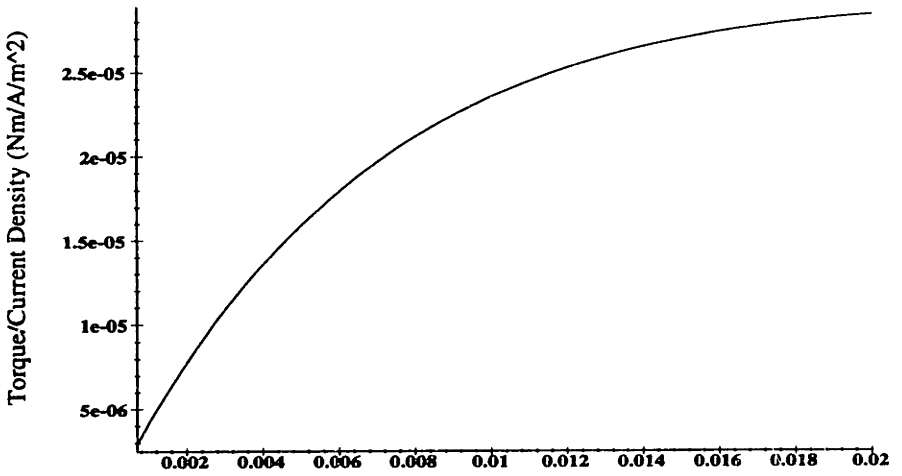

(b) Torque per current density in windings under constant power dissipation

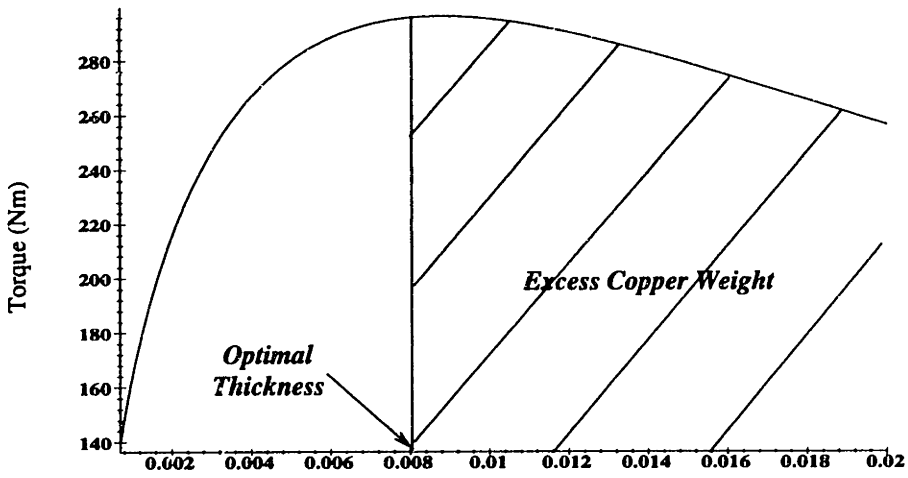

(c) Optimal thickness of stator windings for maximum torque production

Figure 2-7: Optimal thickness of armature windings for high torque production.

back-iron, the excess copper increases the thermal resistance of the stator windings. In general, the optimal thickness of copper would decrease with the number of pole-pairs, N, mainly because the magnetic field decays faster within the airgap for high N.

2.4.2 Halbach vs. Conventional Rotor: Torque Comparison

Figure 2-8 shows 3-D plots of the peak motor torque within a commutation interval against the magnet mass M_{mag} and the magnet pole-arc to pole-pitch ratio β. In both plots, the motor parameters are the same as in Section 2.4.1 and the armature winding thickness is set to its optimal value of 0.8 cm for the given number of pole-pairs. The plot in Figure 2-8(a) compares conventional and Halbach rotor designs with a permeable rotor backing while that in Figure 2-8(b) compares the same designs with a *non*-permeable rotor backing. Note that for fixed R_1, as the magnet volume increases, R_{Cu} and R_{so} decrease to accommodate the additional magnets while maintaining the optimal copper thickness. The usefulness of these plots is to determine, for a given magnet mass and hence magnet cost, which rotor magnet configuration yields the highest torque and what is the corresponding optimal β.

The plot of Figure 2-8(a) shows that for designs with a permeable rotor backing, the conventional array produces higher torque than the Halbach array when the magnets are thin. In this region of the design space, the magnets are *not* full pitch (i.e. $\beta < 1$) and higher torque is produced by shaving off magnets from the pole edges where the magnets abut, and using this magnet material to increase the radial length of the pole magnets. For thick magnets, however, the Halbach array produces higher torque irrespective of β. Note that the optimum β changes with the thickness (mass and hence volume and cost) of the magnets and $\beta = 1$ corresponds to a conventional arrangement where the magnets are full-pitch. For $\beta = 1$, the Halbach becomes equivalent to the conventional design with full-pitch magnets as expected. The plot in Figure 2-8(b), however, shows that for designs with a non-permeable rotor backing, the Halbach array *always* produces higher torque than the conventional array. The use of a permeable rotor backing in both the Halbach and conventional design allows the same torque to be produced with less magnets as the corresponding design with a non-permeable rotor backing. The above conclusions hold

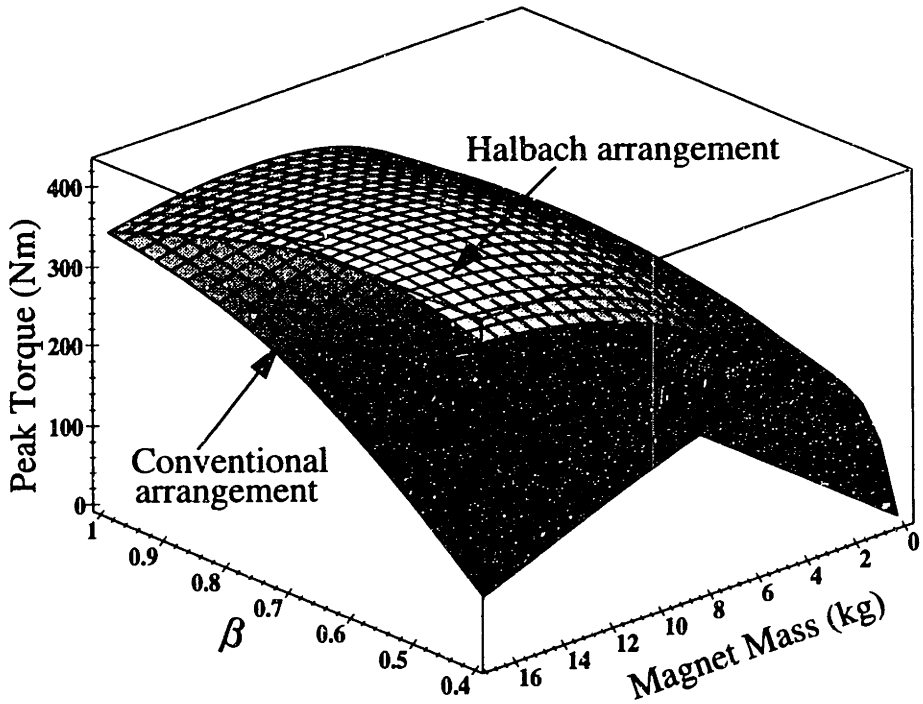

(a) Achievable peak torques with magnetic rotor backing.

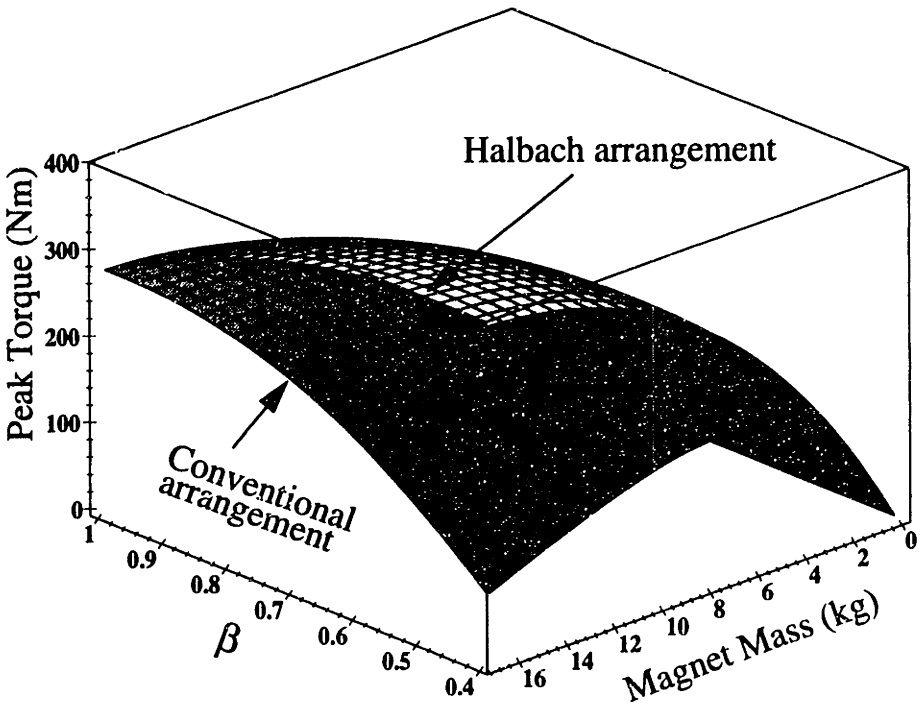

(b) Achievable peak torques with non-magnetic rotor backing.

Figure 2-8: Torque production in Halbach and conventional rotor magnet arrays with and without a permeable rotor backing

in general and are not specific to the illustrative example in Figure 2-8. In general, when the magnets become very thick, the designs *with* and *without* a permeable rotor backing approach each other but the torque "saturation" level of the Halbach rotor is higher than the conventional rotor.

The plots in Figure 2-8 are for the peak torque within a commutation interval but the average torque also exhibits similar dependence the magnet mass and β, except that the optimum β and the crossover magnet thickness (for magnetically backed rotors) are slightly different from those of the peak torque. Notice that in both designs (with and without a permeable rotor backing) the highest torque within the fixed mechanical envelope is achieved with the Halbach design. However this high torque is only achievable with a large volume of magnets which may be prohibitive from an economic point of view. Thus from an economic point of view, a slotless motor is not a good choice for a wheel motor which may be required to produce about 450 Nm of torque, as magnet mass in excess of 16 kg would be required. By shortening the electromagnetic airgap via armature slotting, once can reduce the magnet mass necessary to establish the required airgap flux density and forgo the benefits of high efficiency and low cogging associated with slotless motors.

2.5 Intuitive Explanation of Torque Production with Halbach and Conventional Magnet Arrays

To gain an intuitive understanding of the foregoing results, it is useful to think of the source of electromagnetic force not as the cross product of the radial component of the no-load airgap flux density and the armature current density but rather as the tangential component of the magnetic field from the armature conductors acting on the magnetic charges. Figure 2-9 shows the magnetic field lines from two excited phases of the armature windings. Also shown in the figure are the magnetic charges associated with the magnet arrays; the conventional array is shown in Figure 2-9(a) and the Halbach array is shown in Figure 2-9(b). In both figures, the volume of magnets is kept the same and the rotor magnets and armature conductors are aligned to produce maximum torque.

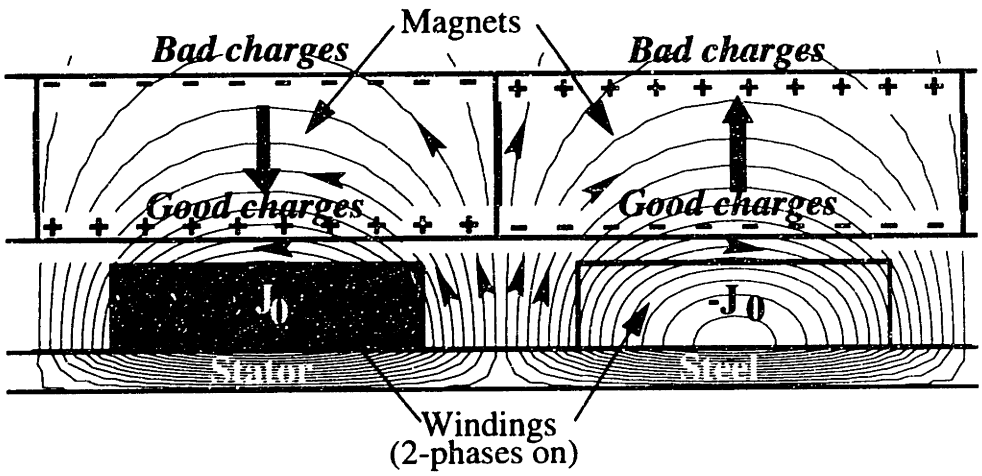

(a) Distribution of magnetic charges in conventional array

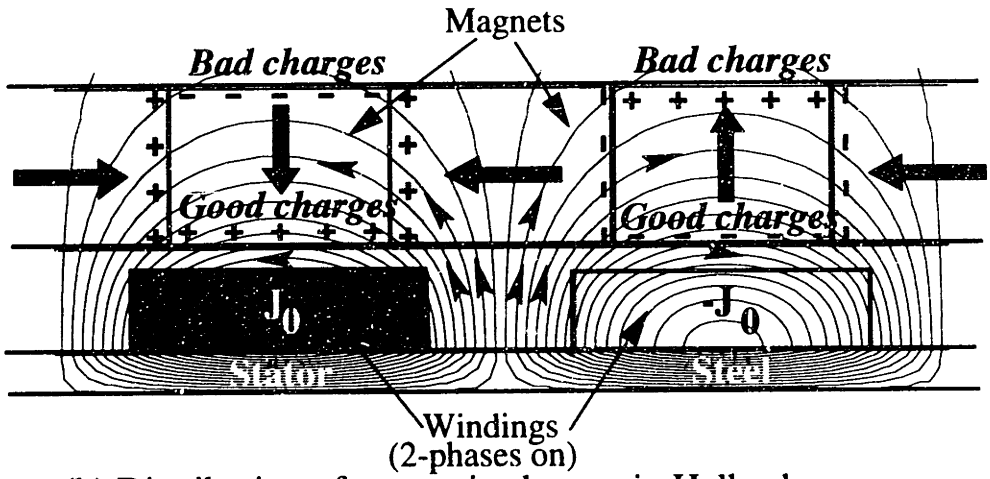

(b) Distribution of magnetic charges in Halbach array

Figure 2-9: Intuitive explanation of torque production in with non-magnetic rotor backing.

The "good" charges interact with the tangential component of armature conductor magnetic field to produce positive torque. The "bad" charges, on the other hand, interact with the tangential magnetic field to produce retarding torque. Note that the strength of the magnetic field interacting with the "bad" charges is low for reasonable magnet thicknesses so there is a *net* positive torque. The shaded charges in Figure 2-9(a) are the "useless" charges. The magnetic field lines interacting with these charges are effectively radial so they produce no *tangential* force. By cutting the magnet pieces containing these "useless" charges and rotating them 90° as shown in Figure 2-9(b), these charges now experience a substantial tangential magnetic field, and hence become "good" charges producing positive

torque. This is the benefit of the Halbach arrangement. Once again, note that the magnet volume remains unchanged.

A similar explanation can be offered for designs with a permeable rotor backing by considering the reflection of the magnetic charges in the steel via the method of images. Note that with both rotor and stator back-iron present, there are infinite reflections. However the overall effect of magnetic backing can be understood by focusing on the primary reflection of the magnetic charges through the rotor back-iron. Figure 2-10(a) shows that a permeable magnetic backing effectively doubles the length of the magnets with radial magnetization. The effect is to further remove the negative charges which produce retarding torque from regions where the armature reaction is strong. Thus there is a significant boost in motor torque when thin radial magnets are backed with steel. The azimuthal magnets, however, reflect the wrong way as shown in Figure 2-10(b). The image charges tend to cancel the otherwise "good" charges. Thus for thin magnets, the "good" charges created by introducing azimuthal magnetization may be completely cancelled by their image charges and hence produce no additional torque. In this situation, one does better by using the azimuthal magnet material to lengthen the radial magnets. When the radial magnets become thick enough such that the effect of magnetic backing is negligible, then one does better by introducing azimuthal magnetization since with thick azimuthal magnets, there is only partial cancellation of charges at the magnet-steel interface, and some "good" charges now appear in regions where there is strong tangential armature reaction. The above intuitive explanations reinforce the generality of our conclusions about the torque production characteristics of Halbach and conventional magnet arrays.

2.6 A Halbach Winding for Stator Design?

The Halbach array without a permeable backing has two desirable attributes: (i) the flux density pattern is single-sided, which makes it attractive in applications where shielding of magnetic fields is important, and (ii) the magnitude of the flux density on the reinforced side is factor of $\sqrt{2}$ higher than that of a conventional array for the same volume of magnets, making it attractive when magnet cost is an issue. One may therefore be tempted to believe

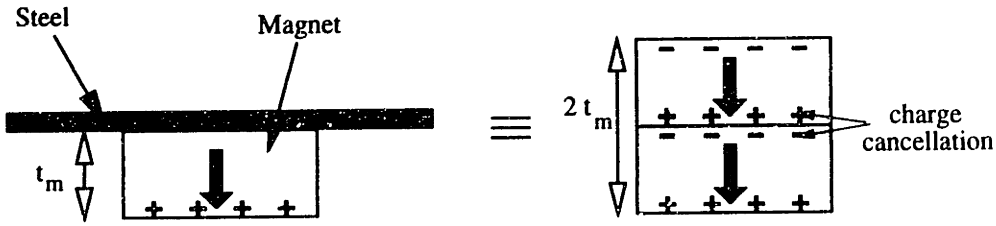

(a) Reflection of radial magnetic charges via method of images

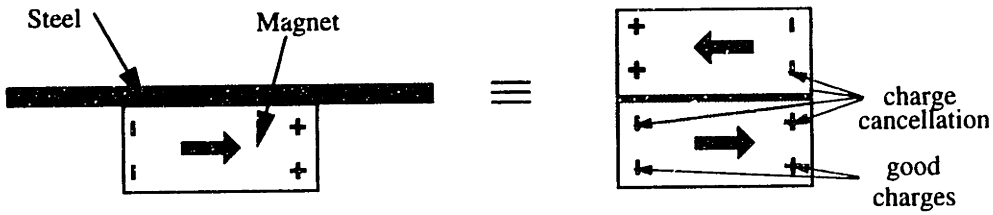

(b) Reflection of azimuthal magnetic charges via method of images

Figure 2-10: Intuitive explanation of torque production in with permeable rotor backing.

that in iron-less motors, a stator winding configured in a Halbach fashion may produce a higher armature reaction than a conventional winding. Unfortunately, to obtain the single-sidedness of magnetic flux density offered by a Halbach magnet array with windings, power is dissipated in windings whose sole function is to cancel the flux on one side of the array. Thus the flux density on the reinforced side, per unit power dissipated in the windings, is lower than that of a conventional array. A detailed analysis of a Halbach winding can be found in [40]. Although a Halbach stator winding in not attractive for the design of power-efficient motors, superconducting electromagnets configured in a Halbach fashion may be useful in shielding passenger compartments in a maglev application. [40]

2.7 Conclusions

We conclude that, for permanent-magnet synchronous motors where the application precludes the use of a magnetic back-iron, the Halbach array always produces higher torque than the conventional array, for the same volume of magnets. The use of a magnetic back-iron in both designs increases the achievable torque. However, for magnetically-backed rotors, the conventional array (with an optimized pole-arc to pole-pitch ratio) produces

higher torque than the Halbach array in the regime of low magnet volume and hence thin magnets. When the cost of magnets is not prohibitive, and thick magnets can be used, the Halbach array will produce higher torque within the fixed mechanical envelope.

The optimal β, in general, depends on the number of excited phases and changes with the magnet volume as was shown in Section 2.4. As β approaches unity for Halbach designs, the resulting aspect ratio of the azimuthally-oriented magnets makes them prone to demagnetization even at no-load. This problem gets worse with an increasing number of pole-pairs and magnet volume, as the azimuthal magnets become flat. For magnets with relatively low coercive force such as ceramic Ferrites, demagnetization of the azimuthal magnets severely limits the range of useful β and number of pole-pairs. Thus, in optimizing β for high torque, one has to guard against demagnetization of the azimuthal magnets even at no-load.

For the direct-drive wheel motor application, the cost of magnets alone preclude the use of a slotless motor despite its attractive features of high efficiency and low cogging. A slotted motor will be a better choice for this application since the reduction of the electromagnetic airgap by the introduction of stator slots reduces the required magnet volume. With thin magnets mounted on a permeable back-iron, a conventional magnet arrangement is preferred to a Halbach array.

Chapter 3

Prototype Wheel Motor: Design and Construction

3.1 Introduction

Figure 3-1 shows a photograph of the Ford Motor Company PNGV concept vehicle, dubbed the Synergy 2010, a futuristic fuel-efficient aerodynamic vehicle with enough room for a family of six. The vehicle is a hybrid electric vehicle that consists of a small 1.0-liter direct-injection, compression-ignited engine that serves as the prime mover for a generator which produces electricity to power four wheel motors through four power electronic inverters shown in Figure 3-2. An energy storage flywheel captures the vehicle's excess engine and regenerative braking energy which is later used to supply the vehicle's peak power demands. In this chapter, we will be concerned with the design and construction of a 20 hp PM motor that fits in the hub of a 19-inch wheel shown in Figure 3-2.

Despite the high remanent flux of Nd-Fe-B magnets, a substantial amount of magnets is still needed to establish a high enough magnetic flux density in the armature windings of a slotless motor, even with a Halbach magnet arrangement. The plots of maximum achievable torques in Figure 2-8 show that, with a slotless armature, about 16 kg of magnets is needed to achieve 400 Nm of peak torque within a 19-inch rim. This magnet cost is excessive and does preclude the use of a slotless armature in an economical wheel motor design. Therefore, we take a look at a slotted armature for the design of the prototype wheel motor.

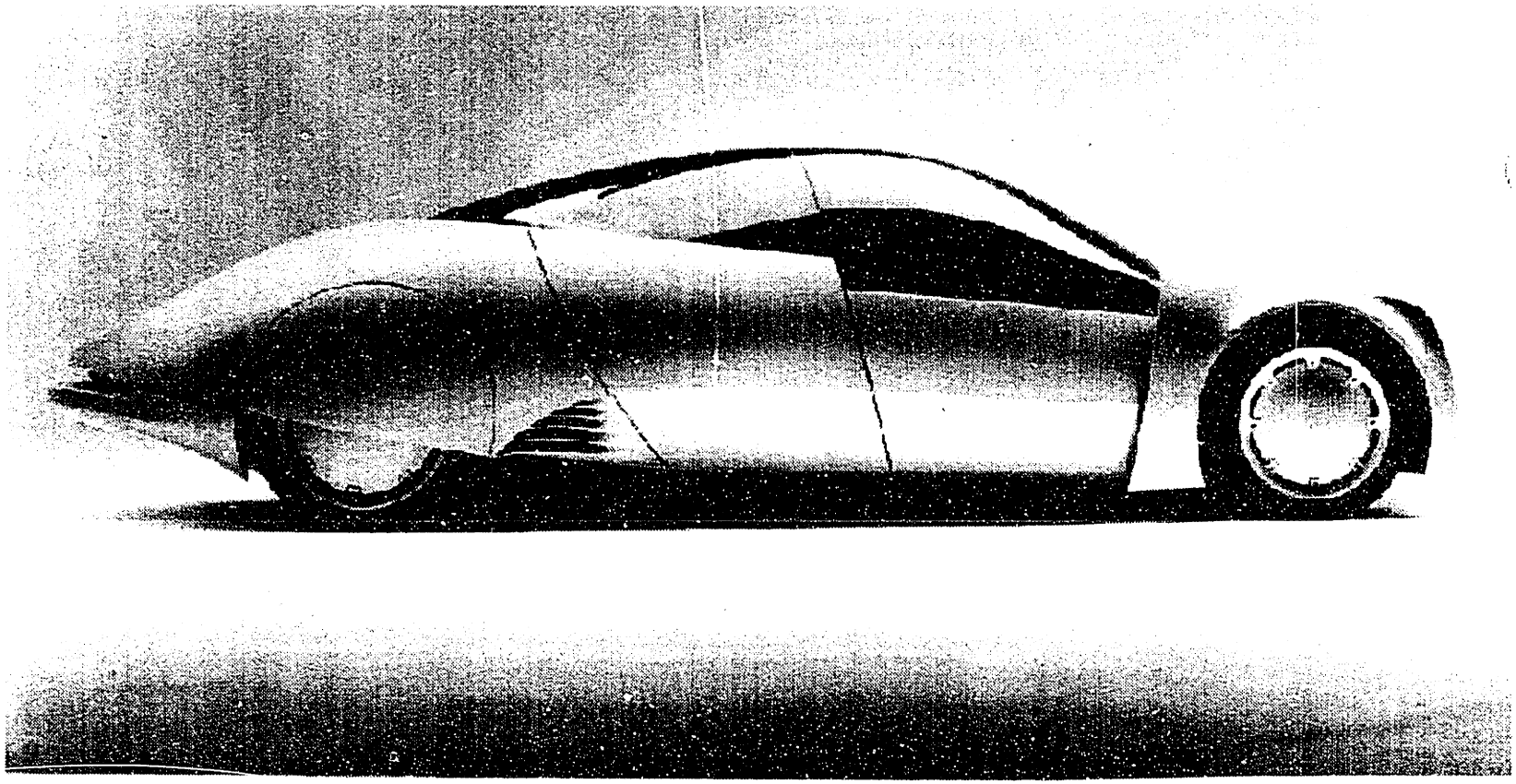

Figure 3-1: Photograph of the Synergy 2010 hybrid electric vehicle.(Courtesy: Ford Motor Company.)

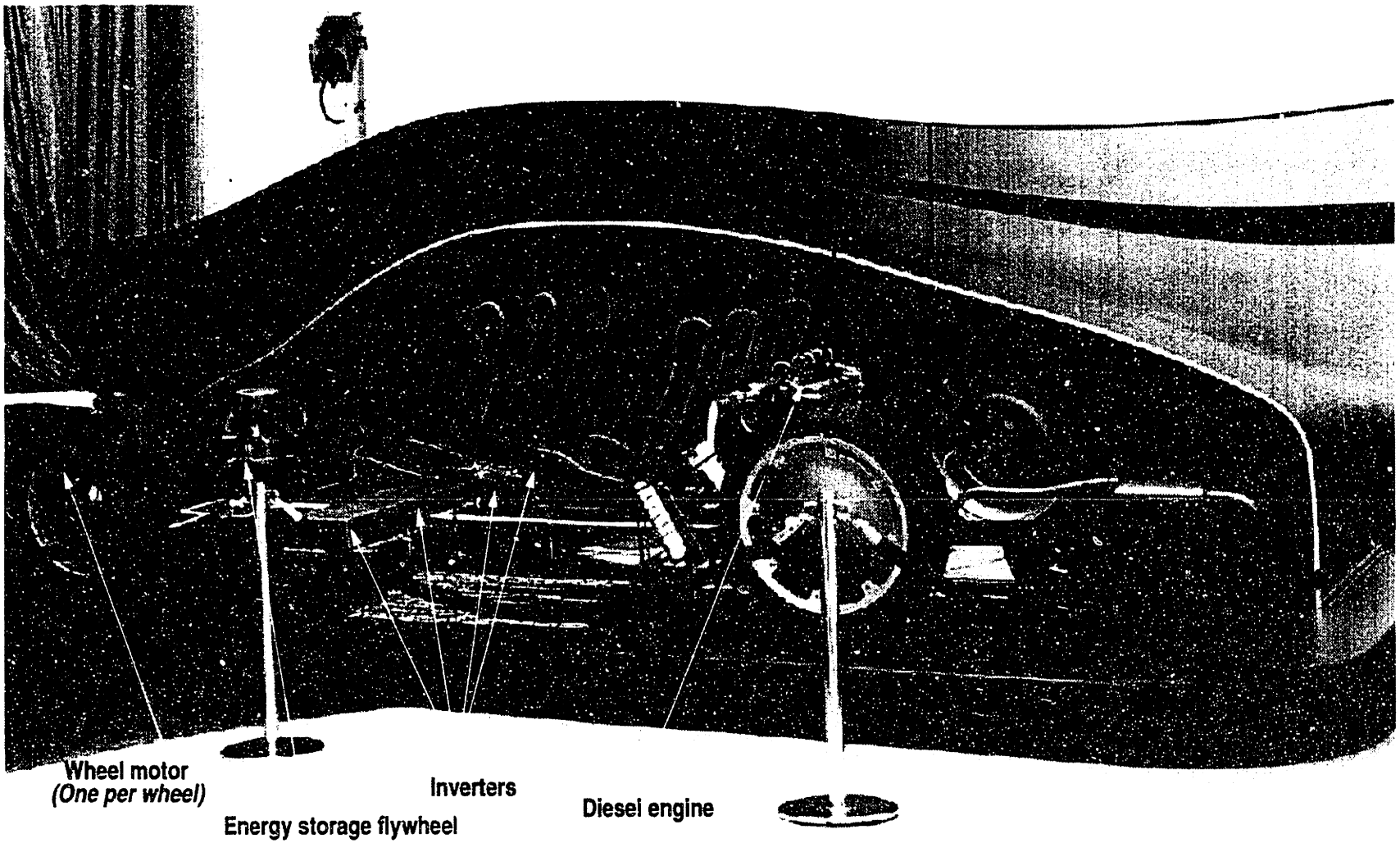

Figure 3-2: Cutaway of the Synergy 2010 hybrid electric vehicle.(Courtesy: Ford Motor Company.)

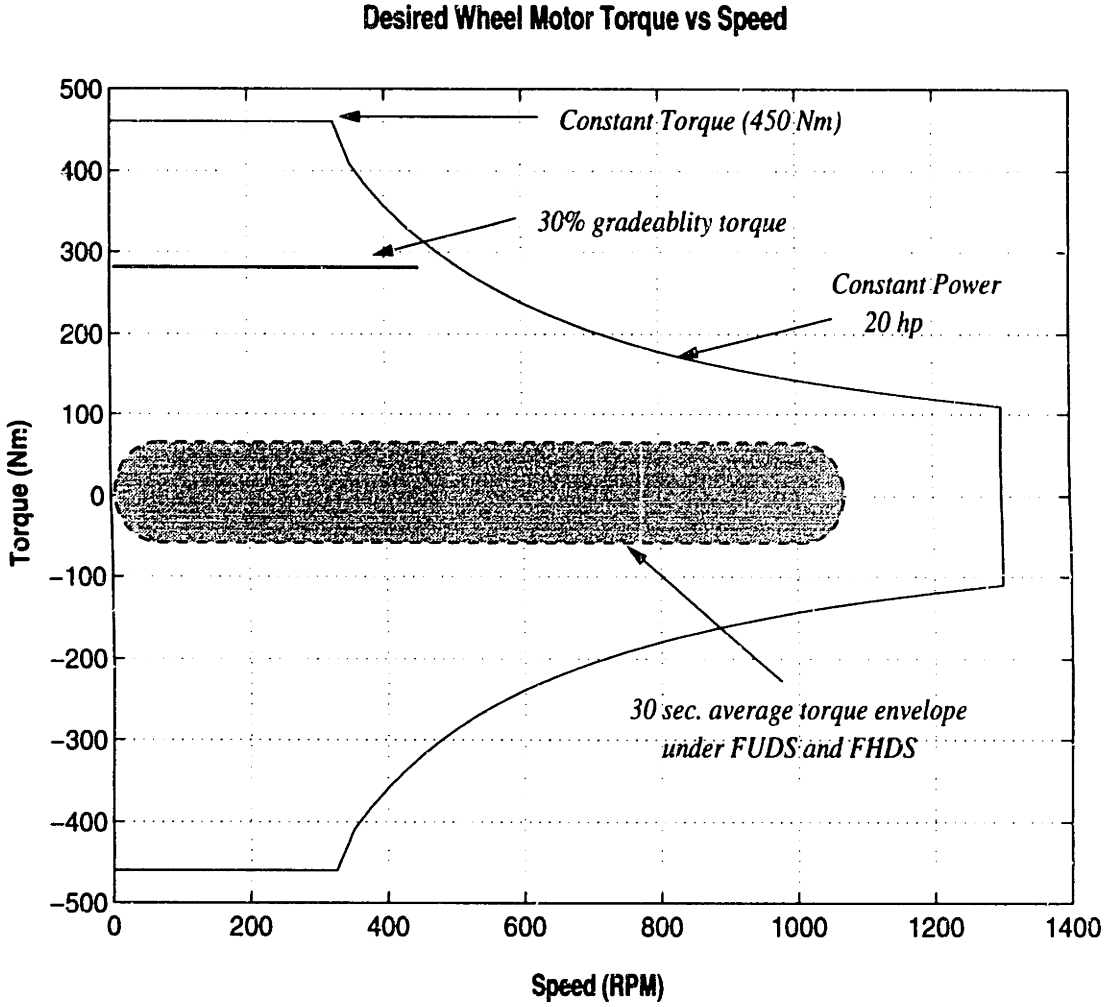

Figure 3-3: Desired torque-speed envelope of wheel motor.

By slotting the stator, the electromagnetic airgap is reduced and hence thinner magnets mounted on a magnetic back-iron can be used. In Chapter 2, we learned that for thin magnets backed by a permeable back-iron, a conventional magnet arrangement is a better choice. Therefore the wheel motor designed in this Chapter will feature the conventional magnet arrangement. The resulting wheel motor design will be fabricated and tested in Chapter 6.

3.2 Desired Mechanical and Performance Specifications

Figure 3-3 shows the desired torque-speed envelope of the prototype wheel motor. In commanding negative torque, the motor is used as a generator to capture the vehicle's

braking mechanical energy. A constant peak torque of 450 Nm is desired up to 325 rpm. Above this "corner" rpm, a constant mechanical power of 15 kW (20 hp) is required up to a maximum speed of 1300 rpm. This maximum rpm corresponds to a top road speed of about 100 mph for a 19-inch wheel.

In normal vehicle operation, shock and vibration forces of about 20 g are not uncommon, thus the wheel motor must have a running clearance of at least 0.5 mm (20 mils) for survivability [38]. Allowing for tolerances in machining the magnet arcs, rotor back iron and stator laminations, a running clearance of 0.625 mm (25 mils) is be used.

In a typical midsize sedan, the ratio of sprung to unsprung mass is about 6:1 [42]. Therefore for the PNGV vehicle whose curb weight[1] is about 900 kg, the weight of each wheel motor with its brake assembly and connecting structural members should be less than 37.5 kg if the vehicle suspension is not to be re-designed. For our design, a target mass of 25 kg for the active part of the motor will be used, leaving 12.5 kg for the remaining mechanical structures.

3.3 Integration of Motor into Wheel

Before embarking on the electromagnetic design of a wheel motor, it is necessary to determine the allowable mechanical envelope for the motor and how to mechanically integrate it into the wheel. This design was done in conjunction with Mr. Allan Gale, Mr. Brad Bates and mechanical engineers at Ford Motor Company in Dearborn, MI. Figure 3-4 shows how the PM propulsion motor is integrated with the wheel. The motor occupies an annular region bounded by an outer radius of 206 mm (8.11 in), an inner radius of 160 mm (6.30 in) and an axial length of 96 mm (3.66 in) including end turns. The spacing between the outer periphery of the motor and the rim of the tire is necessary to provide a running clearance since the rim undergoes flexure when negotiating a turn. The hollow area bounded by the inner periphery of the stator back-iron houses a mechanical brake which consists of a standard disc-rotor/caliper combination. The wheel rim and the end-bell of

[1]Curb mass is the mass of an operational vehicle fitted with all standard equipment without a driver or payload

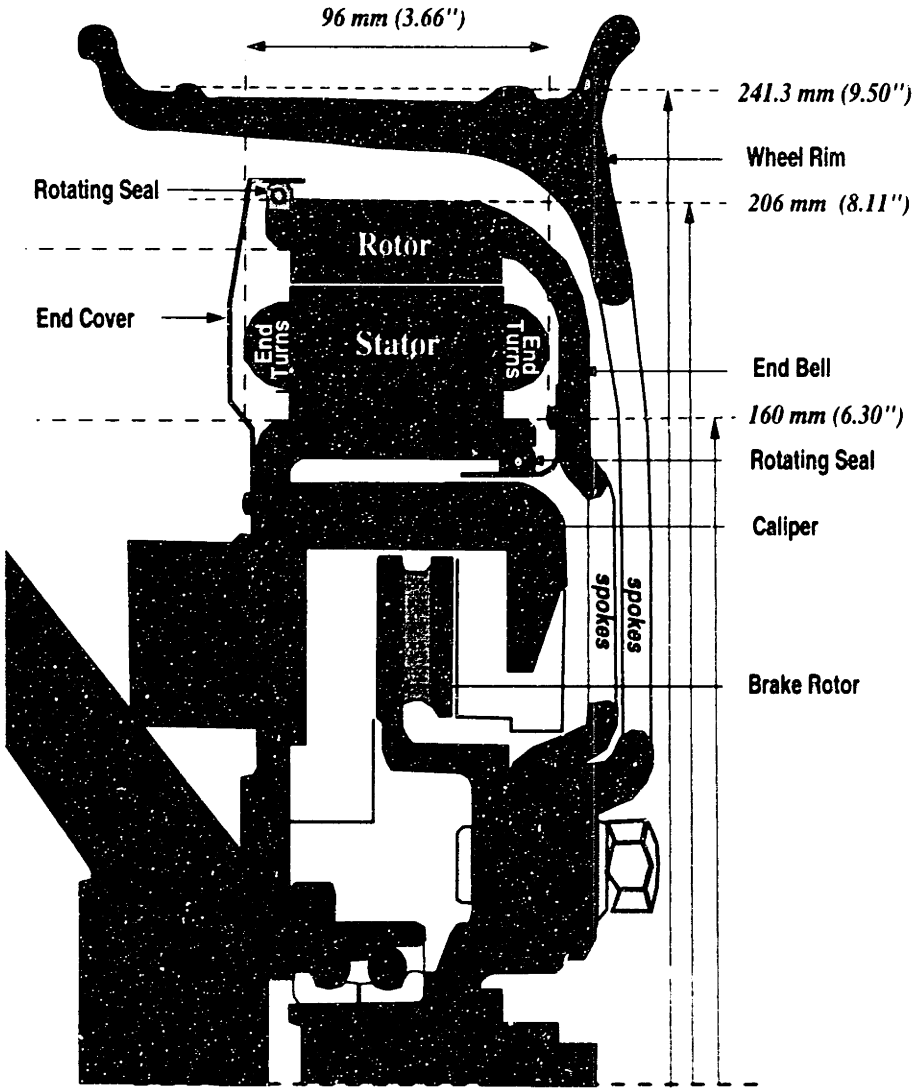

Figure 3-4: Integration of PM motor into wheel.

the motor are spoked to facilitate convective heat transfer from the inner periphery of the motor. An inside-out stator-rotor configuration facilitates the transfer of the rotary motion from the rotor to the rim of the tire. An additional benefit of an inside-out design is the elimination of a structural retaining hoop for the rotor magnets since the centrifugal force from the wheel rotation presses the magnets against the rotor back-iron.

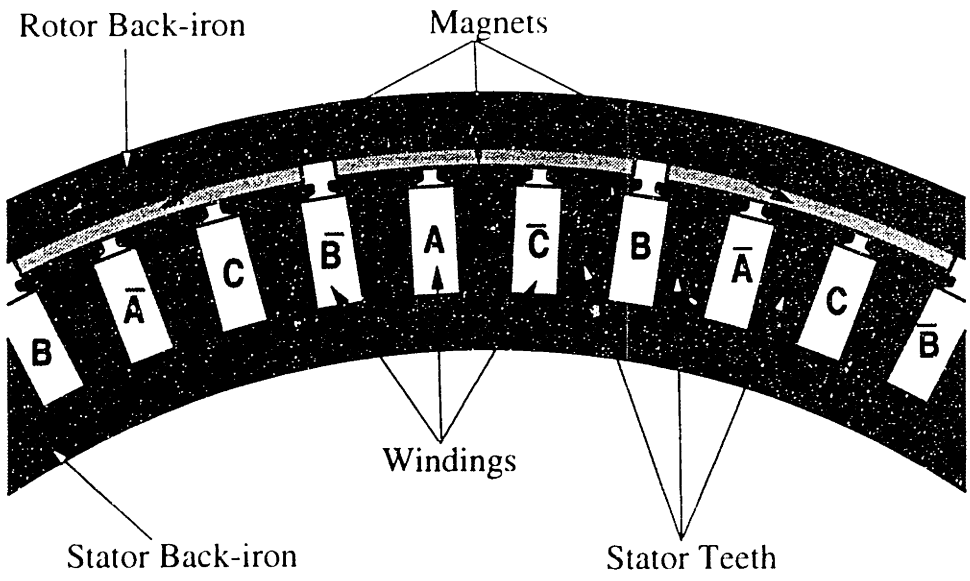

Figure 3-5: Schematic cross section of slotted motor.

3.4 Electromagnetic Modeling

The introduction of stator teeth reduces the electromagnetic airgap of the motor compared to a slotless armature and allows thinner magnets to be used. We learned in Chapter 2 that for thin magnets backed by a permeable rotor, the conventional magnet arrangement is preferred to the Halbach arrangement. Thus the rotor magnets will be arranged in the conventional fashion.

Figure 3-5 shows the cross section of a 3-phase slotted motor with one slot per phase per pole. A small running clearance exists between the magnet arcs and the outer periphery of the stator teeth. The slots have parallel edges to accommodate square wire for increased copper packing factor.

With a running clearance of 0.625 mm and an remanent flux of about 1.1 T, a back of the envelope magnetomotive-force-divider calculation yields a radial airgap flux density of about 0.9 T for a magnet thickness of 3 mm, assuming infinitely permeable rotor and stator back-iron. For equal tooth-to-slot width, the flux in the stator teeth is about 1.8 T, which is close to the saturation flux density of most electrical steels.

One of the distinguishing features between a wheel motor and a conventional motor is that a wheel motor is usually designed to maximize efficiency over a drive cycle, whereas

a conventional motor is designed for efficient operation at full rated load. As a result, conventional motors tend to have a much thicker back-iron that a wheel motor, since the back-iron is sized to carry both the magnet and the peak armature reaction flux efficiently. Motors with thick enough back-iron lend themselves to a linear magnetic circuit analysis where infinite permeability for the steel regions can be assumed. In developing analytical models to guide a first-pass design of the wheel motor, it is assumed that the rotor and stator back-iron are thick enough to permit the assumption of infinite permeability. The stator teeth will, in general, be highly saturated at high electrical loading and hence does require a nonlinear magnetic analysis. The motor is then designed to produce more torque than needed and the thickness of the rotor and stator backings are gradually reduced through experimentation with finite element analysis to reduce motor mass. We underscored in Chapter 2 the need to reduce the no-load losses in the motor for drive cycle efficiency maximization; see Figure 2-2. We therefore use 29-Gage laminations of M-19 nonoriented electrical steel for the stator teeth and back-iron, to reduce eddy-current and hysteresis losses.

3.4.1 No-Load Airgap Flux Density

The ability to account for tooth saturation is important in predicting machine torque, since the permeability of the stator teeth significantly affects the equivalent electromagnetic airgap. In a slotted motor, the magnet flux in the airgap is well guided by the teeth as shown in Figure 3-6, thereby making a one-dimensional magnetic circuit analysis adequate. However, we employ a two-dimensional analysis for the no load airgap flux distribution for consistency with our approach in Chapter 2. In order to include the effects of tooth saturation in the computation of the airgap flux we solve the magnetic circuit of Figure 3-7. The rotor and stator back-iron are assumed to be infinitely permeable.

Figure 3-7 consists of three regions; the region with permanent magnetization denoted as region (a), the free space region that constitutes the running clearance denoted as region (b) and the stator teeth region denoted as region (c). Even though region (c) contains slots, it is modeled as a uniform region. The slotting is taken into account when computing the

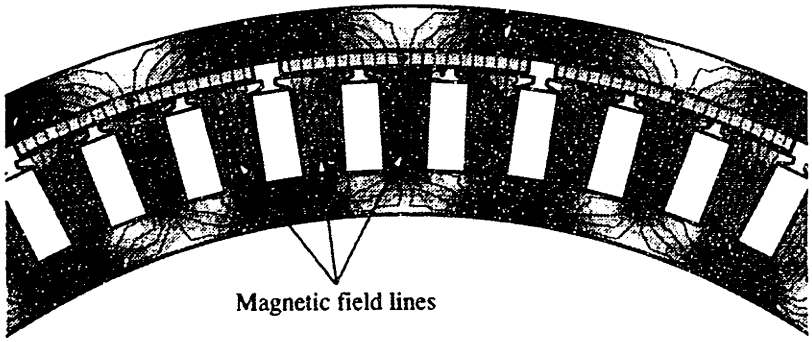

Figure 3-6: Finite element simulation of no-load magnetic flux distribution in a slotted motor.

magnetic field density in the teeth region to iteratively determine the tooth permeability. We do this by multiplying the flux density in the uniform region by a flux concentration factor which accounts for diversion of magnetic flux away from the slots into the teeth. The permeability of region (c) is related, in a nonlinear manner, to its magnetic flux density as shown in Figure 3-8(b). Therefore, to solve for the magnetic flux density in any of the three regions we need to iteratively solve for a self consistent flux density and permeability in region (c).

As was done in Chapter 2, the radial magnetization vector in region (a) can be modeled as

$$\mathbf{M}_{rad} = \sum_{k\ odd}^{\infty} \frac{R_m}{r} \frac{4M_0}{k\pi} \cdot (-1)^{\frac{k-1}{2}} \sin k\beta\pi \cdot \sin kN\phi\hat{\mathbf{r}} \tag{3.1}$$

where M_0 is the maximum magnetization and is related to the remanent flux density B_{r0} by $M_0 = B_{r0}/\mu_0$, where N is the number of pole-pairs, β is the pole-arc to pole-pitch ratio and k is the harmonic number. Note that in this conventional arrangement, there is no azimuthal magnetization. The divergence of each of the Fourier components of $\mathbf{M}_{rad}$ is zero, therefore the magnetic field in all three regions (a), (b), and (c) are governed by Laplace's Equation.

A. Boundary conditions

We denote the Laplacian scalar potentials for the magnet, running clearance, and teeth region as $\Psi^{mag}_{(a)}$, $\Psi^{mag}_{(b)}$, and $\Psi^{mag}_{(c)}$ respectively. Due to the infinite permeability assumption

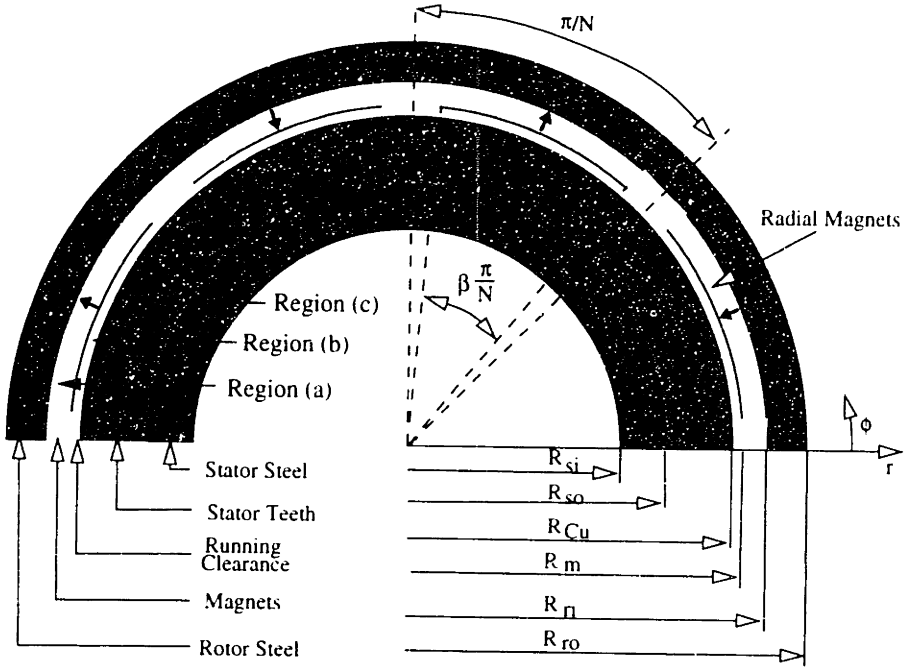

Figure 3-7: Magnetic circuit used to compute no-load airgap flux density.

for the rotor and stator back-iron, the scalar potential vanishes at these two boundaries, i.e.

$$\Psi_{(a)}^{mag} = 0 \text{ at } r = R_{ri} \tag{3.2}$$

and

$$\Psi_{(c)}^{mag} = 0 \text{ at } r = R_{so} \quad . \tag{3.3}$$

The scalar potential and normal magnetic flux density are continuous across $r = R_m$ and $r = R_{cu}^*$, where R_{cu}^* is the physical boundary R_{cu} less 5% of the running clearance to account for the lengthening of the electromagnetic airgap from stator slotting. This is equivalent to modifying the length of the airgap by the Carter coefficient.

B. Solutions

The solutions for the magnetic scalar potentials in the three regions are of the form

$$\Psi_{(a)}^{mag} = \sum_{k\ odd}^{\infty} C_1 \left[\left(\frac{r}{R_{ri}} \right)^{kN} - \left(\frac{R_{ri}}{r} \right)^{kN} \right] \cdot \sin kN\phi \tag{3.4}$$

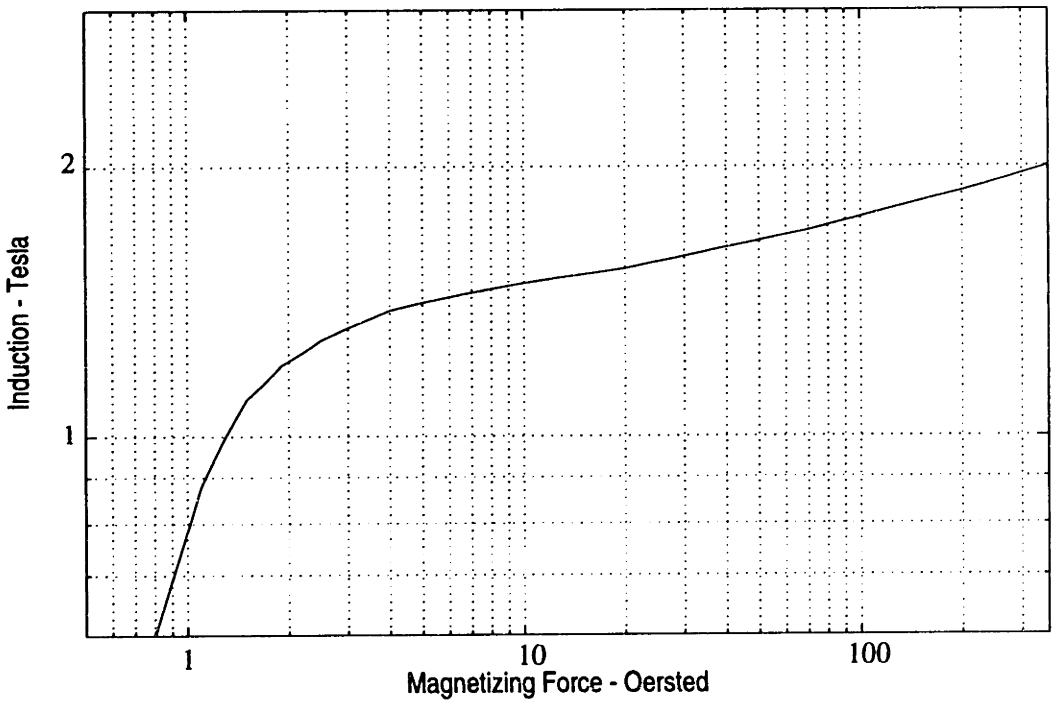

(a) B-H Curve for 29-Gage M-19 Steel

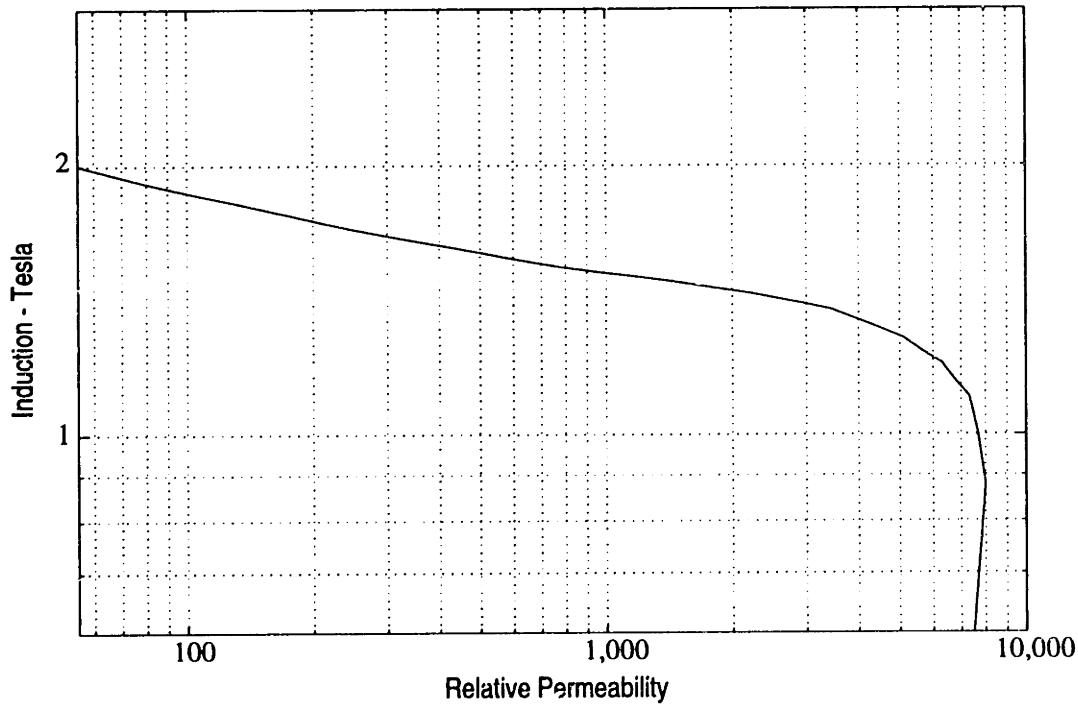

(b) B- μ Curve for 29-Gage M-19 Steel

Figure 3-8: B-H and B-μ curves for 29-Gage M-19 nonoriented steel[45].

$$\Psi_{(b)}^{mag} = \sum_{k\ odd}^{\infty} \left[C_2 r^{kN} - C_3 r^{-kN}\right] \cdot \sin kN\phi \tag{3.5}$$

$$\Psi_{(c)}^{mag} = \sum_{k\ odd}^{\infty} C_4 \left[\left(\frac{r}{R_{so}}\right)^{kN} - \left(\frac{R_{so}}{r}\right)^{kN}\right] \cdot \sin kN\phi \quad . \tag{3.6}$$

It is easily checked that Equations (3.2) and (3.3) are automatically satisfied. The unknown arbitrary constants C_1 - C_4 are determined via Maple V, by ensuring scalar potential and tangential magnetic field intensity continuity across $r = R_m$ and $r = R_{Cu}$. The Maple V source code is included in Appendix D. The magnetic field strength in the various regions, $\mathbf{H}_{(\cdot)}$, is the negative gradient of the corresponding scalar potential. That is,

$$\mathbf{H}_{(\cdot)}^{mag} = -\nabla \Psi_{(\cdot)}^{mag} \tag{3.7}$$

and the corresponding magnetic flux densities are given by

$$\mathbf{B}_{(a)}^{mag} = \mu_0(\mathbf{H}_{(a)}^{mag} + \mathbf{M}) \tag{3.8}$$

$$\mathbf{B}_{(b)}^{mag} = \mu_0 \mathbf{H}_{(b)}^{mag} \tag{3.9}$$

$$\mathbf{B}_{(c)}^{mag} = \mu_t \mathbf{H}_{(c)}^{mag} \tag{3.10}$$

where the permeability μ_t in the teeth region, which is related in a nonlinear fashion to the sum of the magnet and armature reaction flux density, is yet to be determined. If we denote ratio of the slot width to the slot pitch at $r = R_{so}$ as δ, then the no-load flux density in a tooth B_{tooth}^{mag} at a radius r is given by

$$B_{tooth}^{mag}(r) = B_{(b),r}^{mag}(r = R_{cu}) \cdot \underbrace{\frac{R_{cu}}{r - \delta R_{so}}}_{CF} \tag{3.11}$$

where $B_{(b),r}^{mag}$ denotes the radial component of the magnet's flux density in region (b) and CF is the flux concentration factor in the tooth.

It is easy to see that for finite ohmic power dissipation, $\delta = 0$ produces no torque since there is no room for windings, and $\delta = 1$ produces little torque since this configuration corresponds to a slotless armature. The optimum δ therefore lies between zero and one, and

through experimentation we learned that $\delta \approx 0.5$ is about optimum for torque production.

3.4.2 Armature Reaction Fields

In order to compute the motor torque, we need to compute the magnetic field intensity across the electromagnetic airgap due to current excitation in the stator windings, since it is this component of the stator winding magnetic field that interacts with the rotor magnets to produce torque. Figure 3-9 shows the geometrical structure of the stator and the associated magnetic fields. The stator has one slot per pole per phase, and only two out of the three phases are excited at a time as shown in the figure. A square-wave winding is used because the interaction of trapezoidal currents with trapezoidal flux densities produces more torque than sinusoidal currents with sinusoidal flux for the same rms armature current[43].

The slotting of the stator does not make the stator magnetic circuit amenable to a distributed two-dimensional analysis. The traditional approach of converting the total stator ampere-turns into an equivalent surface current over the outer periphery of the teeth severely overestimates machine torque, since tooth saturation and flux leakage across slots are ignored by this approach. A one-dimensional magnetic circuit analysis, that approximately models the effects of tooth saturation and leakage across slots and tooth tips is employed since flux paths of the armature reaction fields are easily traced, as shown in the finite element simulation in Figure 3-9(b). In computing the armature reaction fields, the permanent magnetization is "turned off" but keep in mind that the effective permeability of the teeth is dependent on the *total* flux through them, which includes the magnet flux. Therefore the solution for the armature reaction fields still contains the permeability of the tooth region μ_t which is iteratively determined from the sum of the magnet and armature reaction fields. The tooth permeability is computed using the total flux density at one-third the distance from the base of the tooth and the resulting permeability is assumed constant along the whole tooth. This approximation results in an underestimation of motor torque since the tooth permeability is much higher towards the top of the tooth due to tapering resulting from the parallel slots.

Before writing the governing equations and solving for the unknown fields indicated in

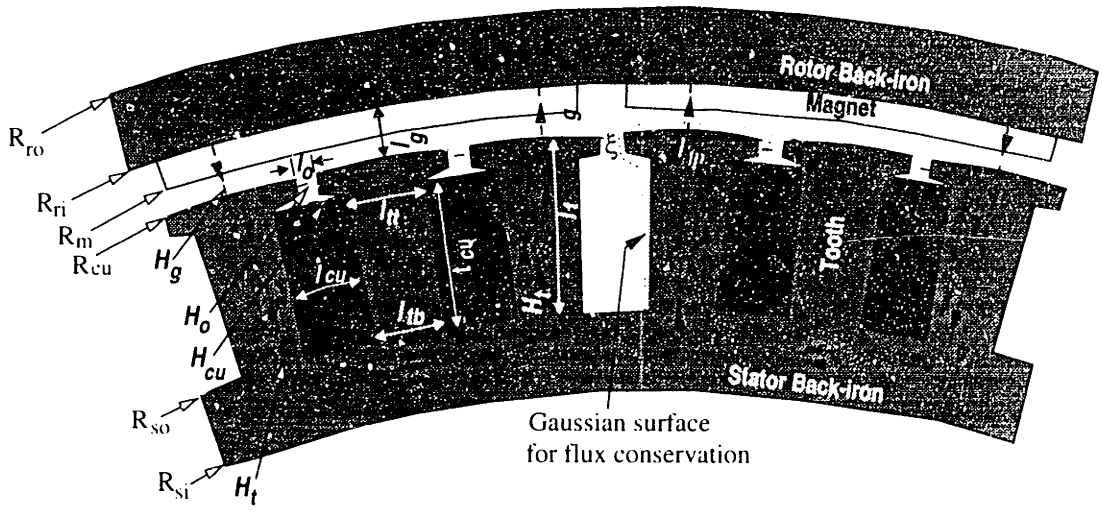

(a) Pertinent armature reaction flux paths and motor dimensions

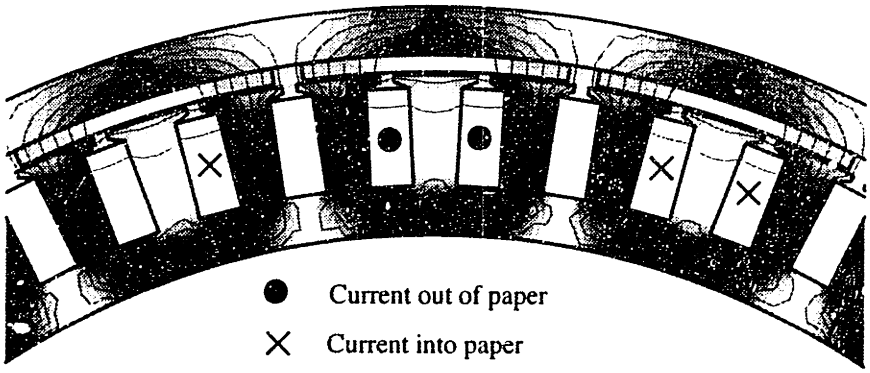

(b) Finite element simulation showing armature reaction flux paths

Figure 3-9: Stator geometry and armature reaction fields.

Figure 3-9, it is instructive to make a few qualitative comments about the torque production characteristics of the slotted machine as it relates to its geometrical parameters. First, the stator slots cannot be made too deep as a substantial fraction of the H-field from the current excitation leaks across the slots through the winding area. These leakage fields increase with decreasing permeability in the teeth. Secondly, for a given number of pole-pairs, there would be an optimal thickness (depth) of copper that maximizes machine torque per unit I^2R power dissipation in the armature windings since the leakage fields depend on the aspect ratio of the slot. A high number of pole pairs reduce the width of the slot and hence

the depth of the winding, if excessive leakage fields are to be avoided. Thus for a given mechanical envelope, the optimal thickness of copper windings is inversely proportional to the number of poles. This phenomenon is equivalent to what we saw earlier for the slotless machines. Thirdly, a wide slot opening reduces the leakage fields across the tooth tips and therefore increases airgap flux and hence the machine torque. However, a wide slot opening makes the airgap flux nonuniform, and exacerbates the torque ripple and eddy current losses in the magnets due to substantial variation of the airgap permeance from slot to tooth. Therefore the slot opening should be made only wide enough to pass the armature conductors through. To eliminate torque ripple from magnet cogging, the stator laminations are skewed by one slot pitch [44].

The unknown armature reaction fields of interest are, (i) the magnetic field intensity at the base of the stator teeth H_t^{arm}, (ii) the leakage magnetic field intensity in the slots at the outer periphery of the windings H_{cu}^{arm}, (iii) the leakage magnetic field intensity in the slot opening H_o^{arm}, and (iv) the magnetic field intensity in the electromagnetic airgap, H_g^{arm}, which consists of the running clearance and the magnet region. These field quantities are denoted as H_t, H_{cu}, H_o, and H_g in Figure 3-9 respectively for clarity. To compute magnitude of these armature reaction fields, we perform contour integration along the three Amperian paths indicated in Figure 3-9(a), and utilize Gauss's Law for magnetic flux continuity around a stator tooth, as also shown in the Figure. A $1/r$ dependence is assumed for the radial variation of the H-field within the teeth and the airgap. The strength of the leakage field across the slots is proportional to the current which it encloses and therefore increase linearly with the radial distance from the bottom of the slots. Proceeding as outlined above, we obtain the following four equations:

$$2H_t^{arm}R_{so}\ln\left(\frac{R_{cu}}{R_{so}}\right) + 2H_{gs}^{arm}R_{cu}\ln\left(\frac{R_{ri}}{R_{cu}}\right) = 2J_0A_{cu} \tag{3.12}$$

$$2H_t^{arm}R_{so}\ln\left(\frac{R_{cu}}{R_{so}}\right) + 2H_o^{arm}l_o + 2\frac{\mu_0}{\mu_t}H_o^{arm}l_{tp} = 2J_0A_{cu} \tag{3.13}$$

$$2H_t^{arm}R_{so}\ln\left(\frac{R_{so}+t_{cu}}{R_{so}}\right) + 2H_{cu}^{arm}l_{cu} + 2\frac{\mu_0}{\mu_t}H_{cu}l_{tt} = 2J_0A_{cu} \tag{3.14}$$

$$\mu_0 H_{cu}^{arm}\frac{t_{cu}}{2} + \mu_0 H_o^{arm}\xi + \mu_0 H_g^{arm}l_{tp} = \mu_t H_{ts}^{arm}l_{tb} \tag{3.15}$$

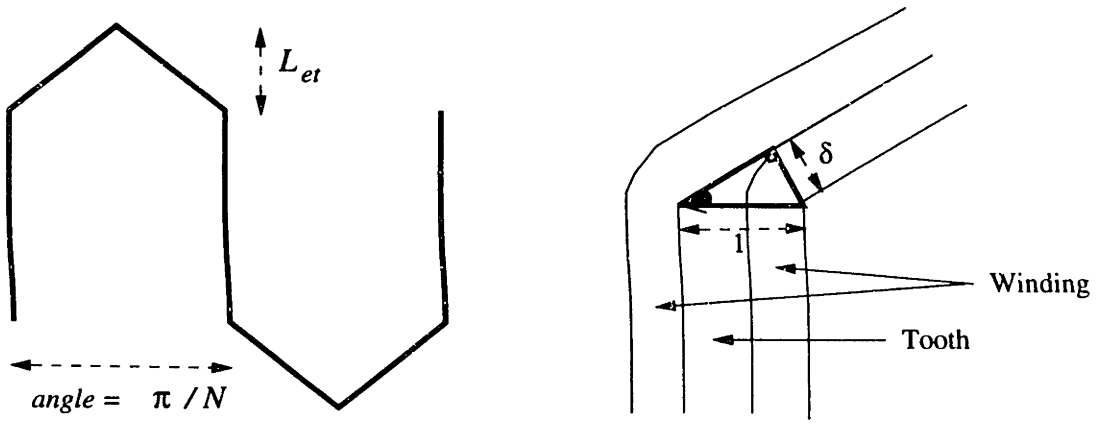

Figure 3-10: Length of end-turns.

where the dimensions l_{tp}, l_{tb}, l_{cu}, and l_{tt} are given by

$$l_{tp} = \frac{2\pi R_{cu}}{6N} - l_o \tag{3.16}$$

$$l_{tb} = (1-\delta)\frac{2\pi R_{so}}{6N} \tag{3.17}$$

$$l_{cu} = \delta\frac{2\pi R_{so}}{6N} \tag{3.18}$$

$$l_{tt} = \frac{2\pi(R_{so}+t_{cu})}{6N} - l_{cu} \tag{3.19}$$

all of which are indicated in Figure 3-9(a). A_{cu} denotes the area occupied by copper and ξ depends on the slot opening l_o. Equations (3.12), (3.13) and (3.14) are associated with Amperian contours across the airgap, across the slot opening, and around the outer periphery of the winding respectively. Equation (3.15) simply states that the flux entering the bottom of the tooth from the stator back iron is equal to the sum of the flux that leaks across the slot through the copper area, the leakage flux across the slot opening and the airgap flux. Equations (3.12 - (3.15) are solved simultaneously for the magnetic field strengths in terms of the unknown tooth permeability μ_t.

Assuming the end turns of the armature windings are arranged to conform to the triangular pattern shown in Figure 3-10, then the axial protrusion of the end turns beyond the stator lamination stack L_{et} is estimated as

$$L_{et} = \frac{\pi(R_{so}+R_{cu})}{2N} \cdot \frac{\delta}{\sqrt{1-\delta^2}} \tag{3.20}$$

and the equivalent end-turn length for computing power dissipation, $L_{et,ohm}$ corresponds to the hypothenuse, whose length is given by

$$L_{et,ohm} = \frac{\pi(R_{so} + R_{cu})}{2N} \cdot \frac{1}{\sqrt{1-\delta^2}} \quad . \tag{3.21}$$

The maximum current density J_0 in the windings is related to the ohmic power dissipation in the armature P_{ohm} via

$$J_0 = \sqrt{\frac{\sigma P_{ohm}}{2N \cdot 2A_{cu}(W_{ohm} + 2L_{et,ohm})}} \quad . \tag{3.22}$$

where W_{ohm} is the length of the winding in the slot and A_{cu} is the area within the slot occupied by copper. The winding length, W_{ohm}, the stack length, W_s, and the skew angle, θ_{sk}, are related by

$$W_{ohm} = \frac{W_s}{\cos\theta_{sk}} \quad . \tag{3.23}$$

where θ_{sk} is related to the angular slot pitch and other motor geometrical constants by

$$\theta_{sk} = \arctan\left[\frac{\left(\frac{R_{so}+R_{cu}}{2}\right)\tan\frac{\pi}{3N}}{W_s}\right] . \tag{3.24}$$

The copper area is computed as

$$A_{cu} = k_{pf}\frac{\pi R_{so}}{6N}t_{cu} \tag{3.25}$$

where k_{pf} is the copper fill factor and t_{cu} is the thickness of the copper or equivalently, the depth of the slot. The copper conductivity σ is related to the winding temperature T in $^\circ C$ by

$$\sigma = 5 \times 10^7 \frac{234.5 + 20}{234.5 + T} \quad . \tag{3.26}$$

As was mentioned earlier, the total magnetic flux density in the teeth is the sum of the contribution from the magnets and the armature reaction. The magnet flux and armature reaction flux oppose each other in the tooth underneath the leading edge of the magnet and aid each other in the tooth underneath the trailing edge of the magnet as shown in

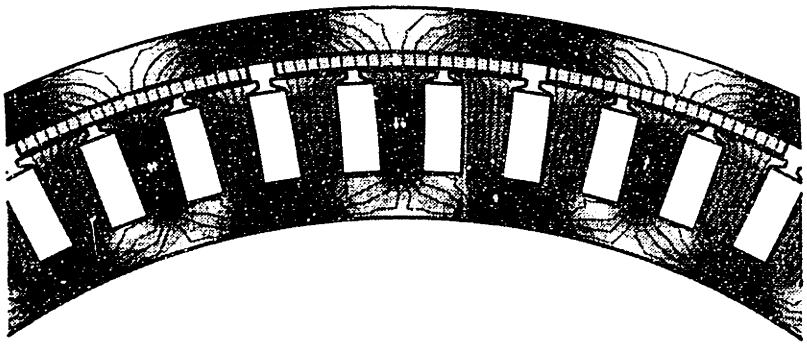

(a) Magnet flux

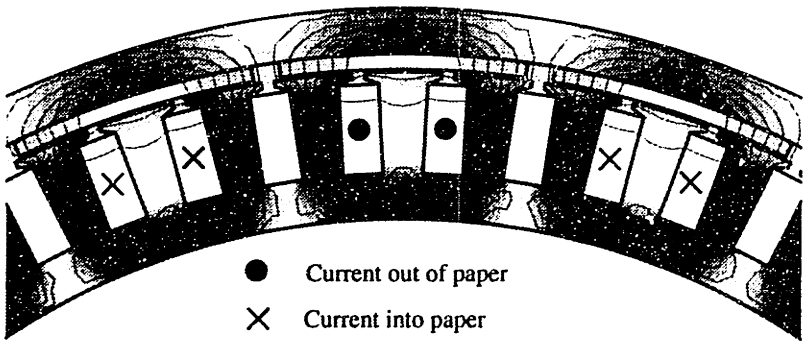

(b) Winding flux

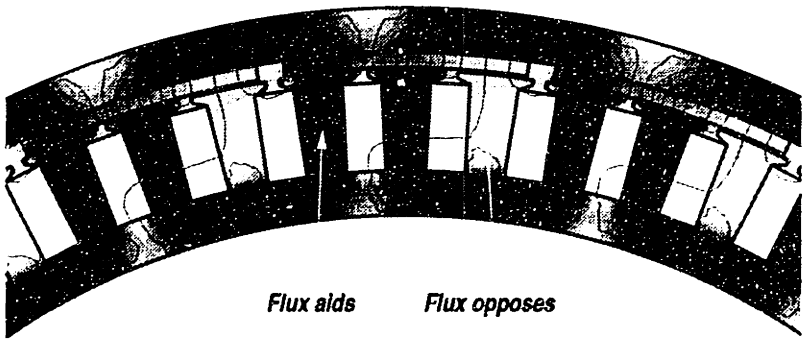

(c) Total flux

Figure 3-11: Illustration of aiding and opposing magnet and armature fluxes in stator teeth.

Figure 3-11(c). For motor torque and loss calculations in the teeth, we use the reinforced flux density at one-third the distance from the base of the tooth. Thus B_{tooth}

$$B_{tooth} = \left[\underbrace{|B^{mag}_{(b),r}(r = R_{cu})| \cdot \frac{R_{cu}}{r - \delta R_{so}}}_{magnet} + \underbrace{|\frac{\mu_t H^{arm}_t R_{so}}{r}|}_{armature} \right]_{r = R_{so} + \frac{t_{cu}}{3}} . \tag{3.27}$$

and the tooth permeability μ_t is iteratively solved to be self consistent with B_{tooth}. Note that this flux density can be quite high at full load and therefore the resulting permeability for the tooth can be quite low. This low permeability, assumed for all the teeth, yields a pessimistic estimate of the motor torque. However, keep in mind that since infinite permeability has been assumed for the rotor and stator backings, the actual flux densities and motor torque will be lower than that predicted by our models when the rotor and stator back-iron are reduced via finite element analysis to reduce motor mass.

3.4.3 Torque

Once the magnetic-field H in the airgap from the armature reaction is known, the peak machine torque which corresponds to the quadrature rotor-stator alignment shown in Figure 3-9 is computed as

$$\tau_m = 2N\mu_0 M_0 \int_{R_m}^{R_{ri}} \frac{R_{cu} H_{gs}}{r} \cdot r dr \hat{\phi} \tag{3.28}$$

$$= 2N R_{cu} \mu_0 M_0 H_{gs} \underbrace{(R_{ri} - R_m)}_{magnet\ thickness} \hat{\phi} \quad . \tag{3.29}$$

3.4.4 Back-EMF

The peak back-emf of the motor is calculated by equating the output mechanical power to the input electrical power in the absence of losses. Thus the motor torque constant k_t equals the motor back-emf constant k_e. Therefore,

$$k_t = k_e = \frac{\tau_m}{I_m} \tag{3.30}$$

where τ_m is the maximum motor torque and I_m is the motor current.

3.4.5 Back-Iron Flux Density

The rotor and stator back-iron carry the fluxes created by the magnets and the armature windings, less the leakage flux in the teeth and copper areas. In normal operation these two fluxes are in quadrature, and the peaks do not occur at the same location, as shown in

Figure 3-11(a) and Figure 3-11(b). The total back-iron flux is therefore approximated by the vector sum of the magnet and current fluxes. The magnet flux in the rotor back-iron Φ_{rbi}^{mag} is computed by integrating the flux density over one-half a pole face at the inner surface of the rotor back-iron. The corresponding flux in the stator back-iron Φ_{sbi}^{mag} is similarly computed by integrating the airgap flux density at the outer periphery of the teeth. Thus

$$\Phi_{rbi}^{mag} = \int_0^{\frac{\pi}{2N}} B_{(a),r}^{mag}(r = R_{ri}) R_{ri}\, d\phi \tag{3.31}$$

$$\Phi_{sbi}^{mag} = \int_0^{\frac{\pi}{2N}} B_{(b),r}^{mag}(r = R_{cu}) R_{cu}\, d\phi \quad . \tag{3.32}$$

Equation (3.32) assumes that there is no flux leakage across the stator slots, which is not so for heavily saturated teeth, thus Equation (3.32) is a conservative estimate of the magnet component of the flux in the stator back-iron. The contribution to the back-iron flux from the currents acting alone is given by

$$\Phi_{rbi}^{arm} = W_{eff}\, \mu_0 H_t^{arm}\, l_{tp} \tag{3.33}$$

$$\Phi_{sbi}^{arm} = W_{eff}\, \mu_t H_t^{arm}\, l_{tb} \quad . \tag{3.34}$$

Therefore, the total flux density in the rotor B_{rbi} and in the stator B_{sbi} are given by

$$B_{rbi} = \frac{\sqrt{|\Phi_{rbi}^{mag}|^2 + |\Phi_{rbi}^{arm}|^2}}{W_{eff}\, t_{rbi}} \tag{3.35}$$

$$B_{sbi} = \frac{\sqrt{|\Phi_{sbi}^{mag}|^2 + |\Phi_{sbi}^{arm}|^2}}{W_{eff}\, t_{sbi}} \tag{3.36}$$

where t_{sbi} is the thickness of the stator back-iron and t_{rbi} is the thickness of the rotor back-iron. The rotor and stator back-iron thicknesses that yield a low enough flux density for the assumption of infinite permeability to be valid tend to be quite large and add unnecessarily to the mass of the motor without significant improvement of the drive cycle efficiencies. Our analytical models help us to determine appropriate dimensions for the outer radius of the stator back-iron R_{so} and the inner radius of the rotor back-iron R_{ri}. Through finite element simulations, the thickness of the stator back-iron and rotor back-iron are reduced

until the desired motor torque is reached.

3.4.6 Eddy Current and Hysteresis Losses

Figure 3-12 shows the core loss data for 29-Gage M-19 nonoriented steel for sinusoidal excitation. To obtain an analytical expression for the core loss per pound P_c, the core manufacturer's data was fitted to the equation

$$P_c = \underbrace{k_e f^2 B^2}_{P_{eddy}} + \underbrace{k_h f \left(\frac{B}{1T}\right)^{\alpha}}_{P_{hyst}} \tag{3.37}$$

using a nonlinear least-squares fit algorithm. In Equation (3.37), f represents the excitation frequency in Hz and B is the magnetic flux density within the steel in Tesla. The parameter k_e models the eddy current losses while k_h and α model the hysteresis loss. These parameters were computed to be $k_e = 32.183 \times 10^{-6}\, W/lb/Hz^2/T^2$, $k_h = 10.664 \times 10^{-3}\, W/lb/Hz$, and $\alpha = 1.793$. The resulting analytical expression is also plotted on Figure 3-12 for comparison. The core loss obtained from Equation (3.37) show reasonable fit with the manufacturer's loss data, as shown by the closeness of the circles and corresponding dots in Figure 3-12.

The core loss in the stator teeth $P_{c,teeth}$ and stator back-iron $P_{c,sbi}$ are given by

$$P_{c,teeth} = 2.02 M_{teeth} \left[k_e f^2 B_{tooth}^2 + k_h f B_{tooth}^{\alpha}\right] \tag{3.38}$$

$$P_{c,sbi} = 2.02 M_{teeth} \left[k_e f^2 B_{sbi}^2 + k_h f B_{sbi}^{\alpha}\right] \tag{3.39}$$

where M_{teeth} and M_{sbi} are the masses of the stator teeth and back-iron respectively in kilograms. The rotor back-iron, to first order, does not suffer any losses since it moves in synchronism with the stator flux. Asynchronous losses from azimuthal variations in the airgap permeance and eddy-current losses from commutation (both in magnets and back-iron) are deemed to be small.

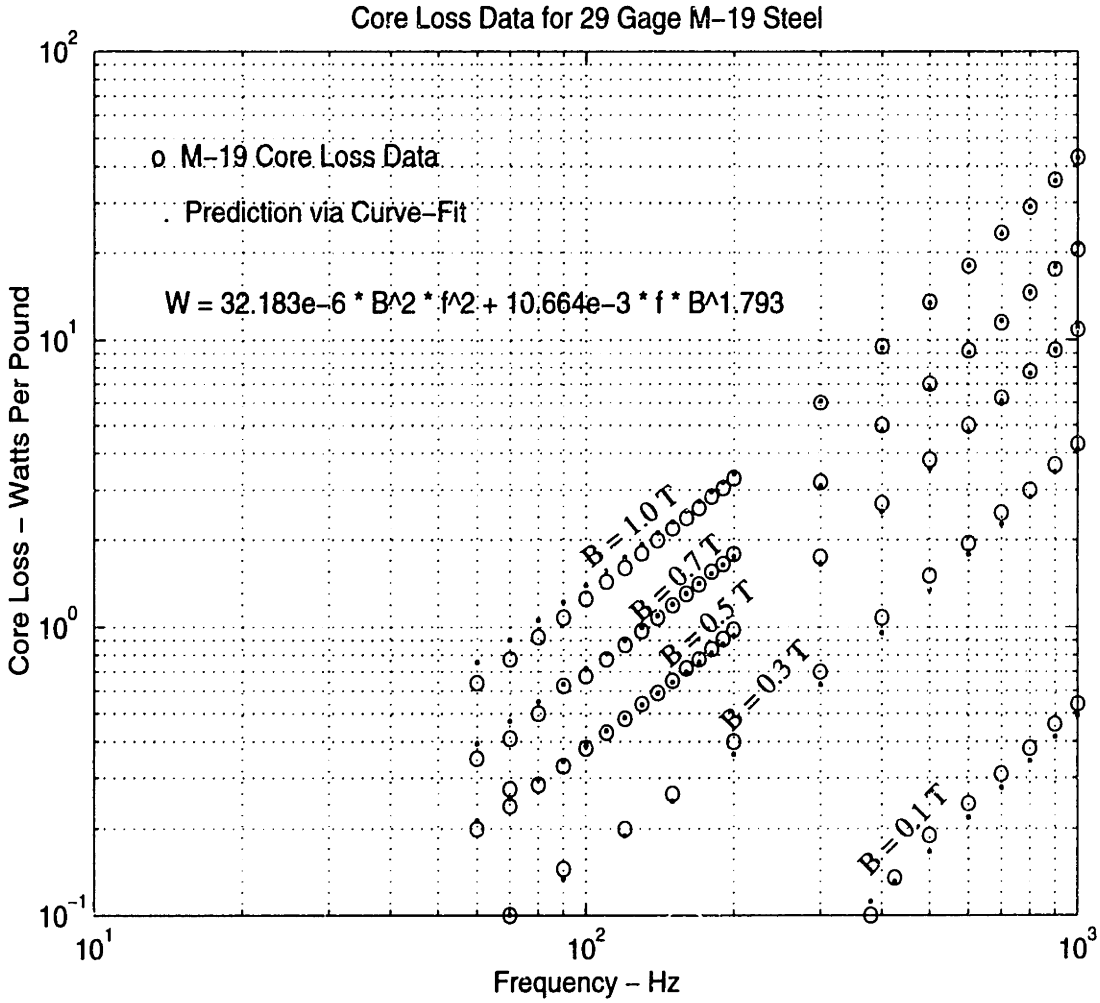

Figure 3-12: Core loss data for 29 Gage M-19 nonoriented steel[45].

3.4.7 Motor Efficiency

The efficiency of the motor η_m is given by

$$\eta_m = \frac{\tau_m \omega_m}{\tau_m \omega_m + P_{ohm} + P_c} \tag{3.40}$$

where P_{ohm} is the dc ohmic loss and P_c is the sum of the eddy current and hysteresis losses in the stator teeth and back-iron. The motor efficiency over a given drive-cycle η_m^{cycle} is given by

$$\eta_m^{cycle} = \frac{\sum_{cycle} \tau^{(i)} \omega_m^{(i)} t^{(i)}}{\sum_{cycle} \left[\tau^{(i)} \omega_m^{(i)} + P_{ohm}^{(i)} + P_c^{(i)} \right] t^{(i)}}, \tag{3.41}$$

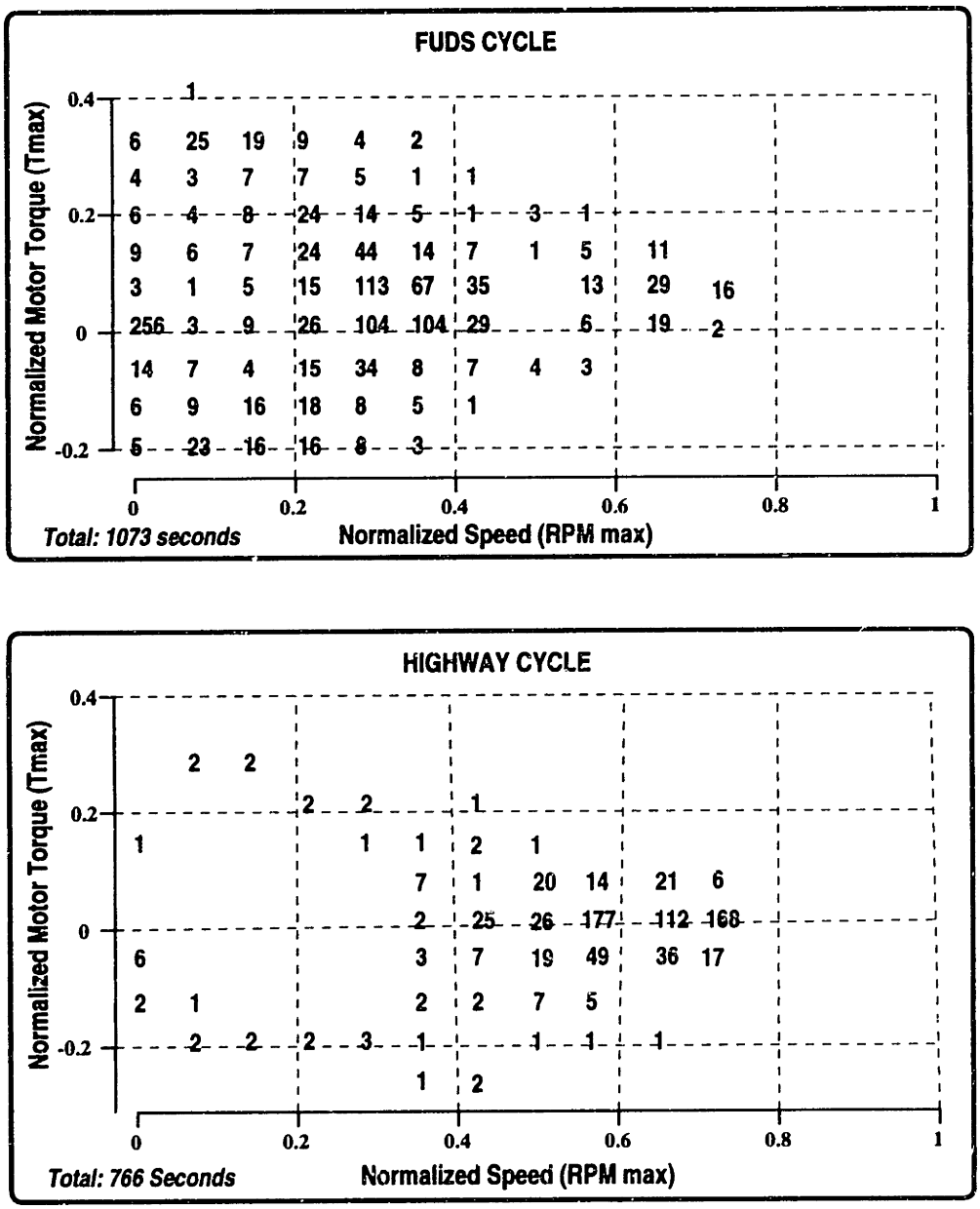

Figure 3-13: Time spent at various operating point under urban and highway drive cycles[38].

where $t^{(i)}$ denotes the time spent in seconds at the operating point (i) underneath the torque-speed envelope. These numbers are shown in Figure 3-13. Since a PM machine produces negative torques as efficiently as positive torques, the negative torques shown in Figure 3-13 are converted to postive for the drive-cycle efficiency calculations. All these calculations are done with Maple V and the source code is included in Appendix D.2.

3.5 Results

3.5.1 Number of Pole-Pairs

One of the results that stem from our analytical models is that a high number of pole-pairs N is desired for the following reasons. A high number of poles reduces the length of the end turns, and hence the power dissipated in this part of the armature windings that produces no useful torque. The total flux that the rotor and stator back-iron have to carry also reduce with increasing N. Thus a high number of pole-pairs is desirable from the point of view of motor mass reduction. The number of poles however cannot be made too high, as fringing in the airgap and leakage in the stator slots become substantial. Another undesirable feature associated with an increased number of poles is the increase in the electrical frequency of the motor which increase hysteresis and eddy current losses, and reduces the time available for motor commutation. Furthermore, for a given number of slots per pole per phase, the stator teeth become very thin and their mechanical integrity become compromised, problems with machining notwithstanding. In view of the foregoing, N = 10 was found, through experimentation, to yield an adequate balance between the above conflicting design parameters.

3.5.2 Optimal Winding Thickness

As was alluded to earlier, for a given number of pole-pairs and fixed power dissipation in the armature, there is an optimum thickness of windings beyond which adding extra copper to the motor adds unnecessarily to the weight of the machine. Figure 3-14 shows a plot of peak motor torque with winding thickness t_{cu} for 10 pole-pairs and 2.7 kW ohmic power dissipation in the stator widings. The magnet mass used for Figure 3-14 is 1.7 kg, the stack length is 6 cm and the running clearance is 25 mils (0.625 mm). The inner radius of the rotor R_{ri} (which is the same as the outer radius of the magnets, see Figure 3-7) is set to 19.6 cm and the magnet and winding temperatures are set to 110°C. A slot opening of 3.1 mm is assumed because we anticipate using AWG #10 square wire. The jitter of the curve with increasing t_{cu} is due to the decrease in the tooth width at its base and the

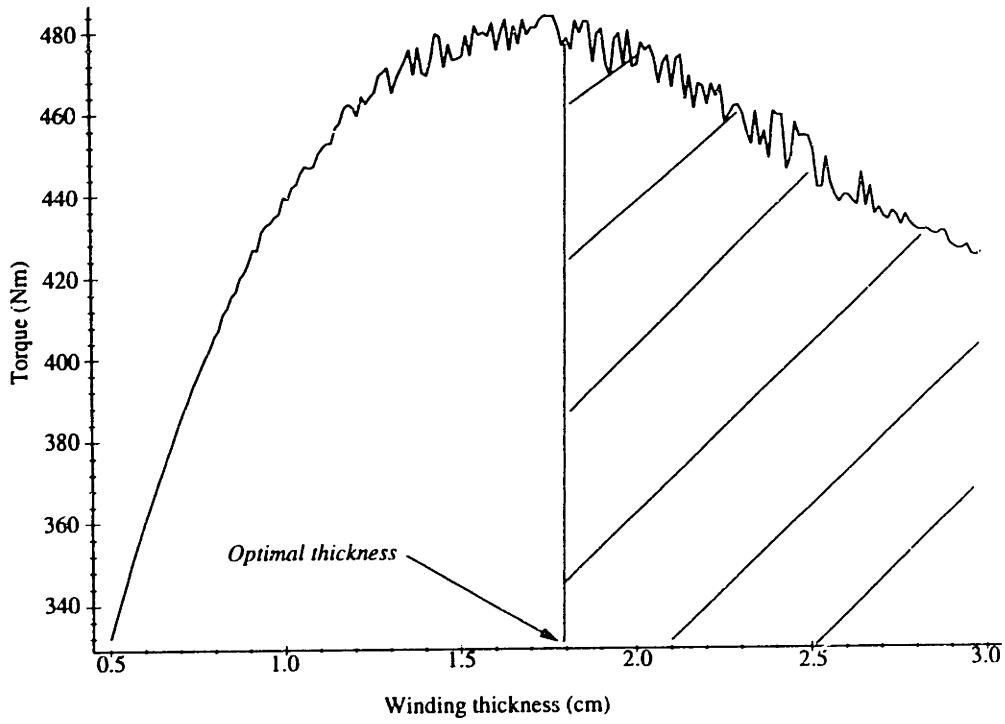

Figure 3-14: Variation of peak motor torque with depth of armature windings.

associated reduction in permeability. At flux densities beyond 1.8 T the slope of plot of flux density with relative permeability is reduced (see Figure 3-8(b)) and the algorithm to find a self-consistent operating point along the nonlinear curve does not easily converge so we reduce the acceptable convergence tolerance. Figure 3-14 is useful in deciding how deep to make the slots. For our candidate wheel motor, we pick t_{cu} to be approximately 1.9 cm. Increasing the copper thickness beyond this value degrades motor torque while increasing motor mass. Furthermore, the thermal performance of the motor is compromised since it is difficult to remove heat from the copper in the slots. Figure 3-14 shows that for the given magnet mass, armature excitation and optimal winding thickness, a peak torque of 472 Nm is achievable.

3.5.3 Performance Parameters of Prototype motor

Figure 3-15 shows a transverse and longitudinal section of the prototype wheel motor. Figure 3-16 shows the detailed geometry and dimensions of the stator slots and rotor magnets. The depth of the slots is optimized to produce the highest peak torque per power

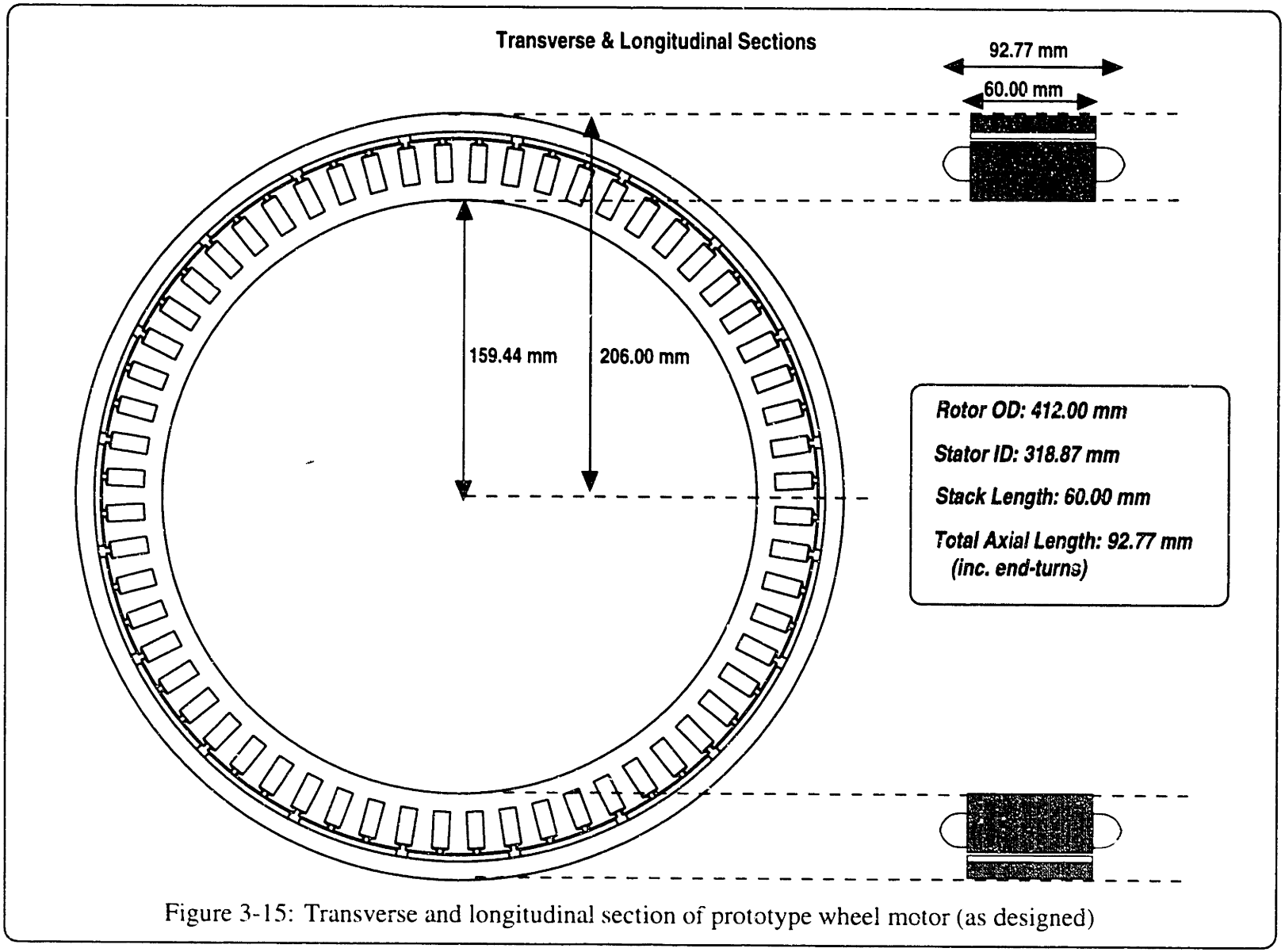

Figure 3-15: Transverse and longitudinal section of prototype wheel motor (as designed)

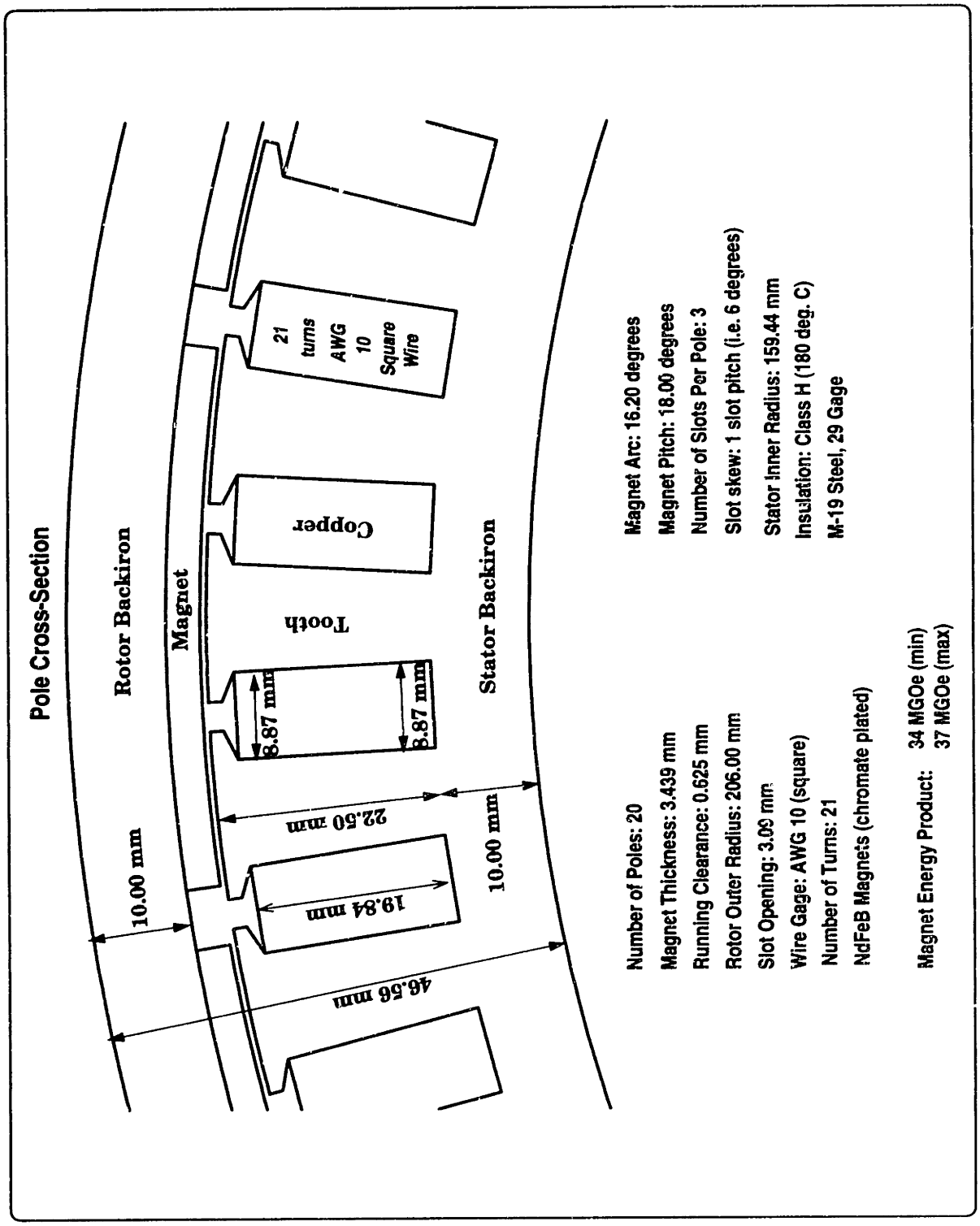

Figure 3-16: Detailed cross-section of motor (as designed).

dissipation in the armature windings. The magnet mass of 1.7 kg, which results in a magnet thickness of 3.44 mm, is the minimum magnet mass needed to achieve 472 Nm of peak torque with 2.7 kW of ohmic power dissipation in the armature at 110°C. The ohmic power dissipation limit of 2.7 kW is chosen for thermal considerations as discussed in Section 3.5.4. The running clearance is set to 25 mils to allow for manufacturing tolerances and survivability of the airgap under road shock and vibration forces. A magnet pole-arc to pole-pith ratio of 0.9 is chosen to reduce the alignment torque ripple [46]. The gap between adjacent magnets is also necessary to facilitate the assembly of the pre-magnetized magnet pieces on the rotor. The width of the slot opening is determined by the wire size which in turn depends on the number of turns per phase. It is set to 3.1 mm to accommodate AWG #10 wire. The choice of the number of turns for the motor has significant implications on the power-electronic inverter and a detailed discussion of this is deferred till the next chapter.

The thickness of the rotor and stator back-iron were determined from finite-element simulations using the finite-element analysis program QuickField. The rotor and stator back-iron were initially made 5 cm thick and the motor torque, as computed by QuickField, was 496 Nm which is in excess of the target motor torque of 450 Nm. This result shows that our analytical modeling underestimates motor torque as expected but it is within 5% of the finite element result. The thickness of the rotor and stator back-iron were then thinned out to to 10 cm and the torque dropped to 460 Nm due to saturation of the steel. At this torque value, the finite element iteration was halted, as the motor torque is likely to reduce through imperfections in the fabrication process.

Figure 3-17 lists the key performance parameters as designed including an efficiency map of the candidate wheel motor. The motor has a mass of 25 kg and produces a minimum of 450 Nm of peak torque while dissipating 2.7 kW in the armature windings at 110°C. The motor torque, self and mutual inductances are computed via finite element analysis using the QuickField. The torque computation is performed via evaluating the Maxwell stress tensor on a closed contour in the airgap. The torque and back-emf constants in Figure 3-17(a) are computed at the maximum armature excitation at a temperature of 110°C. Thus these numbers are expected to be higher at light loads and low temperatures.

Motor's Performance Parameters [as designed]

Minimum Peak Torque at 110 deg. C	450 Nm
Max Phase Current at 110 deg. C	75 A
Minimum Torque Constant at 110 deg. C	6 Nm/A
Minimum Back-EMF Constant at 110 deg. C	6 V/rad-s
FHDS Efficiency	91%
FUDS Efficiency	85%
Temperature rise at full load	60 deg. C
Phase-Neutral Inductance	1.5 mH
Mutual Inductance	0.7 mH
Leakage Inductance	1.7 mH
Motor Resistance at 20 deg. C (phase-phase)	0.34 Ohms
Active Motor Mass	25.1 kg

Rotor: Magnets (1.7 kg), Back-Iron (5.9 kg)

Stator: Teeth (6.6 kg), Back-Iron (4.8 kg), Copper (6.1 kg)

(a) Simulated motor parameters [as designed]

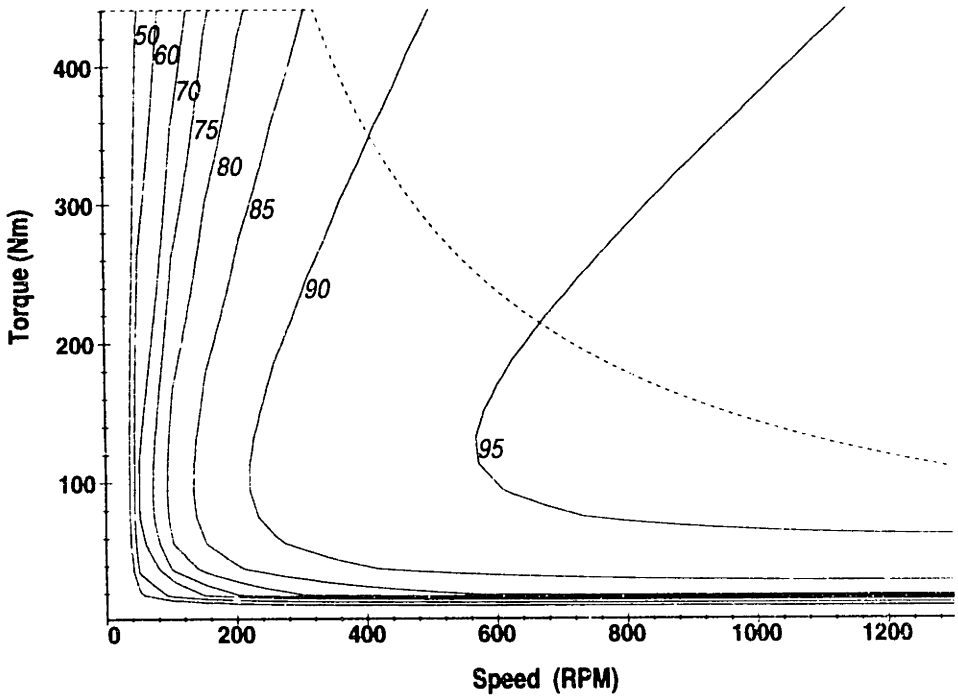

(b) Simulated efficiency map of motor [as designed]

Figure 3-17: Summary of motor's performance parameters and efficiency map.

The self L_s, mutual L_m and leakage L_{lk} inductances *per turn* are computed from two experiments. First one of the three phases is excited with a test current I_{test} the total stored magnetic energy W_{ms} measured. Then two of the phases are excited with the same test current I_{test} and the corresponding stored magnetic energy W_{mm} measured. The measured energies in the above two experiments are related to the test current and the inductances by the equations

$$W_{ms} = \frac{1}{2}(L_s + L_{lk})I_{test}^2 \tag{3.42}$$

$$W_{mm} = ((L_s + L_{lk}) + L_m)I_{test}^2 \quad . \tag{3.43}$$

For a set of three-phase windings displaced by 120°, the mutual inductance is one-half the self-inductance, assuming perfect coupling. Thus we can write relate L_s to L_m by

$$L_s = 2L_m \quad . \tag{3.44}$$

Solving Equations (3.43) - (3.44) simultaneously gives

$$L_s = \frac{2(W_{ms} - W_{mm})}{I_{test}^2} \tag{3.45}$$

$$L_m = \frac{2W_{ms} - W_{mm}}{I_{test}^2} \tag{3.46}$$

$$L_{lk} = 2\frac{3W_{ms} - W_{mm}}{I_{test}^2} \quad . \tag{3.47}$$

Therefore for N_t number of turns per phase, all the inductances are multiplied by N_t^2. Note that because of the nonlinearity of the steel these inductances are nonlinear and depend on the current excitation level. From the power electronics point of view these nonlinearities have negligible consequence.

3.5.4 Thermal Performance

Once the target motor torque specifications have been met, the temperature profile in the motor is simulated via finite element analysis. To find the temperature rise in the motor, we assume that the inner surface of the stator back-iron and the outer surface of the rotor

back-iron are at ambient temperature. We compute the total I^2R losses in the motor while producing maximum torque at stall and assume that no heat is conducted longitudinally through the inner and outer periphery of the motor. In practice, there will be some heat convected away from the end turns and the exposed axial surfaces of the motor. Therefore, by ignoring these modes of heat transfer, the temperature rise obtained here is conservative. Figure 3-18(a) shows the temperature profile in the motor for 2.7 kW of total power dissipation.

To facilitate conductive heat transfer in the winding area, the windings are assumed to be vacuum impregnated with STYCAST-2850FT epoxy encapsulating resin with Catalyst 11 hardener. The thermal conductivity of the epoxy-hardener mixture is is 1.8 W/m-$^\circ C$ [47], and the slots are lined with 5 mils of Nomex paper, whose thermal conductivity is 1 W/m-$^\circ C$. The thermal conductivity thermal conductivity of the copper is 390 W/m-$^\circ C$. The effective thermal conductivity of the winding, insulation, encapsulant, and slot-liner mixture is difficult to compute analytically. In [48], Torquato and Lado computed bounds on the effective conductivity σ_e of a composite material consisting of infinitely long conducting circular cylinders of conductivity σ_2, randomly distributed through an insulating medium of conductivity σ_1, for volume fractions of up to 65%. The effective conductivity σ_e lies between the Milton's fourth order lower bound $\sigma_L^{(4)}$ and the fourth order upper bound $\sigma_U^{(4)}$, where

$$\sigma_U^{(4)} = \sigma_2 \left[\frac{(\sigma_1+\sigma_2)(\sigma_1+\langle\sigma\rangle) - \phi_2\xi_1(\sigma_2-\sigma_1)^2}{(\sigma_1+\sigma_2)(\sigma_2+\langle\bar{\sigma}\rangle) - \phi_2\xi_1(\sigma_2-\sigma_1)^2} \right] \tag{3.48}$$

$$\sigma_L^{(4)} = \sigma_1 \left[\frac{(\sigma_1+\sigma_2)(\sigma_2+\langle\sigma\rangle) - \phi_1\xi_2(\sigma_2-\sigma_1)^2}{(\sigma_1+\sigma_2)(\sigma_1+\langle\bar{\sigma}\rangle) - \phi_1\xi_2(\sigma_2-\sigma_1)^2} \right] \tag{3.49}$$

where

$$\langle\sigma\rangle = \sigma_1\phi_1 + \sigma_2\phi_2 \tag{3.50}$$

$$\langle\bar{\sigma}\rangle = \sigma_2\phi_1 + \sigma_1\phi_2 \tag{3.51}$$

and ϕ_2 and ϕ_1 are the volume fractions of the cylinders and host material respectively, and

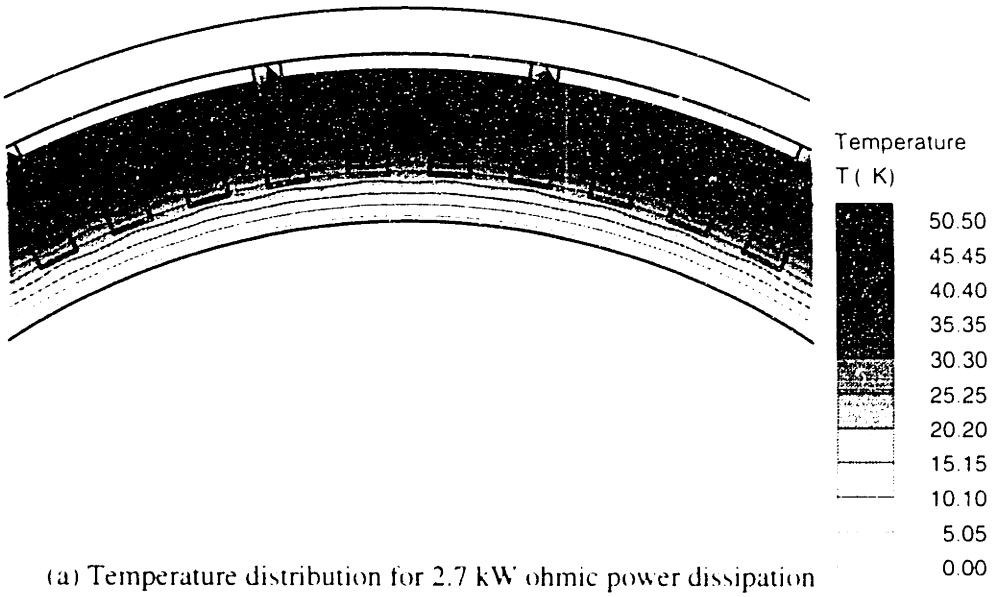

(a) Temperature distribution for 2.7 kW ohmic power dissipation

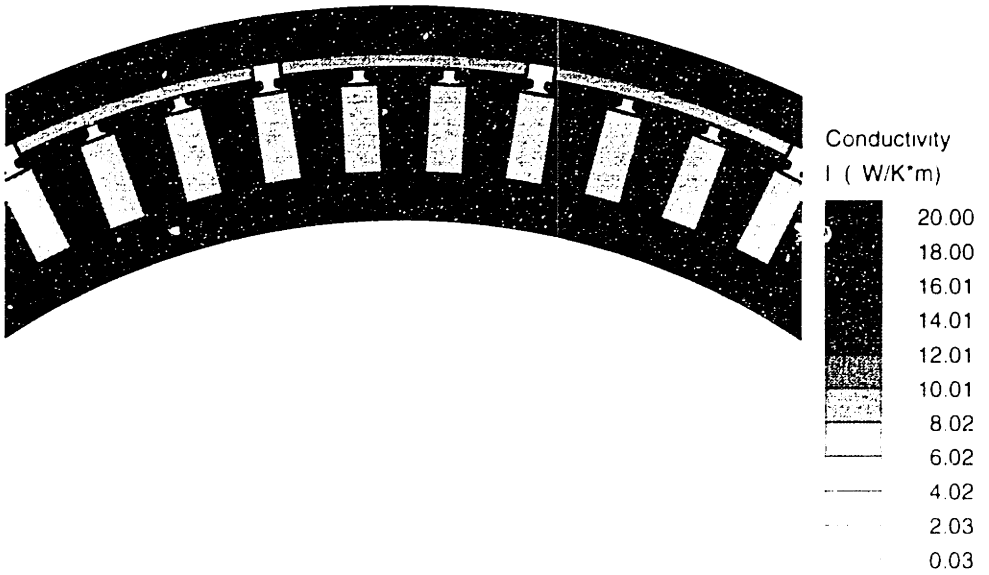

(b) Thermal conductivity profile

Figure 3-18: Finite element simulation of temperature distribution with 2.7 kW of armature power excitation.

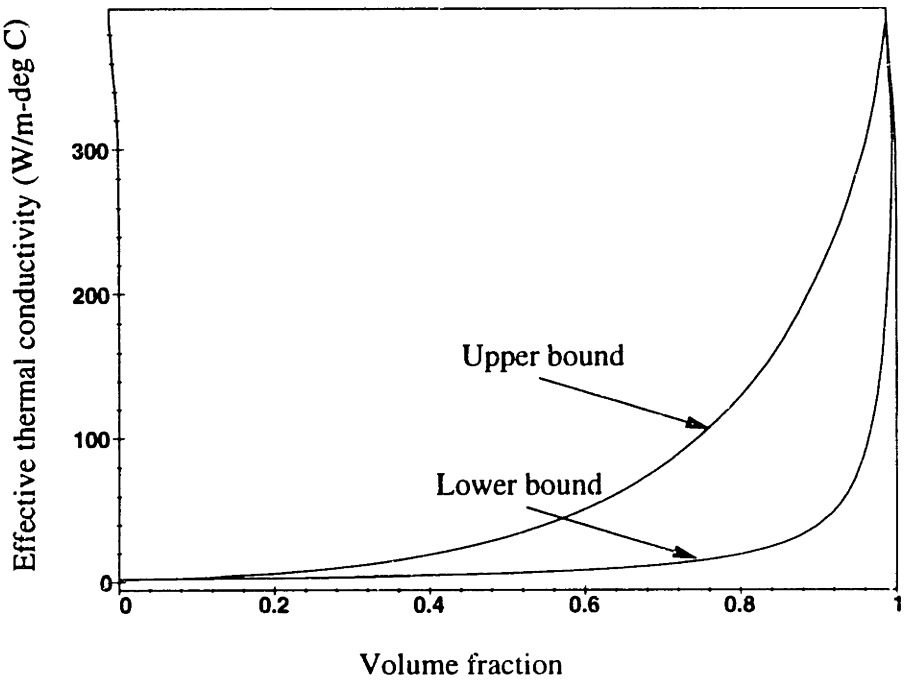

Figure 3-19: Variation of Milton's fourth order bounds on effective thermal conductivity with volume fraction.

are related by

$$\phi_2 = 1 - \phi_1 \quad . \tag{3.52}$$

The parameters ξ_1 and ξ_2 in Equations (3.48) and (3.49) model the cylinder-to-cylinder interactions for volume fractions up to 0.65 and are computed in [48] to be

$$\xi_2 = \frac{\phi_2}{3} - 0.05707\phi_2^2 \tag{3.53}$$

$$\xi_1 = 1 - \xi_2 \quad . \tag{3.54}$$

Figure 3-19 shows the upper and lower bounds on the effective thermal conductivity of parallel cylindrical inclusions with conductivity 390 W/m-°C embedded in a host material with conductivity 390 W/m-°C. Assuming that the volume fraction of the magnet wire insulation and the slot liner within a slot is small compared to that of the copper and epoxy, we estimate the effective thermal conductivity of the copper-epoxy mixture to be between 8.18 W/m-°C and 51.41 W/m-°C for a copper volume fraction of 0.6. For the simulation in Figure 3-18, an effective thermal conductivity of 2 W/m-°C is assumed for the whole slot, and the thermal conductivities for the remaining bulk regions are 9 W/m-°C for the

magnets, 0.033 W/m-°C for the air in the running clearance and 20 W/m-°C for the rotor and stator steels, as shown in Figure 3-18(b).

Figure 3-18(a) shows that there is a 50 °C rise within the motor and the hot-spot occurs in the airgap, close to the magnets. Assuming that the inner surface of the stator back-iron is kept at 70°C (i.e 10°C above the maximum operating ambient temperature of 60°C) while removing all the head radially, the hot spot within the motor attains a temperature of 120 °C. The winding insulation is Class H and can withstand 180°C, and the Curie temperature of Nd-Fe-B is 300 °C but we need to guard against demagnetization of the rotor magnets by the armature reaction fields. At 120°C the coercive force of the magnets is 350 kA/m, down by 65% from its value at of 1000 kA/m 20°C. At temperatures above 75°C, the "knee" of the demagnetization curve moves into the second quadrant. To prevent magnet demagnetization at 120°C the the magnetic flux density in the leading edge of the magnets must be kept below 0.4 T. From finite element analysis, we find that the flux density at the leading edge of the magnets at full load is 0.36 T. Therefore we risk demagnetization of the permanent magnets if the armature current is raised above 75 A. Operation at -40°C is not a problem for Nd-Fe-B magnets since the coercive force has a negative temperature coefficient. In short, the peak torque can be maintained indefinitely *if* all the 2.7 kW of heat can be removed while keeping the inner periphery of the stator back-iron at 70°C.

For operation over the Urban and Highway drive cycles, the average motor torque is about 90 Nm, a factor of one-fifth lower than the peak constant torque. Therefore the power dissipation associated the the torque-producing current is down by a factor of 25. Total hysteresis and eddy current losses when commanding this amount of torque at the maximum speed of 1300 rpm is estimated to be 300 W. Therefore, we expect a temperature rise of about 9°C within the motor. Thus under normal driving conditions, the motor can be air cooled due to the reduced losses.

If the motor is to be air cooled, then it is necessary to obtain a conservative estimate of how long the peak torque can be sustained. To obtain this estimate we assume that all the heat dissipated in the copper goes to raise the temperature of the copper and stator steel.

Thus the time, $t_{(50°C)}$, to attain a 50°C temperature rise in the motor can be computed by

$$t_{(50°C)} = \frac{50}{60} \frac{(M_{ss}c_{ss} + M_{cu}c_{cu})}{P_{ohm}^{max}} \text{ mins} \tag{3.55}$$

where M_{ss} and M_{cu} is the mass in kilograms of the stator steel and copper respectively. The specific heat capacity of the stator steel, c_{ss}, is 502 J/kg/°C and that of copper , c_{cu}, is 384 J/kg/°C. With M_{ss} = 11.4 kg, M_{cu} = 6.1 kg, and an ohmic power dissipation of 2.7 kW, the maximum torque can be sustained for 2.5 minutes before there is a 50°C temperature rise within the motor.

Chapter 4

Wide Speed Range Operation of PMSMs Without Flux Weakening

4.1 Introduction

Traction drives generally require operation at constant torque up to a corner speed ω_c and constant power up to a top speed ω_{max} as shown in Figure 4-1. The ratio of ω_{max} to ω_c is normally referred to as the speed range. For machines with variable rotor field excitation, such as wound-field synchronous motors, the speed at which the transition from constant torque to constant power operation is made has been traditionally referred to as the base speed. This speed normally corresponds to that at which the back-emf of the motor at full field equals the battery or dc bus voltage.

To make better utilization of the inverter's power semiconductor devices, the field current is made inversely proportional to motor speed in the constant power region to reduce the airgap flux so as to keep the back-emf of the motor constant with speed, as also shown in Figure 4-1. The armature current is however kept constant so that the motor torque decreases in an inverse proportion to its speed to produce constant mechanical power.

Unlike the wound-field synchronous motor, where the field current can be reduced to lower the back emf of the motor for constant power operation, PMSMs operate under a fixed airgap flux. Therefore, left alone, the back-emf grows linearly with speed and consequently makes PMSMs top-speed-limited up to the dc supply voltage.

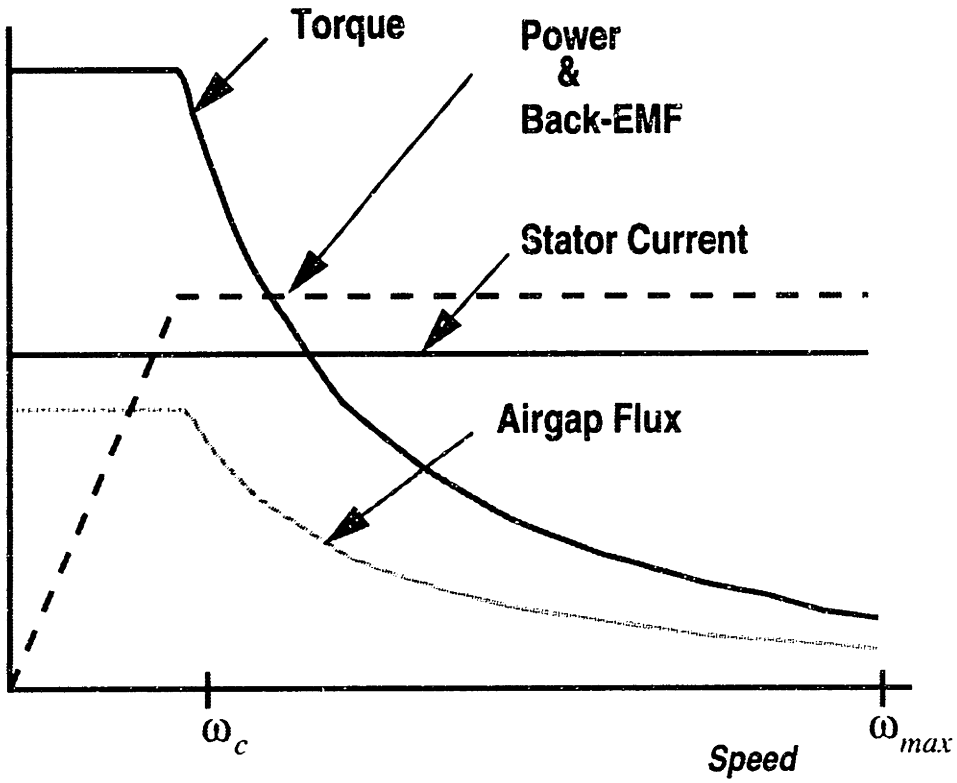

Figure 4-1: Relationships between motor torque, airgap flux, back-emf, armature current and mechanical power under flux-weakening.

To extend the speed range of PMSMs, flux weakening control has been the common practice[49, 50]. The basic idea of flux-weakening control is to use additional armature current to create a magnetic field that opposes or weakens the airgap flux so that the motor's back-emf can be kept constant. For efficient flux-weakening control, the PM rotor has to exhibit negative saliency so that direct-axis current used to weaken the airgap flux also produces reluctance torque. This requirement often results in complicated rotor designs such as the buried magnet (interior or inset) type, which have different direct and quadrature axes inductances; and are often more difficult to manufacture compared to their surface-mounted counterparts. Operation under flux-weakening control, compromises motor efficiency since the direct-axis current used to weaken the airgap flux dissipates heat and produces little or no reluctance torque. In motors with square-wave winding distribution, where the back-emf of the motor is close to trapezoidal, the term "phase-advance" is used to describe

the flux weakening process. Under phase-advance operation, the inverter leg driving the commutating phase of the motor is turned on some time before the peak of the back-emf of that phase, allowing current to build up in the commutating armature winding during the rising edge of its back-emf waveform.

In addition to poor efficiency, phase advance yields only a modest increase in speed range and significant torque ripple, which is undesirable in direct-drive applications at low speeds. Thus in EV propulsion applications where system efficiency and torque ripple at low speeds are important, flux weakening or phase-advance is a sub-optimal method of achieving an extended speed range operation [53]. The problem of rotor magnet demagnetization, furthermore, becomes exarcebated during the flux-weakening mode of operation. As mentioned earlier, one of the benefits of flux-weakening is the better utilization of the Volt-Ampere (V-A) rating of the power semiconductor devices. However, if the power semiconductor devices are not rated to withstand the highest motor back-emf, in the unlikely but possible event where the microprocessor controlling the inverter undergoes a reset, large currents can be injected into the traction battery or dc power supply by the motor. This failure mode can be catastrophic in a vehicle propulsion application.

In summary, even though flux-weakening control permits savings on the V-A ratings of power semiconductors, this mode of operation complicates rotor design and fabrication, and increases torque ripple which is undesirable especially at low speed. It also lowers motor efficiency while increasing its cooling requirements, and makes the drive system prone to potentially catastrophic failures. In view of the above shortcomings of flux weakening, we seek an alternative to efficiently extend the operating speed range of a PM synchronous motor.

Figure 4-2 shows how the motor torque, airgap flux, back-emf, armature current and mechanical power vary with motor speed when flux weakening is not employed. In this mode of operation, the power semiconductor switches are rated to withstand the highest back-emf of the motor so that the catastrophic failure mode described above is avoided. The back-emf is allowed to grow linearly with motor speed and the motor's number of turns is adjusted so that the peak back-emf is below the dc bus voltage at top speed. The advantages accruing from this mode of motor operation include extended constant power speed range,

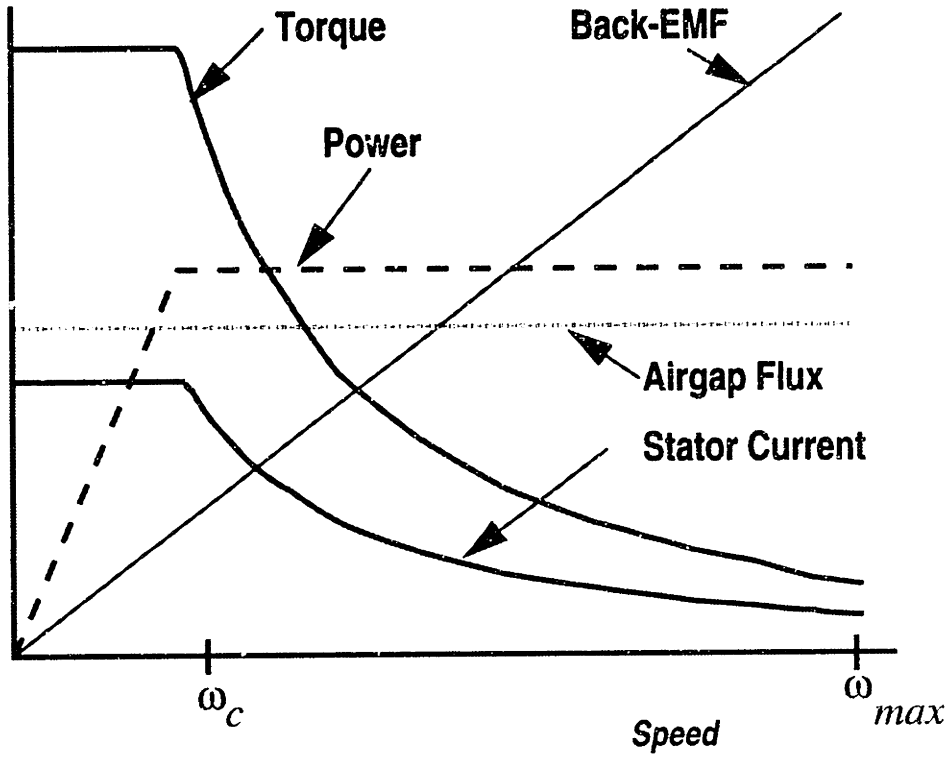

Figure 4-2: Relationships between motor torque, airgap flux, back-emf, armature current and mechanical power without flux-weakening.

reduced torque ripple and more importantly, reduced heat removal requirements while producing constant power. This reduced thermal burden stems form the fact that backing off on the stator current for lower motor torque reduces substantially the I^2R losses in the motor which is the major contributor to heat generation in the motor. Consequently, air cooling may be successfully employed in cooling the motor over the drive cycle.

Given that the power semiconductor switches are sized to withstand the highest back-emf of the motor for the reasons outlined above, the question that remains is how to choose the number of turns of the motor. Should the number of turns be chosen so that the back-emf never exceeds the battery voltage, resulting in a low-voltage/high-current drive which allows the use of a standard three-phase voltage-source inverter or are there some benefits in going to a high-voltage/low-current drive? We show shortly that there are substantial gains in inverter efficiency by employing a high-voltage/low-current drive, in addition to

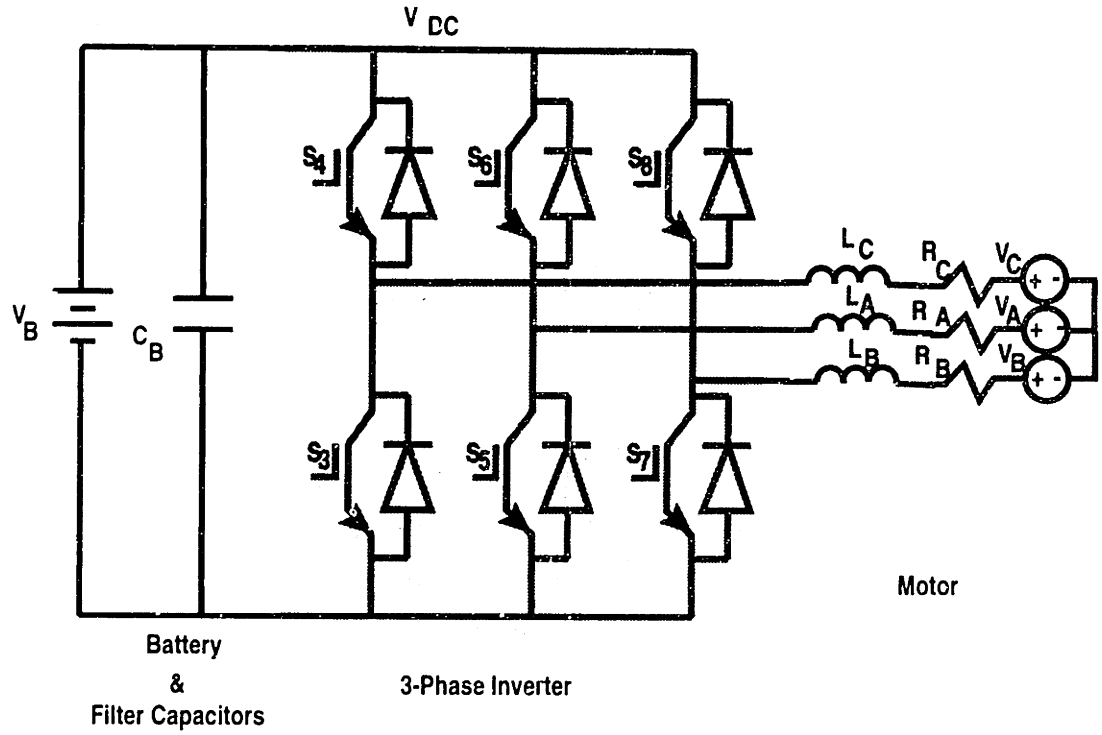

Figure 4-3: Power circuit of a standard 3-phase IGBT voltage source inverter.

reduced snubbing and switching current filtration requirements.

4.2 Standard 3-Phase Voltage Source Inverter

Figure 4-3 shows the power circuit for a standard 3-phase IGBT voltage source inverter. Three two-quadrant half-bridges are used to chop the battery voltage to match the motor back-emf as well steer currents in the appropriate phase windings to ensure smooth and continuous motor rotation. Two-quadrant operation of the inverter is necessary for regenerative braking, where the traction motors are used as generators to capture the kinetic energy of the vehicle.

Consider a 15 kW (20 hp) traction drive that operates from a nominal battery voltage of 250 V. Allowing about 50 V of headroom for commutation at top speed, the inverter has to supply a dc current of 300 A at the corner speed where the motor back-emf is 50 V, in order to achieve a 4:1 constant-power speed range. In other words, the inverter has to process the total 15 kW plus its power conversion and motor losses at 50 V. Current state-of-the-art IGBT modules are available in two voltage ratings, namely 600 V and 1200

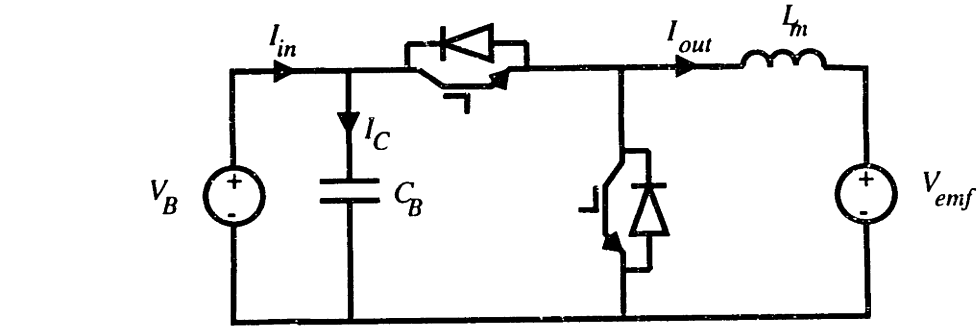

(a) Buck converter

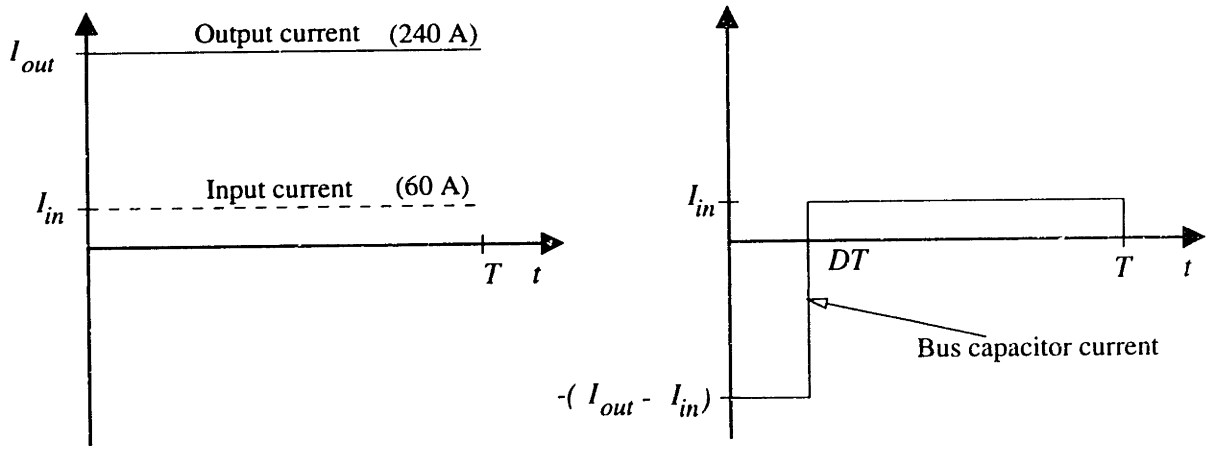

(b) Current waveforms

Figure 4-4: Idealized inverter and associated currents.

V. With a forward voltage drop of 2.7 V, conduction losses in the IGBT modules amount to 1.62 kW since there are always two devices in the conduction path of the topology in Figure 4-3. Neglecting all other losses, conduction losses *alone* constitute an efficiency drop of 9.7 %. Associated with this drop in power conversion efficiency is the problem of heat removal from the devices. If the back-emf of the motor were increased to say 200 V at the corner speed, 1200 V IGBTs will be needed in order to be able to withstand the motor back-emf at top speed, and the conduction losses can be cut down by a factor of four since the on-state voltage for 1200 V, low-current IGBT modules is essentially the same as that for 600 V high-current modules [20].

Another problem with the low-voltage/high-current inverter is the large rms current that the bus capacitors must filter. Consider the buck converter shown in Figure 4-4(a), which represents one leg of the standard 3-phase inverter shown in Figure 4-3. For the sake of

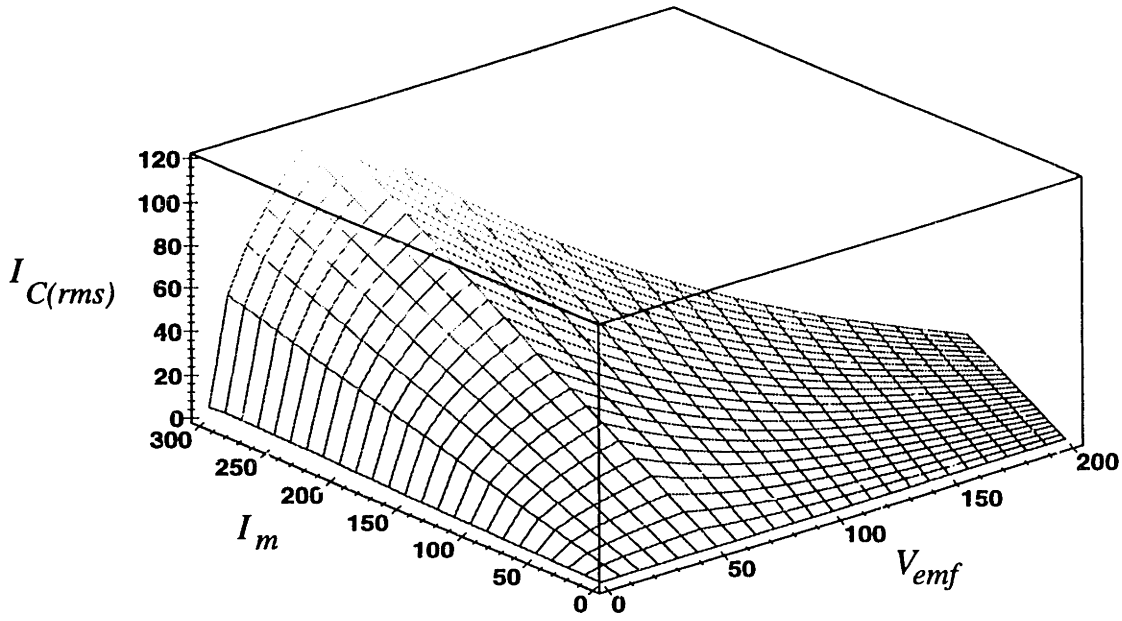

Figure 4-5: RMS current through bus capacitors over the entire region of operation of the motor.

discussion, the motor inductance L_m is assumed to be infinite so that the motor current is essentially dc. The armature resistance is assumed to be zero so that ohmic losses in the motor can be ignored. With a 300 A motor current, the dc battery current is 60 A, assuming perfect conversion efficiency. The resulting duty cycle is 20%. Thus, during 20 % of the time when the motor is directly connected to the dc bus, C_B sources 240 A of current as shown in Figure 4-4(b). During the remaining 80 % of the time when the motor current is freewheeling through the low-side diodes, C_B is charged by the 60 A of battery current. The net ac current that C_B has to filter at this operating point is 120 A rms. Figure 4-5 shows the rms current through C_B over the entire region of operation of the motor using the methodology above. Note that, in general, the rms ripple current through C_B is zero at both zero and unity duty cycles and the maximum value occurs at 0.5 duty cycle. The rms current is also proportional to the motor current. For the standard inverter under discussion, the maximum rms ripple current through C_B occurs at the "corner point" (as shown in Figure 4-5) since operation at 0.5 duty cycle, for this inverter, occurs in the constant power mode of operation at which point the motor current is down by a factor of

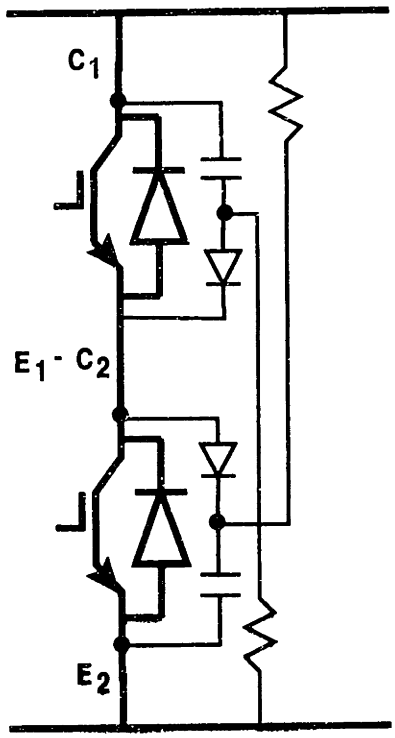

Figure 4-6: Resistor-Capacitor-Diode snubber for high-current IGBTs.

2.5 from its constant torque value. This peak current filtration requirement is harsh on the bus capacitors which are often electrolytic and are limited in their ripple current carrying capability, and hence require several capacitors to be paralleled even though the additional capacitance is not necessary from an impedance point of view.

While switching large currents, the IGBTs have to be adequately snubbed to keep them in the safe operating region. The voltage overshoots that occur in switching transients is proportional to the amount of current being switched. For proper device operation, the recommended snubber for a 600-V 300-A IGBT require the complicated resistor-capacitor-diode (RCD) combination shown in Figure 4-6, in conjunction with intricate low-impedance bus designs to minimize the increased current-related voltage overshoots associated with switching large currents [20].

In addition to the above drawbacks of a low-voltage/high-current design from the power-electronics point of view, the motor that matches the low-voltage inverter requires fewer turns, which necessitates that the windings be made of large conductors. Larger gauge wires are difficult to wind and their end turns are difficult to control. Larger slot openings are

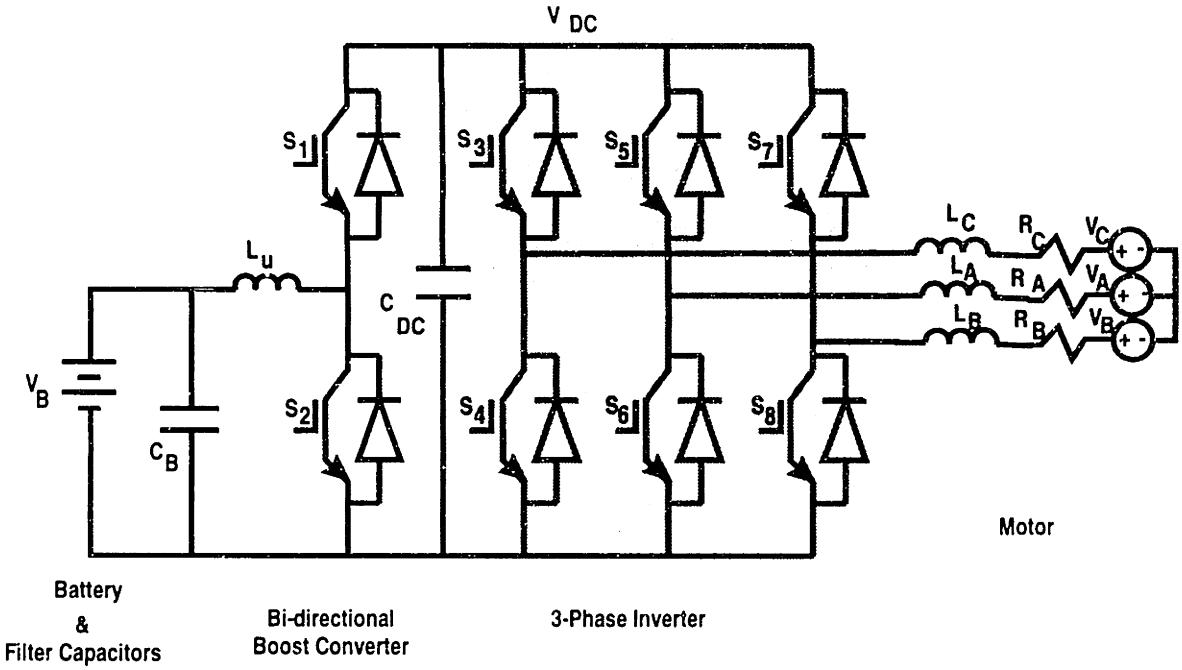

Figure 4-7: New inverter topology.

required, and if the parallel conductors are used, the wires have to be properly transposed to minimize circulating currents. To address the above concerns, we explore the use of an unconventional inverter design that permits motor operation at high voltage.

4.3 Novel 3-Phase Voltage Source Inverter

Figure 4-7 shows a modification of the standard 3-phase voltage source inverter to include a bi-directional boost converter in the dc-link. This modification makes possible efficient wide speed range operation of PMSMs without flux weakening while circumventing the problems associated with the standard voltage source inverter discussed in the previous section. In this inverter topology, a constant power bi-directional boost converter is used to step up the traction battery voltage as necessary to match the motor back-emf [51, 52].

The operation of the inverter is as follows. When the back-emf of the motor is below the battery voltage, the boost converter is disabled by turning off S_1 and S_2 and the inverter operates as a standard voltage source inverter where the switches $S_3 - S_8$ are used to chop the battery voltage as well as commutate the motor. When the back-emf exceeds the battery voltage, the boost converter is used to step up the battery voltage to match the motor back

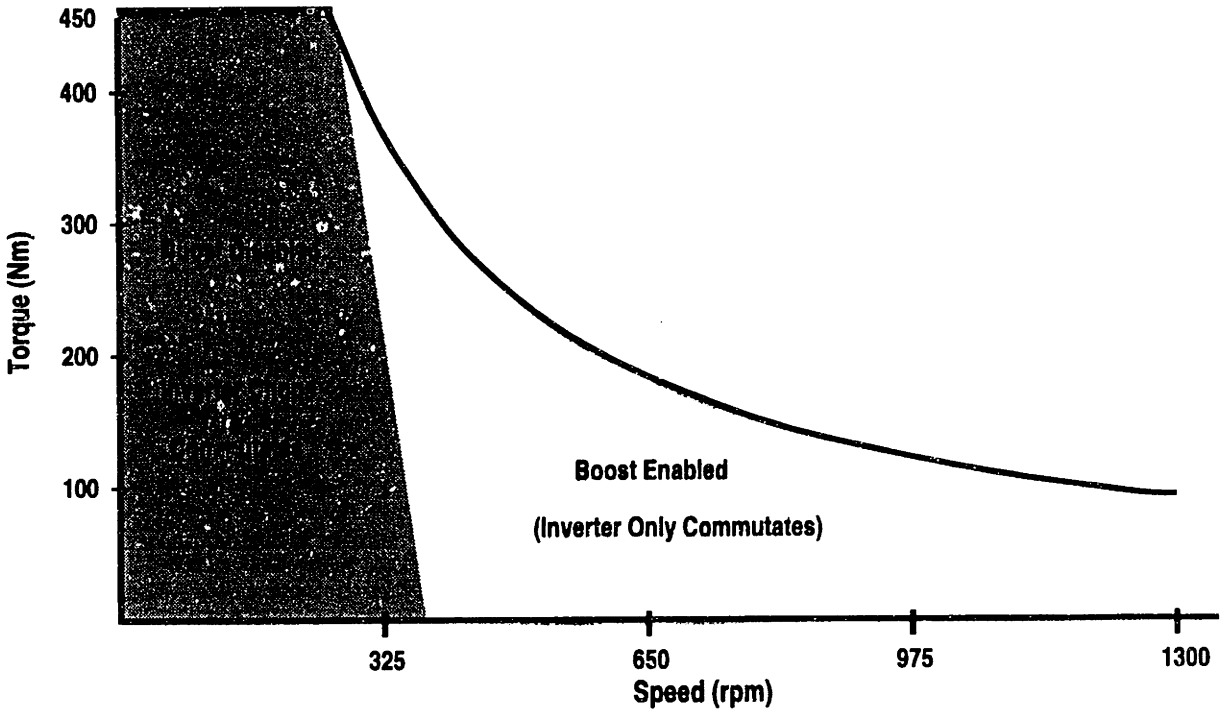

Figure 4-8: Regions of operation of buck and boost sections of inverter.

emf and the switches $S_3 - S_8$ are *only* used to commutate the motor. This way, we minimize additional switching losses associated with high-frequency pulse-width modulation (PWM). The regions under the torque-speed curve where the inverter operates in the buck and boost modes are schematically shown in Figure 4-8. The slope to the buck/boost boundary is due to the voltage that develops across the non-zero motor resistance.

To implement regenerative braking when the motor back-emf is below the battery voltage, $S_3 - S_8$ are used to boost the motor back emf to match the battery voltage, thus capturing the motor regenerative energy and storing it in the battery. In this mode of operation, S_2 is turned on while S_1 remains off. When the back-emf is greater than the battery voltage, then the switches $S_3 - S_8$ are used to rectify the motor's back-emf and down-converted to match the battery voltage by pulse-width modulating S_2. In the regenerative braking mode of operation, mechanical energy from the vehicle is converted to electric energy and stored in the traction battery or a high-power intermediate energy storage device such as a flywheel.

In the remaining sections of this chapter, we compare the relative merits and shortcomings of the two inverter topologies in terms of energy storage component requirements,

power conversion efficiency, installed V-A capacity, snubbing requirements, cost, and control complexity.

4.4 Energy Storage Requirements

The only energy storage components required in the standard inverter topology of Figure 4-3 are the capacitors across the traction battery, which are required to filter the ripple currents generated by the switching of the three half-bridge inverter switches. As we have shown earlier, these bus capacitors have to filter 120 A rms at the "corner point". For operation with the high-voltage inverter shown in Figure 4-7, the number of turns of the motor is adjusted by a factor of four to yield a back-emf of 200 V at the "corner point". Remember that for the low-voltage inverter, we allowed a margin of 50 V above the back-emf to effect commutation. To achieve the same rate of current buildup in the commutating winding as before, we now require 200 V of voltage margin above the back-emf since the inductance increases as the number of turns squared, and the commutation current is inversely proportional to the number of turns. Thus for a back-emf of 800 V at top speed and an additional 200 V for commutation, we have a headroom of 200 V to accommodate current related voltage overshoots and switching voltage ripple. As mentioned earlier the ripple current in the bus capacitors is a maximum when switching the maximum current at 50% duty cycle.

Using the ripple current computation methodology illustrated in Figure 4-4, we calculate the rms current through the bus capacitors when the inverter is operating in the buck mode, and the resuit is shown in Figure 4-9. With the increase in the number of turns by a factor of four, the torque constant increases by the same factor and the maximum constant torque current is now 75 A dc. The resulting rms current ripple that must be filtered by the bus capacitors is only 37.5 A, a factor of 3.2 reduction. The maximum rms current in the boost mode is lower than that of the buck moded due to the current smoothing action of the boost inductor.

At a switching frequency of 20 kHz and a traction battery internal resistance of about 0.3 Ω, 265 μF of capacitance constitutes an impedance that is one-tenth that of the battery,

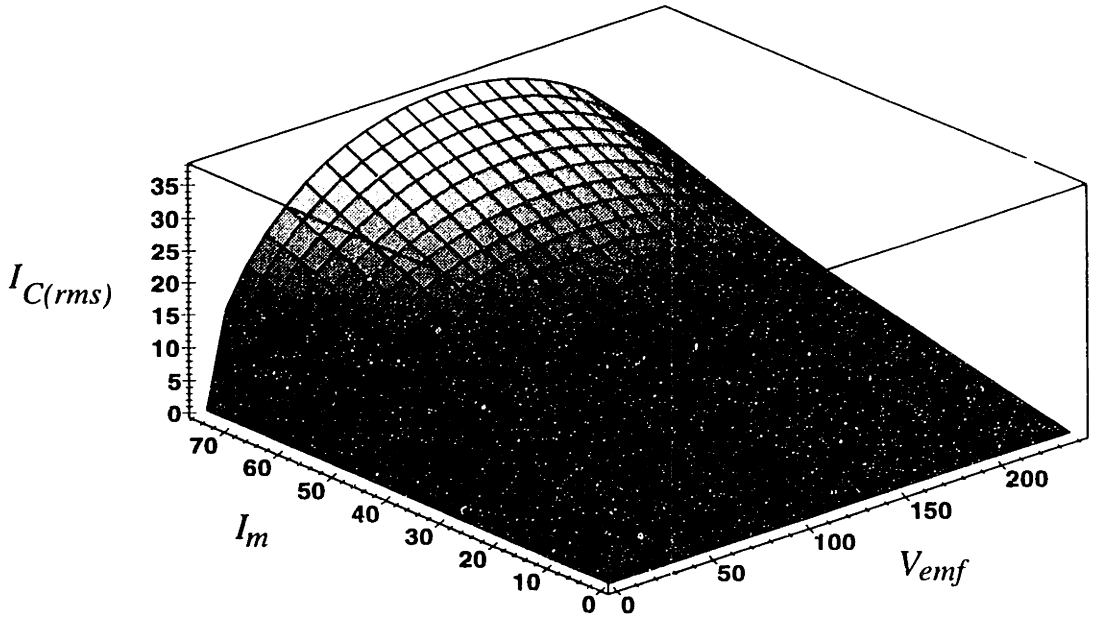

Figure 4-9: RMS current through bus capacitors in the buck mode of operation.

thus constituting an adequate low-impedance path for current filtering. This amount of capacitance is readily obtainable in a single electrolytic capacitor, but not enough current filtering capability due to the high dissipation factor of electrolytics. Therefore, the number of capacitors needed is often proportional to the rms current. In view of the rms ripple current that must be filtered, the novel inverter requires less than a third of the number of bus capacitors needed for the standard voltage source inverter.

The novel inverter of Figure 4-7 requires two additional energy storage elements; a front end inductor L_u and an output capacitor C_{DC} for the bi-directional boost converter. The size of an inductor is, in general, proportional to the amount of energy the inductor must store. Therefore we determine the boost inductor parameters by minimizing the amount of energy that it must store. The peak energy E_{Lu} stored in an inductor of inductance L_u , carrying a peak current I_{pk} is given by

$$E_{Lu} = \frac{1}{2} L_u I_{pk}^2 \quad . \tag{4.1}$$

For a constant power boost converter with an input voltage V_{in} and an output voltage V_{out}

switching at a constant frequency f_{sw}, the energy stored in the boost inductor is minimized when the converter is operating at the edge of discontinuous conduction. The critical inductance $L_{u,crit}$ that minimizes the energy storage is given by

$$L_{u,crit} = \frac{V_{in}^2}{2P_{out}f_{sw}}\left[1 - \frac{V_{in}}{V_{out}}\right] \tag{4.2}$$

where P_{out} is the power processed. At the edge of discontinuous conduction, the peak inductor current is equal to twice the average input current I_{in}. The corresponding minimum magnetic energy stored is therefore given by

$$E_{Lu,min} = \frac{P_{out}}{f_{sw}}\left[1 - \frac{V_{in}}{V_{out}}\right] \quad . \tag{4.3}$$

For V_{in} = 250 V, V_{out} = 1000 V, f_{sw} = 20 kHz, and P_{out} = 15 kW, the critical inductance $L_{u,crit}$ = 78 μH and the required magnetic energy stored by the boost inductor is 0.56 J. The output capacitor C_{DC} is chosen to be 40 μF to yield an output ripple voltage of 25 V peak-to-peak. The electric energy storage E_C is given by

$$E_C = \frac{1}{2}C_{DC}V_{pk}^2 \quad = \quad 25J \tag{4.4}$$

for V_{pk} of 1025 V. Thus the new inverter requires about 0.56 J of additional magnetic energy storage and 25 J of high-voltage electric energy storage.

4.5 Conversion Efficiency

By moving the "corner point" of the inverter to 200 V, the conduction losses go down by a factor of four since the current is reduced by one-fourth. However, since we have one extra device conducting in the boost converter in the new topology, the total conduction losses is only lowered by a factor of 2.67, from 1.62 kW to 606 Watts. With our switching strategy of pulse-width modulating only one section of the converter at a time, the switching losses to first order are the same for both converters, ignoring the switching losses associated with the low-frequency six-step commutation when the boost converter is in operation. Additional

energy is lost in the boost inductor but will be ignored in this qualitative comparison, since the exact loss is not known until the inductor has been designed.

4.6 Installed Volt-Ampere Capacity

The standard inverter requires six 600-V, 300-A two-quadrant switches, making the installed V-A capacity 1.08 MVA, whereas the modified inverter requires eight 1200-V, 75-A two quadrant switches, resulting in 0.72 MVA. This corresponds to a factor of 1.5 reduction in installed V-A capacity for the new inverter.

4.7 Snubbing Requirements

The reduced switching current requirement in the new high-voltage inverter, in conjunction with a low-inductance bus structure, allows the use of the simple snubber in shown in Figure 4-10, where low-inductance high-voltage polypropylene snubber capacitors are connected across the collector and emitter of the half-bridge as opposed to the complicated RCD snubber shown in Figure 4-6.

4.8 Component Cost

The total cost of the power circuit in the standard inverter is effectively a weighted sum of the installed V-A capacity of the power semiconductors and energy storage in the bus capacitors, and the cost of snubber components. We have shown in the previous sections that by using the new inverter topology, the cost of the electrolytic bus capacitors is reduced by a factor of 3.2 and we save on the power semiconductor V-A ratings by a factor of 1.5. Furthermore, the snubber for the standard inverter is more costly than that in the new inverter due to the added diodes. It is anticipated that, in general, the cost savings deriving from the reduced energy storage in the bus capacitors, reduced power semiconductor V-A ratings, and simplified snubber will more than compensate for the added cost of a boost inductor and boost output capacitors and two additional gate drives.

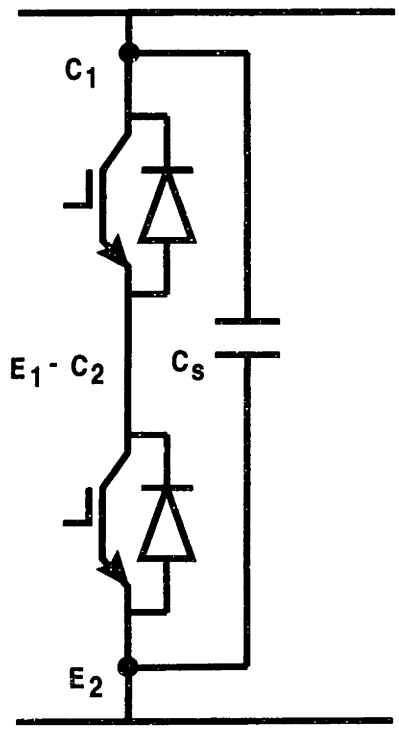

Figure 4-10: Capacitive snubber for low-current IGBTs.

4.9 Control Complexity

Torque control in the standard 3-phase voltage source inverter is easily accomplished with as simple proportional plus integral (PI) digital controller. In the new inverter, however, in addition to a PI controller for the buck section of the inverter, we require additional controllers for the boost section which operates mostly in discontinuous mode. These different controllers in the new inverter have to relinquish control to each other as needed, in response to the torque demands of the motor. Although the control algorithm for the new inverter is more complex than the standard inverter, it can be implemented at no additional cost with a microcontroller.

4.10 Conclusions

In applications where energy efficiency is at a premium, the use of power electronics instead of flux-weakening to extend the speed range of PMSMs offers significant advantages in motor efficiency and cooling requirements, while avoiding potentially catastrophic failure

modes associated with inverter reset during operation in the flux-weakening mode. By using the unconventional high-voltage inverter described in this chapter, the efficiency of the inverter is improved due to lower semiconductor conduction losses. The installed V-A capacity is reduced as well as the snubbing and current filtration requirements of the dc bus capacitors. Total semiconductor and energy storage component cost is about the same, if not less, for the new inverter compared to the standard inverter.

Chapter 5

Prototype Wheel Motor: Power Electronics and Control

5.1 Introduction

In this chapter, we design the prototype inverter that will be used to drive the wheel motor designed in Chapter 3. We start by specifying component values for the power circuit and then proceed to derive averaged plant models to be used for control. We then design digital controllers around these plants and implement these controllers with an MC68HC16Z1 microcontroller. For our computations in this chapter, the traction battery will be modeled as a 336-V voltage source in series with a 0.3 Ω series resistance[42].

5.2 Power Circuit

The power circuit of the of the novel inverter is reproduced in Figure 5-1 for ease of reference. In this section, we discuss the design of the experimental inverter to be used with the prototype wheel motor designed in Chapter 3, with regard to semiconductor and energy storage component specification and compute the theoretical efficiency of the inverter. Our original intent was to switch the inverter at 20 kHz to avoid audible noise, but this PWM frequency was not readily obtainable from the MC68HC16Z1 microcontroller used for control. Therefore the inverter was switched at 16.44 kHz, which is the closest

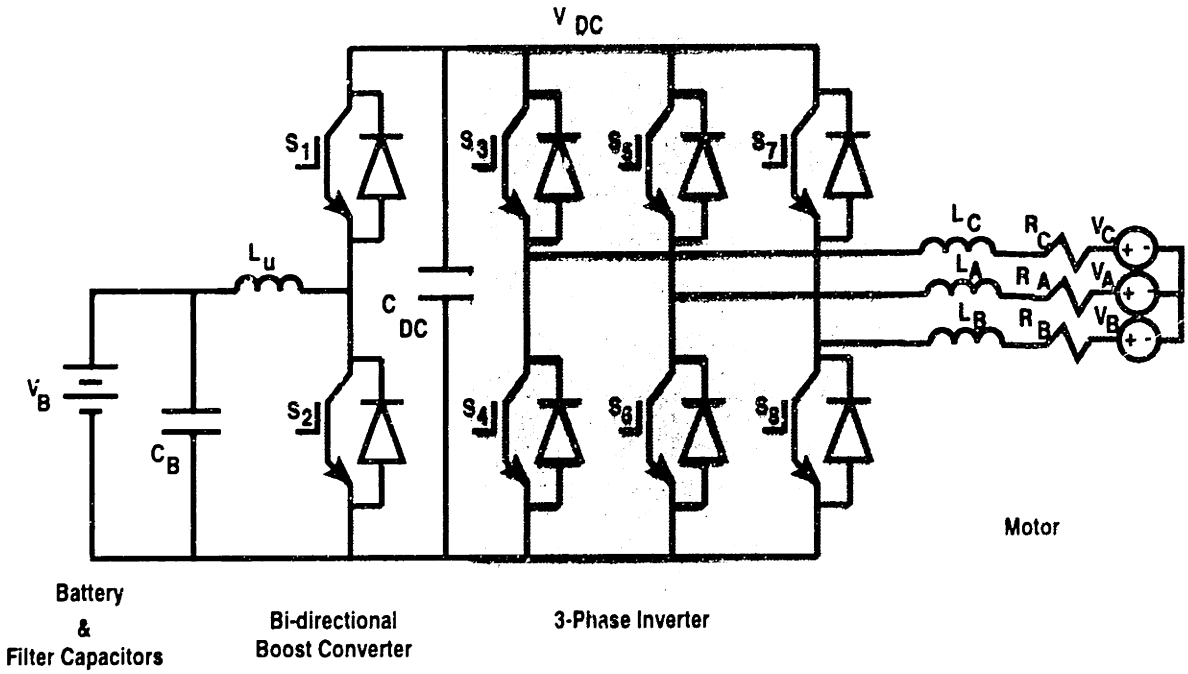

Figure 5-1: Inverter topology.

programmable frequency to 20 kHz.

5.2.1 Semiconductor Component Specification

As discussed in Chapter 4, to achieve efficient wide speed range operation without flux weakening, the semiconductor switches must be sized to withstand the highest back-emf of the motor and have adequate headroom for the extra voltage needed for commutation. In addition, one must also ensure that the switching-related voltage ripple on the output capacitors of the boost converter does not cause the voltage rating of the IGBTs to be exceeded. With a back-emf constant of 6 V/rad-s, the expected maximum back-emf at 1300 rpm is 800 V. Budgeting 200 V for commutation, 1200 V IGBTs will be used. The maximum constant torque required sets the current rating of the IGBTs. Since 75 A is required to produce 450 Nm of torque, we select 100 A devices to allow a margin for safety. To simplify the layout of the power circuit and gate-drive circuitry we use half-bridge intelligent IGBT modules from Powerex which have integral gate-drive and protection circuitry.

5.2.2 Energy Storage Component Specification

A. Bus Capacitors

As shown in Chapter 4, the maximum rms current that the bus capacitors must filter is 38 A. From an impedance point of view, 322 μF constitutes an impedance of 0.03 Ω (one-tenth the battery impedance) at the switching frequency of 16.44 kHz. Power electrolytic capacitors have high dissipation and are therefore limited in the ripple current they can filter. For example, a 2,400 μF, 450 VDC high-ripple electrolytic capacitor can only handle 9.4 A rms of ripple current at 20 kHz[1] [54]. The ripple current carrying capability can only be increased by increasing the capacitance. Therefore, in general, several capacitors must be paralleled for high ripple current filtration. For the prototype inverter, we parallel six Mallory CGH242T450W4L capacitors to yield a ripple current capability of 56.4 A. Notice that the resulting capacitance 14.4 mF is very much in excess of what is needed from an impedance point of view.

B. Boost Inductor

As shown in Chapter 4, the inductance $L_{u,crit}$ that minimizes the magnetic energy storage is given by

$$L_{u,crit} = \frac{V_{in}^2}{2P_{out}f_{sw}}\left[1 - \frac{V_{in}}{V_{out}}\right]. \tag{5.1}$$

With a maximum output voltage of 1050 V (800 V from the back-emf, 200 V for commutaion and 50 V for Ohmic drops and current related overshoots), a low battery voltage of 250 V [42], and a maximum output power of 15 kW while switching at 16.44 kHz, the inductance required is 97 μH. The corresponding inductor was constructed by winding 48 turns of AWG 12 Litz wire (259 strands of AWG 36) on a 4-inch outer diameter, Hi-Flux^{TM} powder (HF) toroidal core[2] [56]. The resulting copper and core losses at full power is 106 W and 170 W respectively.

HF cores are composed of 50% nickel and 50% iron, and have a higher saturation flux density (1.5 T) compared to Molybdenum Permalloy Powder (MPP) or ferrites which have

[1] Mallory Part no. CGH242T450W4L
[2] Arnold Engineering Part no. HF-400060-2

saturation flux densities of 0.7 T and 0.3-0.5 T, respectively. The high saturation flux of HF cores make them suitable for applications requiring high magnetic energy storage, yielding significant reduction in inductor size and cost compared to ferrites or MPP. The permeability of HF cores is also less sensitive to changes in ac excitation, dc bias and temperature.

C. Boost Output Capacitors and Snubbers

The function of the capacitors at the output of the boost converter is to hold the output voltage while the boost inductor is being charged. These capacitors must filter significant ripple current as charge is dumped into them periodically from the boost inductor. Therefore these capacitors must have a low dissipation factor in order to prevent excessive heating. Both polypropylene capacitors or low dissipation electrolytic capacitors may be used for this application. However, the required voltage rating of 1200 V precludes the use of single electrolytics since 1200 V is well above the voltage rating of commercially available electrolytics. Furthermore, as we saw earlier, attaining a reasonable ripple current handling capability requires a large capacitance. Excessive capacitance at the output of the boost converter is undesirable since it limits our ability to dynamically shape the output voltage to control the motor current in response to rapid changes in torque demand.

With 100 μH of boost inductance, a capacitance value of 40 μF is chosen as a reasonable balance between output ripple voltage and capacitor cost. With this amount of output capacitance, the maximum ripple voltage across the output capacitor is computed to be 25 V and the rms ripple current is 30 A. Due to difficulty in procuring a standard capacitor with these voltage and current ratings, the 40 μF output capacitor is implemented with four 10 μF, 1500 V capacitors[3]. Each of the 10 μF capacitors procured is capable of filtering 207 A of ripple current, thus the capacitors are extremely oversized for the current handling capability required [55]. Furthermore, the size of a capacitor is proportional to the energy storage, which is proportional to the square of the voltage. Thus, rated at 1500 V, these capacitors are a factor of 1.56 larger than necessary, but no appropriate capacitor was readily available.

[3]GE Part no. 97F8625

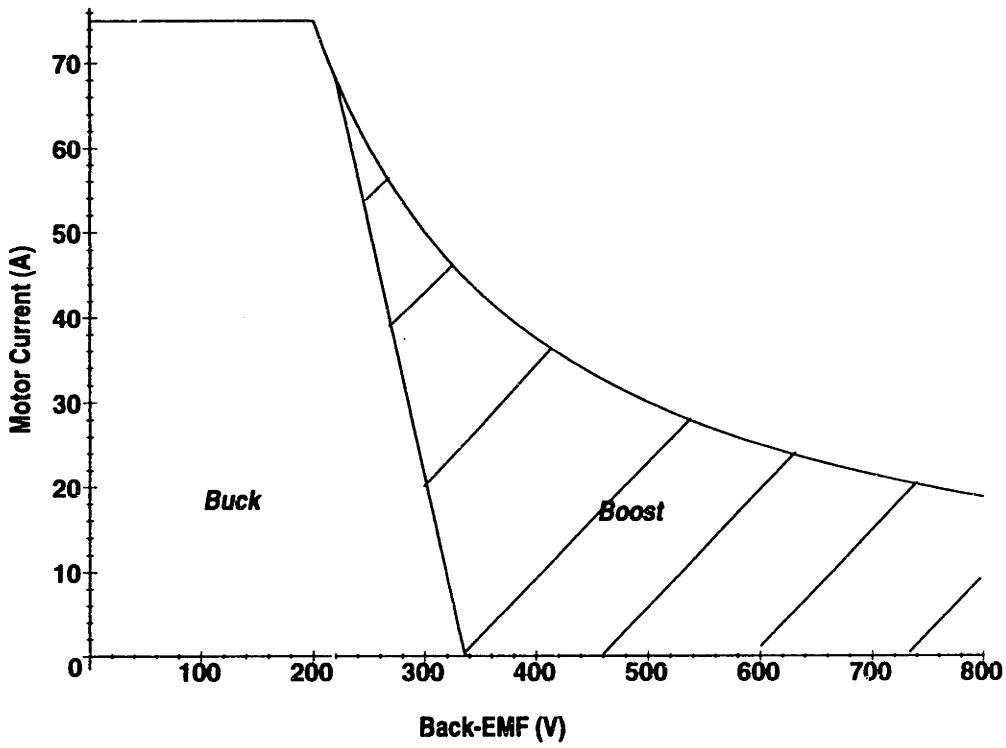

Figure 5-2: Operating boundaries of buck and boost converters.

To minimize current-related voltage overshoot during switching transients, 2-μF low-inductance polypropylene snubber capacitors are connected directly across the collector and emitter of the IGBT half-bridge modules.

5.2.3 Semiconductor Losses

The inverter in Figure 5-1 is effectively a cascade of hard-switched boost and buck converters, and Figure 5-2 shows the regions of operation of the buck and boost converters. As mentioned earlier, the buck converter is used to drive the motor until its terminal voltage (the sum of the back-emf and the resistive voltage drop) becomes equal to the inverter input voltage, at which point the boost converter takes over.

Figure 5-3(a) shows the magnitude of the dc input current input current into the inverter in its entire region of operation. This plot is generated with Maple V (source code in Appendix D.3) under the assumption that the inverter is 100 % efficient, and all four wheel motors are operating simultaneously at the same point underneath the torque-speed

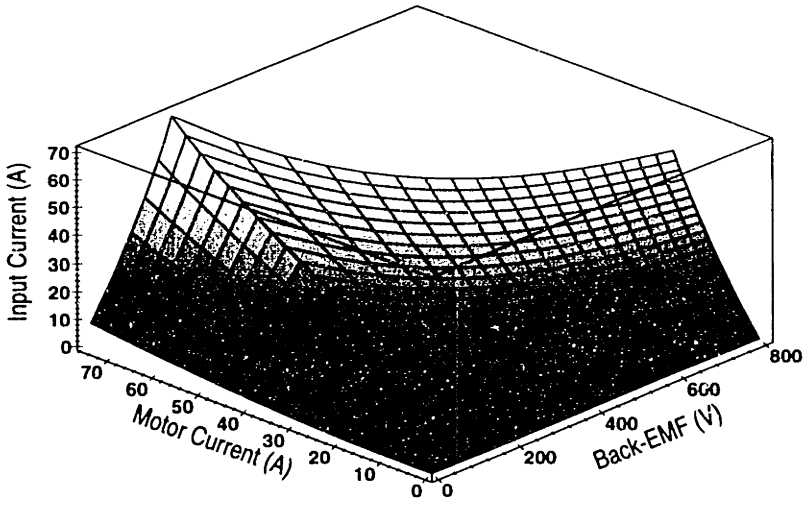

(a) Input current to inverter

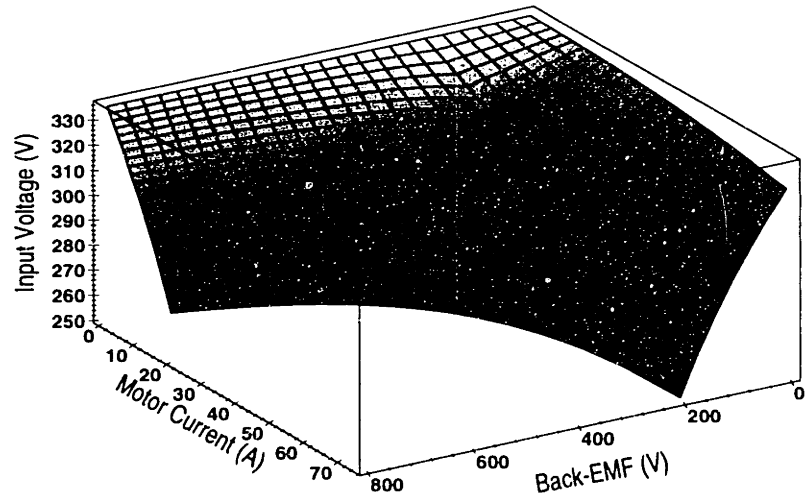

(b) Input voltage to inverter

Figure 5-3: Variation of inverter's input current and input voltage with motor current and back-emf.

envelope. Under these circumstances, the dc current into the inverter I_{in} can be written as

$$I_{in} = \frac{V_{B,(oc)} - \sqrt{V_{B,(oc)}^2 - 16R_{int}V_{out}I_{out}}}{8R_{int}} \tag{5.2}$$

where I_{out} is the inverter output dc current, V_{out} is the inverter output voltage, $V_{B,(oc)}$ is the battery open circuit voltage and R_{int} is the battery internal resistance. The output voltage V_{out} is related to the motor resistance R_m and the back-emf V_{emf} by

$$V_{out} = V_{emf} + I_{out}R_m \quad . \tag{5.3}$$

Figure 5-3(b) shows the corresponding input voltage V_{in} to the inverter. The input voltage is the battery open-circuit voltage less the voltage drop across its internal resistance, and is given by the equation

$$V_{in} = V_{B,(oc)} - 4I_{in}R_{int}. \tag{5.4}$$

The slope to the line in Figure 5-2 that forms the boundary between the buck and boost regions of operation of the inverter is due to the drop in the input voltage with increased motor current and to a small extent the resistive drop across the motor that increases with increased motor current.

Hard-switched converters incur switching losses at both the turn-on and turn-off transitions. Figure 5-4 shows typical switching waveforms for a half-bridge intelligent module and an illustration of the associated power loss. The energy lost during switching transitions, which correspond to the shaded areas in Figure 5-4(b), is proportional to the voltage and current being switched and the duration of the switching interval. The average power loss is therefore the energy loss per switching cycle multiplied by the switching frequency. Graphical data on the energy dissipated during both turn-on and turn-off transitions including diode reverse recovery losses are available from the power semiconductor manufacturer's data sheets [20].

Figure 5-5(a) shows the variation of switching losses with the motor's back-emf at various motor currents. This figure is generated with Maple V subroutines in Appendix D.3 using the graphical data on switching and conduction losses provided in [20]. Note that the back-emf is proportional to speed and the motor current is proportional to torque, thus the Figure can be interpreted as representing the switching losses underneath the torque-speed envelope. Our switching approach of not switching both converters simultaneously help to reduce the total switching losses. In the buck mode of operation, the switching losses for a given current is independent of motor speed since the inverter is switched at a constant PWM frequency from a fixed bus voltage. In the boost mode however, even though the boost converter switches at a constant PWM frequency, the ouput voltage of the boost converter is proportional to the motor speed and hence we expect the switching losses to increase with the increased ouput voltage. Furthermore, in this mode of operation, the three

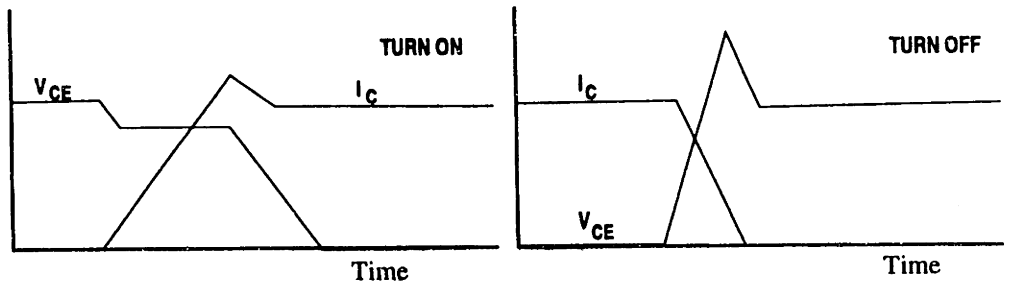

(a) Switching waveforms at Turn-on and Turn-off

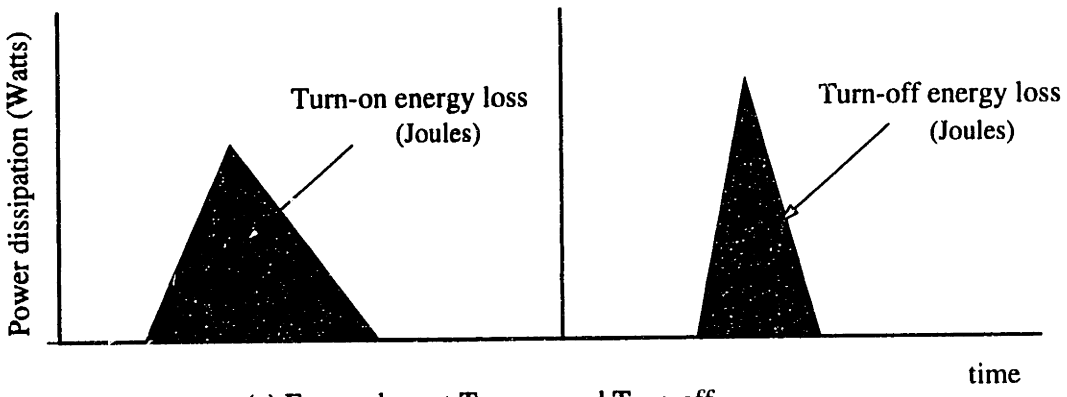

(a) Energy loss at Turn-on and Turn-off

Figure 5-4: Typical switching waveforms and associated energy loss for a hard-switched half-bridge.

inverter legs are operated in a six-step fashion to commutate the motor. Not only is the commutation frequency proportional to the motor speed, the switching losses deriving from this section of the inverter is also proportional to the output voltage. These two phenomena explain the increase of the switching losses with the motor speed as shown in Figure 5-5(a). Note that the maximum commutation frequency is 1300 Hz at top speed, thus the maximum switching losses from the six-step commutation is less than one-tenth of the losses from the high frequency PWM section.

Due to the non-zero collector-to-emitter voltages of the IGBTs, and non-zero forward

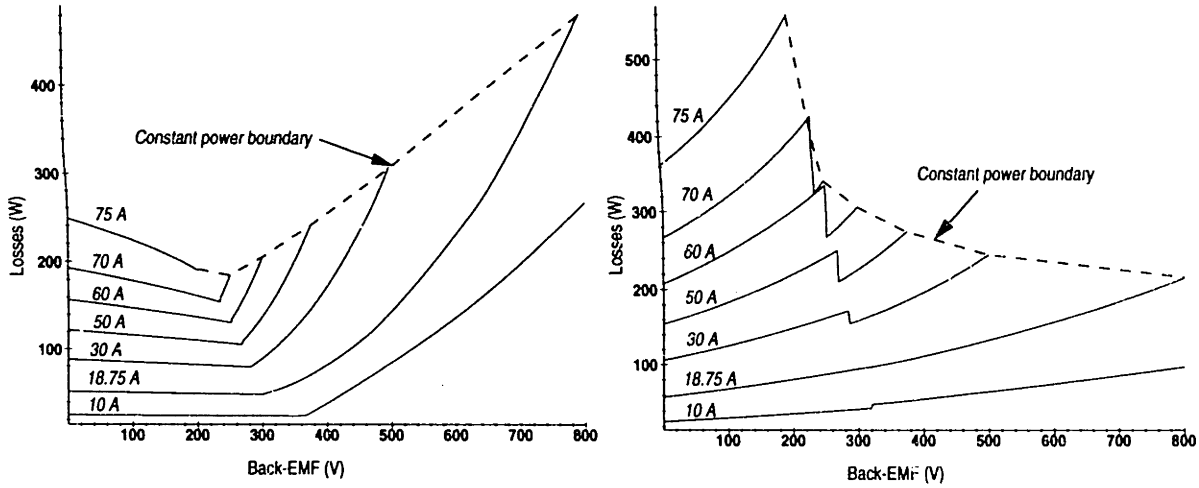

(a) Switching losses

(b) Conduction losses

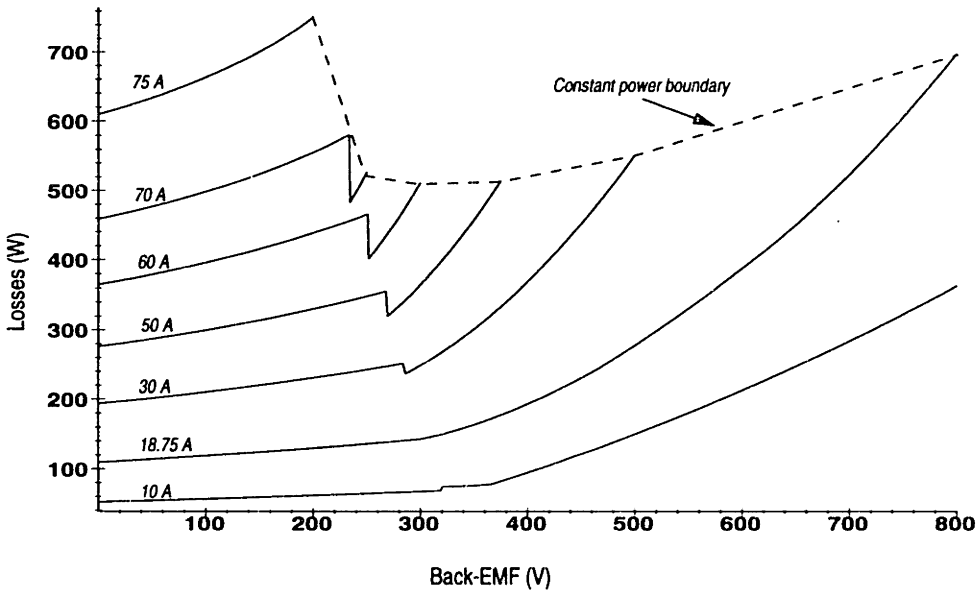

(c) Sum of switching and conduction losses

Figure 5-5: Inverter's semiconductor switching and conduction losses.

voltages of the anti-parallel diodes, power is dissipated in the IGBT module when conducting current. Graphical data on the on-state voltage drop across the power device are also provided in the power semiconductor manufacturer's data sheets [20]. The conduction power loss in a device is the time-average of the integral of the product of the voltage across and current through the device. Figure 5-5(b) shows the conduction losses in the inverter. The conduction losses are highest in the buck regime of operation for two reasons: (i) the highest currents are switched in this constant torque regime of operation, and (ii) there is an

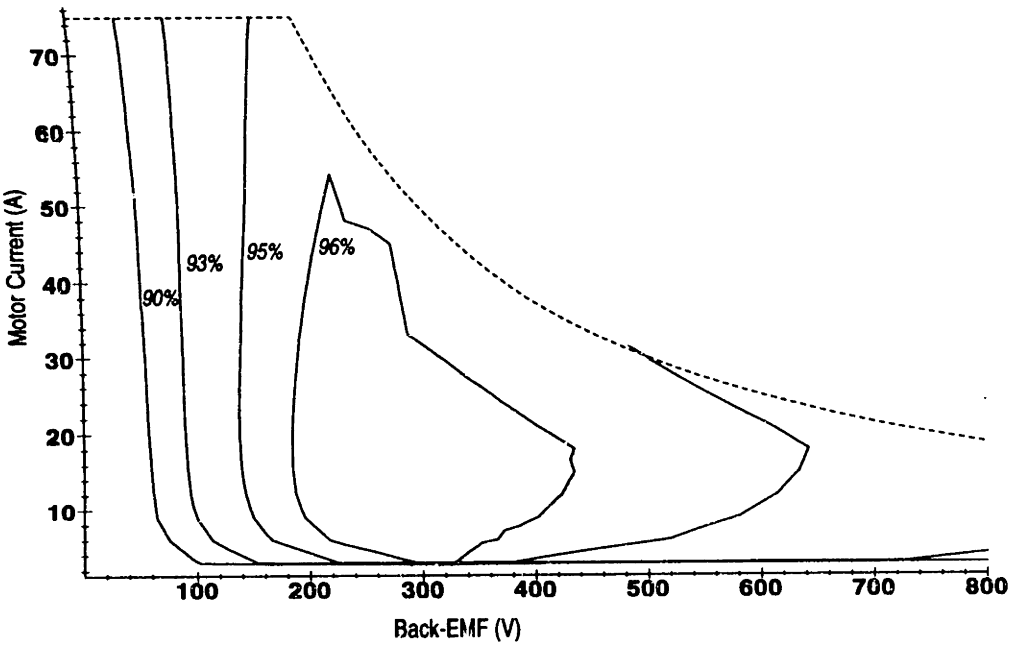

Figure 5-6: Simulated inverter efficiency.

extra diode from the disabled boost converter in the power flow path from input to output. The sharp drop in conduction losses in traversing the buck/boost operating boundary is due to the elimination of an extra junction drop form the power flow path.

Figure 5-5(c) shows the total semiconductor losses, which is the sum of the switching and conduction losses. From the figure we see that the maximum semiconductor loss is about 750 W and it occurs at the "corner-point" of the inverter.

5.2.4 Inverter Efficiency

The efficiency of the inverter η_{inv} is computed as

$$\eta_{inv} = \frac{V_{out} I_{out}}{V_{out} I_{out} + P_{semi} + P_{ind} + P_{gd}} \tag{5.5}$$

where P_{semi} is the sum of the switching and conduction losses of the power semiconductors, P_{ind} is the copper and core loss in the boost inductor, and P_{gd} is the power loss in the gate drives and control electronics, assumed to be 20 W. Figure 5-6 shows the theoretical efficiency map of the inverter as computed with Maple V in Appendix D.3. The medium torque, medium speed region attains efficiencies in excess of 96%. The weighted efficiencies

over the Urban and Highway drive schedules are 94 % and 95 %, respectively.

5.3 Control

The inverter in Figure 5-1 has four modes of operation. The first mode of operation is the "buck-motoring" mode, when the motor is motoring with a back-emf below the battery voltage. The second mode of operation is the "boost-motoring" mode, when the motor is motoring with a back-emf is above the battery voltage. The third mode of operation is the "boost-regenerative" mode, when the motor is regenerating with a back-emf below the battery voltage, and the fourth mode of operation is the "buck-regenerative" mode, when the motor is regenerating with a back-emf above the battery voltage. In all operating modes, we are interested in closing a feedback loop around the output current of the inverter, which is the motor current when motoring, and the battery charging current when regenerating.

In this thesis, control loops will be implemented for the first two modes of operation where electrical power is converted to mechanical power via the motor and transferred to an inertial load, as operation in these two regimes is enough to characterize the torque production capabilities and efficiency of the motor.

5.3.1 Average Models

In order to close the current feedback loop, we must develop average models that describe how the "plant", which consists of the power circuit of the inverter and the electrical section of the motor, respond to the control variable of our choice in an average sense. In the "buck-motoring" mode of operation, the control variable of choice is the duty cycle of the buck converter since the transfer function from control to output is contains only a single pole.

Figure 5-7(a) shows an averaged circuit model of the plant in the "buck-motoring" mode of operation. The average motor current $\bar{i}_m$ is related to the duty cycle $\bar{d}$ via the equation

$$\bar{i}_m = \frac{\bar{d}V_{in} - V_{emf}}{sL_m + R_m} \tag{5.6}$$

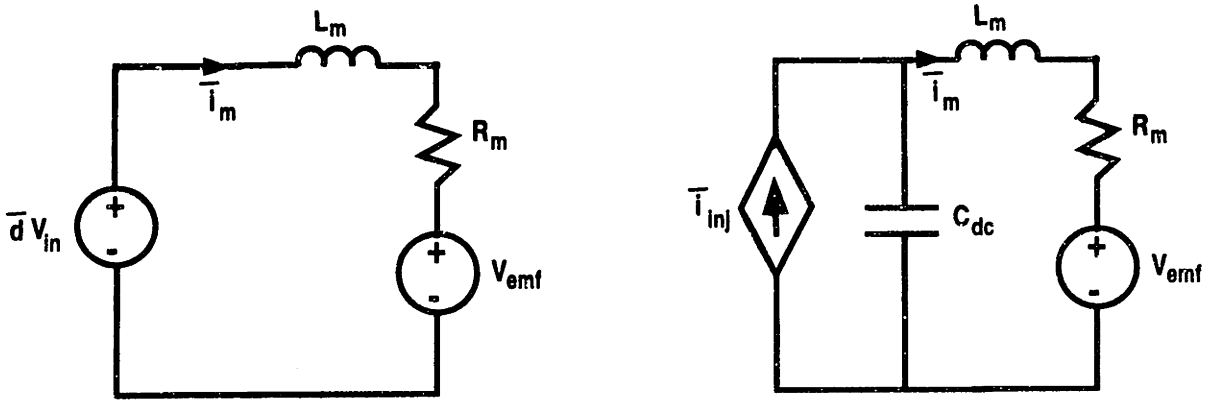

(a) Buck converter

(b) Boost converter

Figure 5-7: Average circuit models of buck and boost converters driving wheel motor.

where L_m is the synchronous inductance of the motor and R_m is the series resistance of two motor phases, a long as s is well below the switching freqency.

Figure 5-7(b) shows an averaged circuit model of the plant in the "boost-motoring" mode of operation. In this mode of operation the converter operates mostly in discontinuous conduction. Peak current-mode control is employed to suppress the dynamics associated with the boost inductor. We can therefore model the response of the motor current to the average injected current $\bar{i}_{inj}$ into the LCR tank circuit consisting of the boost output capacitors C_{dc}, the synchronous inductance of the motor L_m, and the phase to phase motor resistance R_m by

$$\bar{i}_m = \frac{1}{L_m C_{dc} s^2 + R_m C_{dc} s + 1} \bar{i}_{inj} - \frac{sC_{dc}}{L_m C_{dc} s^2 + R_m C_{dc} s + 1} V_{emf} \qquad (5.7)$$

Note that, unlike the buck operating mode, the plant has second-order dynamics which, in general, is more difficult to control compared to a first-order plant. The average motor current $\bar{i}_m$ is affected by the rate of change of the motor back-emf. Since we control $\bar{i}_m$ through $\bar{i}_{inj}$, the back-emf appears as a disturbance, the effect of which must be corrected by the feedback control system.

In discontinuous mode operation, the average injected current $\bar{i}_{inj}$ is related to the boost

inductor peak current I_{pk} by

$$\bar{i}_{inj} = \frac{L_u}{2T(V_{out} - V_{in})} \cdot I_{pk}^2 \quad . \tag{5.8}$$

Thus

$$I_{pk} = \sqrt{\frac{2T}{L_u}(V_{out} - V_{in})\bar{i}_{inj}} \tag{5.9}$$

and therefore to keep the loop linear, the microcontroller has to compute the proper peak inductor current from $\bar{i}_{inj}$ as shown in Equation (5.9).

5.3.2 Digital Controllers

The motor current control loops are implemented digitally with the MC68HC16Z1 microcontroller. The bandwidth of the vehicle controller which interprets driver commands and issues a torque command to the wheel motor controller is 20 Hz [21]. Therefore the bandwidth of the wheel motor torque controller has to be an order of magnitude above that of the vehicle controller to allow the two controllers to be designed independently. Thus, we aim to achieve closed loop bandwidths of 200 Hz for our motor current control loops.

Figure 5-8(a) shows the general block diagram of the discrete-time torque control system and Figure 5-8(b) shows the sequencing of events during a control interval. On the kth control cycle, the (k-1)th ouput of the controller is applied to the plant and the motor current, boost converter output voltage, and inverter input voltage are sampled and digitized. The digitized motor current is subtracted from the commanded current to generate a current error signal. This error signal is passed through a proportional plus integral (PI) compensator, the integral part being necessary to ensure zero steady-state error. The result is then added to a scaled version of the (k-1)th controller output to be applied to the plant at the next control cycle. When the motor is operating in the regime where the boost converter is active, the boost converter output voltage is also used in computing the output of the controller, as shown by the dashed line in Figure 5-8(a).

To compute the feedback gains necessary to yield our desired response, we need to represent our control system in discrete time state-space form. The state equations for

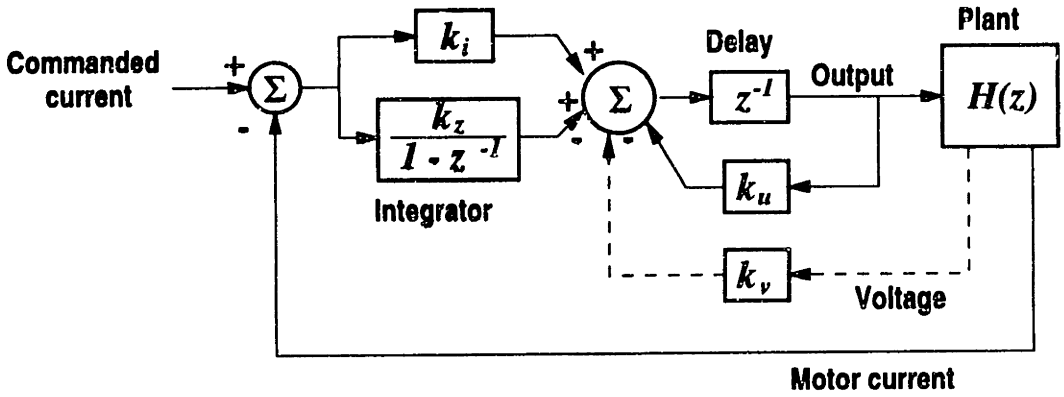

(a) Block diagram of controller. (Dashed line indicate voltage feedback for boost converter)

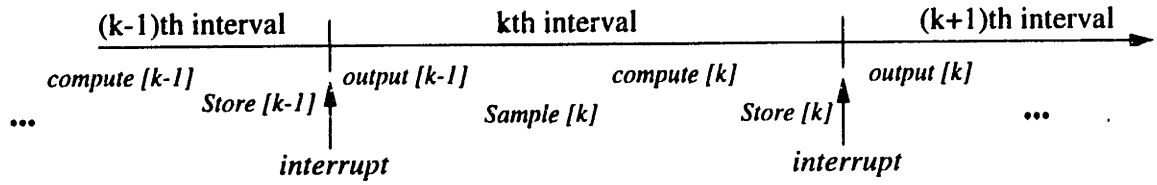

(b) Sequence of control events

Figure 5-8: General block diagram of buck and boost control loops.

continuous time linear time-invariant (LTI) system can be written in matrix form as

$$\mathbf{x}(t) = \mathbf{A}\mathbf{x}(t) + \mathbf{B}\mathbf{u}(t) \tag{5.10}$$

where $\mathbf{A}$ is the dynamic-coefficient or system matrix, $\mathbf{x}(t)$ is the state vector, $\mathbf{B}$ is the input-coupling matrix and $\mathbf{u}(t)$ is the input vector. Equation (5.10) can be represented in discrete time as

$$\mathbf{x}[k+1] = \mathbf{F}\mathbf{x}[k] + \mathbf{G}\mathbf{u}[k] \tag{5.11}$$

where

$$\mathbf{F} = e^{\mathbf{A}T_s} \tag{5.12}$$

$$\mathbf{G} = \mathbf{A}^{-1}\left(e^{\mathbf{A}T_s} - \mathbf{I}\right)\mathbf{B} \tag{5.13}$$

and T_s is the sampling period.

For the buck mode of operation, the continuous-time state-space equation for the plant

is given by

$$\frac{d}{dt}\bar{i}_m = -\frac{R_m}{L_m} + \frac{1}{L_m}(\bar{d}V_{in} - V_{emf}) \tag{5.14}$$

where the **A** and **B** matrices are scalars given by $-R_m/L_m$ and $1/L_m$ respectively. The discrete-time dynamic system that incorporates the integrator and the one-sample delay shown in Figure 5-8(a) is given by

$$\begin{bmatrix} \bar{i}_m[k+1] \\ z[k+1] \\ u[k+1] \end{bmatrix} = \underbrace{\begin{bmatrix} \mathbf{F} & 0 & \mathbf{G} \\ 1 & 1 & 0 \\ 0 & 0 & 0 \end{bmatrix}}_{\mathbf{M}} \begin{bmatrix} \bar{i}_m[k] \\ z[k] \\ u[k] \end{bmatrix} + \underbrace{\begin{bmatrix} 0 \\ 0 \\ 1 \end{bmatrix}}_{\mathbf{N}} q[k] \tag{5.15}$$

where the **F** and **G** matrices are defined as in (5.12) and (5.13). In Equation 5.15, the state variables z and u represent the output of the integrator and and one-sample delay element and the input $q[k]$ represents the controller's output in the kth control interval.

For the boost mode of operation, the continuous-time, state-space equation for the plant (assuming a constant back-emf) is given by

$$\frac{d}{dt}\begin{bmatrix} \bar{v}_{dc}(t) \\ \bar{i}_m(t) \end{bmatrix} = \underbrace{\begin{bmatrix} 0 & -\frac{1}{C_{dc}} \\ \frac{1}{L_m} & -\frac{R_m}{L_m} \end{bmatrix}}_{\mathbf{A}} \begin{bmatrix} \bar{v}_{dc}(t) \\ \bar{i}_m(t) \end{bmatrix} + \underbrace{\begin{bmatrix} \frac{1}{C_{dc}} \\ 0 \end{bmatrix}}_{\mathbf{B}} \bar{i}_{inj}(t) \quad . \tag{5.16}$$

In this case, the corresponding discrete-time dynamic system that incorporates the integrator and the delay shown in Figure 5-8(a) is given by

$$\begin{bmatrix} v_{dc}[k+1] \\ \bar{i}_m[k+1] \\ z[k+1] \\ u[k+1] \end{bmatrix} = \underbrace{\begin{bmatrix} \begin{bmatrix} F_{11} & F_{12} \\ F_{21} & F_{22} \end{bmatrix} & \begin{bmatrix} 0 \\ 0 \end{bmatrix} & \begin{bmatrix} G_{11} \\ G_{21} \end{bmatrix} \\ 0 & 1 & 1 & 0 \\ 0 & 0 & 0 & 0 \end{bmatrix}}_{\mathbf{M}} \begin{bmatrix} v_{dc}[k] \\ \bar{i}_m[k] \\ z[k] \\ u[k] \end{bmatrix} + \underbrace{\begin{bmatrix} 0 \\ 0 \\ 0 \\ 1 \end{bmatrix}}_{N} q[k] \tag{5.17}$$

where the **F** and **G** matrices are again as defined in (5.12) and (5.13).

Given a row vector **P** which contains the desired pole locations of the closed loop system, the **M** and **N** matrices in (5.15) and (5.17) are used to compute the state feedback

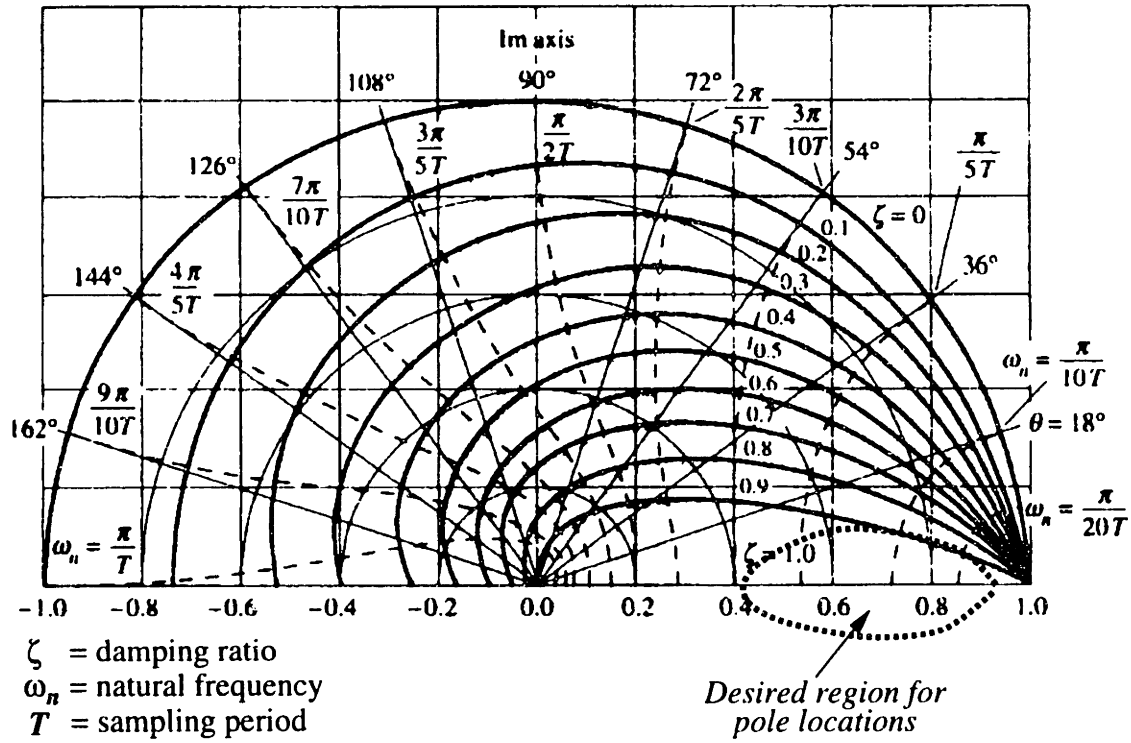

Figure 5-9: Desired region for pole placement

matrix **K** such that the eigenvalues of **M** – **NK** are those specified in vector **P**. The elements of **K** are the feedback gains k_i, k_z, k_u, and k_v when operating in the boost mode. Given the state-transition matrix **M**,the input vector **N**, and the desired pole location vector **P**, the "place" routine in the Matlab[4] control toolbox is used to compute the state feedback matrix **K**.

Figure 5-9 shows the relationship between the pole locations in the z-plane and the natural frequency ω_n and the damping ratio ζ for a standard all-pole, second-order system [57]. Even though our two control systems are of higher order (third order for the buck and fourth order for the boost) we will approximate their response to be second order by placing the poles such that there is a dominant complex pole-pair. Unlike the standard all-pole second-order system, ours contains transmission zeros. Thus for a given damping ratio ζ, our system response will exhibit a higher overshoot than a all-pole second order

[4]Matlab is a registered trademark of The Mathworks, Inc., 24 Prime Park Way, Natick, MA 01760

system. The settling time T_{st} to a step input can be approximated as

$$T_{st} = \frac{4}{\zeta \omega_n}. \tag{5.18}$$

For our control loops, we seek a settling time 5 ms or less. Thus for a sampling period of 244 μs we seek to place our closed loop poles in the general area demarcated by the dotted line in Figure 5-9. Once initial feedback gains are obtained from Matlab, the control loops are simulated and fine-tuned with Simulink[5]. Simulations of the response of the two control systems are given in Chapter 6.

5.4 Experimental Circuit Implementation

Figure 5-10 shows a schematic diagram of how the inverter power circuit, microcontroller and user interface are interconnected. Desired motor torque and motor direction commands are input via a potentiometer and a keypad. The microcontroller interprets user input commands and controls the switching of the IGBTs S_1 - S_8 to meet user demands. The battery voltage, boost converter output voltage, boost inductor current, and two of the motor phase currents are sensed and used for control. A shaft encoder is implemented via three Hall-effect sensors, the signals from which are not only used for commutation but also for motor speed calculations. A 16-character by 4-line Optrex Liquid Crystal Display (LCD)[6] is used to display relevant input and output data which may consist of commanded motor torque, motor speed, battery voltage and other parameters of interest.

5.4.1 Commutation circuits

To determine rotor magnet position relative to the stator windings, we use SS461A latching, open collector, digital Hall sensors by Micro Switch [58]. These devices have an operating temperature range of -40°C to +150°C, and operate from a dc supply voltage of 3.8 - 24 V. The maximum operate and minimum release points are 100 Gauss and -100

[5]Simulink is a registered trademark of The Mathworks, Inc., 24 Prime Park Way, Natick, MA 01760
[6]Optrex Corporation part no. DMC16433

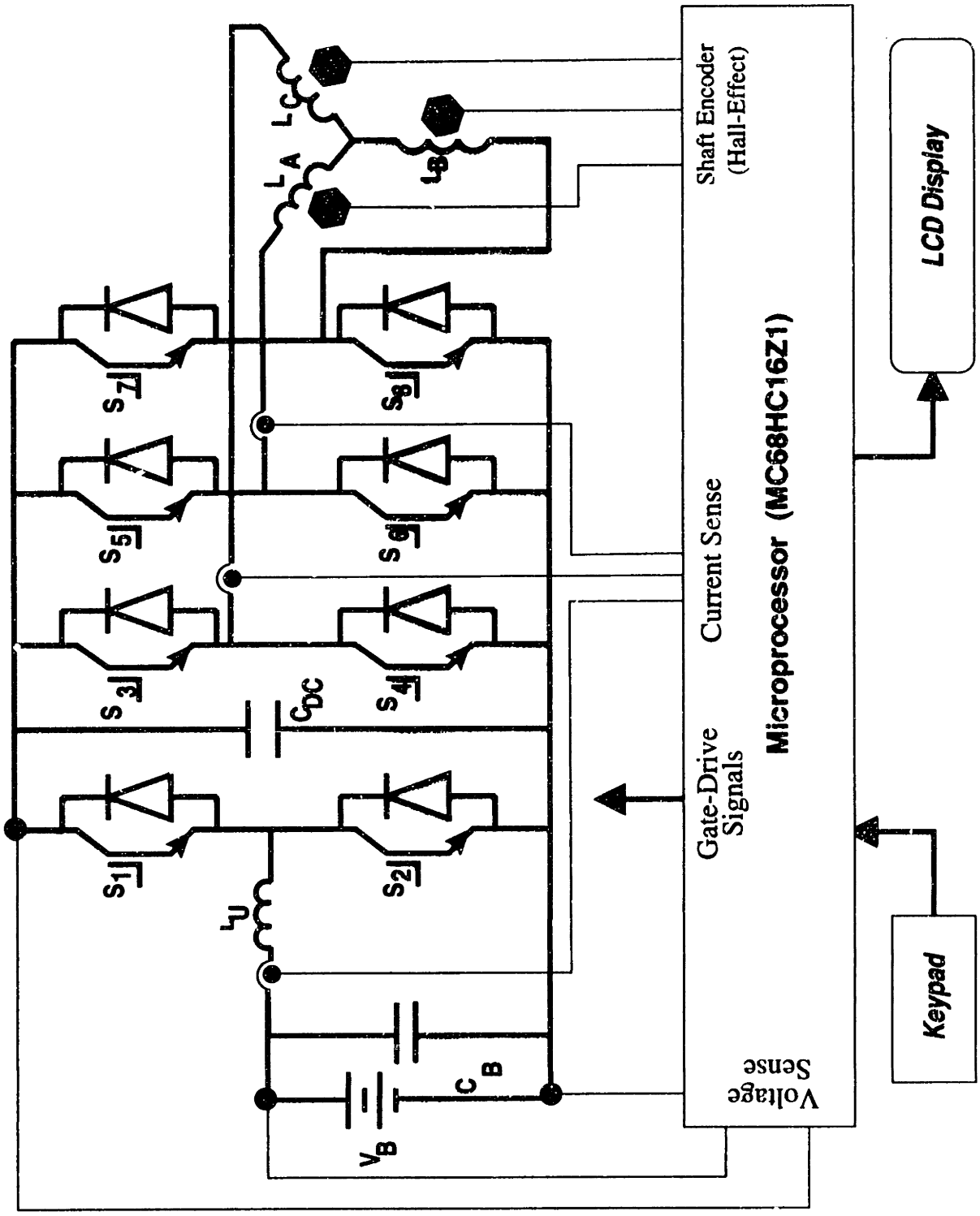

Figure 5-10: Schematic diagram of inverter implementation.

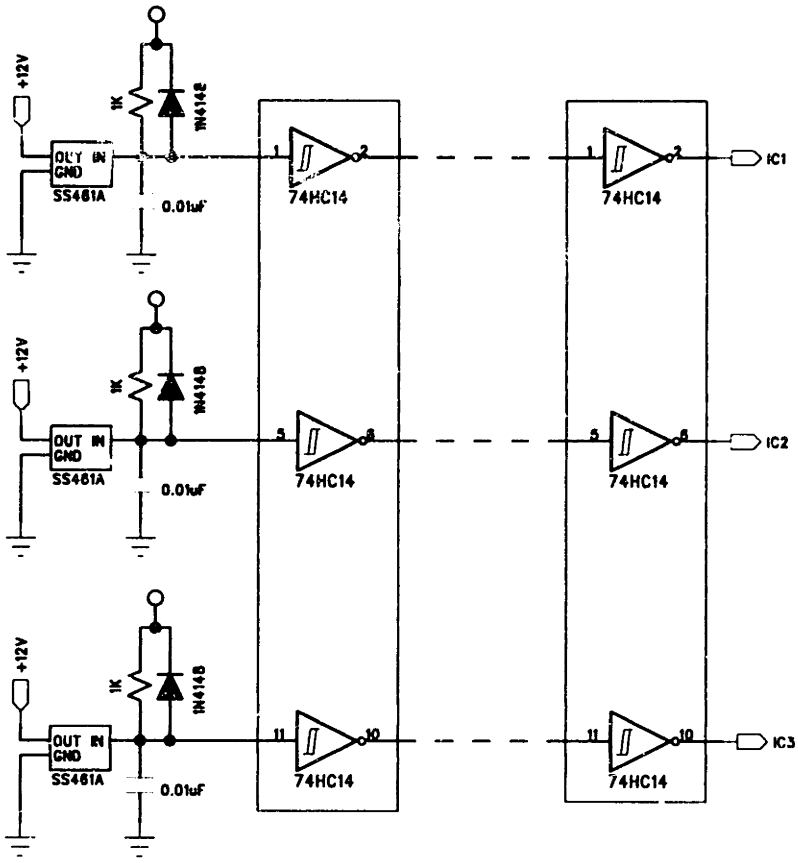

Figure 5-11: Hall sensor - microcontroller interface circuitry

Gauss respectively[7]. Figure 5-11 shows the circuitry that interface the Hall sensors to the microcontroller. The three Hall sensors are mounted 120° on the stator to detect the rotor magnet's fringing fields, and the resulting 3-phase digital output signals are transported to the input-capture port of the General Purpose Timer (GPT) of the microcontroller. The Hall signals are phase-locked in sofware within the microcontroler and are used to compute motor RPM. The RPM computed is used to estimate the motor's back-emf constant as well as adjust the user-commanded torque accordingly when it falls outside the constant power boundary. The phase-locked signals, which can be phase advanced in software to better align the Hall signals to the motor back-emf waveforms, are output through the output-compare pins of the GPT and used as inputs to combinational logic used to commutate the motor.

[7]Operate and release points are strength of the magnetic fields needed to turn on and off the open collector transistor repectively

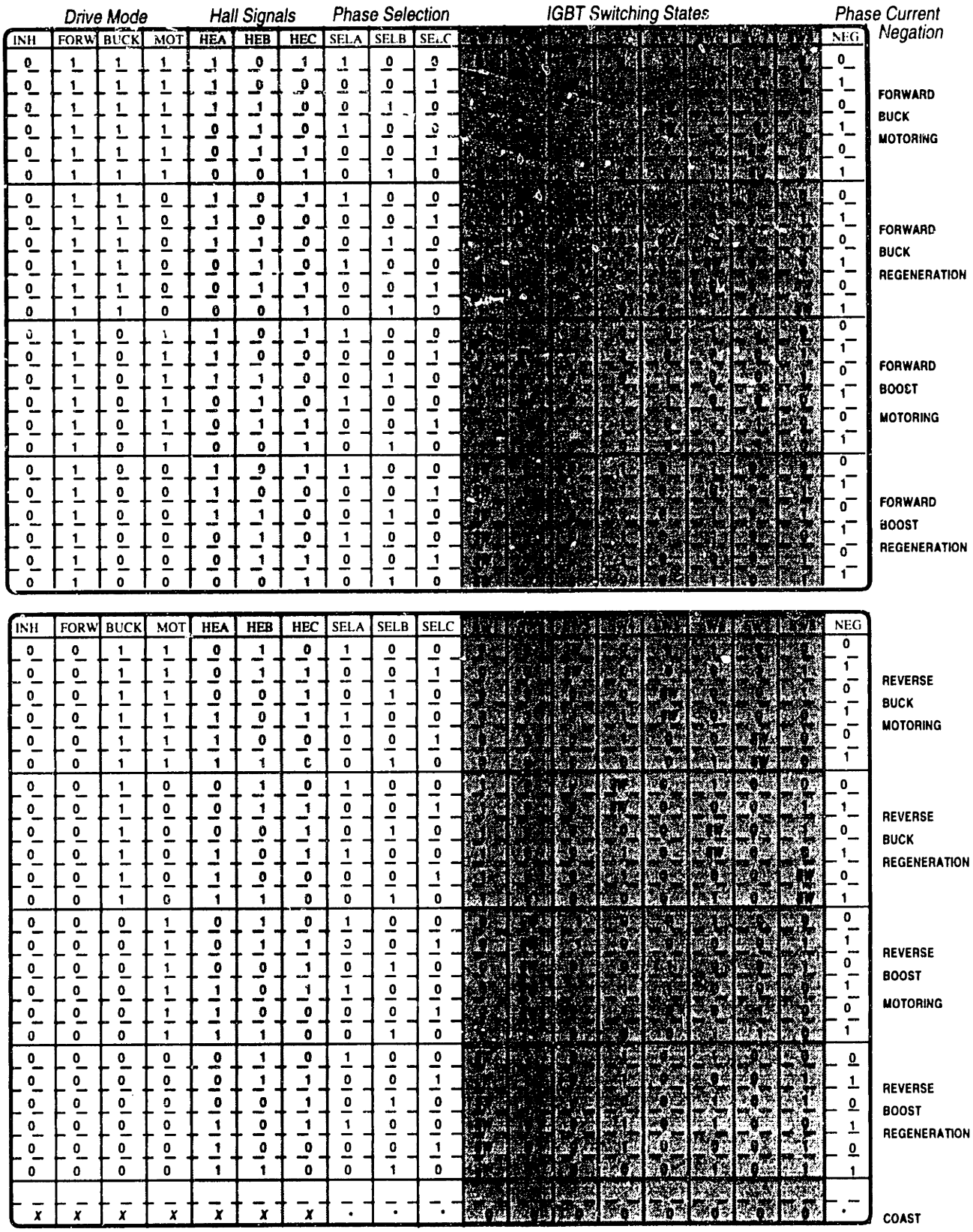

* *Phase selection and negation does not depend on INH*

Figure 5-12: Truth table for motor commutation and phase selection.

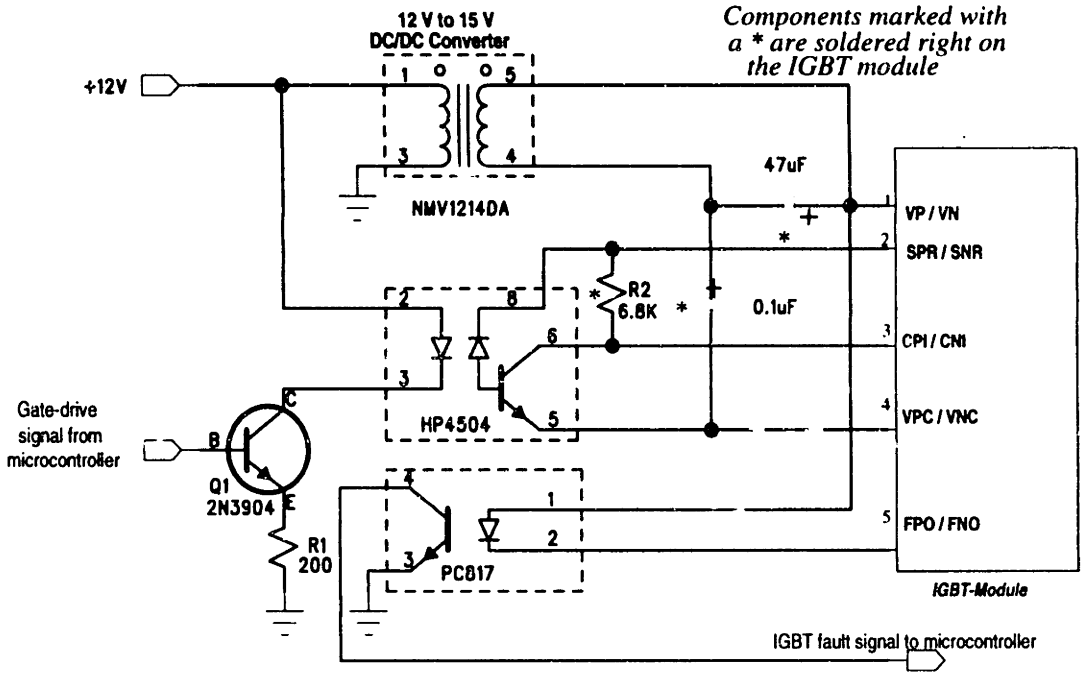

Figure 5-13: Gate-drive interface circuitry.

Figure 5-12 is a truth-table that shows how the IGBTs are switched depending on the mode of operation of the inverter. When the INH signal is asserted the drive is disengaged and the motor coasts. The FORW signal sets the direction of motor rotation to forward. The BUCK signal indicate that the motor back-emf is below the battery voltage and the MOT signal indicate that the motor is motoring as opposed to regeneration. The signals HEA, HEB, and HEC are Hall-effect signals for phases A, B, and C respectively. The SELA, SELB, SELC signals indicate the phase current to be used for the torque feedback loop, and NEG indicates whether the corresponding phase is sourcing or sinking current. Finally, the switching of the IGBTs are controlled by SW1-SW8. The combinational logic for phase-current selection and the switching of the IGBTs are implemented in programmable gate-array logic chips (GALs) and the source code for programming these GALs are included in Appendix B.1 and B.2 respectively.

5.4.2 Gate Drive Circuits

The half-bridge Intellimod IGBT modules contain integral gate-drive and protection circuitry. A NMV1215DA 12 V to 15 V isolated dc-dc converter is used to provide power

to module's internal circuitry as shown in Figure 5-13[8]. Gate-drive signals from the microcontroller are supplied to the module via an HP4504 high-speed optocoupler. IGBT fault signals are retrieved through the low-speed PC-819 optocouplers. In principle, only the power supplies to the high-side IGBTs must be isolated, but in the interest of noise minimization and protection of the control board in the event of an IGBT fault, each IGBT is provided with its own isolated supply.

5.4.3 Analog Instrumentation Circuits

The battery voltage, boost converter output voltage, boost inductor current, and two of the motor phase currents are needed for control and display purposes. These low-level analog signals must be acquired from the noisy power circuit environment and transported to the analog/digital control board for amplification and filtering before being used for control. Figure 5-14(a) and (b) show the analog circuits used to acquire the input and output voltages of the inverter. The input voltage and the boost converter output voltage are attenuated via a Zener-protected, high-impedance resistive divider. These signals are transported as differential pairs to the analog/digital control board via a ribbon cable where they are filtered and amplified by Burr Brown INA105 instrumentation amplifiers[9]. The instrumentation amplifiers are preceded by voltage followers for improved common-mode rejection. Both signals are fed into the analog-to-digital (A/D) converter where they are digitized and used for control. The boost converter output voltage signal is also used in conjunction with an analog comparator, as shown in Figure 5-14(c), to generate an output-overvoltage signal which is used to quickly disable the boost converter when its output voltage gets too high.

The boost inductor current is needed for current mode control of the boost converter and also to for controlled charging of the battery during regenerative braking. The current is sensed with a closed-loop Hall-effect current sensor, the output current of which represents the inductor current divided by 2000. The output current of the sensor is converted to a voltage by loading it with a 50 Ω, 1 % precision resistor. The resulting voltage signal,

[8]NMV1215DA is a product of International Power Sources Inc., 200 Butterfield Dr., Ashland, MA 01721
[9]Connections through the ribbon cable are indicated by dashed lines in the figures

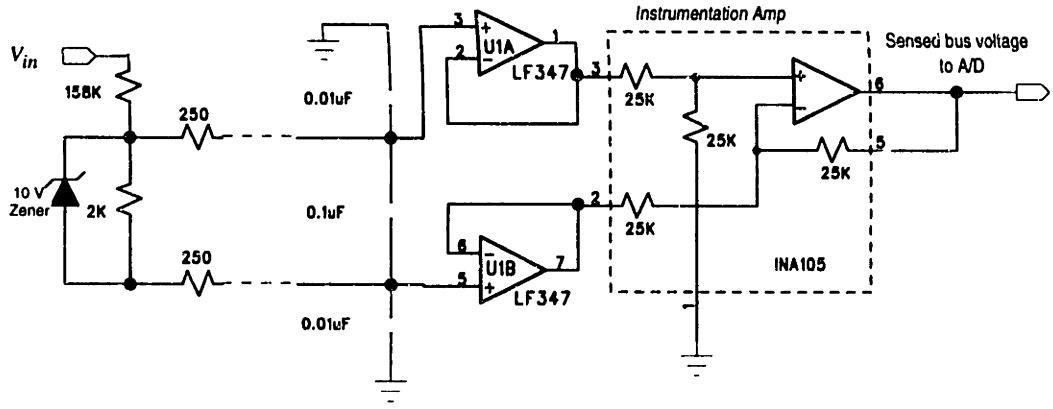

(a) Bus voltage sensing circuit

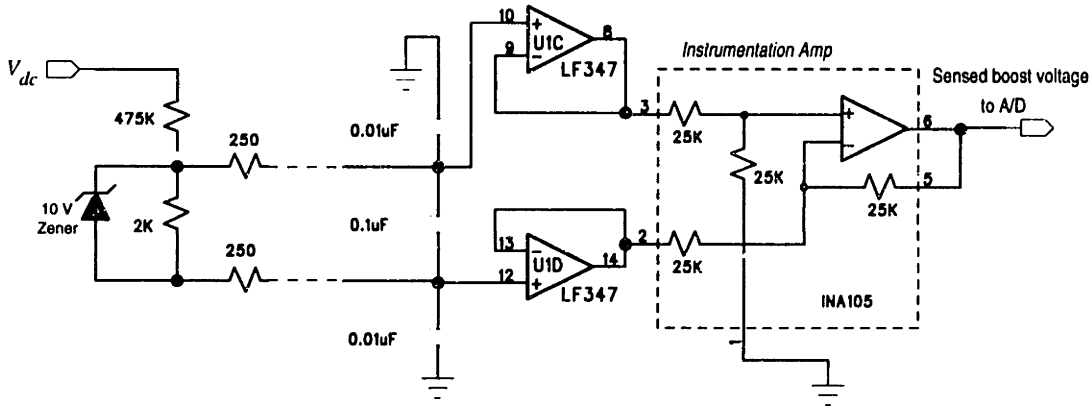

(b) Boost voltage sensing circuit

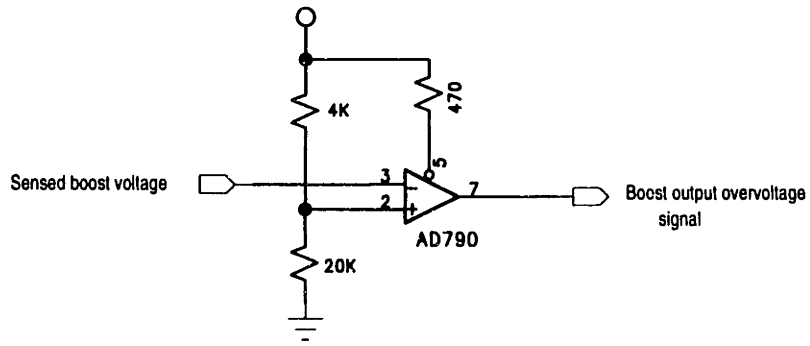

(c) Boost overvoltage comparator

Figure 5-14: Bus voltage and Boost output voltage sensing circuit.

along with its ground, is transported through the ribbon cable to the analog/digital control board where it is filtered and amplified by a Burr Brown INA111 instrumentation amplifier, as shown in Figure 5-15(a). The sensed inductor current is scaled and level shifted for digitization by the A/D converter as shown in Figure 5-15(b). The current signal is also

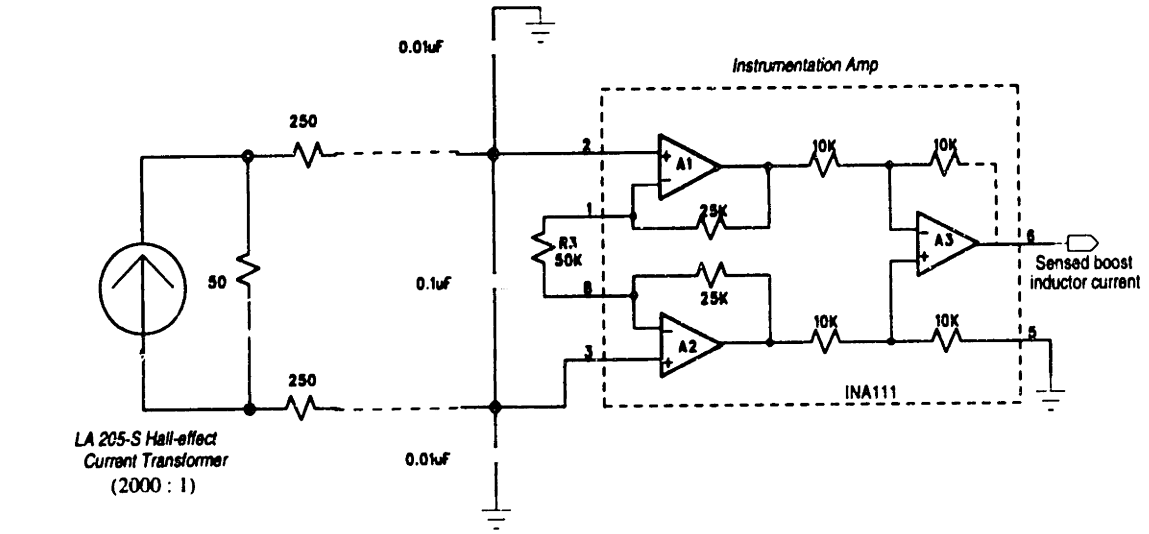

(a) Boost inductor current sensing circuit

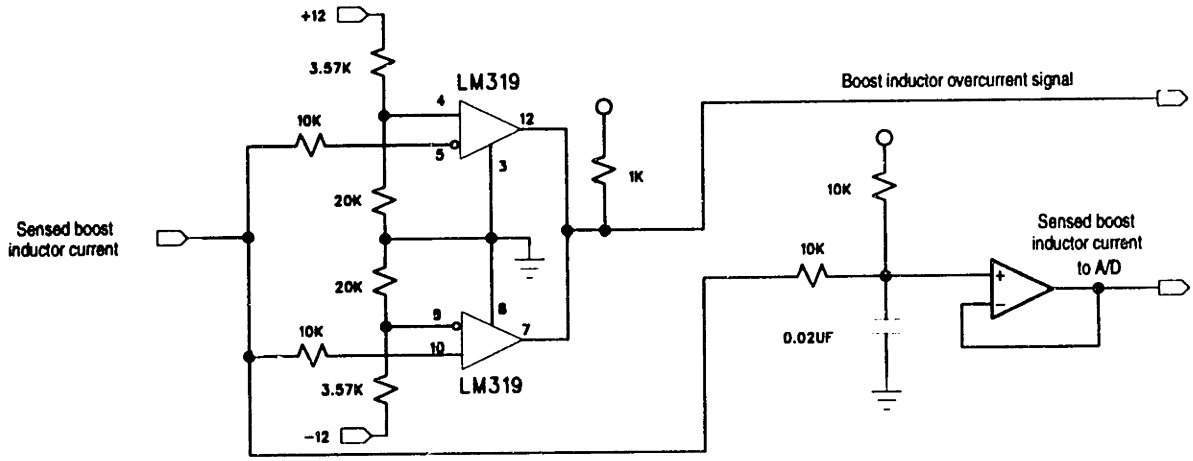

(b) Boost inductor overcurrent circuit and A/D pre-filtering circuit

Figure 5-15: Boost inductor current sensing circuit.

used to generate an over-current signal which is used as additional protection for the semiconductor switches.

The three motor phase currents always sum to zero. We therefore sense two of the phase currents and generate the third electronically, as shown in Figure 5-16(a). Under normal operation, except during commutation, only two phases conduct current at a time; one being the source and the other being the sink. To regulate the motor current, we close a feedback loop around the current in one of the current-carrying phases. To speed up the commutation of current between phases, we close the feedback loop around the newly commutated motor phase. This control strategy has the effect of raising the voltage available

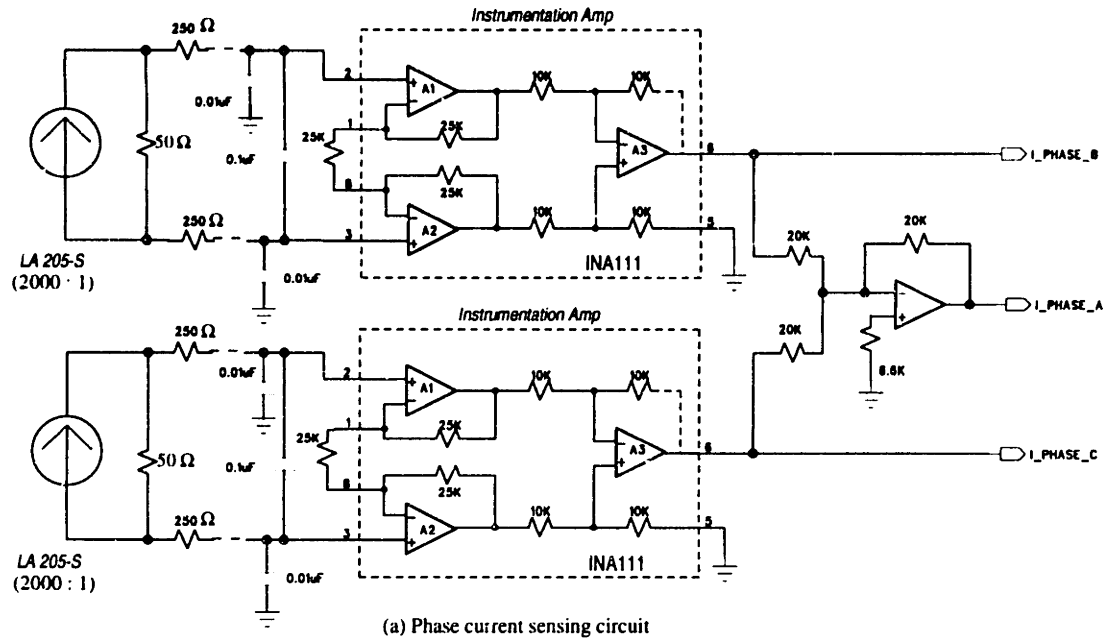

(a) Phase current sensing circuit

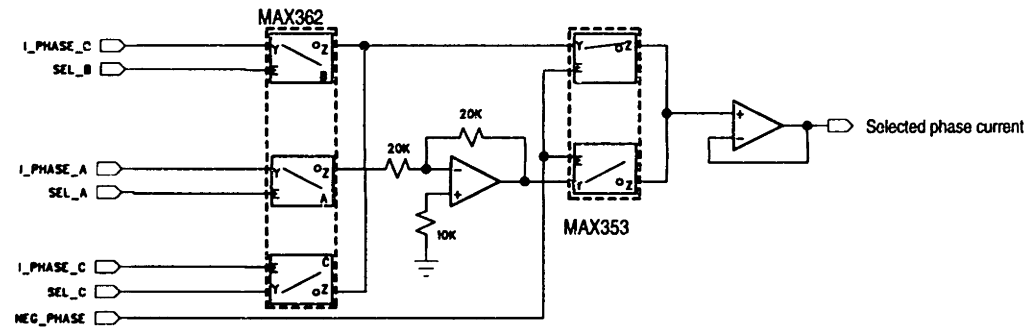

(b) Phase current selection circuit

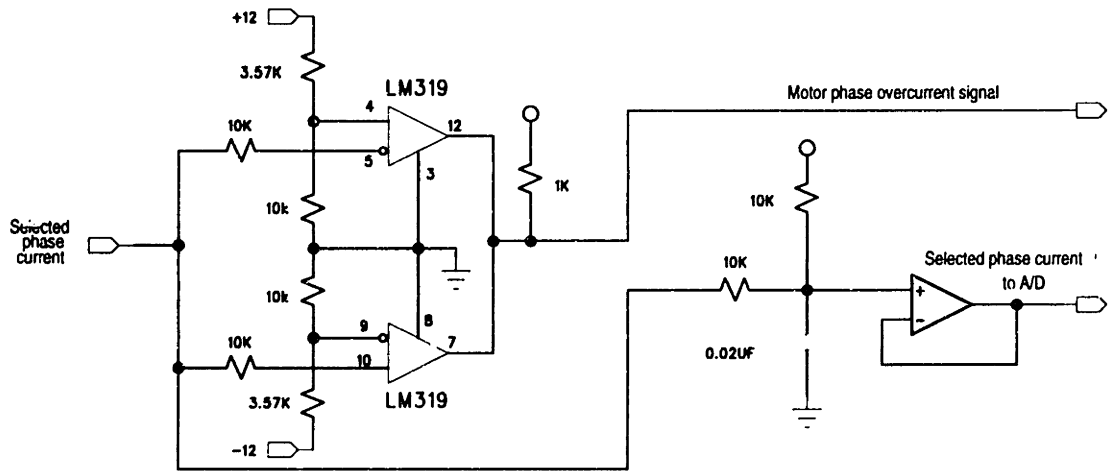

(c) Motor overcurrent and A/D pre-filtering circuit

Figure 5-16: Phase current sensing and selection circuitry.

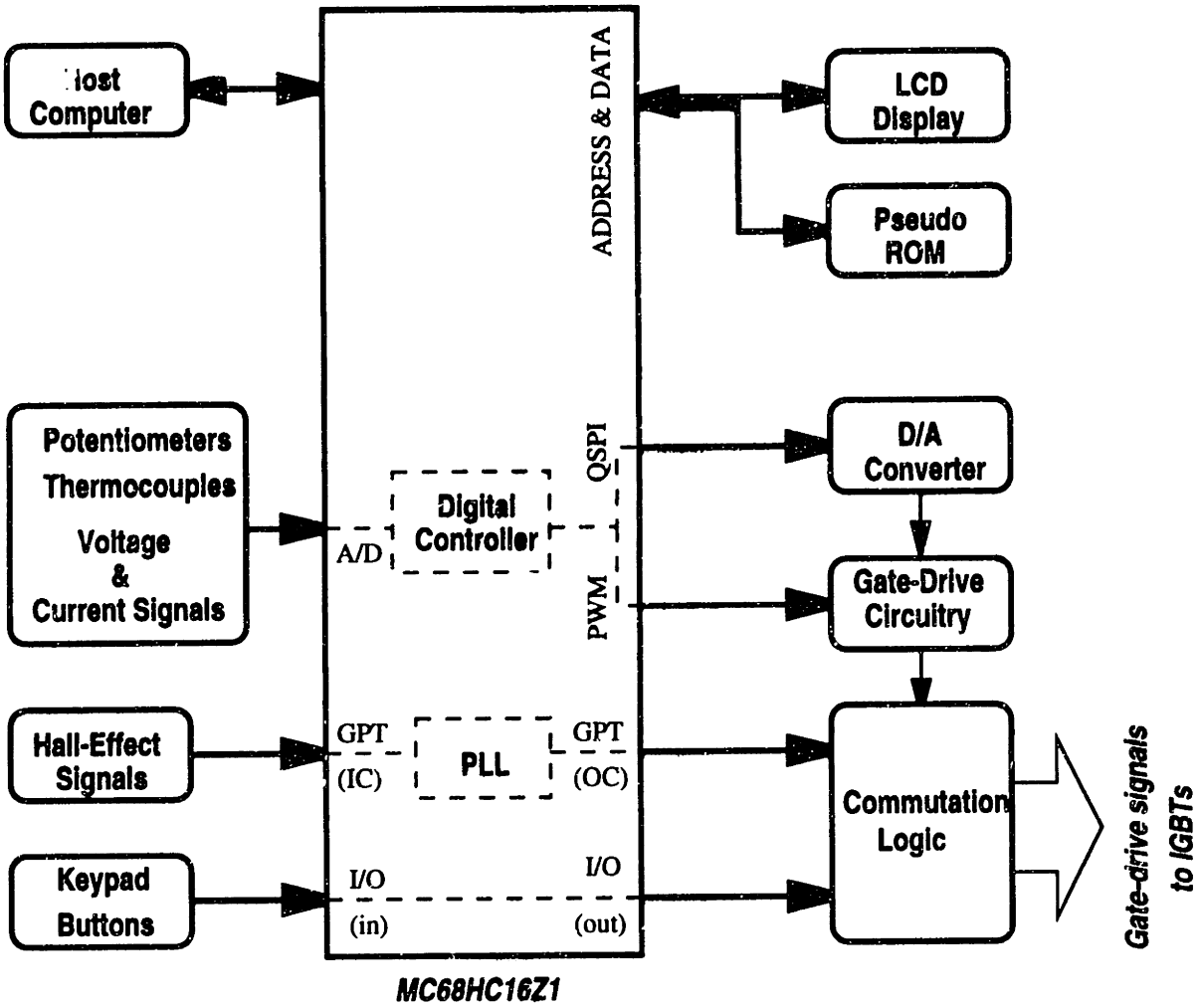

Figure 5-17: Connectivity and data flow between the MC68HC16Z1 and its peripherals.

to build up current in the newly commutated motor phase. The selected phase current in Figure 5-16(b) is scaled and level-shifted for digitization by the A/D converter as shown in Figure 5-16(b). The phase current signal is also used to generate a motor over-current signal to prevent demagnetization of the rotor permanent magnets.

5.4.4 Microcontroller and Peripheral Digital Circuits

The microcontroller used in our experimental prototype is the Motorola MC68HC16Z1, a sixteen-bit microcontroller with 1K of on board Random Access Memory (RAM). A system block diagram showing the connectivity and data flow between the microcontroller to its peripherals is shown in Figure 5-17. The MC68HC16Z1 is equipped with two

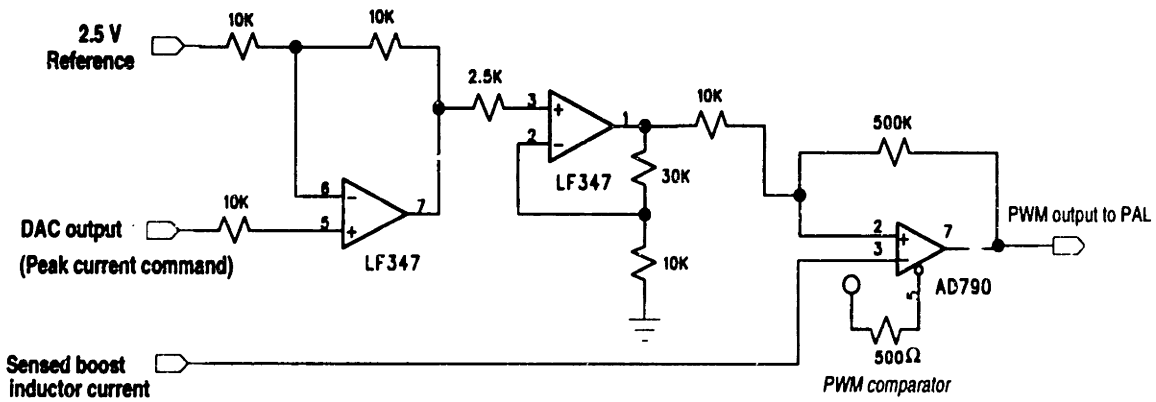

Figure 5-18: DAC post-processing circuit and current-mode PWM implementation.

programmable pulse-with modulator (PWM) ports, one of which is used to implement duty-cyle control of the buck portion of the inverter, while the other is used to implement current-mode control of the boost section of the inverter.

The MC68HC16Z1 features an eight-channel, 10-bit A/D converter with 10 μs conversion time. This A/D converter is used to sequentially digitize the battery voltage, boost converter's output voltage, the selected motor phase current, the boost inductor current, the torque and brake user commands which are issued via potentiometers, and the motor's winding temperatures supplied via thermocouples.

The Queued Serial Peripheral Interphase (QSPI) is used transmit the computed value of peak current for the boost inductor for each control interval to a 12-bit serial D/A converter (DAC). The DAC used is the MAX537 by Maxim Integrated Products. The output of this 12-bit serial DAC is unipolar. Therefore additional external circuitry is needed to implement a bipolar output. As shown in Figure 5-18, the output voltage of the DAC is level shifted and amplified so that the 0 V - 2.5 V output swing of the DAC is mapped to -10 V and +10 V. This voltage is fed into one input of a high-speed comparator with hysteresis which is compared with the sensed boost inductor current to generate a current-mode PWM signal.

User torque commands are input to the controller via a potentiometer on the analog/digital control board. In addition to a torque command input, the user can set the direction of rotation of the motor, engage and disengage the drive via an array of pushbutton switches shown in Figure 5-19.

The MC68HC16Z1 processor comes on an evaluation board (MC68HC16Z1EVB)

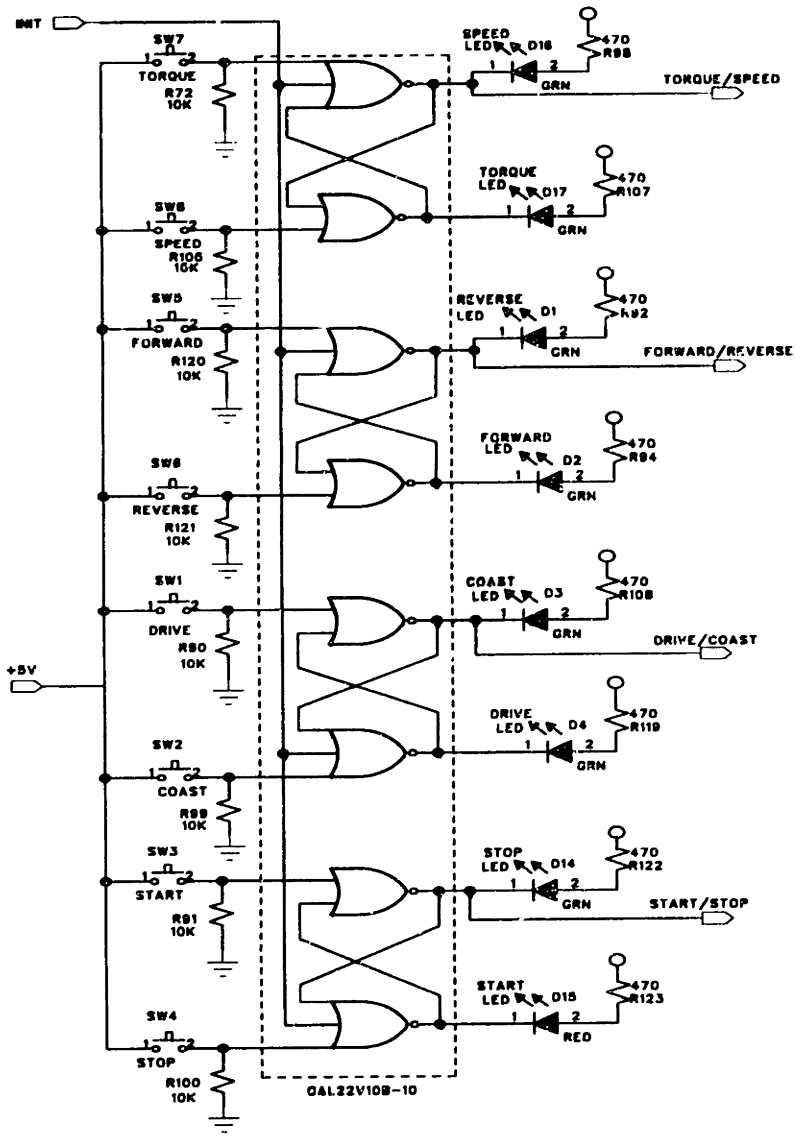

Figure 5-19: Schematic of user-input keypad.

which facilitates the downloading of assembled code from the host computer into a 32Kx16 block of RAM (used as pseudo-ROM) for execution by the microcontroller. The evaluation board also facilitates debugging by allowing the user the capability of displaying and modifications of memory locations, stack manipulations, and control over program execution. Figure 5-20 shows a simplified flow chart of the microcode for the experimental prototype described in this thesis. The complete assembly language code is included in Appendix E.

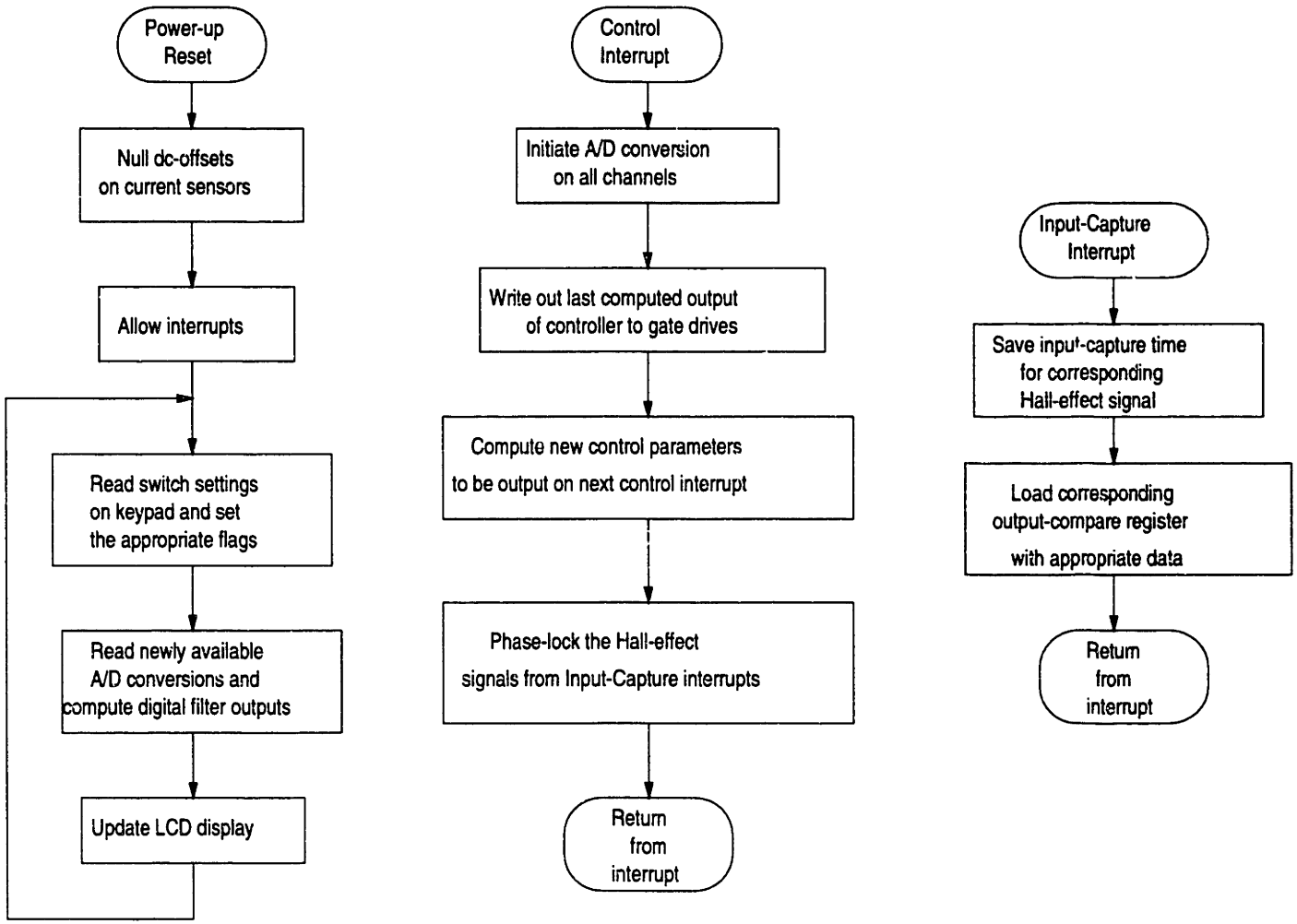

Figure 5-20: Simplified flow chart of microprocessor control code.

Chapter 6

Prototype Fabrication and Experimental Results

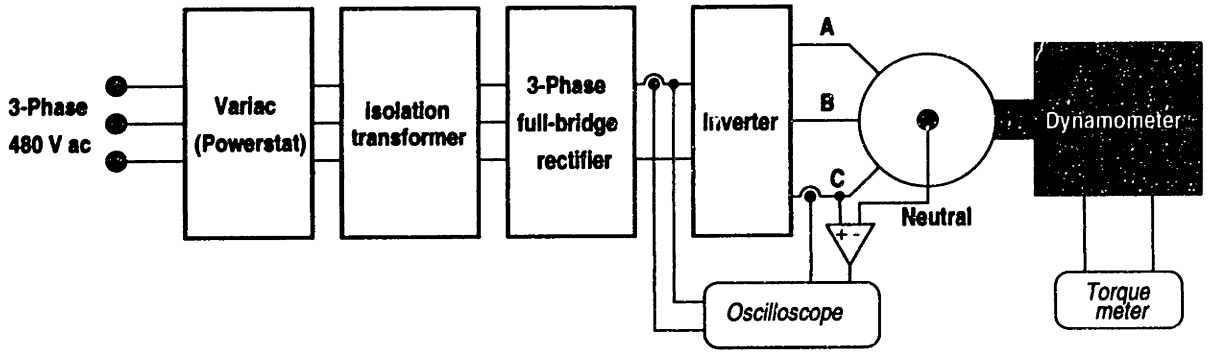

Figure 6-1: Schematic diagram of experimental setup.

Figure 6-1 shows a schematic diagram of the experimental system used to evaluate the performance of the prototype wheel motor and inverter. Due to the unavailability of a traction battery at the test site, the inverter was powered off a rectified 3-phase ac source. As shown in the figure, a variable autotransformer (Powerstat[1]) was powered off a 480 V line. The output of the Powerstat, which was variable from 0 to 240 V, was fed into a 30 kVA 3-phase isolation transformer. The output of the isolation transformer was then full-wave rectified by a 3-phase diode bridge and used as the input power source to the inverter. The wheel motor was connected to a dynamometer which was controlled by a four-quadrant

[1]Powerstat is a registered trade-mark of Superior Electric Company.

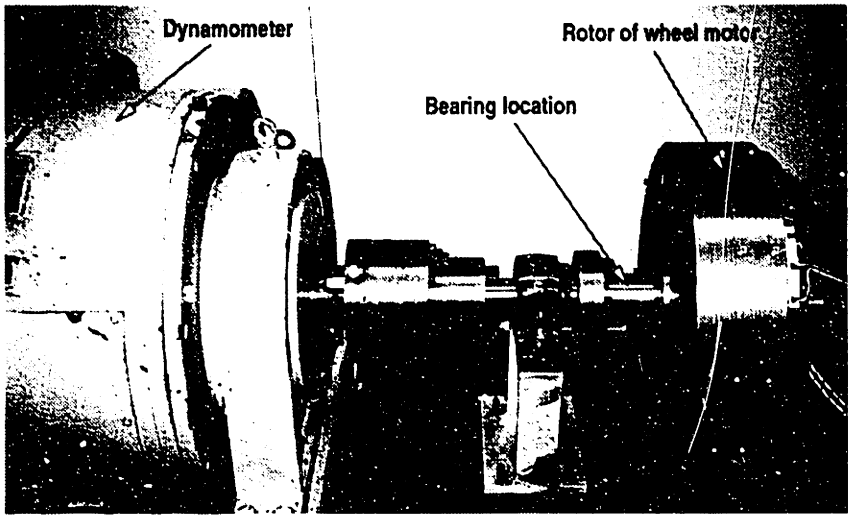

(a) Photograph showing coupling of wheel motor to dynnamometer

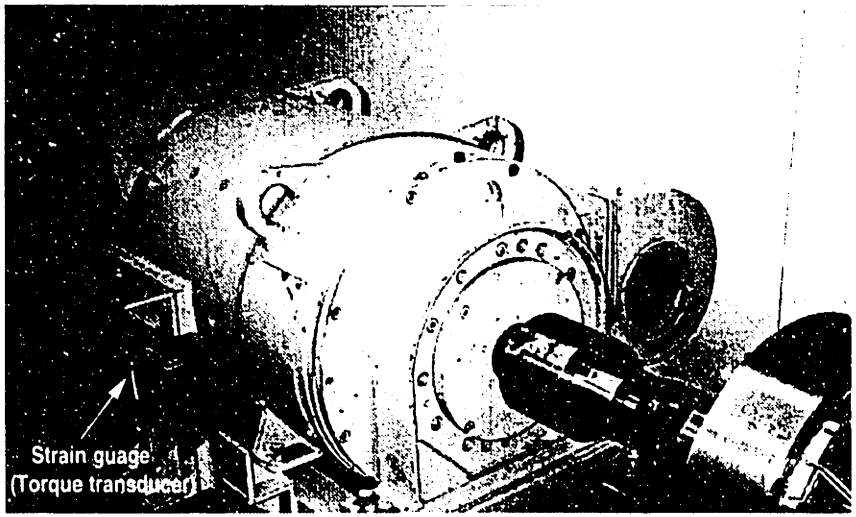

(b) Photograph of dynamometer showing torque transducer

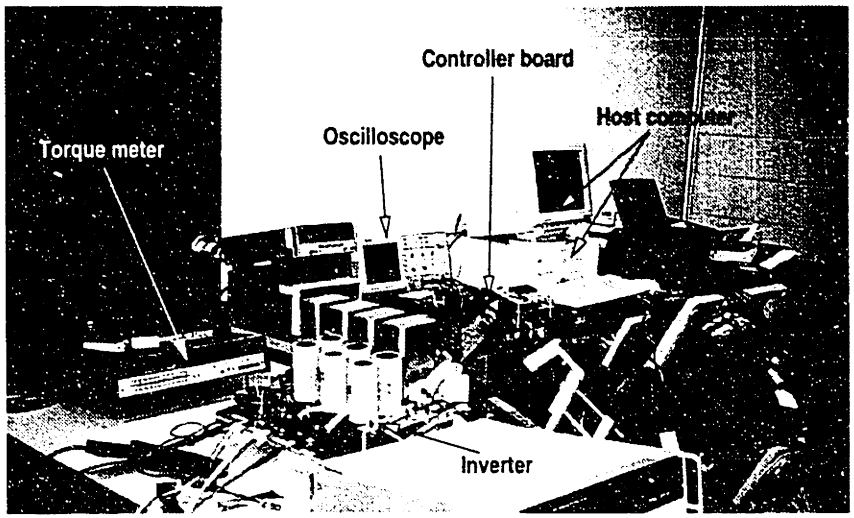

(c) Photograph of torque meter, inverter, contr ler board, host computer and other instrumentation equipment

(d) Photograph of inverter for dynamometer

Figure 6-2: Photographs of experimental setup.

inverter. The torque output, as measured with a strain guage on the dynamometer, was fed to a digital readout. The inverter input voltage, input current, and the motor phase-to-neutral input voltage and phase current were measured with a four-channel Tektronix TDS520 digital oscilloscope[2]. The inverter input current and motor phase currents were sensed with a 100 A Tektronix dc current probe. Figure 6-2 shows photographs of the experimental setup.

6.1 Inverter Construction

Figure 6-3 shows the inverter at various stages of construction. To remove switching and conduction losses, the IGBT modules were mounted on a water-cooled aluminum heatsink as shown in Figure 6-3(d). Low-inductance polypropylene snubber capacitors were mounted directly across the terminals of the IGBT modules, as shown in Figure 6-3(a)to minimize voltage overshoot and undershoot from the switching of the power devices. The boost converter output capacitors, shown in Figure 6-3(b), are connected to the IGBTs via the use of L-shaped copper tabs, machined to yield a low inductance connection. The high-voltage buss bar at the output of the boost converter was separated from neighboring conductors by at least 1 cm to prevent flashover from dielectric breakdown. As mentioned in Section 5.2.2, due to the unavailability of appropriate 1200 V capacitors at the time of inverter construction, 1500 V capacitors were used, thus making the boost converter output capacitors 1.5 times larger than necessary.

The isolated dc-dc converters and optocoupler circuits for the gate drives to the IGBTs were wire-wrapped on a perforated board and mounted vertically in close proximity to the IGBTs as shown in Figure 6-3(c). A multiconductor ribbon cable connected this board to the analog/digital control board which in turn connected to the MC68HC16Z1 evaluation board. Detailed schematic diagrams of the inverter's low-voltage electronics are attached in Appendix A.

[2]The phase-to-neutral voltage was measured with a Tektronix P5200 high-voltage differential probe.

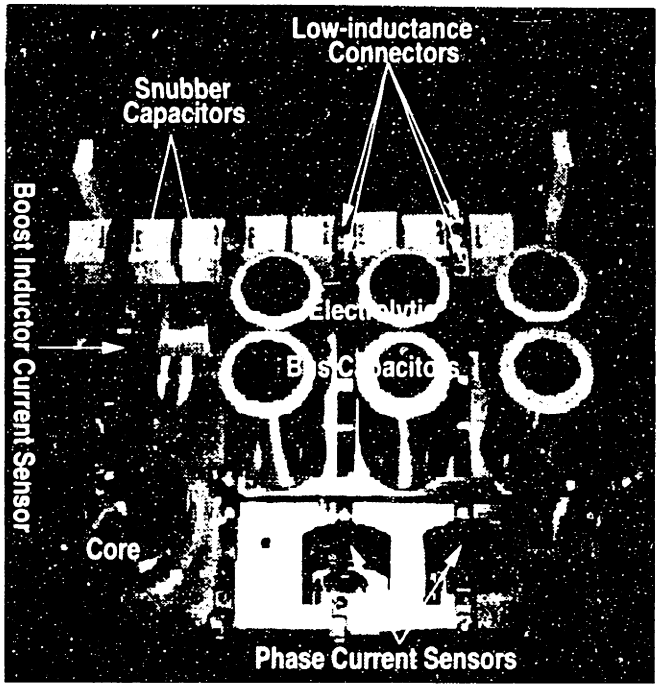

(a) Top view showing snubber capacitors and low-inductance connector tabs

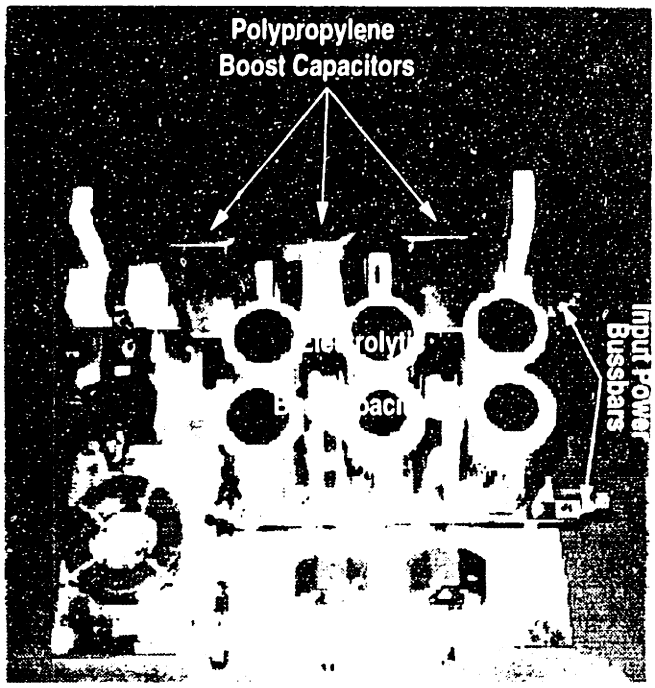

(b) Top view showing assembly of boost converter output capacitors

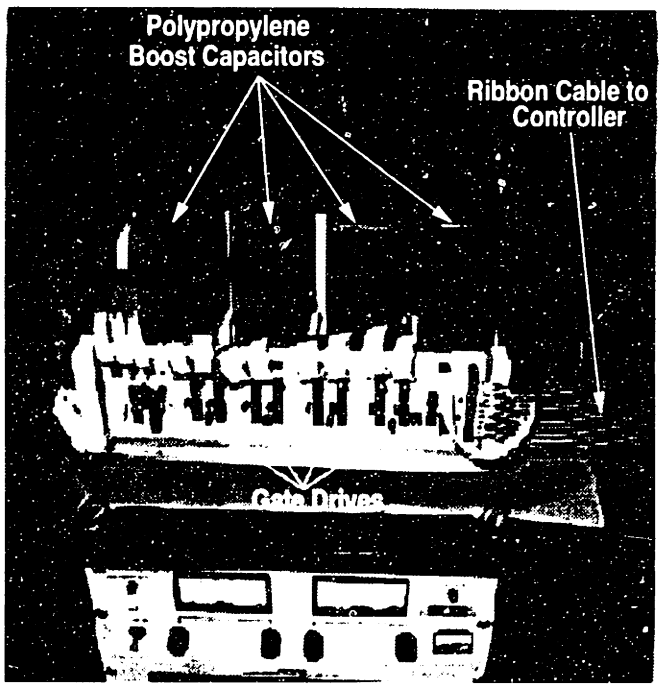

(c) Front view showing gate drives

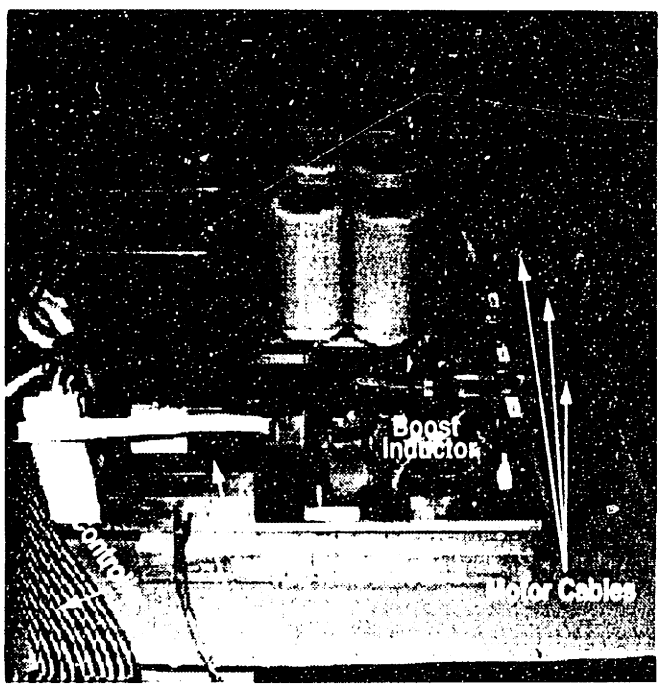

(d) Side view showing IGBT module, heatsink, and connecting cables

Figure 6-3: Prototype inverter at various stages of construction.

6.2 Motor Construction

The fabrication of the prototype wheel motor was subcontracted to the Superior Electric Company, a motor manufacturing company in Bristol, CT. Figures 6-4 and 6-5 show the motor at various stages of construction. The rotor magnets were machined to the specifications in Figure 3-16 out of Hicorex ND Grade H-97CB material and were supplied by Hitachi Magnetics Corporation in Edmore, MI. The magnets were chromate plated to prevent rusting and had an energy product of 33.44 MGOe. Due to equipment limitations in machining the magnet arcs, each magnet pole was made out of four pieces and glued together. The magnets were then glued on the rotor back-iron as shown in Figure 6-4(a). The rotor back-iron was made out 1018 HF steel supplied by Normag Inc. at Bridgeport, CT. Unlike the stator steel which experiences substantial changes in its magnetic flux density, the rotor turns at the synchronous speed and therefore does not experience substantial variations in magnetic flux density. Therefore the rotor back-iron was made from solid steel, instead of glued laminations, to insure structural integrity. Figure 6-4(b) shows the assembled rotor with the end-bell attached. Due to our desire to keep one end of the motor open for ease of instrumentation, the rotor was cantilevered with bearings on only one side of the stator.

Figure 6-4(c) shows the jig used to skew the stator laminations. The stator laminations were laser-cut from M-15, 29 gauge (14 mils), fully-processed, nonoriented electrical steel. The lamination stack was skewed by one slot pitch. The skewing was accomplished with the aid of two bars, slanted at the skewing angle of 17° from vertical, which guided the laminations as they were stacked. Figure 6-4(d) shows the the glued stator lamination stack mounted for winding. This photograph was taken during the second attempt to wind the motor with a 5-mil Kapton slot-liner. Both attempts resulted in high-potential failures due to abrasion caused by the uneven edges of the skewed lamination stack within slots. To guard against punchthrough of the slot-liner by the edges of the skewed laminations, 10-mil Nomex slot-liners were used. Initial attempts were made to wind the motor with AWG 10 solid square wire, but the wire was difficult to bend and the endturns became unmanageable, as they built up rapidly radially. In order to prevent the radial buildup where the phases cross over each other at the endturns, parallel strands of smaller gauge wires were used so

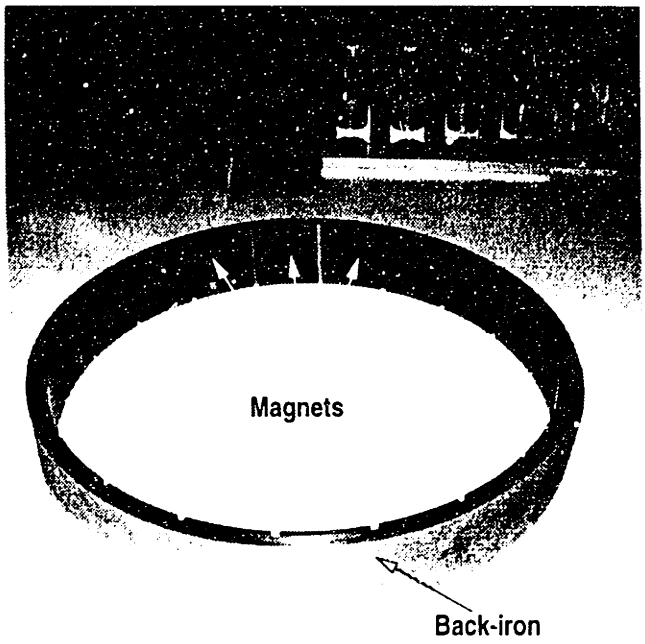

(a) Rotor magnets assembled on solid back-iron

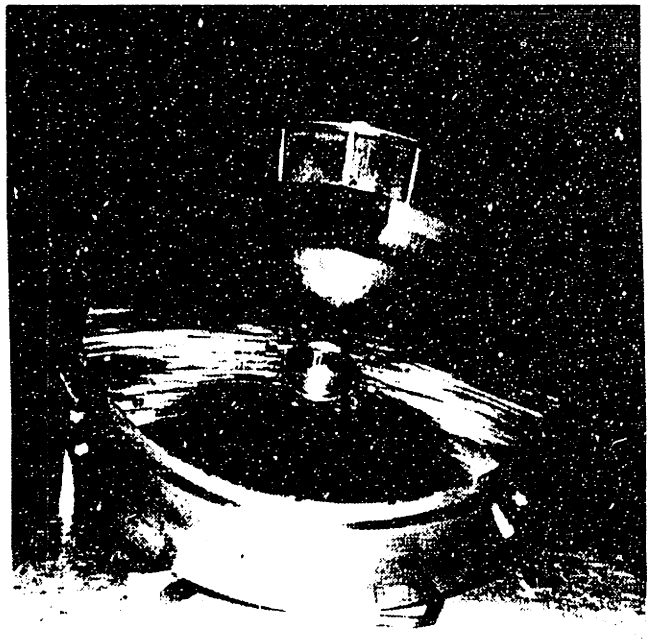

(b) Rotor with single endbell, cantilevered on a bearing

(c) Stacking and skewing of stator laminations

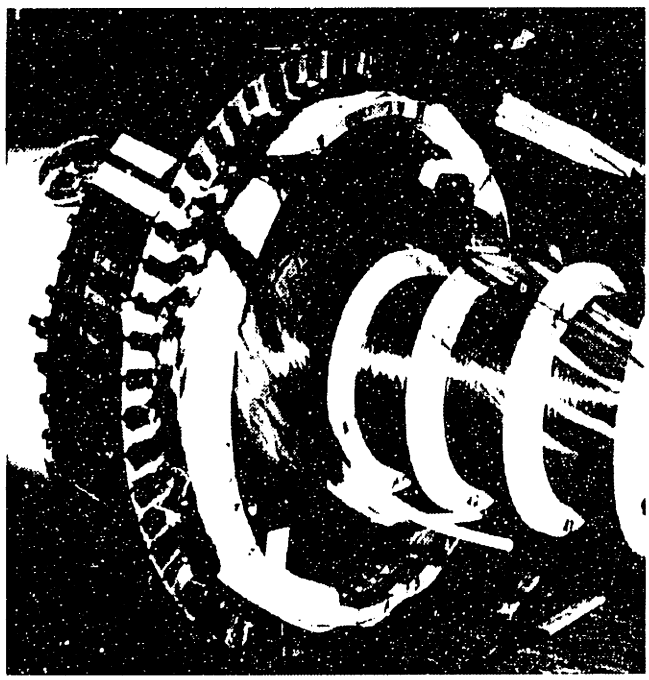

(d) Winding the stator

Figure 6-4: Prototype motor at various stages of construction.

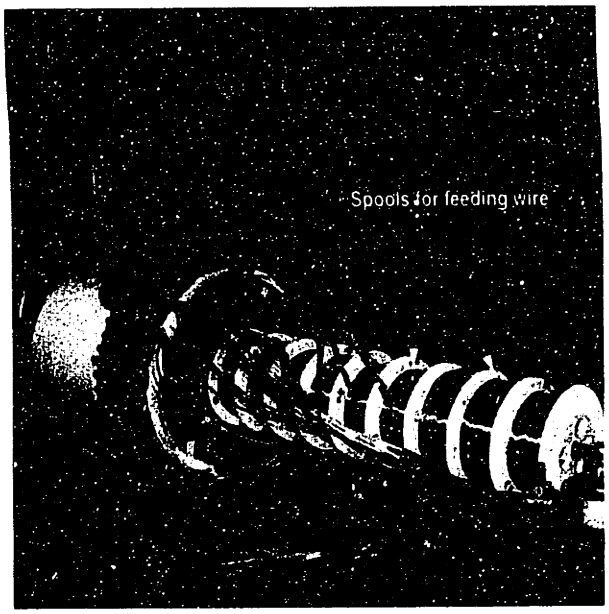

(a) Winding setup showing wire feeding system.

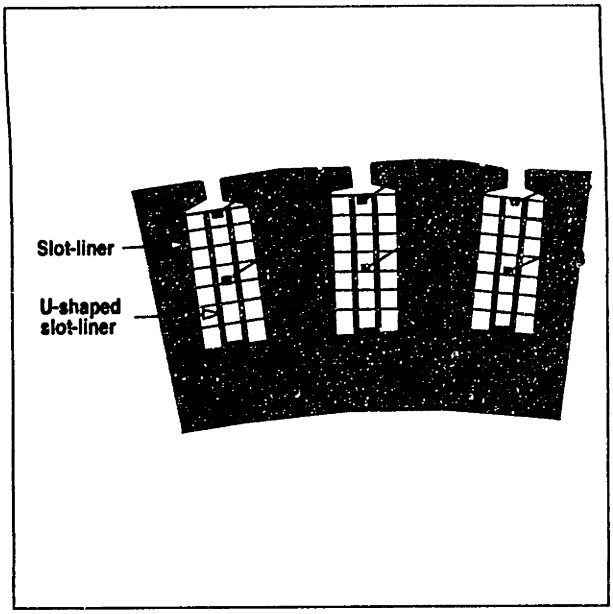

(b) Schematic showing U-shaped slot-liner and location of thermocouples within the slots.

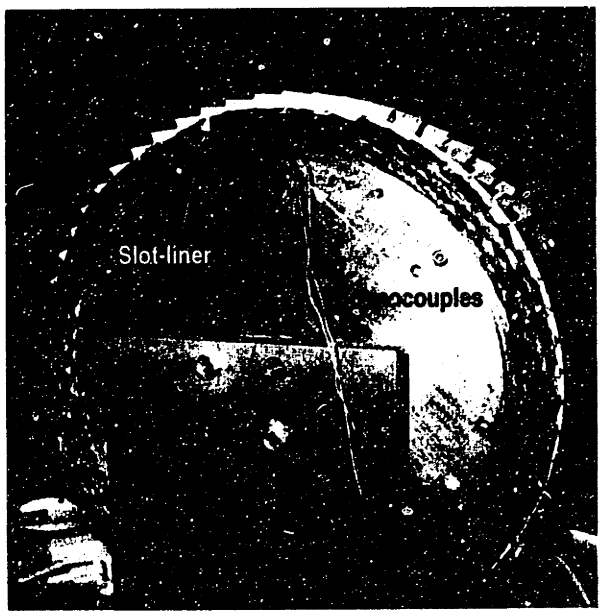

(c) Wound stator prior to trimming slot-liners and varnishing.

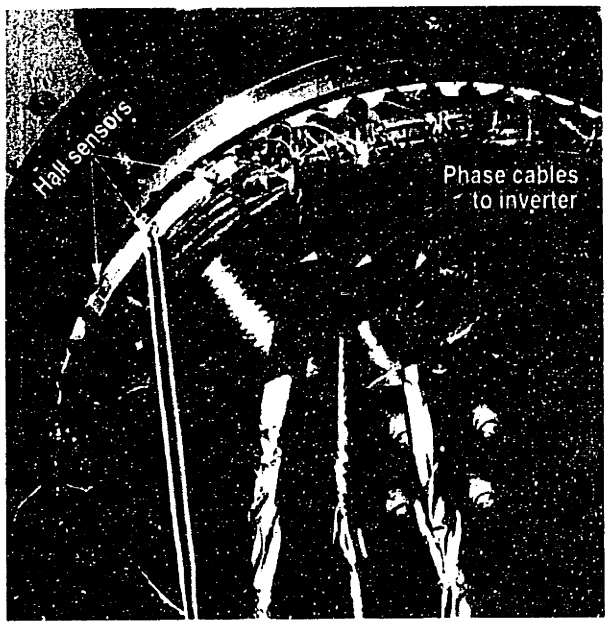

(d) Assembled motor.

Figure 6-5: Prototype motor at various stages of construction.

that the wires can be flattened at locations where the phases overlap. The price paid for this setup is longer endturns.

The final winding of the prototype motor was done by the author with initial instruction from Dr. Peter Senak, an employee at the Superior Electric Company. The armature conductors were made out of 24 strands of AWG 25 round wire, resulting in an equivalent conductor size of slightly less than AWG 11. The motor was wound in layers of 3 conductors at a time, which were finally connected in series. To minimize the chances of a high-potential failure from winding to winding, U-shaped 10-mil Nomex slot-liners were used to provide additional dielectric isolation between conductors as shown in Figure 6-5(b). Due to several factors including the reduction in slot area by the slot-liners, our desire to keep the axial length of the endturns in check, and lack of experience on the part of the author in winding motors, we were only able to fit 20 out of the designed 21 turns. Thus in winding the 7th layer, one of the three conductors was dropped as indicated by the unshaded conductor section in Figure 6-5(b). The measured winding-to-frame capacitance was 0.01 μF. The wound stator, shown in Figure 6-5(c), was high-potential tested at 2500 V dc from winding to frame, 1500 V dc between phases, and 600 V dc between windings in the same slot. The winding-to-winding high-potential test was performed before the windings were series-connected.

To measure winding temperature, thermocouples were embedded between the 3rd and 4th layer and on top of the 7th layer as shown in Figure 6-5(b). The stator was not vacuum impregnated with a STYCAST-2850FT epoxy encapsulant as was anticipated in Chapter 3 due to unavailability of an appropriate impregnation tank. Furthermore, we wanted to retain the flexibility of re-winding the motor if necessary. Thus, a Sterling 79WS-028 high-bond polyester varnish was used instead. The high-potential tests described above were successfully repeated after the stator was varnished and the rotor and stator were assembled together as shown in Figure 6-5(d).

The cantilever design of the rotor made it difficult to keep a uniform airgap all around the periphery of the stator. Part of the uneveness of the airgap can also be ascribed to machining and manufacturing tolerances. The average measured airgap of the motor was about 15 mils instead of 25 mils. This reduction of the airgap constitutes a 7% increase in the no-load

airgap flux density (given a Carter coefficient of 5%) which more than compensates for the 4.7% reduction in the back-emf constant arising from the dropping of 1 out of 21 turns during the winding of the motor.

The phase-to-phase motor resistance R_m and the phase-to-phase motor inductance L_m were measured by measuring the step response of the motor to a step of voltage excitation across two of the windings with the third open-circuited. The motor resistance was determined as the ratio of the magnitude of the voltage excitation to the final value of the motor current, and the inductance was computed from the time constant of the current waveform. The measured resistance and inductance were 0.47 Ω and 3.5 mH respectively. The measured inductance was much less than that predicted by the QuickField finite-element program in Chapter 3 from the stored magnetic energy. The discrepancy may be due to inadequate nodes used in mesh generation. The low inductance is actually desirable as it shortens the time for current commutation from one phase to the other. The measured resistance is 38% higher than our original design target of 0.34 Ω. This increase in motor resistance is due to the reduced copper packing factor and longer endturns resulting from our desire to prevent radial buildup of enturns.

6.3 No-Load Back-EMF

To measure the no-load back-emf, the prototype motor was spun at different speeds and the peak value of the phase-to-neutral voltage was measured. The results, plotted in Figure 6-6 shows a linear relationship between the motor back-emf and speed as expected for a PMSM. The no-load back-emf constant, given by the slope in Figure 6-6, is computed to be 0.76 V/rpm or 7.25 V/rad-s. The no-load back-emf constant is 21% higher than the full-load back-emf value quoted in Figure 3-17 in Chapter 3. Part of this can discrepancy is due to teeth saturation at full-load which reduces the teeth permeability. Also, the magnet temperature in Figure 3-17 was 110°C, which reduces the remanent flux of the rotor magnets by 10%. Furthermore, as explained earlier, the reduction of the airgap from 25 mils to 15 mils amount to a 7% increase in the no-load airgap flux density which more than compensates for the 4.7% reduction in the back-emf constant arising from the reduced

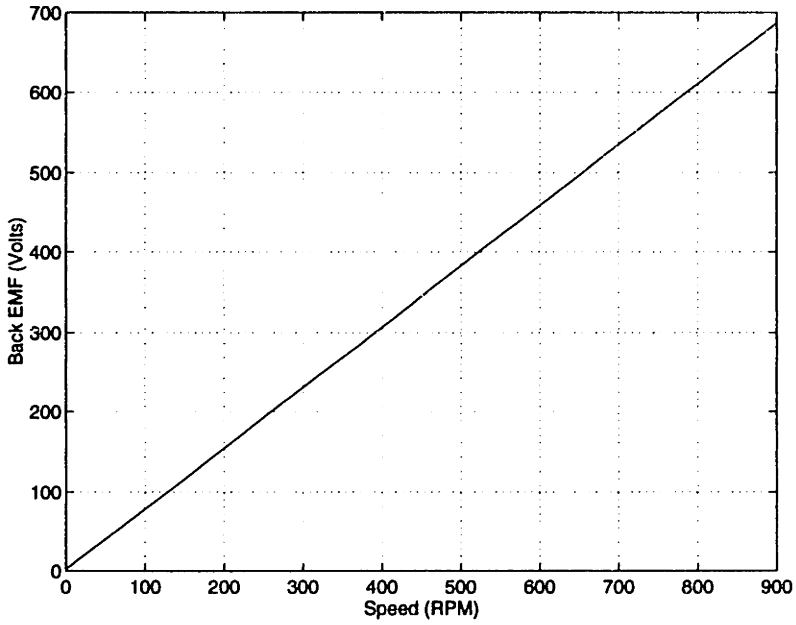

Figure 6-6: Variation of no-load peak phase-to-neutral voltage with motor speed.

number of turns.

Figure 6-7 shows the no-load phase-to-neutral back-emf waveforms at three different speeds. These waveforms not only confirm linearity between motor speed an back-emf, but show the trapezoidal nature of the back-emf which is expected from a surface-mounted PMSM with square-wave windings.

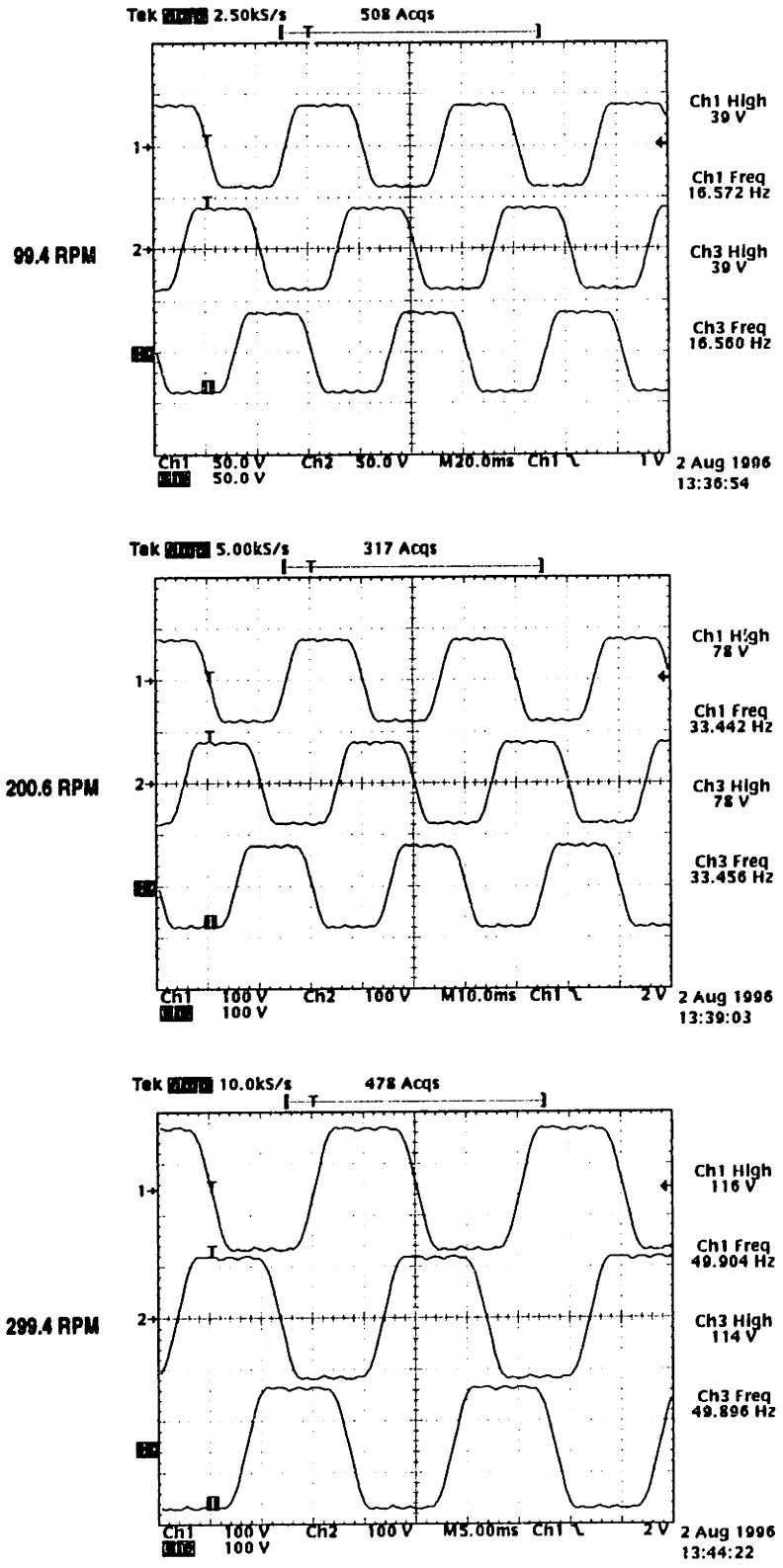

Figure 6-7: No-load phase-to-neutral back-emf waveforms at three different speeds.

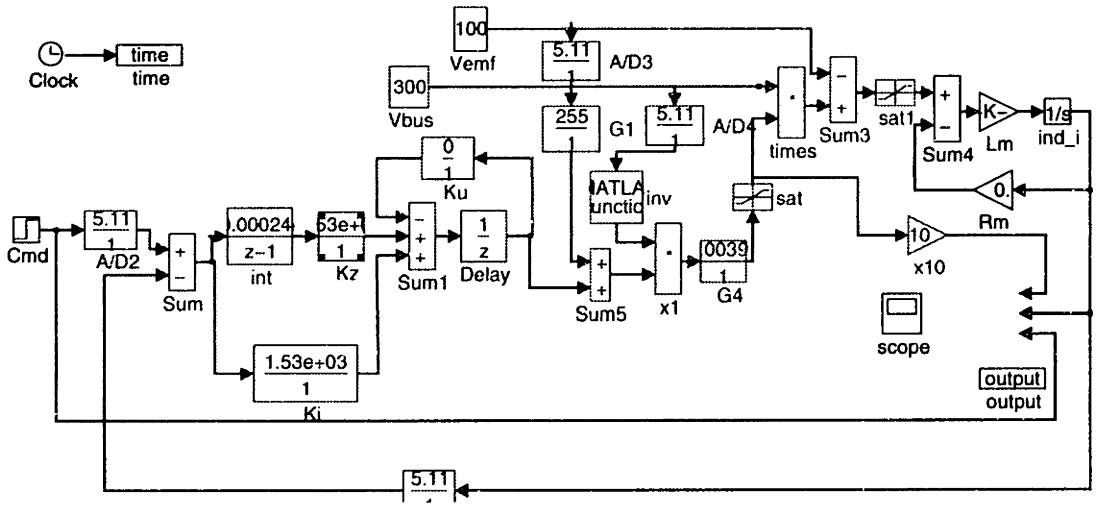

(a) Simulink block diagram of buck control loop

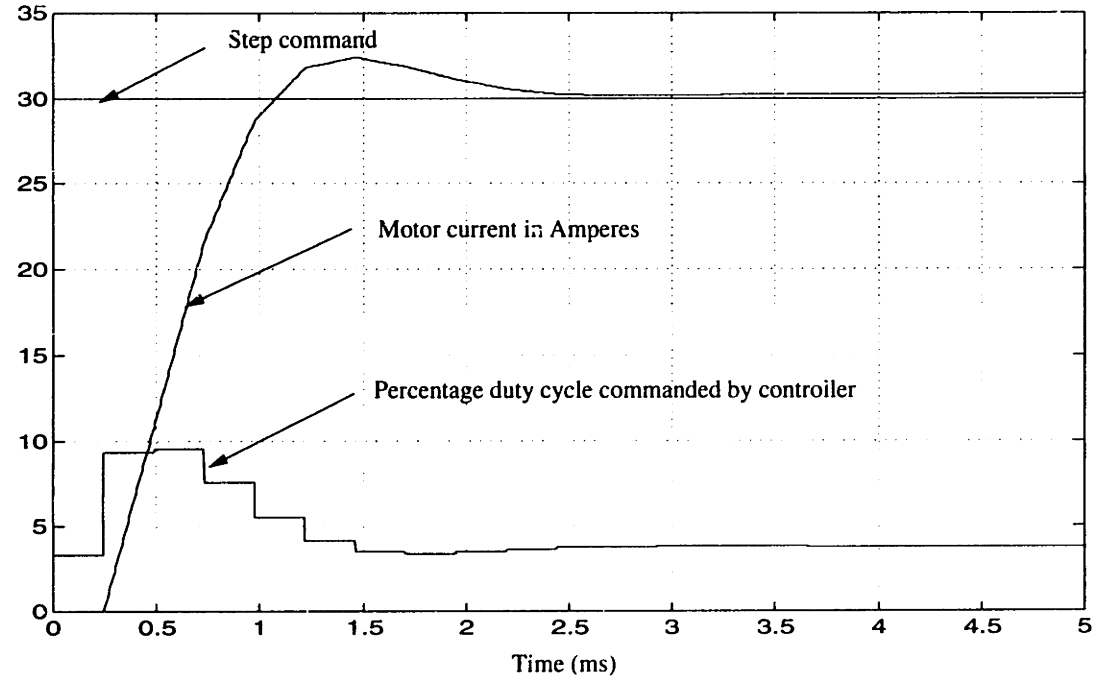

(b) Simulated step response of buck control loop

Figure 6-8: Simulink block diagram and simulated step response of the buck control loop.

6.4 Control Loop Simulations

With the measured phase-to-phase motor inductance and motor resistance, feedback gains for the buck and boost digital control loops were determined as described in Section 5.3.2. Since the desired vehicle controller bandwidth is 20 Hz, the bandwidth of the torque controller should be a factor of 10 higher in order to separate the dynamics of the two

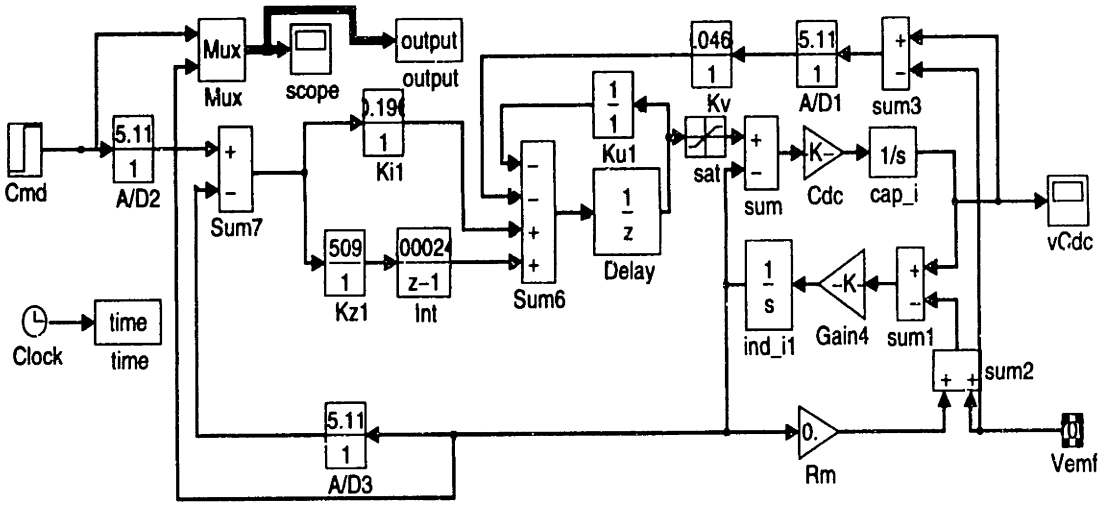

(a) Simulink block diagram of boost control loop

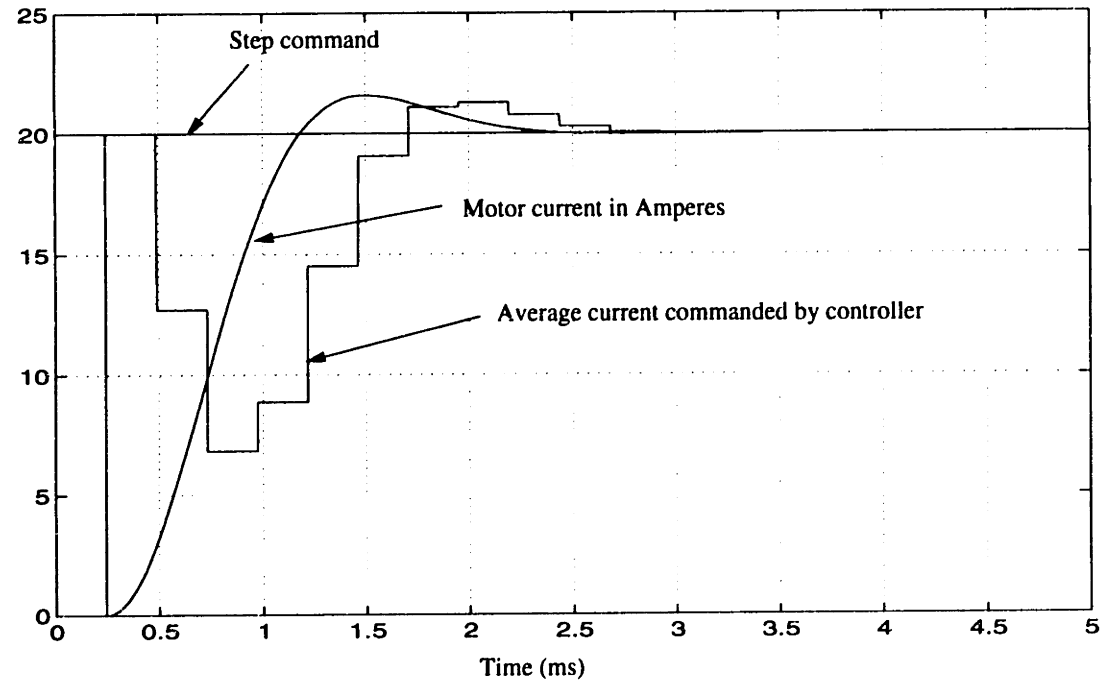

(b) Simulated step response of boost control loop

Figure 6-9: Simulink block diagram and simulated step response of the boost control loop.

systems [42]. Thus, the closed-loop bandwidth of the torque controller should be at least 200 Hz. The current loop is closed around the newly commutated phase so that the controller provides additional voltage to speed up the commutation of motor current from one phase to another[3]. Therefore a closed-loop bandwidth greater than 200 Hz is desirable. The feedback gains for the buck and boost control loops were determined with the Matlab script

[3]Phase current commutation can be further sped up by phase-advance

for pole placement attached in Appendix C. Initial feedback gains were determined by placing the poles in the general area demarcated in Figure 5-9 and the resulting gains were fine-tuned via a simulation of the control system in Simulink.

The poles of the buck control loop were placed at 0.5043±1.2609j and 0.9632 in the z-plane, and the resulting feedback gains were $k_i = 6\ A^{-1}$, $k_z = 900\ A^{-1}$, and $k_u = 0$, given an additional gain of 5.11 from the A/D conversion where 100 V and 100 A are converted to 511 (1FF HEX). The pole locations were specially chosen such that previous command feedback gain k_u was zero to reduce computation time. Figure 6-8(a) shows the Simulink block diagram of the buck control loop. The simulated response of the loop to a step in torque command is shown in Figure 6-8(b). The bus voltage for this simulation is 300 V and the motor back-emf is 100 V. Bus voltage feed-forward is implemented in this simulation as shown by the initial non-zero duty cycle. The settling time of the loop to a step input, discounting the long tail, is about 3 ms which is well below the maximum desired settling time of 5 ms.

The poles of the boost control loop were placed at 0.3523±0.408j and 0.4847±0.2385j in the z-plane and the resulting feedback gains were $k_v = 0.046$ A/V, $k_i = 0.196$ A/A, k_z =509 A/A, and $k_u = 1$ A/A, including the additional gain of 5.11 from the A/D converter. Figure 6-9(a) shows the Simulink block diagram of the boost control loop. The simulated response of the loop to a step in torque command is shown in Figure 6-9(b). The initial delay of the evolution of the motor current is due to the one-sample delay in the controller, which is also shown in the figure by the average current commanded by the controller. The back-emf for this simulation is 700 V. The settling time of the boost loop to a step input is also about 3 ms which is below the maximum desired settling time of 5 ms.

Figure 6-10 shows an oscillogram of a phase-to-neutral voltage and the corresponding phase current with the buck control loop in operation. This figure corresponds to Experiment #7 in Table 6.1, where the motor produced 250 Nm of torque at 75 rpm. The purpose of this figure is to show that buck control loop operates properly, and that the controller reacts to increase or decrease the phase-to-neutral voltage as necessary to speed up commutation. This oscillogram does not quite indicate indicate the settling time of the control loop since the initial transient includes the commutation period. The phase-to-neutral voltage in the

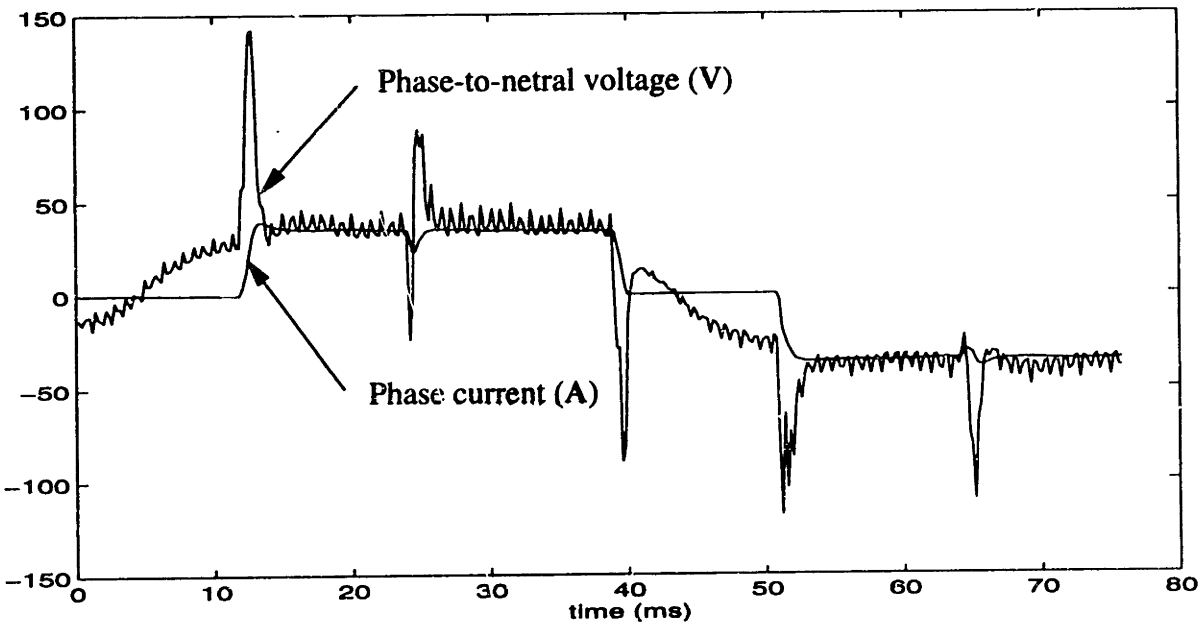

Figure 6-10: Sample phase-to-neutral voltage and corresponding phase current for buck control loop.

figure shows substantial averaging and aliasing, as the oscilloscope severely undersamples the pulse-width-modulated waveform, but the figure gives an indication of the average voltage commanded by the controller.

The boost control loop did not operate as envisioned due to the fact that our plant model assumed that the boost inductor always operated in discontinuous conduction. This assumption turned out not to be valid and therefore the plant dynamics changed as the inductor entered into continuous conduction. Sub-harmonic oscillations were also present when the inductor operated in continuous conduction with a duty cycle greater than 0.5. Therefore the controller, as implemented, chattered and its behavior was erratic. Sub-harmonic oscillations in a boost converter can be cured by ramp compensation where a ramp is added to sensed inductor current [59]. The next iteration of the inverter should explore designing the boost converter to run in continuous conduction or using ramp compensation. To operate the boost converter in continuous conduction, additional energy storage is required. The only disadvantage of ramp compensation is that it reduces the dynamic range of the current PWM comparator.

To be able to operate the prototype wheel motor beyond the corner speed, our switching strategy for the power semiconductors was modified to switch the boost converter open

loop with bang-bang duty cycle control to raise its output voltage 100 V above the motor back-emf or 1100 V, whichever is lower. The 3-phase buck converter should only be used for commutation during boost operation. However, because the boost converter was run open-loop, the 3-phase buck converter was used for current control instead. The penalty paid for this control scheme is a maximum additional switching losses in the 3-phase buck converter of about 500 W at the full power of 15 kW, which corresponds to a 3.3% drop in the efficiency of the inverter.

6.5 Characterization of Motor-Inverter Efficiency

To obtain an accurate measurement of the efficiency of the wheel motor and inverter, one must include the losses in the bearings of the wheel motor-dynamometer assembly, as the wheel motor must supply those losses. To measure the bearing losses, the wheel motor was spun with its windings open circuited at different speeds, and the torque output of the dynamometer was measured. Figure 6-11 shows the plot of the torque necessary to spin the rotor of the wheel-motor-dynamometer assembly at no load. The quantization of the dynamometer torque meter is 2 Nm. The measured data is fitted to a straight line via least-squares error regression. The no-load torque T_0 in Nm is therefore related to the motor RPM by

$$T_0 = 5.5148 + 0.0106 \times \text{RPM} \quad . \tag{6.1}$$

Thus T_0 must be added to the torque output as read on the dynamometer digital readout in order to obtain the true torque supplied by the wheel motor when spinning the shaft of the dynamometer.

To measure the torque capability of the motor, and the efficiency of the wheel motor and the inverter, the dynamometer was operated at different speeds and the wheel motor was driven to oppose the dynamometer. The speed controller of the dynamometer maintained the shaft speed of the motor at the set rpm, and the torque necessary to keep the shaft speed constant was read from the torque meter. For each experiment the phase-locked signals from the Hall sensors were phase-advanced as necessary to keep the phase current in phase

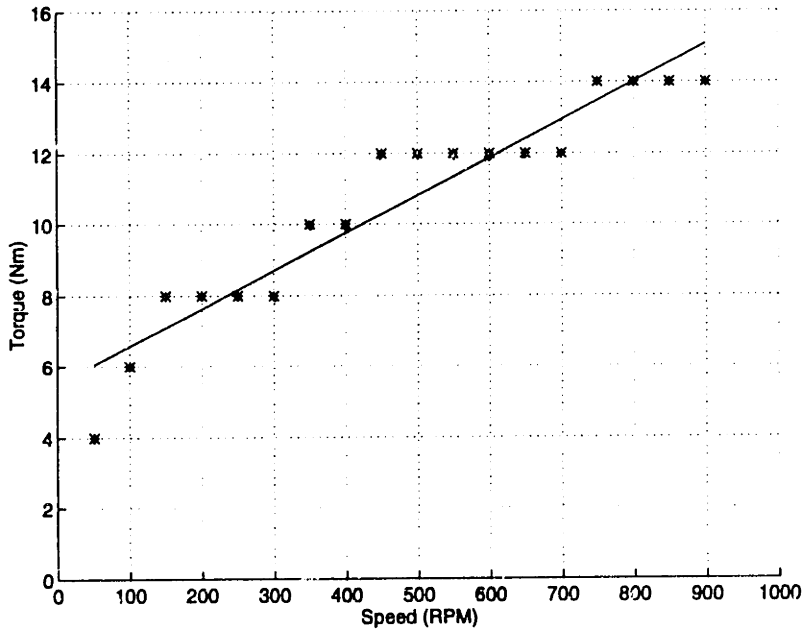

Figure 6-11: No-load torques needed to spin the dynamometer-motor assembly at various RPMs.

with the motor back-emf. The temperature of the winding, measured by thermocouples located between the 3rd and 4th layer and on top of the 7th layer are noted. The inverter input bus voltage, input bus current, motor phase-to-neutral voltage and phase current were captured with the oscilloscope as shown in Figure 6-1. The data was post-processed with Matlab. Note that with this setup the inverter bus capacitors not only filtered the ripple current from the switching of the IGBTs but also served as filter capacitors for the 180 Hz input voltage ripple. Thus, current was drawn by the inverter in short bursts at a frequency of 180 Hz, as shown by the sample voltage and current measurement in Figure 6-12

The input power into the inverter was computed from the bus voltage and bus current data by point-by-point multiplication of the two waveforms and averaging. The output power of the inverter, which is the input power into the motor, was calculated likewise by multiplying the phase-to-neutral voltage by the phase current. The result is averaged over an integral number of cycles and multiplied by 3 to obtain the total power supplied to the three phases of the motor. The no-load back-emf waveforms shown in Figure 6-7 indicate the three phases of the motor are balanced and hence multiplication of the single phase power by 3 is justified. However, from Figure 6-10, we see that the oscilloscope severely

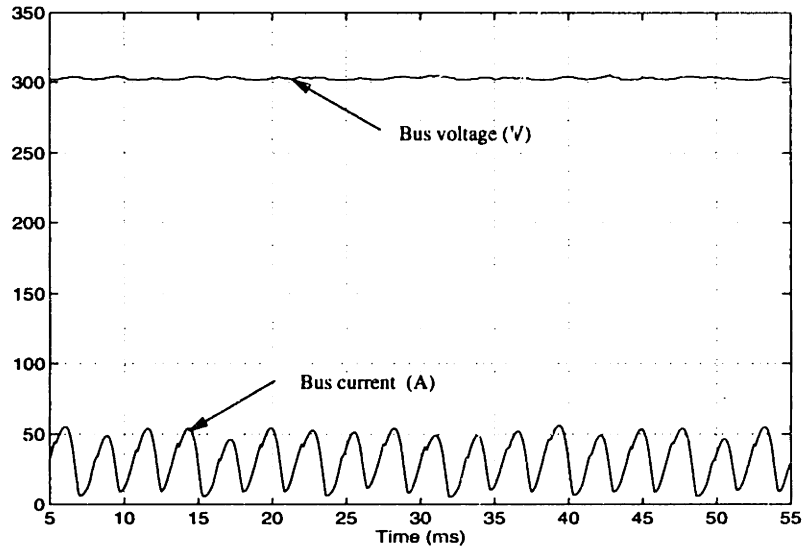

Figure 6-12: Sample inverter input voltage and current waveforms.

undersamples the 16.44 kHz pulse-width-modulated phase-to-neutral waveform, therefore any calculations based on this waveform are subject to unpredictable errors.

It was anticipated that the fringing fields from the sides of the rotor magnets would be enough to activate the Hall sensors, therefore the rotor magnets did not overhang the stack. Although this was true at no-load, the Hall sensors did not operate reliably when the motor was loaded, due to interference from the armature reaction flux. Thus, it was necessary to constantly fiddle with the orientation of the Hall sensors with respect to the rotor magnets in order to get the controller to operate properly. Due to this problem with the Hall sensors, the GALs on the controller board were re-programmed to shut down all gate-drives when a bad Hall-effect signal set (a combination of all ones or all zeros) was detected. Although this temporary fix allowed data to be taken without inverter or motor malfunction, it is imperative that the magnets overhang the stack in future designs for reliable operation. The operation of the Hall sensors deteriorated severely when the winding temperature exceeded 90°C, hence our inability to obtain experimental data above 800 rpm.

The measured torque, speed, winding temperatures, inverter input bus voltage V_{bus}, inverter input power P_{in} and the drive efficiency η_d, which is the combined efficiency of the motor and inverter are given in Table 6.1[4] Due to the lack of a data-acquisition system fast

[4]Due to human operating error, the boost converter switch blew up in the course of our experiments. Thus data for motor operation at 400 rpm and above was taken with the boost 3-phase buck converter operating

Expt. #	Torque (Nm)	Speed (RPM)	Temperature (deg. C)					V_{bus} (Volts)	P_{in} (kW)	η_d (%)
			A_7	A_3	B_7	B_3	Avg.			
1†	157	149	37	38	38	40	38.3	291	3.1	79
2†	159	295	36	37	36	37	36.5	289	5.7	85
3	28	74	35	35	35	36	35.3	300	0.31	71
4	159	151	42	42	40	41	41.3	293	3.1	82
5	158	76	39	40	39	42	40.0	297	1.8	70
6	388	75	51	52	48	52	50.8	290	4.0	76
7	250	75	46	48	47	51	48.0	292	2.9	68
8	199	151	49	47	47	52	48.8	291	3.9	80
9	148	236	46	47	48	49	47.5	289	4.4	83
10	234	248	49	50	49	50	49.5	286	7.0	88
11	30	250	48	48	47	49	48.0	297	1.1	70
12	33	151	47	47	46	47	46.8	298	0.74	70
13	153	301	57	59	57	58	57.8	319	5.6	86
14	75	301	57	56	56	58	58.0	323	2.8	83
15	29	301	57	56	56	58	56.8	328	1.4	65
16	253	301	64	66	62	66	64.5	303	9.1	87
17	309	301	59	61	57	60	59.3	301	11.6	83
18	412	73	62	63	61	63	62.3	307	5.6	56
19	429	150	63	65	61	64	63.3	303	9.7	69
20	402	251	64	66	62	66	64.5	303	13.2	80
21	93	99	35	34	33	36	34.5	324	1.1	89
22	325	325	35	36	34	36	35.3	316	4.9	70
23	94	199	38	38	35	35	36.5	320	2.3	83
24	274	199	43	41	39	41	41	310	7.0	82
25	366	199	42	43	42	43	42.5	308	9.8	77
26†	100	201	48	48	47	48	47.8	293	2.4	87
27*	46	403	52	53	54	55	53.5	416	0.20	968
28	128	402	56	57	56	57	56.5	405	6.0	90
29	238	403	64	66	63	66	64.8	421	11.4	88
30	81	495	69	71	69	71	70	512	4.6	91
31	169	500	75	78	76	78	76.3	500	9.5	93
32	49	595	79	80	78	79	79	602	3.2	92
33*†	50	598	79	81	79	81	80	601	1.8/3.4	173/92
34*	148	586	91	91	86	83	86.5	603	5.2/9.8	169/90
35*	89	696	87	90	88	90	88.8	631	3.7/7.0	173/92
36*	83	796	93	93	91	93	92.5	711	4.1	96
37†	106	800	92	95	93	95	93.8	708	9.5	93
38	106	798	97	100	98	100	98.8	709	9.5	94
39	127	704	102	106	103	106	104.3	685	10.3	91

Table 6.1: Measured experimental data.

enough to accurately capture the PWM phase-to-neutral voltage, the motor efficiency was computed from the mechanical power output P_{mech}, the Ohmic power loss P_{Ohm}, and an estimated core loss P_{core}. With these parameters, the motor efficiency was estimated as

$$\eta_m = \frac{P_{mech}}{P_{mech} + P_{Ohm} + P_{core}} \tag{6.2}$$

where

$$P_{mech} = \tau \times \frac{2\pi}{60}\text{RPM} \tag{6.3}$$

and the estimated core loss is given by

$$\begin{aligned} P_{core} &= 1.30 \times 10^{-5}(1.44 + 1.32 \times 10^{-3}\tau)^2\text{RPM}^2 \\ &\quad + 2.59 \times 10^{-2}(1.44 + 1.32 \times 10^{-3}\tau)^{1.79}\text{RPM} \\ &\quad + 4.4 \times 10^{-5}\text{RPM}^2 + 7.46 \times 10^{-2}\text{RPM} \end{aligned} \tag{6.4}$$

where RPM indicates the motor speed in rpm. Once the motor efficiency η_m was computed, the inverter efficiency η_{inv} was calculated from the drive efficiency by the equation

$$\eta_{inv} = 100\frac{\eta_d}{\eta_m} \quad . \tag{6.5}$$

Note that P_{Ohm}, P_{core}, η_m and η_{inv} are given in Table 6.2. For completeness, motor losses $P_{l,m}$ computed from the equation

$$P_{l,m} = 3v_{pn}i_p - P_{mech} \tag{6.6}$$

where v_{pn} is the motor phase-to-neutral voltage and i_p is the corresponding phase current are also given in Table 6.2. In general, the motor losses computed from Equation (6.6) are higher than the sum of the I^2R losses and the estimated core losses that are also given in Table 6.2. Thus the undersampling of the motor PWM input voltage by the oscilloscope

from a higher dc bus voltage as noted in Table 6.1; i.e. the bus was raised by the autotransformer rather than by the boost converter. The bus current measurement in Experiments marked with * in Tables 6.1 and 6.2 are believed to be erroneous as explained in the text. Experiments marked with † are similar others that are also noted in the text.

lead to an overestimation of the motor input power.

The rotary dial of the Tektronix current probe amplifier used to measure the inverter input current sometimes did not make good contact at the 5A/div setting. This is evident from the low bus currents recorded in Experiments 27, 33, 34, 35, and 36. Thus, bus current data for these experiments are erroneous. Since time did not permit these experiments to be repeated, an attempt was made to correct the bus currents in Experiments 33, 34, and 35. Experiment 32 was carried out at practically the same torque-speed point as Experiment 33, except that the bus current setting in Experiment 32 was 10 A/div and that of Experiment 33 was 5A/div. Therefore the bus current measured in Experiment 33 was multiplied by a scale factor of 1.884 to make the drive efficiencies in these two experiments match. Since the bus current setting was not changed for Experiments 33, 34, and 35, this same scale factor was used to correct the measured bus currents in Experiments 34 and 35. Motor and inverter parameters computed with the corrected bus current are preceded by a / in Table 6.1.

Figures 6-13 to 6-15 show plots of the measured drive efficiency, and the computed motor and inverter efficiencies respectively underneath the torque-speed envelope. Note that the winding temperature was not constant for all the experiments, as noted in Table 6.1. Data from Experiments 27 and 36 are not plotted in Figures 6-13 and 6-15 because the bus current measurement errors in these experiments could not be corrected. These experiments are however included in the computed motor efficiency in Figure 6-14 since the bus current measurements were not used in the motor efficiency computations. To avoid clutter, data from Experiments 1, 2, 26, and 37 are not plotted in any of the graphs since they are similar to Experiments 4, 13, 23, and 38 respectively. Overlaying the grayscale density plot of efficiency weights underneath the torque-speed curve over both the urban and highway drive cycles in Figure 2-2 on the plot of motor-inverter efficiency in Figure 6-13, the drive efficiencies from the dc power source to wheel are estimated at 85% and 92% over the urban and highway drive cycles respectively.

Plots of the inverter bus voltage, inverter input power, average motor winding temperature, Ohmic power loss in the armature windings and the estimated core loss in the stator teeth and back-iron at the various points underneath the torque-speed envelope are given in

Expt. #	P_{Ohm} (W)	P_{core} (W)	$P_{Ohm} + P_{core}$ (W)	$P_{l,m}$ (W)	η_m (%)	η_{inv} (%)
1†	223	22	246	270	91	87
2†	251	48	299	499	94	90
3	8.4	9.8	18	34	92	77
4	246	23	269	430	90	91
5	247	11	258	387	77	83
6	1049	13	1062	767	74	1062
7	625	12	636	816	75	89
8	414	23	438	725	88	91
9	217	37	254	527	94	88
10	578	41	619	1179	91	96
11	14	36	50	258	94	75
12	15	21	36	143	93	75
13	247	48	296	706	94	91
14	71	46	117	537	95	87
15	15	45	60	413	94	70
16	679	52	731	1104	92	95
17	1049	54	1103	1699	90	93
18	1794	12	1806	2116	63	88
19	2121	27	2148	2801	76	91
20	1932	47	1978	2966	84	95
21	83	14	97	168	91	98
22	1036	16	1052	1369	76	91
23	91	29	121	348	94	88
24	731	33	764	1084	88	93
25	1414	35	1449	2232	84	92
26†	103	30	133	278	94	93
27*†	25	64	89	316	96	1012
28	43	67	110	-2392	98	91
29	628	72	115	1478	93	95
30	71	83	154	402	96	94
31	318	89	408	874	96	97
32	25	102	127	128	96	96
33*†	28	103	131	243	96	181
34*	247	107	138	1086	96	176
35*	91	128	146	3851	97	97
36*	25	148	173	37	96	101
37†	144	155	300	1101	97	96
38	142	155	297	815	97	97
39	216	134	350	1280	96	94

Table 6.2: Computed performance parameters from experimental data.

Figures 6-16 to 6-20 for completeness.

6.5.1 Thermal Performance

As described in Chapter 3, the wheel motor is completely sealed in its operating environment. One side of the prototype wheel motor was however left open for ease of experimentation. Furthermore the motor, through its bearings and mechanical couplings, was thermally connected to the dynamometer. Therefore it was impossible to obtain any thermal data representative of motor operation in the hub of a wheel. One point that is worth noting is that the winding temperatures recorded in Table 6.1 indicate that temperature between the 3rd and 4th winding layers, measured by thermocouples A_3 and B_3, are higher than that on top of the 7th layer, as measured by thermocouples A_7 and B_7. Thus the hot spot has shifted to the center of the windings. This result is expected since the airgap is no more adiabatic as was assumed in Section 3.5.4.

Although we were unable to obtain actual temperatures representative of motor operation in the hub of a wheel, Figure 6-21 is of special importance since it shows the amount of heat that must be removed at the various operating point. Note from Figure 6-13 that the motor operates on the average at about 1/5 of its constant torque rating over the drive cycles. As Figure 6-21 shows, the thermal burden of the wheel motor is significantly reduced by the ability to lower the motor current at high speeds and therefore the motor can be air cooled while producing substantial horsepower. This reduced thermal burden is one of the benefits of the buck-boost inverter.

6.6 Summary

A 450 Nm, 20 hp, 25.1 kg permanent-magnet wheel motor and a microprocessor-controlled novel power-electronic drive that incorporates a bidirectional boost converter has been built and tested in a laboratory environment. The wheel motor-inverter combination, designed to operate up to 1300 rpm was tested at various points underneath its torque-speed curve up to 800 rpm. Experimental data for operation above 800 rpm were unobtainable due to unreliable operation of the Hall-effect magnetic field sensors at high temperatures. Due to

human operating error, one of the switches of the boost converter was destroyed therefore operation above a bus voltage of 300 V was achieved by raising the bus voltage with an autotransformer. The drive efficiencies, from the dc power source to wheel, are estimated at 85% over the Federal Urban Drive Schedule and 92% over the Federal Highway Drive Schedule.

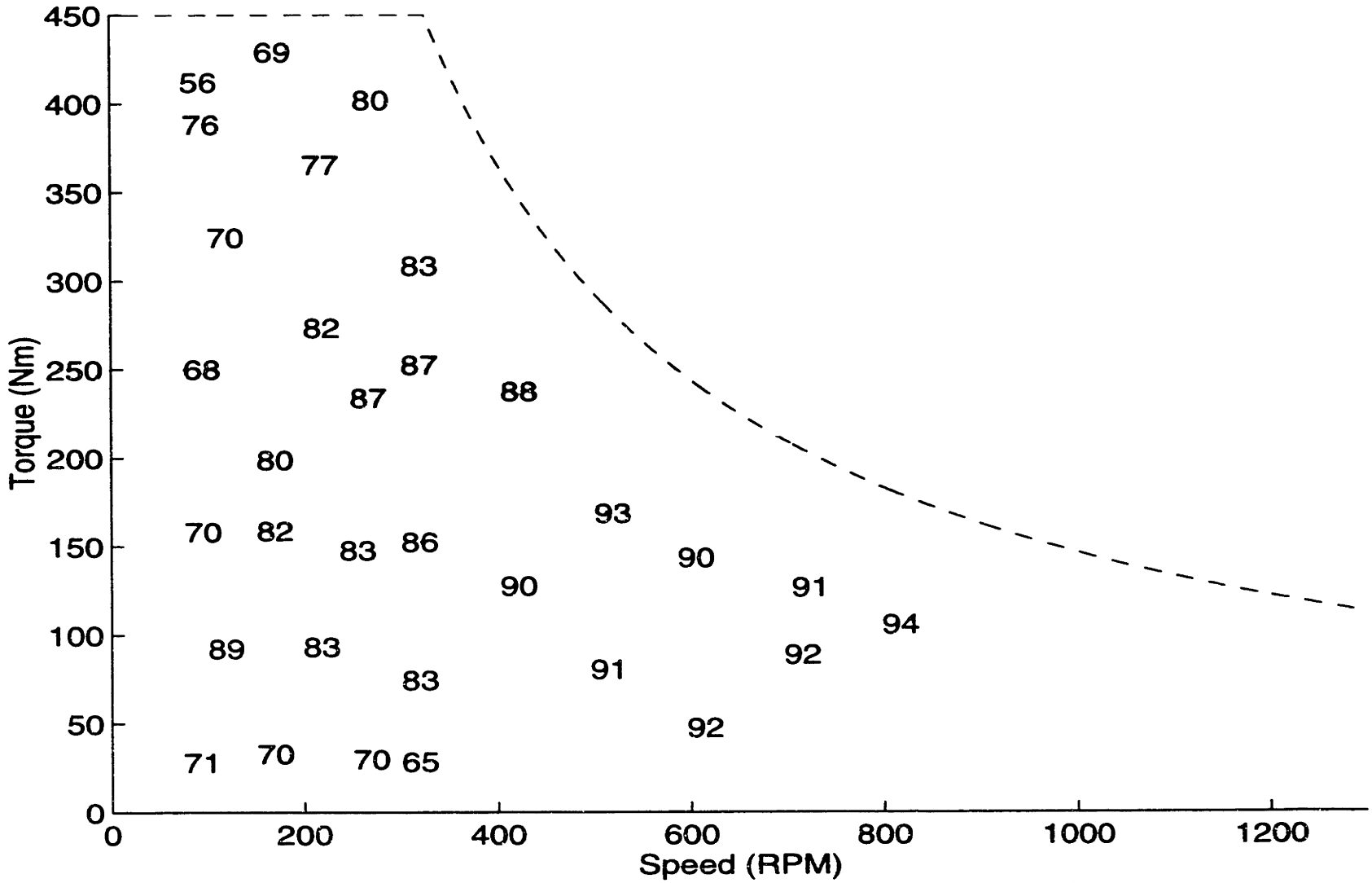

Figure 6-13: Measured efficiency of the inverter motor combination in percent.

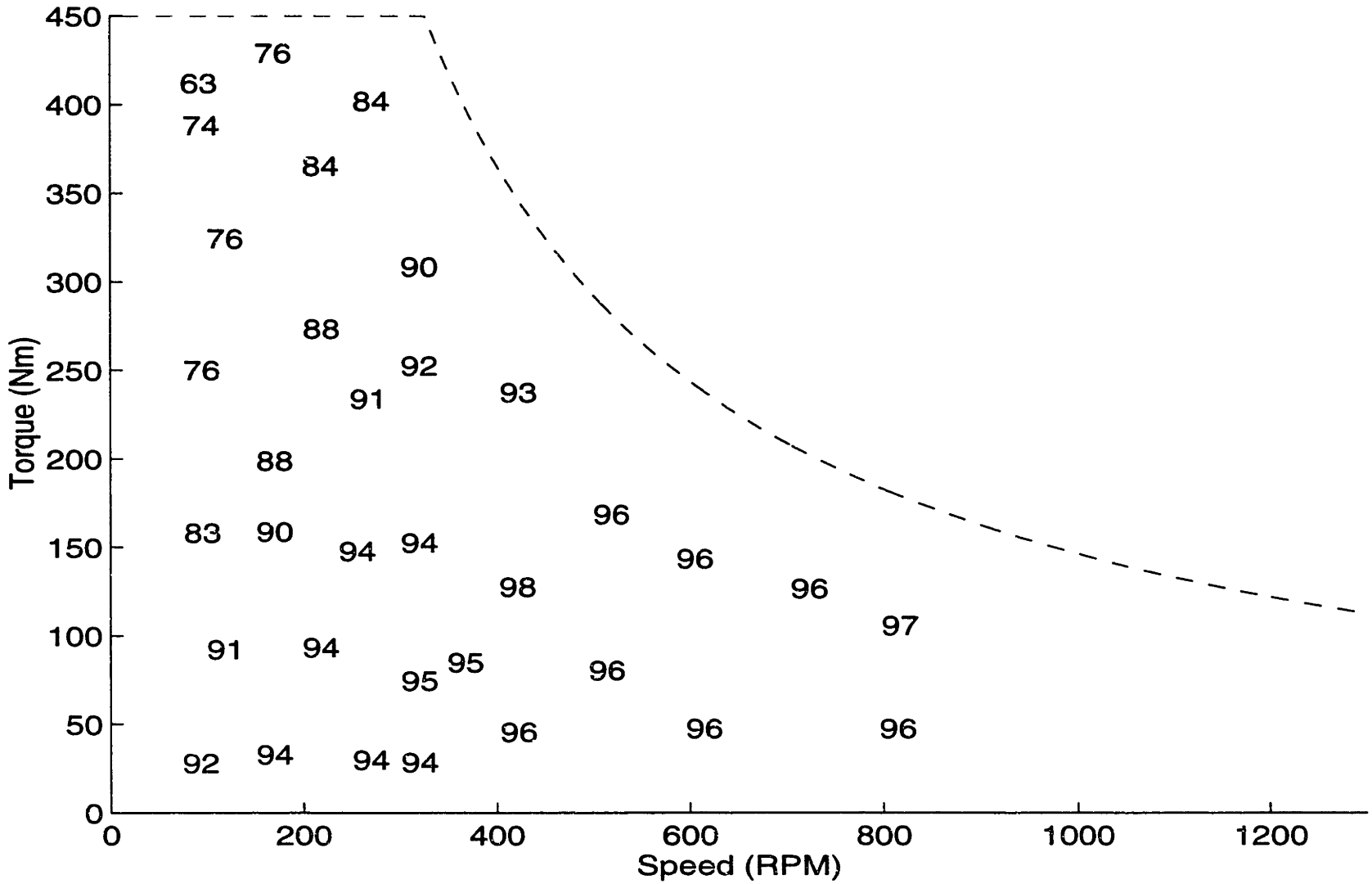

Figure 6-14: Computed efficiency of motor in percent.

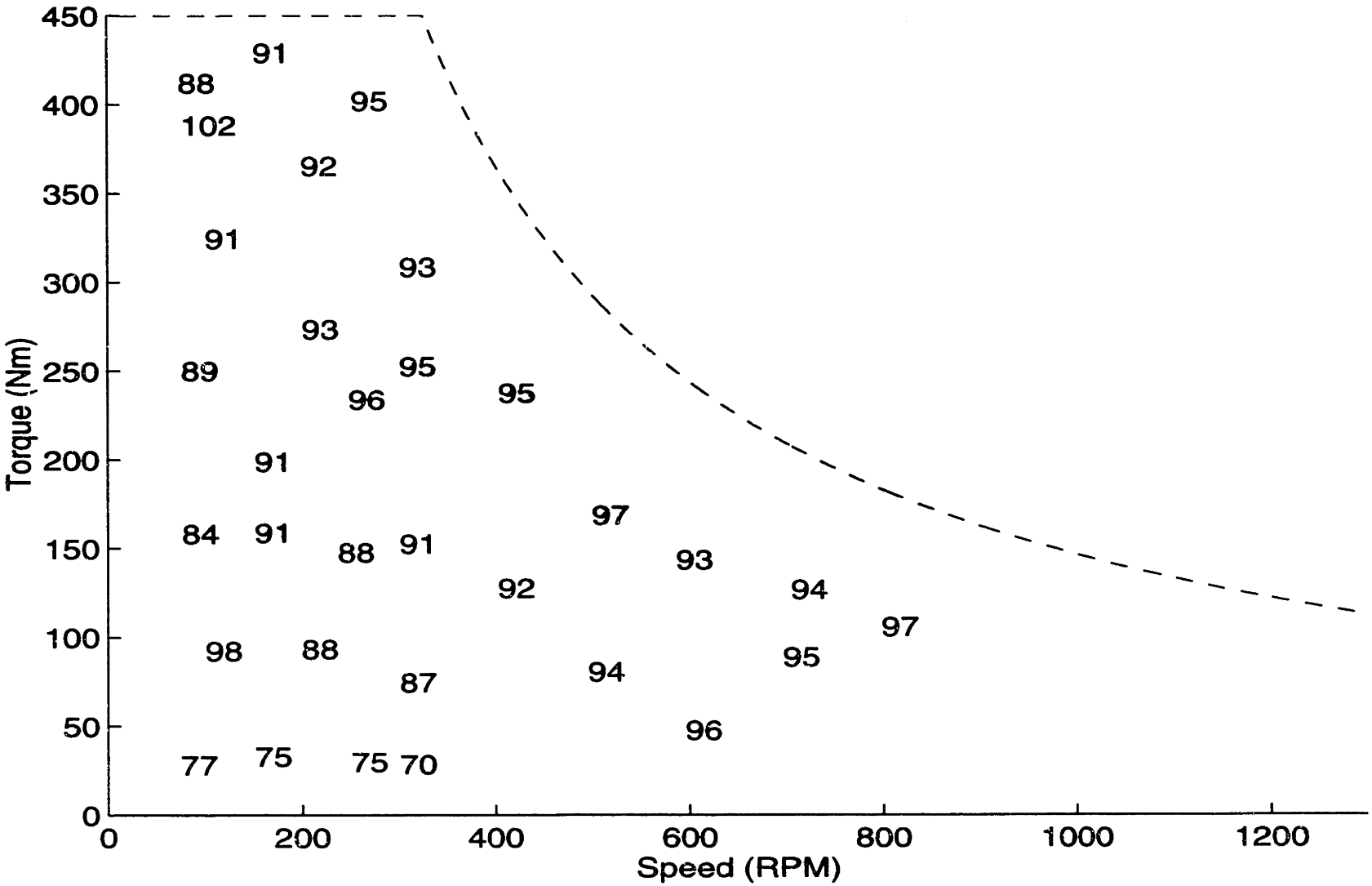

Figure 6-15: Computed efficiency of inverter in percent.

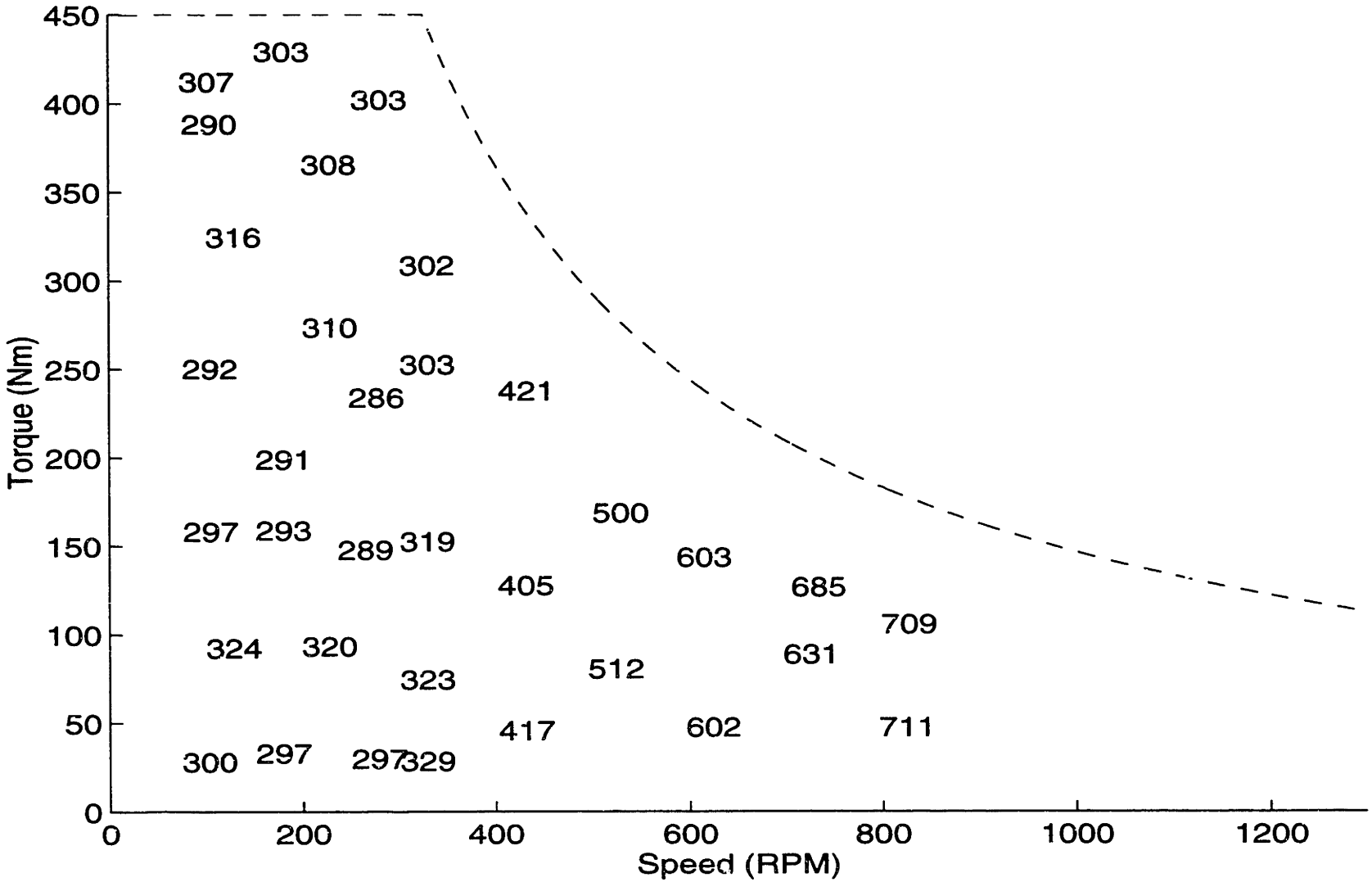

Figure 6-16: Inverter input bus voltage in Volts.

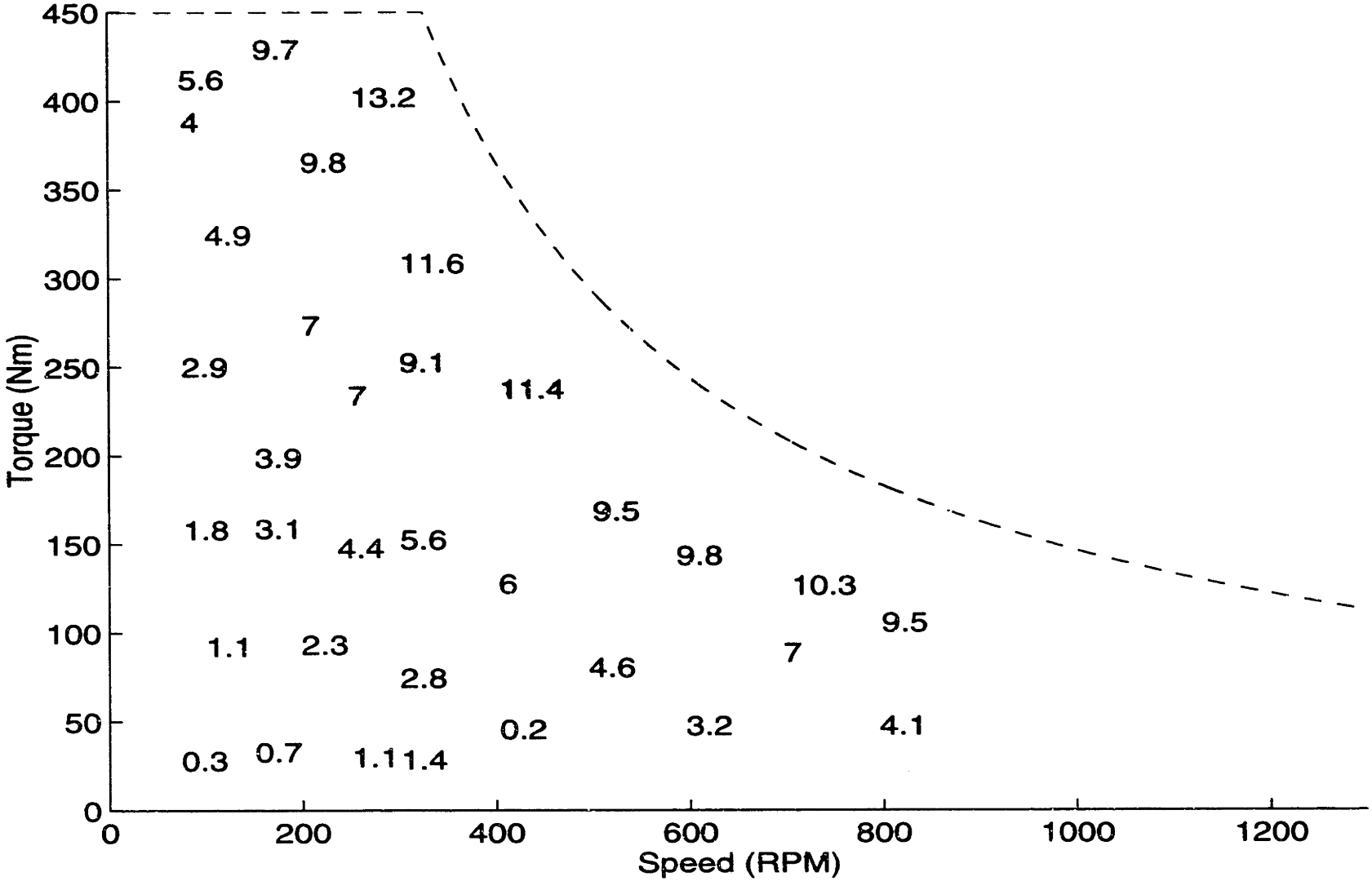

Figure 6-17: Inverter input power in kW.

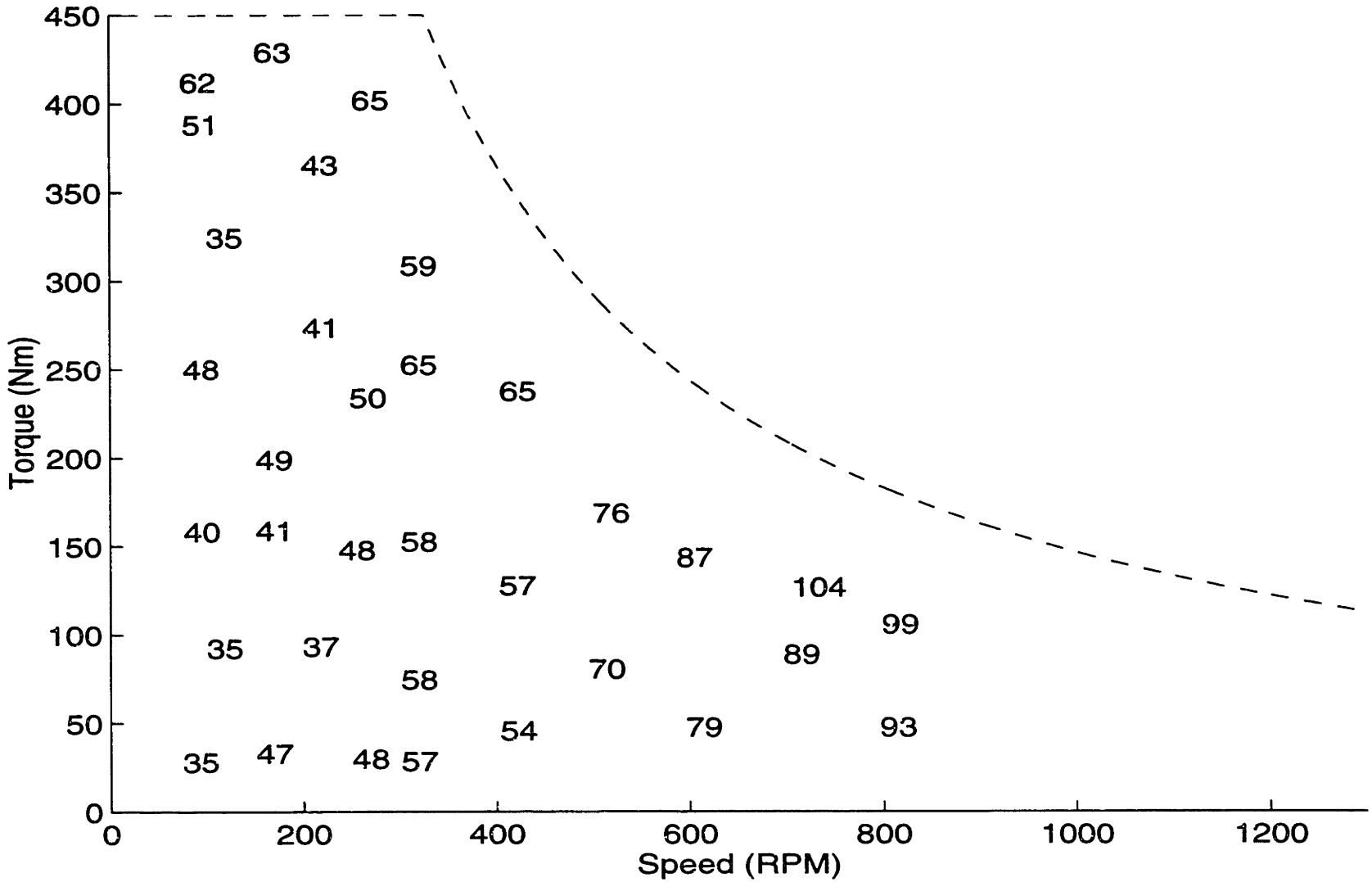

Figure 6-18: Average armature winding temperature in deg. C.

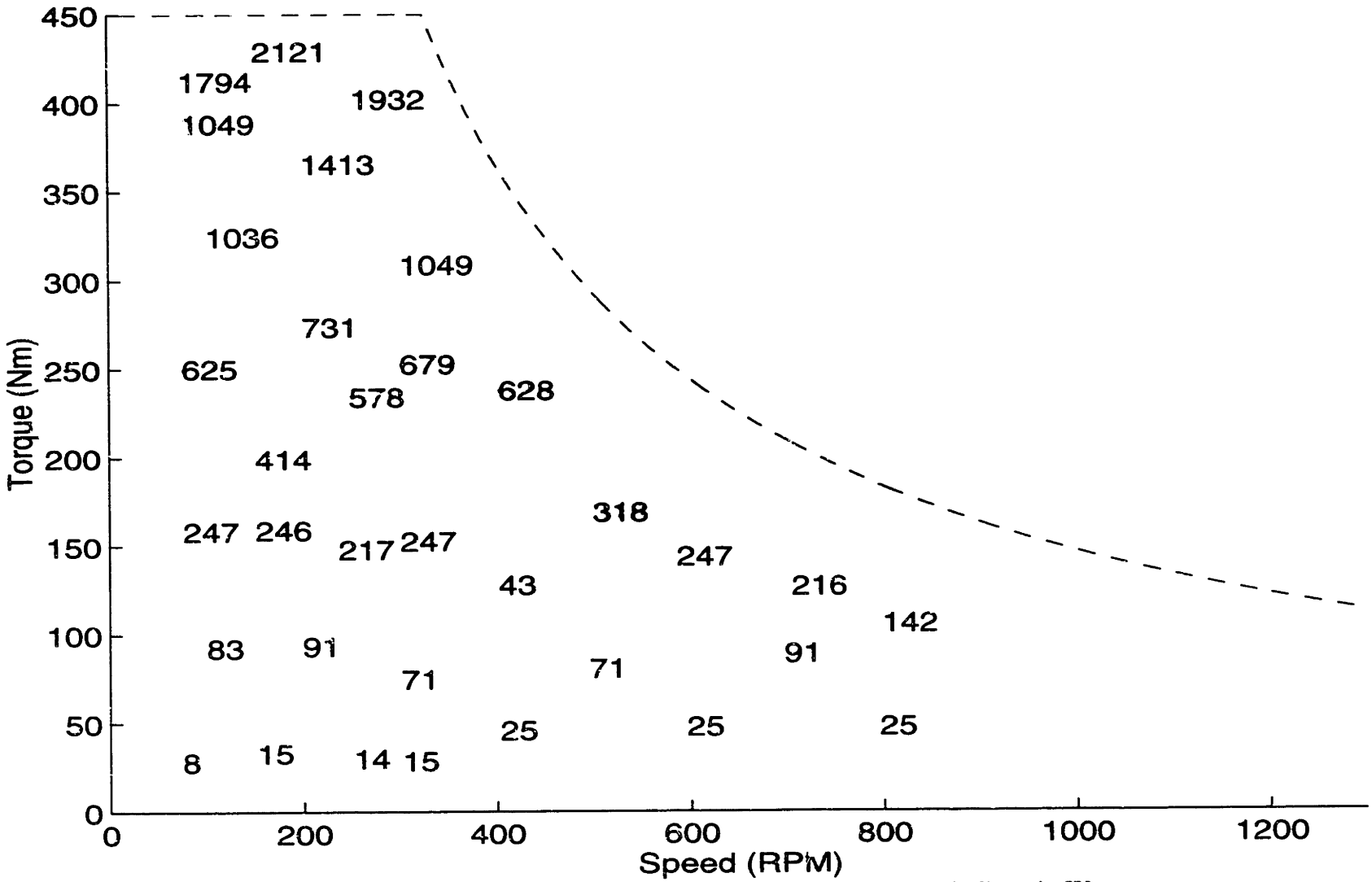

Figure 6-19: Ohmic power dissipation in armature windings in Watts.

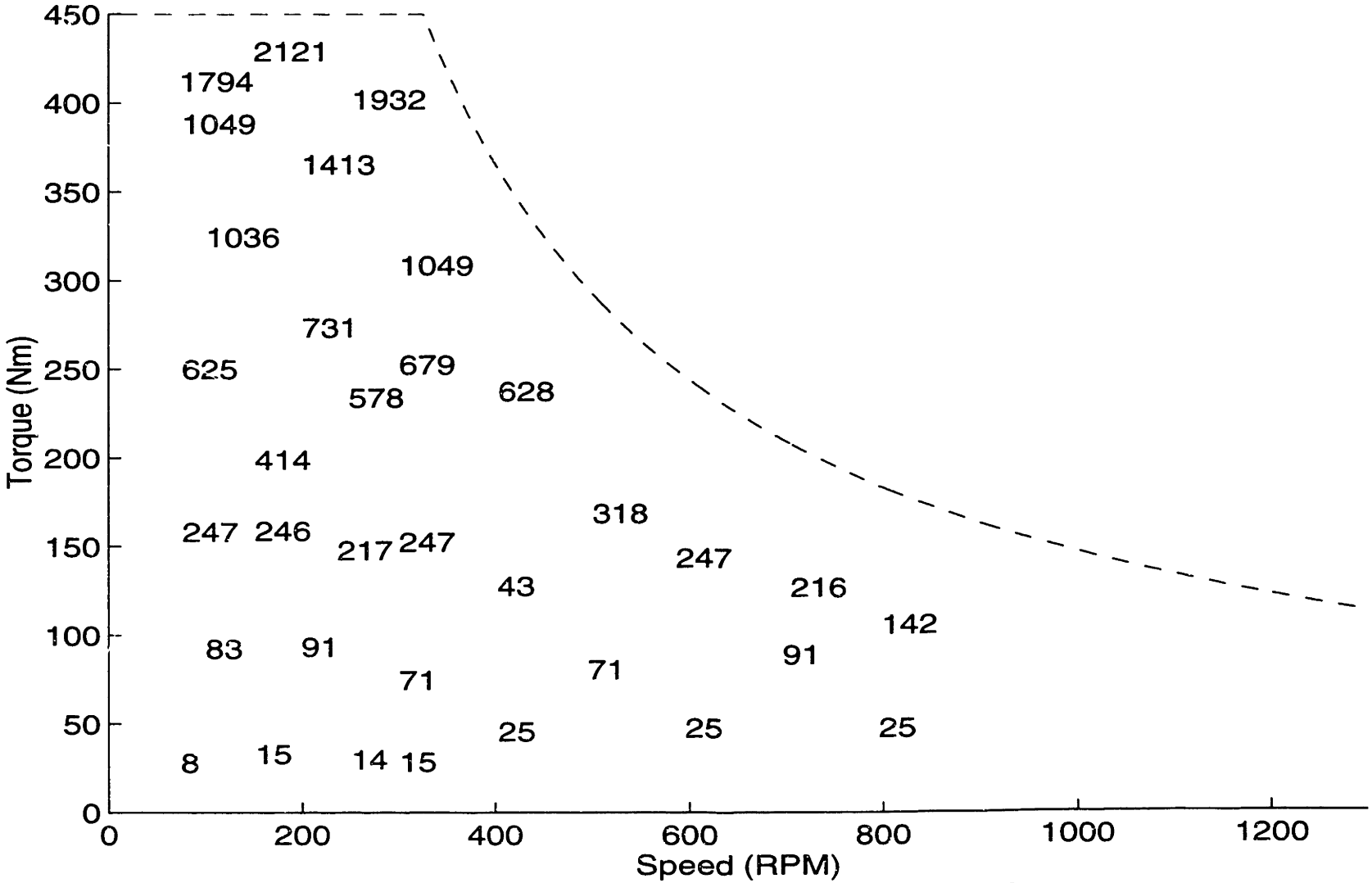

Figure 6-20: Estimated core loss in stator steel in Watts.

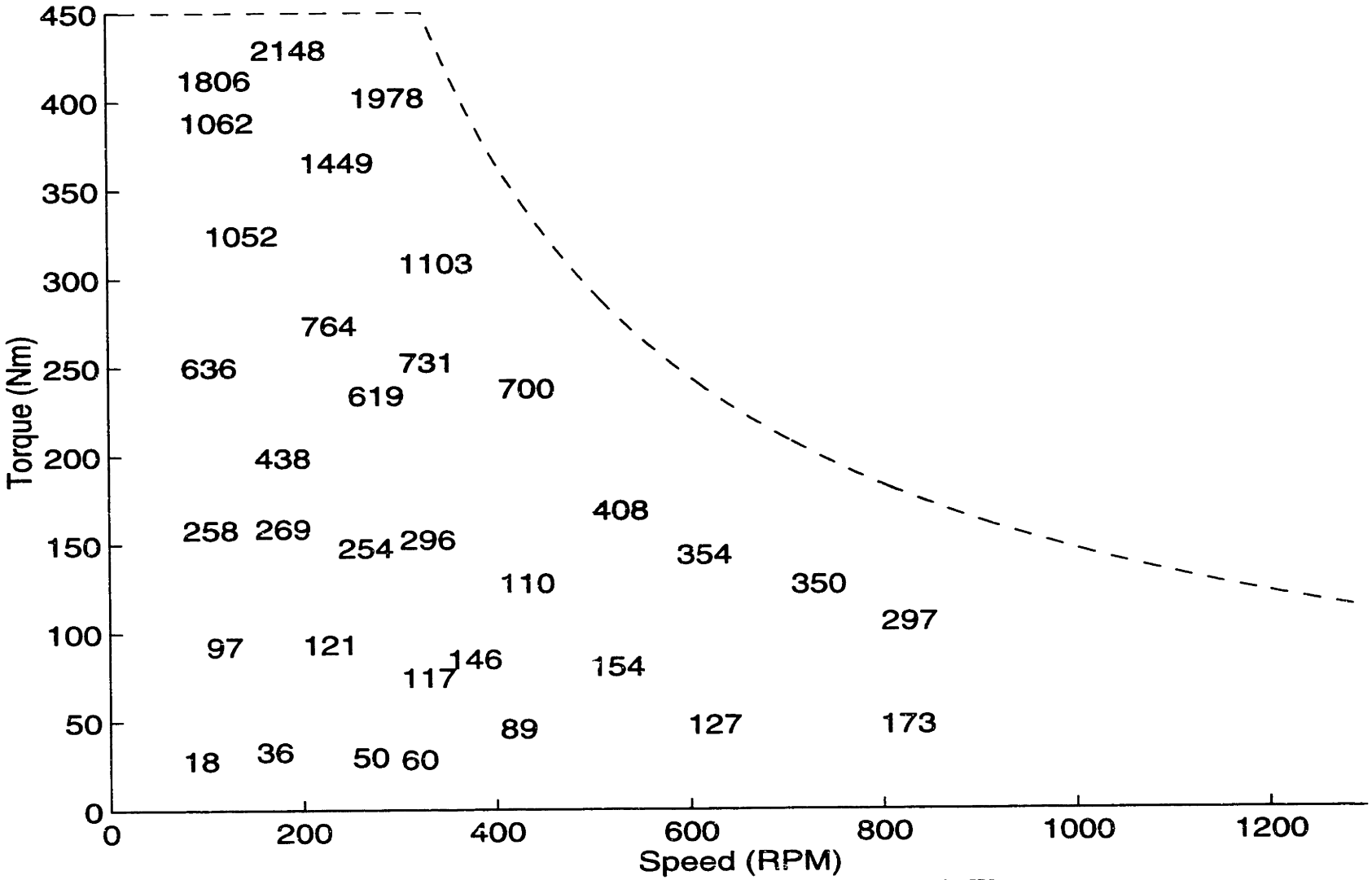

Figure 6-21: Total heat generated in motor in Watts.

Chapter 7

Summary and Conclusions

7.1 Thesis Summary

From an applications viewpoint, this thesis develops a permanent-magnet synchronous motor and a microprocessor-controlled novel power-electronic inverter for use in direct-drive EV propulsion. The development raises a variety of engineering and scientific issues which are addressed as follows.

- Environmental legislation by the CARB to improve air quality in urban areas, coupled with the PNGV initiative by the Federal government and the USCAR, has rekindled interest in the development of EVs as a competitive means of transport to ICEVs. An EV driven by wheel motors has improved powertrain efficiency due to the elimination of losses in the drive line and mechanical transmission; see Figure 1-2. A wheel motor powertrain also offers advantages in the packaging and manufacturing of the vehicle. The elimination of intermediate gearing requires the wheel motors to produce the high torques necessary to accelerate the vehicle in the limited space available in the hub of the wheel. There is also a strong need to reduce the mass of the wheel motors to reduce the unsprung weight of the vehicle so that the ride quality of the vehicle is not compromised. Thus the wheel motor offers a significant technical challenge.

- The use of newly available Nd-Fe-B magnets permits the design of efficient high-torque, low-mass motors and the availability of high-voltage, fast-switching IGBTs

allow these motors and their inverters to operate efficiently at high voltage and reduced currents. The combination can lead to a very low weight and efficient drive, as demonstrated in Chapter 6.

- Unlike an industrial motor, which is designed to operate continuously at rated torque, a wheel motor typically operates at an average of one-fifth of its peak torque rating over a drive cycle. Thus, the ability to produce low torques efficiently at medium and high speeds is key for drive-cycle efficiency maximization.

- The desire to reduce no load losses calls for the exploration of a slotless motor for the wheel motor application. With a slotless armature the electromagnetic airgap is large, since it includes the thickness of the airgap windings. Thus, there is the need to explore magnet arrangements which maximize radial airgap flux density per volume of magnet material used. The torque-production characteristics of a Halbach and conventional rotor magnet arrangement, with and without a permeable rotor back-iron, operating with a magnetically-backed slotless armature was studied in Chapter 2. The results of this study showed that a more economic motor design can be obtained with a slotted armature, and that with a slotted armature the preferred magnet arrangement is the conventional arrangement for the EV application. The study also explained, in an intuitive manner, why and when to use a Halbach array in the design of PMSMs.

- In Chapter 3, we designed a slotted motor with a conventional magnet arrangement that is capable of producing 450 Nm of torque at 110°C. The design methodology was to produce the highest torque per Ohmic power dissipation in the armature windings while keeping magnet cost in check. The motor was optimized in terms of the number of pole-pairs and the thickness of the armature windings. Low-loss M-15, 29 gauge nonoriented electrical steel was used in the stator construction to reduce the no-load losses in the motor. Unlike the stator back-iron which experiences significant changes in magnetic flux density during motor operation, the rotor back-iron was made out of solid 1018 HF steel for enhanced structural integrity. The active mass of the wheel motor is 25.1 kg.

- For efficient operation of the power-electronic inverter, the number of turns of the motor was chosen so that the inverter operates at high voltage and reduced current. Efficient 4:1 speed range operation is achieved with a 3-phase inverter with a bidirectional boost converter in its dc link. By using this novel inverter topology we avoid the need for flux weakening which compromises drive efficiency. The cooling requirements of the motor are also reduced. In addition to improved drive-cycle efficiency, there is a factor of 1.5 reduction in the installed V-A capacity over a low-voltage/high-current inverter that does not utilize flux weakening to achieve wide-speed range operation, and the snubbing requirements are also mitigated. These issues are discussed in Chapter 4.

- Detailed design of the power-electronic inverter and the microprocessor controller are given in Chapter 5.

- The wheel motor and novel inverter were fabricated and tested at the Superior Electric Company in Bristol, CT, as described in Chapter 6. The efficiency of the drive (inverter and motor) over the Urban and Highway drive cycles were estimated at 85% and 92% respectively. The packaging of the motor and its assembly on the dynamometer did not permit a meaningful thermal characterization of the motor.

7.2 Thesis Conclusions

There are three major conclusions that can be drawn from this thesis. The first is that efficient high-torque, low-mass wheel motors are possible. A viable design approach for the motor is to maximize the peak torque produced per Ohmic power dissipated in the armature windings. A slotted stator is desirable in reducing magnet mass and a high number of poles is required to reduce endturn length and the thickness of the rotor and stator back-iron. The use of low-loss electrical steel with thin laminations (14 mils in this thesis) help to reduce eddy-current and hysteresis losses in the stator teeth. The rotor back-iron may be made of solid electrical steel.

Secondly, the use of a 3-phase inverter with a bidirectional boost converter in the dc

link permits efficient operation of the high-voltage/low-current power-electronic inverter. By rating the semiconductor switches to withstand the highest back-emf of the motor, catastrophic failures where the motor injects large currents in to the dc power source such as a traction battery is avoided. The cooling requirements of the motor are reduced by not using flux-weakening as a means to obtain wide speed range operation. The cost of the new inverter is comparable to, if not less than, that of a standard 3-phase voltage-source inverter.

The third conclusion pertains to when to use a Halbach magnet arrangement in the design of a PMSM. Halbach arrays are superior when one is precluded from using a magnetic rotor backing. In such applications the Halbach magnet arrangement produces higher torque than a conventional magnet arrangement. If a magnetic rotor backing can be used, then one does better by using a conventional magnet arrangement when the rotor magnets are thin. Beyond a certain thickness of rotor magnets (this depends on the geometry of the motor in question) a Halbach magnet arrangement becomes beneficial.

7.3 Recommendations for Future Work

In our experimentation, we discovered that the SS461A Hall sensors could not be made to operate reliably with only the fringing fields from the magnets. Therefore the next iteration of the wheel motor design should have the magnets overhang the stack by a couple of millimeters so that the Hall sensors can be located underneath the overhang. This arrangement will insure reliable operation of the Hall sensors over the temperature range of operation of the motor without false triggering from the armature reaction flux. Another way of determining rotor magnet position with respect to the stator windings is to paint the edges of alternating magnets and use an optical emitter-detector pair. Although this approach is less robust than using the Hall magnetic field sensors due to eventual degradation of the optical surfaces from dirt, it may be necessary to implement such an optical shaft encoder to insure reliable operation of the prototype wheel motor. The third approach, which would be ideal if it can be made to work, is to commutate the motor based on the back-emf of the motor, measured through the non-conducting phase. This approach eliminates the need for an additional sensor within the motor housing.

Our original intent of reducing switching losses in the three half-bridges that drive the motor in the boost mode when the motor back-emf was above the dc bus voltage was unachievable since it was not possible to close a robust control loop around the boost converter. This is because the boost inductor sometimes operated in continuous conduction, thus changing the plant dynamics. The absence of ramp compensation also resulted in sub-harmonic oscillations which caused the inductor to chatter. The next iteration of the inverter design should explore adding a ramp to the sensed boost inductor current or operating the boost inductor in continuous conduction. Although adding a ramp to the boost inductor current eliminates sub-harmonic oscillations, ramp compensation has the undesirable effect of reducing the dynamic range of the current-mode PWM comparator. Operating the boost inductor in continuous conduction will prevent the plant dynamics from changing in various regimes of the boost converter's operation. The cost is additional energy storage in the boost inductor.

Due to the lack of proper packaging and mounting of the prototype wheel motor on the dynamometer, it was impossible to obtain meaningful data that could predict the thermal performance of the motor. These measurements remain to be done.

Future designs of the wheel motor should also explore skewing the magnets instead of the slots to reduce cogging, as the skewed slots expose sharp lamination edges which can cut easily through slot liners. Furthermore, unskewed slots will make the motor easier to wind, require less wire and reduce Ohmic losses in the armature windings.

Regenerative braking of the motor was not implemented. This remains to be done. Last but not least, the MC68HC16Z1 is fast enough for the control of a single wheel motor, and therefore the motor commutation and phase current selection logic which are currently implemented in GALs can be implemented in software within the microcontroller.

Appendix A

Circuit Schematics

This Appendix contains the schematics of the low-voltage circuitry on the gate-drive board, control board attached to the MC68HC16Z1 evaluation board and the user interface keypad. Descriptions of these circuits and how they operate are given in Chapter 5.

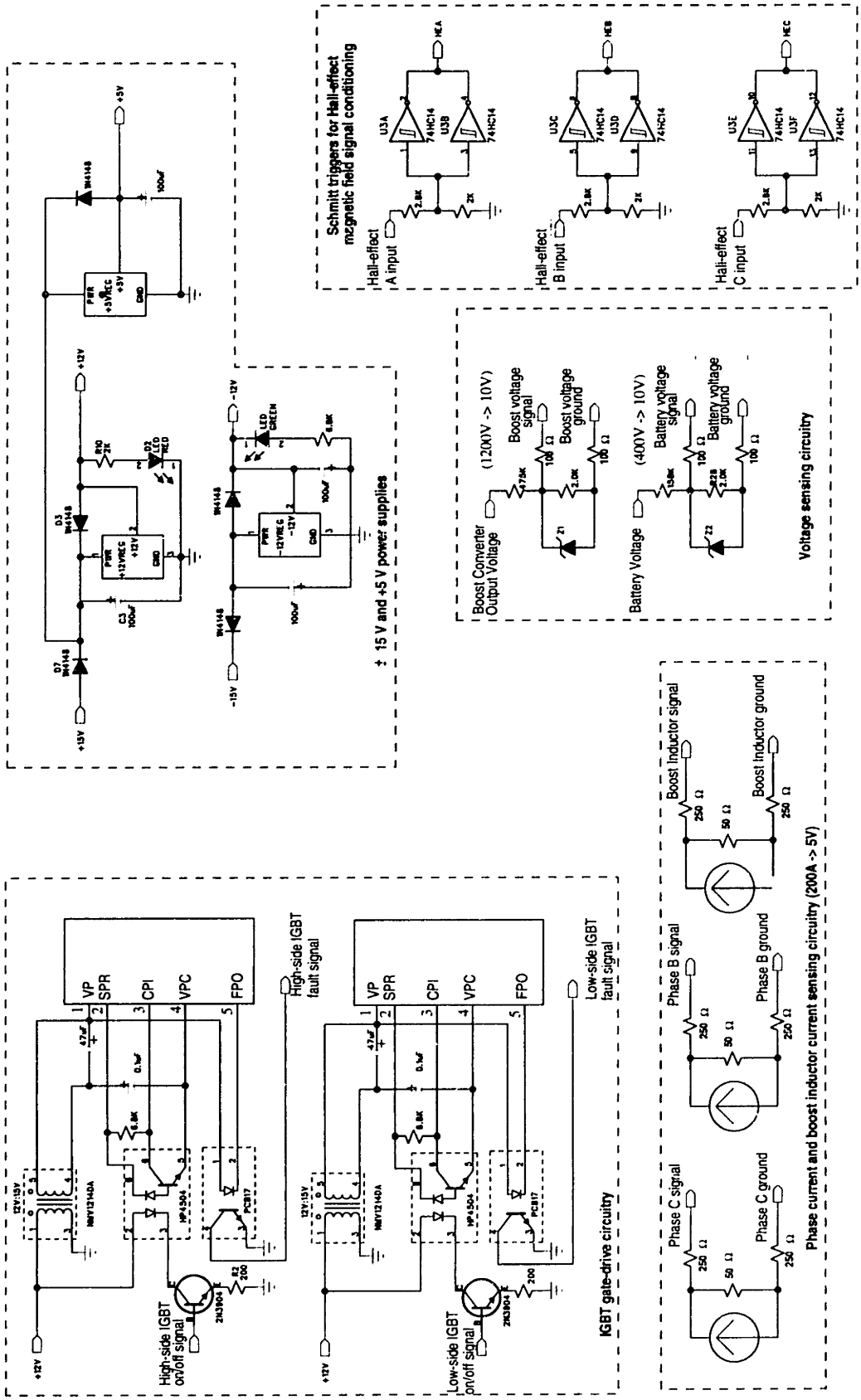

Figure A-1: Circuitry on gate-drive board.

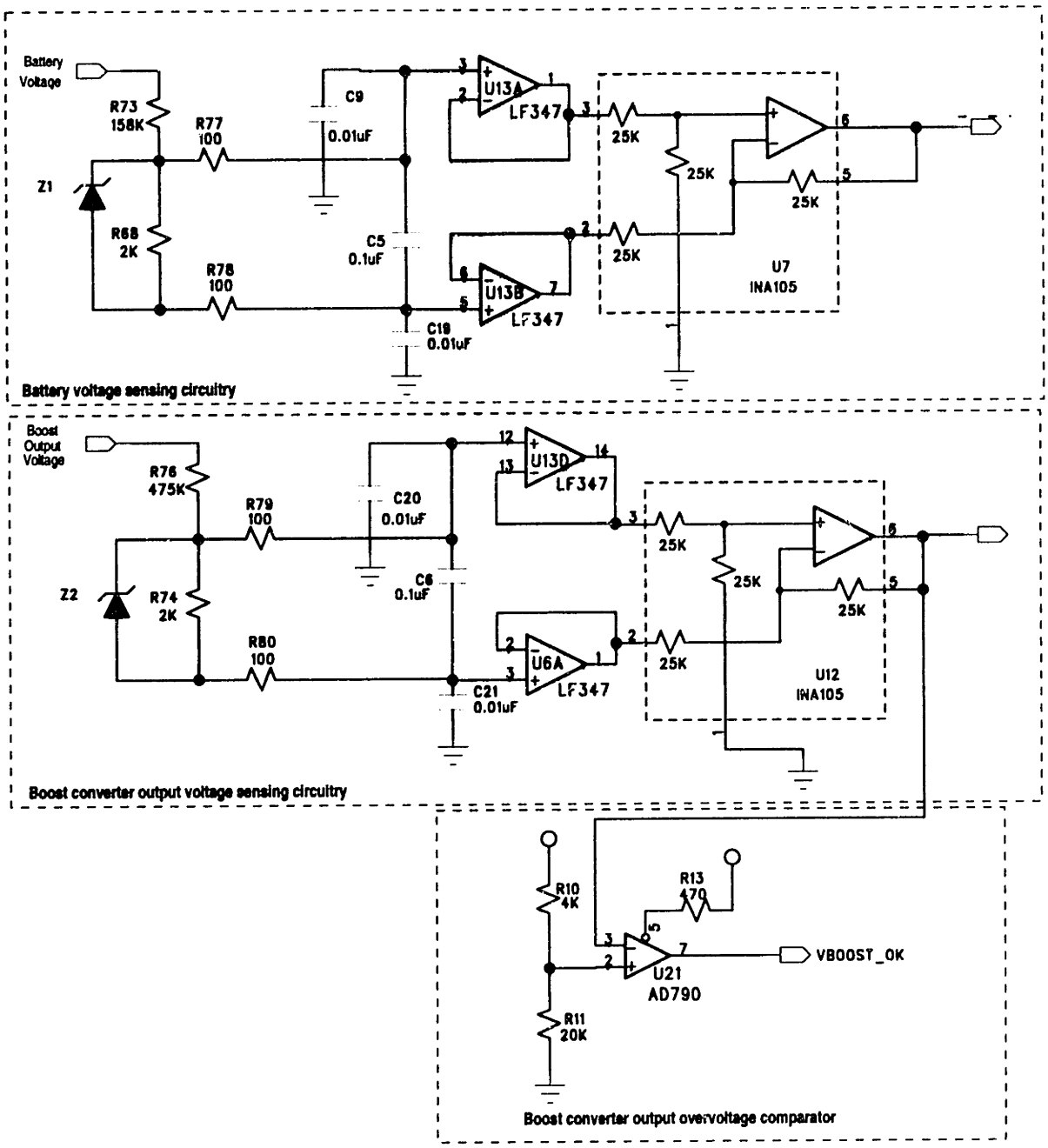

Figure A-2: Voltage sensing circuitry.

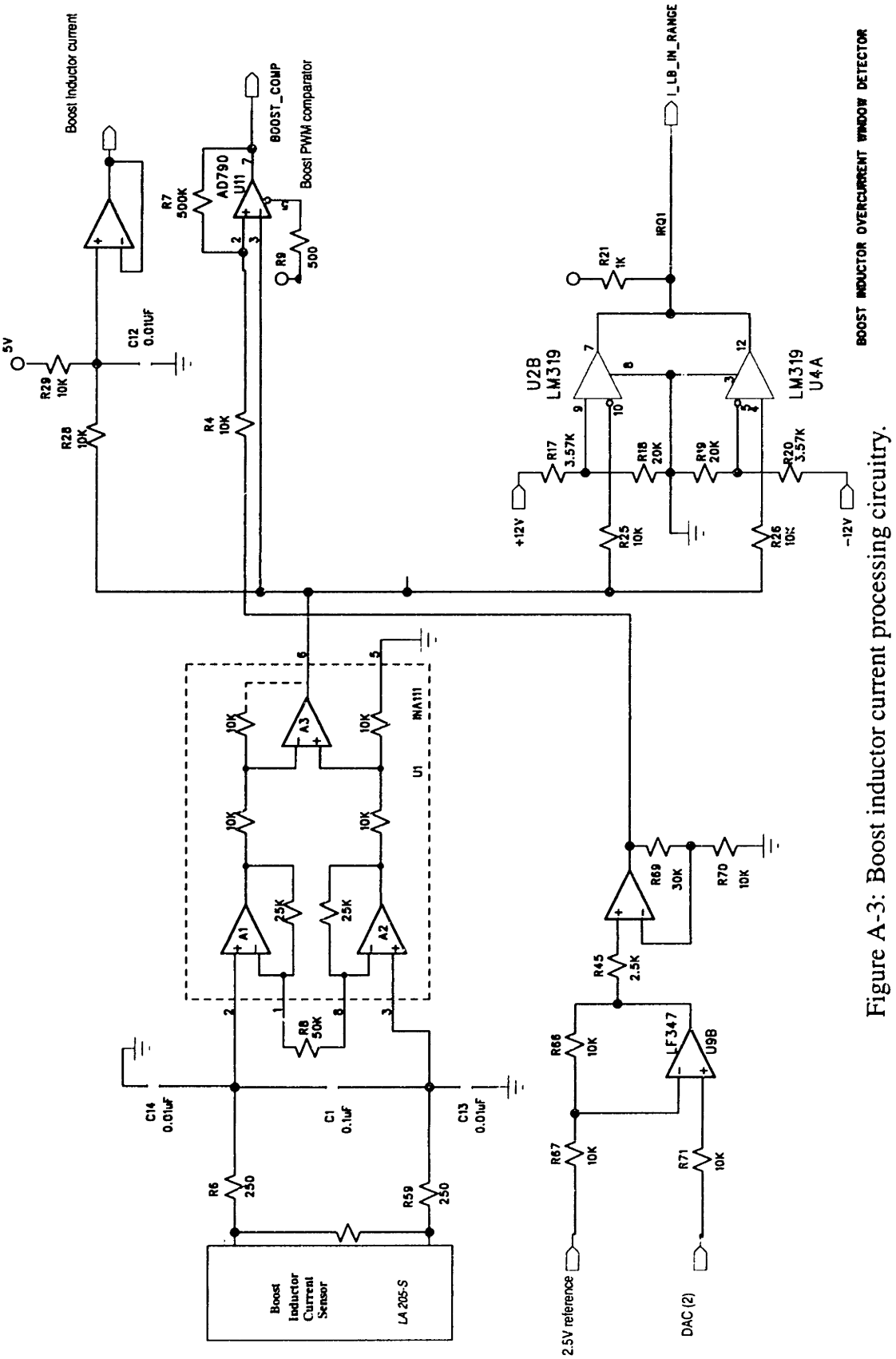

Figure A-3: Boost inductor current processing circuitry.

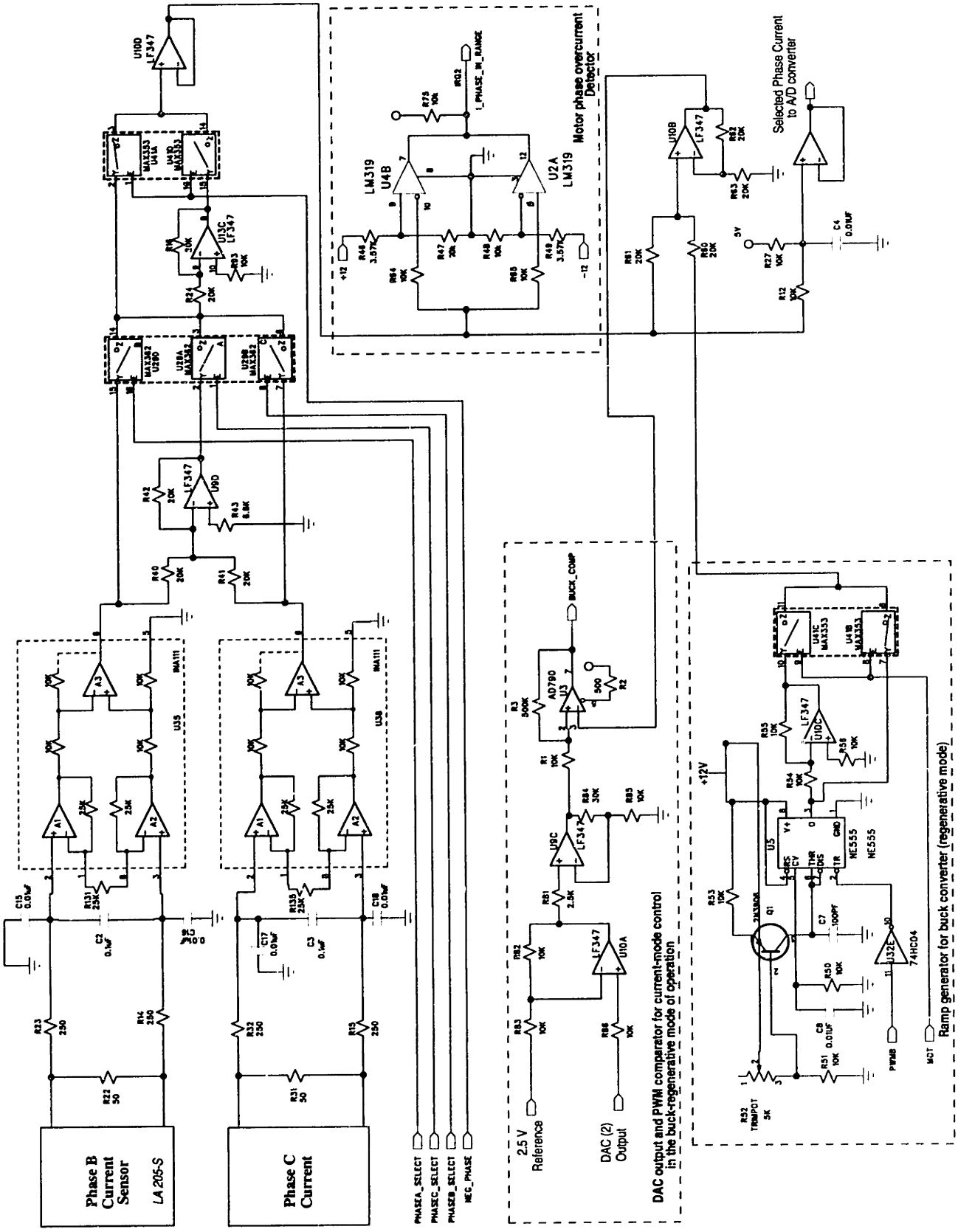

Figure A-4: Motor phase current processing circuitry.

Drawings of GALs indicating chip pinouts are given, along with their programming files, in Appendix B

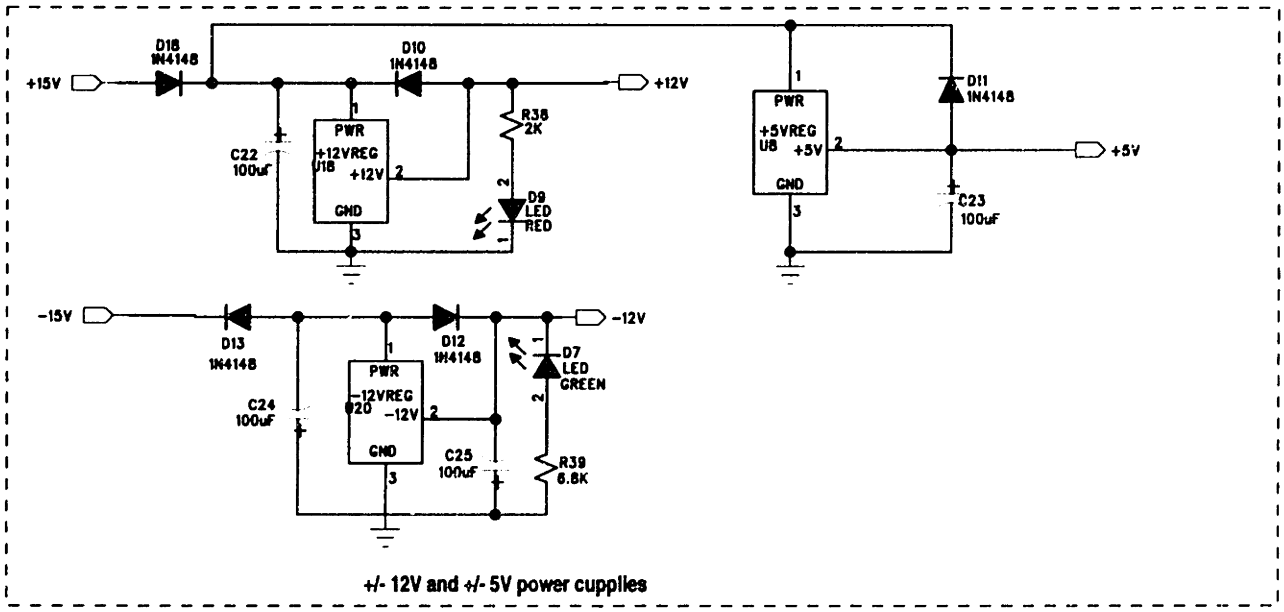

Figure A-5: Gate-Array Logic chips and power supplies for analog/digital board.

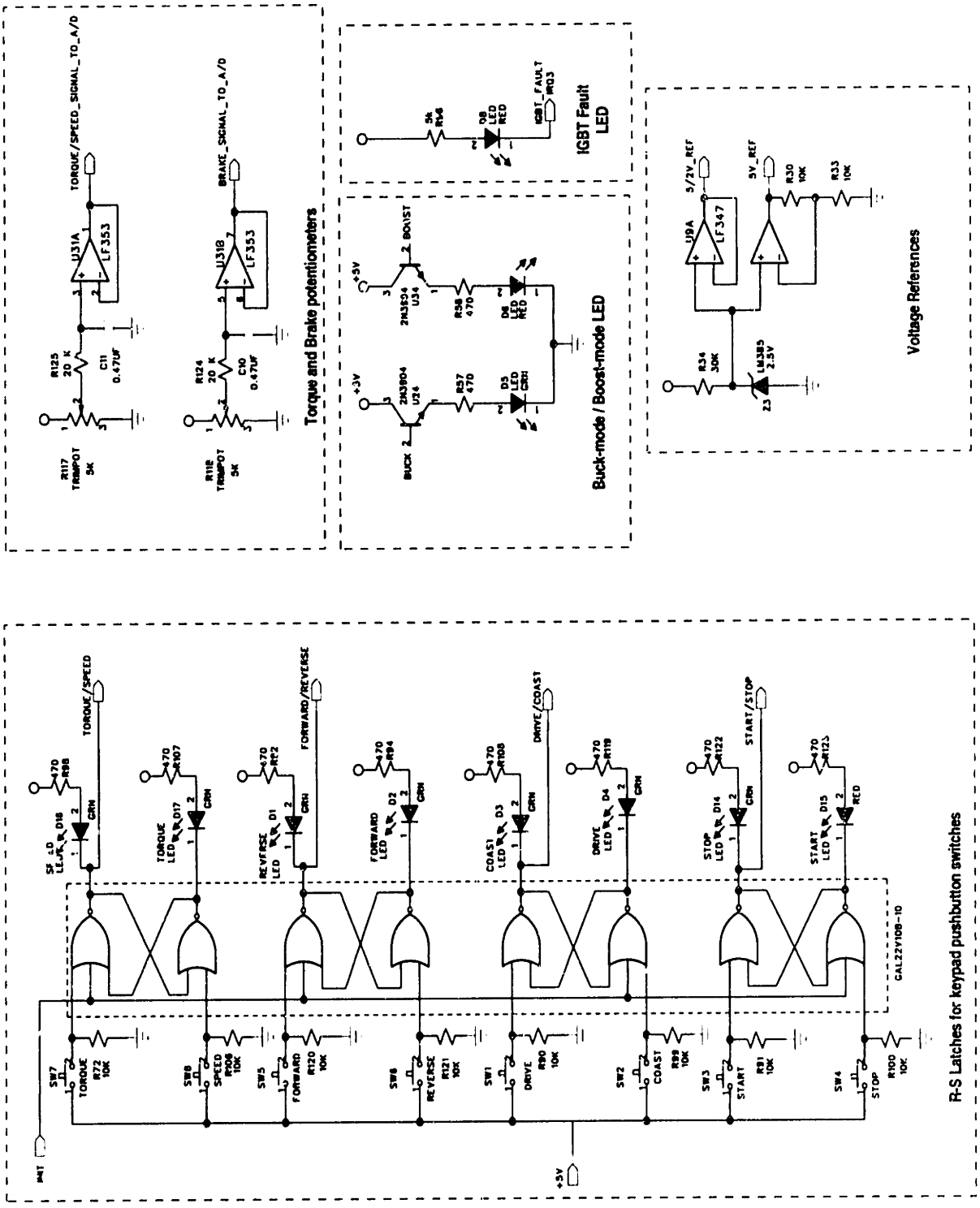

Figure A-6: Circuitry on user keypad and display board

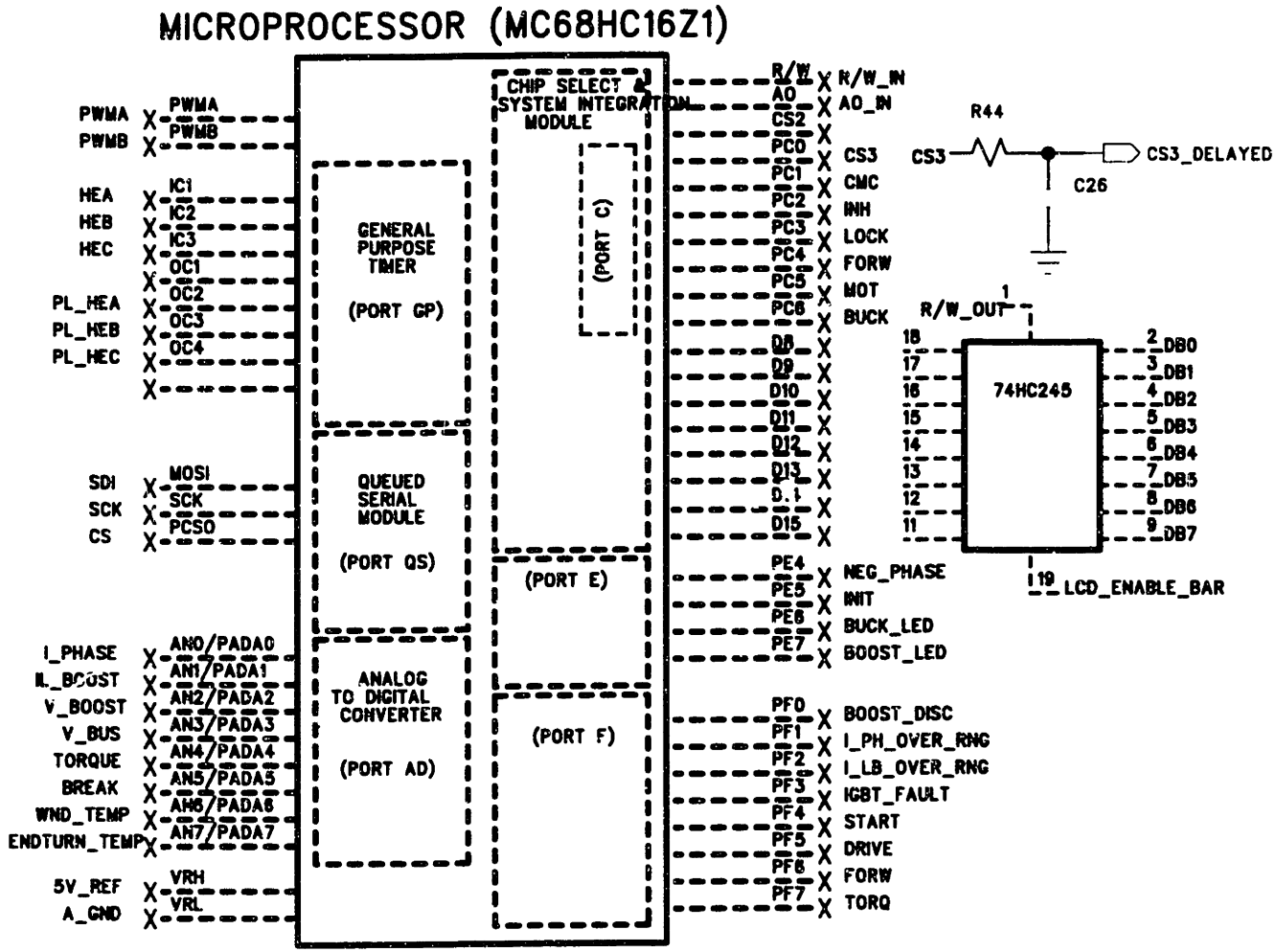

Figure A-7: Simplified schematic of microcontroller showing pins used

Appendix B

GAL22v10 Programming Files

To simplify the wiring of the analog/digital board for the prototype inverter, most of the digital glue logic was implemented with electrically erasable programmable Gate Array Logic (GAL). A total of four GAL22V10 devices were used in the experimental prototype. This chapter contains the source code describing the logic configuration of the devices. A schematic chip diagram is attached at the end of each source code.

B.1 Phase Current Selection Logic

The function of this GAL is to generate the phase current select signals SELA, SELB, SELC, and phase current negate signal, NEG, that are used to determine the motor phase current around which to close the current feedback loop. The truth table of the logic implemented in this GAL is given in Figure 5-12 in Chapter 5. A fault signal is generated in the event of motor-phase ovecurrent, boost-inductor overcurrent, boost-converter overvoltage, or a bad Hall-effect signal combination - which is all zeroes or all ones. The fault signal is used to shut down the IGBTs and is cleared by pushing a button on the user interface keypad.

```
Name      select;
Partno    CA0006 ;
Date      11/28/95;
Revision  01;
Designer  ofori;
Company   MIT;
Assembly  None;
Location  None;
```

```
Device    P22V10;

/*****************************************************************/
/* Phase current select  combinational logic generator           */
/*****************************************************************/

/*****************************************************************/
/* Allowable Target Device Types :  GAL22V10                     */
/*****************************************************************/

/**  Inputs  **/

PIN 1 = INH; /* HIGH TO TURN OFF GATE DRIVES */
PIN 2 = NO_IGBT_FAULT; /* NO IGBT FAULT */
PIN 3 = FORW; /* SPIN MOTOR FORWARD OR REVERSE */
PIN 4 = MOT; /* MOTOR OR REGEN , BUT NOT USED*/
PIN 5 = PL_HEA; /* HALL EFFECT A */
PIN 6 = PL_HEB; /* HALL EFFECT B */
PIN 7 = PL_HEC; /* HALL EFFECT C */
PIN 8 = PWMB; /* BUCK PWM SIGNAL */
PIN 9 = VBOOST_IN_RANGE;    /* HIGH WHEN VBOOST IS IN RANGE */
PIN 10 = IPHASE_IN_RANGE;  /* HIGH WHEN PHASE CURRENT IS IN RANGE */
PIN 11 = ILB_IN_RANGE;    /* HIGH WHEN BOOST IND. CURRENT IS IN RANGE */
PIN 13 = CLEAR_FAULT;     /* HIGH TO CLEAR ALL FAULTS */

/**  Outputs  **/

PIN 23 = SELB;  /* SELECT PHASE B CURRENT */
PIN 22 = SELC;  /* SELECT PHASE C CURRENT */
PIN 21 = SELA;  /* SELECT PHASE A CURRENT */
PIN 20 = NEG_PHASE;      /* HIGH WHEN SENSED PHASE CURRENT IS */
                         /* TO BE NEGATED */
PIN 19 = PWMB_BAR;       /* INVERTED PWMB TO TRIGGER BUCK RAMP */
PIN 18 = FAULT;          /* HIGH DURING IGBT FAULT, BOOST INDUCTOR ... */
                         /* OVER CURRENT, BOOST OVERVOLTAGE, PHASE ... */
                         /* OVER CURRENT, OR BAD HALL EFFECT COMBINATION*/
PIN 17 = NO_FAULT;        /* HIGH WHEN NO FAULT HAS OCCURED */
PIN 16 = BAD_HALL_SIGNAL;
PIN 15 = GOOD_HALL_SIGNAL;

/** Declarations and Intermediate Variable Definitions **/
BAD_HALL_EFFECT = (PL_HEA & PL_HEB & PL_HEC) #
                  (!PL_HEA & !PL_HEB & !PL_HEC);

/** Logic Equations **/

SELA = (!PL_HEA & PL_HEB & !PL_HEC) # (PL_HEA & !PL_HEB & PL_HEC);

SELB = ( !PL_HEA & !PL_HEB & PL_HEC) # ( PL_HEA & PL_HEB & !PL_HEC);
```

```
SELC = ( !PL_HEA & PL_HEB & PL_HEC) # ( PL_HEA & !PL_HEB & !PL_HEC);

NEG_PHASE = ( !FORW & !PL_HEA & PL_HEB & PL_HEC) #
            ( !FORW & PL_HEA & !PL_HEB & PL_HEC) #
            ( !FORW & PL_HEA & PL_HEB & !PL_HEC) #
            ( FORW & PL_HEA & !PL_HEB & !PL_HEC) #
            ( FORW & !PL_HEA & PL_HEB & !PL_HEC) #
            ( FORW & !PL_HEA & !PL_HEB & PL_HEC) ;

PWMB_BAR = !PWMB;

FAULT = !NO_FAULT # !IPHASE_IN_RANGE #
        !ILB_IN_RANGE # BAD_HALL_EFFECT # !NO_IGBT_FAULT;
NO_FAULT = !FAULT # CLEAR_FAULT;

GOOD_HALL_SIGNAL = !BAD_HALL_SIGNAL # CLEAR_FAULT;

BAD_HALL_SIGNAL = !GOOD_HALL_SIGNAL # BAD_HALL_EFFECT;
```

Chip Diagram

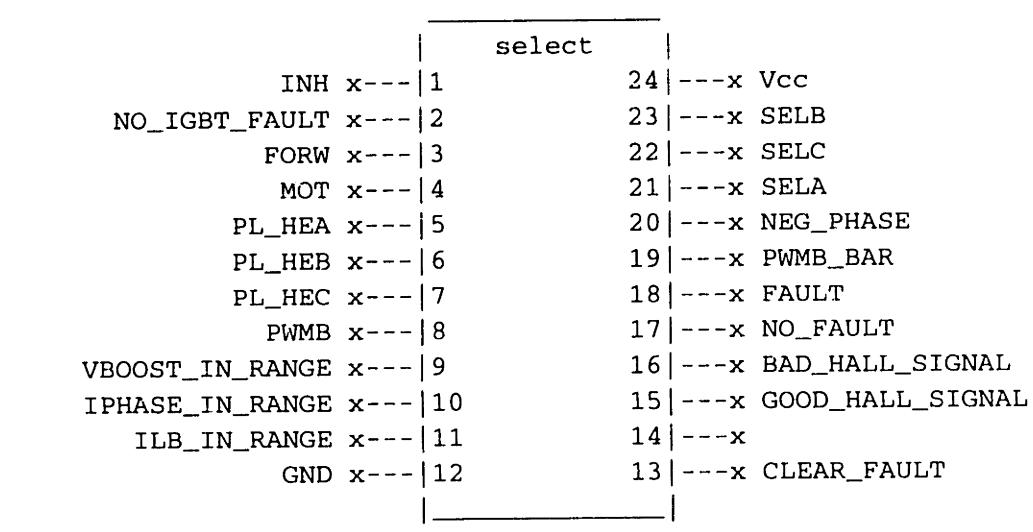

B.2 IGBT Switching Logic

This GAL determines the switching status of all the intellimod IGBTs based on the truth table in Figure 5-12. The SW1 - SW8 signals generated by this GAL is buffered by an octal line driver (74HCT244) and used to drive the gates of the intellimod IGBTs. The inhibit (INH) signal, when high, turns off all the IGBTS. The phase-locked Hall-effect signals (PL_HEA - PL_HEC) in conjunction with the motor rotation direction signal (MOT) are used to commutate the motor. Two different IGBT switching strategy were implemented; one with current-mode control of the boost converter where the 3-phase buck converter just operates as a commutator and the other where the boost converter was switched open loop with bang-bang control and the 3-phase buck converter was used to regulate the motor curent. The code for both versions of the GAL are given below.

B.2.1 Switching Logic for Current-Mode Control of Boost Converter

```
Name      IGBT_SW1;
Partno    CA0006 ;
Date      11/28/95;
Revision  01;
Designer  ofori;
Company   MIT;
Assembly  None;
Location  None;
Device    P22V10;

/*****************************************************************/
/* Switch states combinational logic generator                   */
/*                                                               */
/*****************************************************************/

/*****************************************************************/
/* Allowable Target Device Types :  GAL22V10                     */
/*****************************************************************/

/**  Inputs  **/

PIN 1 = INH; /* HIGH TO TURN OFF GATE DRIVES */
PIN 2 = NOT_USED;       /* CURRENTLY WIRED TO LOCK */
PIN 3 = FORW; /* SPIN MOTOR FORWARD OR REVERSE */
PIN 4 = MOT; /* MOTOR OR REGEN */
PIN 5 = PL_HEA; /* HALL EFFECT A */
PIN 6 = PL_HEB; /* HALL EFFECT B */
```

```
PIN 7 = PL_HEC; /* HALL EFFECT C */
PIN 8 = BUCK;  /* WHEN BATTERY VOLTAGE > BACK EMF */
PIN 9 = PWM_BUCK;  /* PWM SIGNAL FOR BUCK CONVERTER */
PIN 10 = PWM_BOOST; /* PWM SIGNAL FOR BOOST CONVERTER */
PIN 11 = VBOOST_OK;      /* HIGH WHEN VBOOST IS BELOW MAX VALUE */
PIN 13 = NO_FAULT;       /* HIGH WHEN THERE IS NO FAULT */

/* FAULT HERE MEANS BOOST INDUCTOR OVERCURRENT, BOOST OVERVOLTAGE  */
/* PHASE OVERCURRENT, BAD HALL EFFECT SIGNAL, AND IGBT FAULT       */
/* FAULT IS CLEAR BY PUSHING CLEAR FAULT BUTTON  ON KEYPAD         */

/**  Outputs  **/
PIN 23 = SW1; /* TURNON SIGNAL FOR BOOST TOP SWITCH */
PIN 22 = SW2; /* TURNON SIGNAL FOR BOOST BOT SWITCH */
PIN 21 = SW3; /* TURNON SIGNAL FOR PHASE A TOP SWITCH */
PIN 20 = SW4; /* TURNON SIGNAL FOR PHASE A BOT SWITCH */
PIN 19 = SW5;  /* TURNON SIGNAL FOR PHASE B TOP SWITCH */
PIN 18 = SW6; /* TURNON SIGNAL FOR PHASE B BOT SWITCH */
PIN 17 = SW7;  /* TURNON SIGNAL FOR PHASE C TOP SWITCH */
PIN 16 = SW8; /* TURNON SIGNAL FOR PHASE C BOT SWITCH */
PIN 15 = FAULT;   /* HIGH WHEN THERE IS A FAULT */

/** Declarations and Intermediate Variable Definitions **/

DRIVE_OK = !INH & NO_FAULT ;

/** Logic Equations **/

SW1 = (DRIVE_OK & !MOT & !PL_HEA & PL_HEC & PWM_BOOST) #
      (DRIVE_OK & !MOT & !PL_HEA & PL_HEB & PWM_BOOST) #
      (DRIVE_OK & !MOT & PL_HEA & !PL_HEC & PWM_BOOST) #
      (DRIVE_OK & !MOT & PL_HEA & !PL_HEB & PWM_BOOST) #
      (DRIVE_OK & BUCK & !MOT & !PL_HEA & PL_HEC) #
      (DRIVE_OK & BUCK & !MOT & !PL_HEA & PL_HEB) #
      (DRIVE_OK & BUCK & !MOT & PL_HEA & !PL_HEC) #
      (DRIVE_OK & BUCK & !MOT & PL_HEA & !PL_HEB);

/* VBOOST_OK DISABLES BOOST CONVERTER WHEN BUS GETS TOO HIGH */
/* CURRENTLY REDUNDATNT BECAUSE OF THE DEFINITION OF FAULT   */
/* IF ALL WORKS WELL, VBOOST_OK FROM FAULT DEFINITION */

SW2 = (DRIVE_OK & !BUCK & (MOT & VBOOST_OK) & !PL_HEA & PL_HEC & PWM_BOOST) #
      (DRIVE_OK & !BUCK & (MOT & VBOOST_OK) & !PL_HEA & PL_HEB & PWM_BOOST) #
      (DRIVE_OK & !BUCK & (MOT & VBOOST_OK) & PL_HEA & !PL_HEC & PWM_BOOST) #
      (DRIVE_OK & !BUCK & (MOT & VBOOST_OK) & PL_HEA & !PL_HEB & PWM_BOOST);

SW3 = (DRIVE_OK & FORW & MOT & PL_HEA & !PL_HEB & PWM_BUCK) #
      (DRIVE_OK & !FORW & MOT & !PL_HEA & PL_HEB & PWM_BUCK) #
      (DRIVE_OK & FORW & !BUCK & MOT & PL_HEA & !PL_HEB) #
      (DRIVE_OK & !FORW & !BUCK & MOT & !PL_HEA & PL_HEB);
```

```
SW4 = (DRIVE_OK & !FORW & !MOT & !PL_HEA & PL_HEB & PWM_BUCK) #
      (DRIVE_OK & !FORW & !BUCK & !MOT & !PL_HEA & PL_HEB) #
      (DRIVE_OK & FORW & MOT & !PL_HEA & PL_HEB) #
      (DRIVE_OK & FORW & BUCK & !PL_HEA & PL_HEB) #
      (DRIVE_OK & !MOT & PL_HEA & !PL_HEB & PWM_BUCK) #
      (DRIVE_OK & !BUCK & !MOT & PL_HEA & !PL_HEB) #
      (DRIVE_OK & !FORW & PL_HEA & !PL_HEB);

SW5 = (DRIVE_OK & !FORW & MOT & !PL_HEB & PL_HEC & PWM_BUCK) #
      (DRIVE_OK & !FORW & !BUCK & MOT & !PL_HEB & PL_HEC) #
      (DRIVE_OK & FORW & MOT & PL_HEB & !PL_HEC & PWM_BUCK) #
      (DRIVE_OK & FORW & !BUCK & MOT & PL_HEB & !PL_HEC);

SW6 = (DRIVE_OK & !MOT & PL_HEB & !PL_HEC & PWM_BUCK) #
      (DRIVE_OK & !MOT & !PL_HEB & PL_HEC & PWM_BUCK) #
      (DRIVE_OK & FORW & !PL_HEB & PL_HEC) #
      (DRIVE_OK & !BUCK & !MOT & PL_HEB & !PL_HEC) #
      (DRIVE_OK & !BUCK & !MOT & !PL_HEB & PL_HEC) #
      (DRIVE_OK & !FORW & PL_HEB & !PL_HEC);

SW7 = (DRIVE_OK & !FORW & MOT & PL_HEA & !PL_HEC & PWM_BUCK) #
      (DRIVE_OK & !FORW & !BUCK & MOT & PL_HEA & !PL_HEC) #
      (DRIVE_OK & FORW & MOT & !PL_HEA & PL_HEC & PWM_BUCK) #
      (DRIVE_OK & FORW & !BUCK & MOT & !PL_HEA & PL_HEC);

SW8 = (DRIVE_OK & !MOT & !PL_HEA & PL_HEC & PWM_BUCK) #
      (DRIVE_OK & !MOT & PL_HEA & !PL_HEC & PWM_BUCK) #
      (DRIVE_OK & FORW & PL_HEA & !PL_HEC) #
      (DRIVE_OK & !BUCK & !MOT & !PL_HEA & PL_HEC) #
      (DRIVE_OK & !BUCK & !MOT & PL_HEA & !PL_HEC) #
      (DRIVE_OK & !FORW & !PL_HEA & PL_HEC);

FAULT = !NO_FAULT ;
```

```
=============================================================
                      Chip Diagram
=============================================================

                      _______________
                     |   IGBT_SW1    |
           INH x---|1              24|---x Vcc
      NOT_USED x---|2              23|---x SW1
          FORW x---|3              22|---x SW2
           MOT x---|4              21|---x SW3
        PL_HEA x---|5              20|---x SW4
        PL_HEB x---|6              19|---x SW5
        PL_HEC x---|7              18|---x SW6
          BUCK x---|8              17|---x SW7
      PWM_BUCK x---|9              16|---x SW8
     PWM_BOOST x---|10             15|---x FAULT
     VBOOST_OK x---|11             14|---x
           GND x---|12             13|---x NO_FAULT
                     |_______________|
```

B.2.2 Switching Logic for Current-Mode Control of Boost Converter

```
Name      IGBT_SW2;
Partno    CA0006 ;
Date      11/28/95;
Revision  01;
Designer  ofori;
Company   MIT;
Assembly  None;
Location  None;
Device    P22V10;

/*************************************************************/
/* Switch states combinational logic generator               */
/* for the implementation where the boost converter is switched */
/* open loop                                                 */
/*************************************************************/

/*************************************************************/
/* Allowable Target Device Types :  GAL22V10                 */
/*************************************************************/

/**  Inputs  **/

PIN 1 = INH; /* HIGH TO TURN OFF GATE DRIVES */
PIN 2 = NOT_USED;       /* CURRENTLY WIRED TO LOCK */
PIN 3 = FORW; /* SPIN MOTOR FORWARD OR REVERSE */
```

```
PIN 4 = MOT; /* MOTOR OR REGEN */
PIN 5 = PL_HEA; /* HALL EFFECT A */
PIN 6 = PL_HEB; /* HALL EFFECT B */
PIN 7 = PL_HEC; /* HALL EFFECT C */
PIN 8 = BUCK;  /* WHEN BATTERY VOLTAGE > BACK EMF */
PIN 9 = PWM_BUCK;  /* PWM SIGNAL FOR BUCK CONVERTER */
PIN 10 = PWM_BOOST; /* PWM SIGNAL FOR BOOST CONVERTER */
PIN 11 = VBOOST_OK;      /* HIGH WHEN VBOOST IS BELOW MAX VALUE */
PIN 13 = NO_FAULT;       /* HIGH WHEN THERE IS NO FAULT */

/* FAULT HERE MEANS BOOST INDUCTOR OVERCURRENT, BOOST OVERVOLTAGE  */
/* PHASE OVERCURRENT, BAD HALL EFFECT SIGNAL, AND IGBT FAULT       */
/* FAULT IS CLEAR BY PUSHING CLEAR FAULT BUTTON  ON KEYPAD         */

/**  Outputs  **/
PIN 23 = SW1; /* TURNON SIGNAL FOR BOOST TOP SWITCH */
PIN 22 = SW2; /* TURNON SIGNAL FOR BOOST BOT SWITCH */
PIN 21 = SW3; /* TURNON SIGNAL FOR PHASE A TOP SWITCH */
PIN 20 = SW4; /* TURNON SIGNAL FOR PHASE A BOT SWITCH */
PIN 19 = SW5;  /* TURNON SIGNAL FOR PHASE B TOP SWITCH */
PIN 18 = SW6; /* TURNON SIGNAL FOR PHASE B BOT SWITCH */
PIN 17 = SW7;  /* TURNON SIGNAL FOR PHASE C TOP SWITCH */
PIN 16 = SW8; /* TURNON SIGNAL FOR PHASE C BOT SWITCH */
PIN 15 = FAULT;   /* HIGH WHEN THERE IS A FAULT */

/** Declarations and Intermediate Variable Definitions **/

DRIVE_OK = !INH & NO_FAULT & MOT & BUCK;

/** Logic Equations **/

SW1 = 'b'0;

/* VBOOST_OK DISABLES BOOST CONVERTER WHEN BUS GETS TOO HIGH */

SW2 = (DRIVE_OK & VBOOST_OK & PWM_BOOST);

SW3 = (DRIVE_OK & FORW & PL_HEA & !PL_HEB & PWM_BUCK) #
      (DRIVE_OK & !FORW & !PL_HEA & PL_HEB & PWM_BUCK);

SW4 = (DRIVE_OK & FORW & !PL_HEA & PL_HEB) #
      (DRIVE_OK & !FORW & PL_HEA & !PL_HEB);

SW5 = (DRIVE_OK & FORW & PL_HEB & !PL_HEC & PWM_BUCK) #
      (DRIVE_OK & !FORW & !PL_HEB & PL_HEC & PWM_BUCK);

SW6 = (DRIVE_OK & FORW & !PL_HEB & PL_HEC) #
      (DRIVE_OK & !FORW & PL_HEB & !PL_HEC);

SW7 = (DRIVE_OK & FORW & !PL_HEA & PL_HEC & PWM_BUCK) #
```

```
      (DRIVE_OK & !FORW & PL_HEA & !PL_HEC & PWM_BUCK);

SW8 = (DRIVE_OK & FORW & PL_HEA & !PL_HEC) #
      (DRIVE_OK & !FORW & !PL_HEA & PL_HEC);

FAULT = !NO_FAULT ;
```

```
================================================================
                        Chip Diagram
================================================================
```

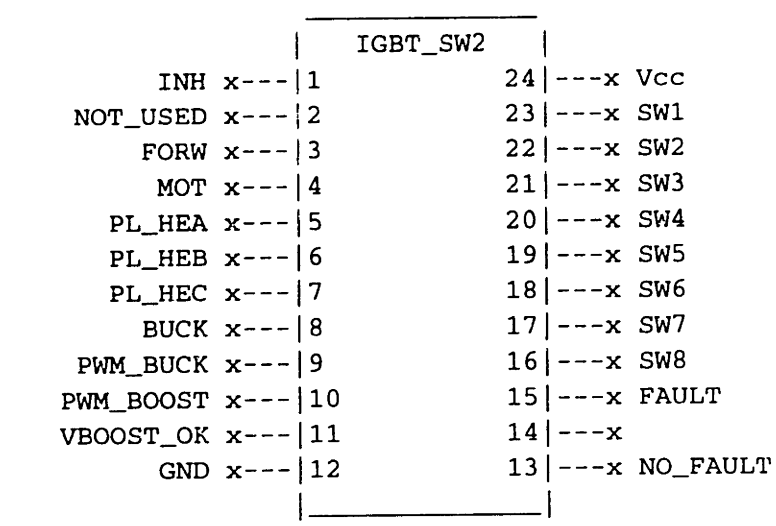

B.3 R-S Latches for User Interface

An eight-button keypad is used to set the drive mode of the motor as shown in Figure 5-19. With these buttons, the user can select a torque feedback loop or a speed feedback loop[1], set the motor's direction of rotation, engage or disengage the motor from the drive, and start or stop the motor. This GAL implements the R-S latches used to latch user keypad commands.

```
Name      switches;
Partno    CA0006;
Date      11/01/95;
Revision  01;
Designer  ofori;
Company   MIT;
Assembly  None;
Location  None;
Device    P22V10;

/*****************************************************/
/* Keypad switches combinational logic  (RS latches)  */
/*****************************************************/
/**  Inputs  **/
PIN 1 = CLK; /* Register Clock */
PIN 2 = TORQUE; /* Torque Mode */
PIN 3 = SPEED; /* Speed Mode */
PIN 4 = FORWARD;     /* Spin in forward direction */
PIN 5 = REVERSE; /* Spin in reverse direction */
PIN 6 = DRIVE;         /* Inverter drives motor */
PIN 7 = COAST; /* Inverter lets motor coast */
PIN 8 = START; /* Start motor */
PIN 9 = STOP; /* Stop motor */
PIN 10 = INIT ;  /* Initialize switch settings */

/**  Outputs  **/
PIN 22 = TORQUE_OUT; /* Debounced torque signal */
PIN 23 = SPEED_OUT; /* Debounced speed signal */
PIN 20 = FORW_OUT; /* Debounced forward signal */
PIN 21 = REV_OUT; /* Debounced reverse signal */
PIN 18 = DRIVE_OUT; /* Debounced drive signal */
PIN 19 = COAST_OUT; /* Debounced coast signal */
PIN 16 = START_OUT; /* Debounced start signal */
```

[1]The speed feedback loop was not implemented in our prototype but the signal is available for use

```
PIN 17 = STOP_OUT; /* Debounced stop signal */

/** Logic Equations **/
TORQUE_OUT = !(TORQUE # INIT # SPEED_OUT);

SPEED_OUT = !(TORQUE_OUT # SPEED);

FORW_OUT = !(FORWARD # INIT # REV_OUT);

REV_OUT = !(REVERSE # FORW_OUT);

DRIVE_OUT = !(DRIVE # COAST_OUT);

COAST_OUT = !(COAST # INIT # DRIVE_OUT);

START_OUT = !(START # STOP_OUT);

STOP_OUT = !(STOP # INIT # START_OUT);
```

```
============================================================
                        Chip Diagram
============================================================

                   _______________
                  |    switches   |
        CLK x---|1             24|---x Vcc
     TORQUE x---|2             23|---x SPEED_OUT
      SPEED x---|3             22|---x TORQUE_OUT
    FORWARD x---|4             21|---x REV_OUT
    REVERSE x---|5             20|---x FORW_OUT
      DRIVE x---|6             19|---x COAST_OUT
      COAST x---|7             18|---x DRIVE_OUT
      START x---|8             17|---x STOP_OUT
       STOP x---|9             16|---x START_OUT
       INIT x---|10            15|---x
            x---|11            14|---x
        GND x---|12            13|---x
                |_______________|
```

B.4 Miscellaneous Logic

This GAL is used to perform several miscellaneous glue logic. It is used to generate the proper ENABLE pulse for the LCD since the timing requirements for the LCD slightly differ from the bus control signals available from the MC68HC16Z1. The chip is to

buffer the microcontroller's READ/WRITE and ADDRESS 0 signals as well as generate the PWM signals for the buck and boost converters. Finally, the chip is used to generate motor over-current and boost inductor over-current signals. Two versions of this GAL were implemented; one for when the boost converter is switched closed-loop with current-mode control and the other when it is switched open-loop. The difference in these two GALs lie in how the PWM clocks to the IGBTs are generated.

B.4.1 Current-Mode Control of Boost Converter

```
Name      misc_1;
Partno    CA0006 ;
Date      11/28/95;
Revision  01;
Designer  ofori;
Company   MIT;
Assembly  None;
Location  None;
Device    P22V10;

/*************************************************************/
/* LCD enable pulse generator and Boost & Buck SR-Latches  */
/*                                                           */
/*************************************************************/

/**  Inputs  **/
PIN 1 = R_W_IN;      /* Read/Write signal from micro */
PIN 2 = CS3;      /* Chip Select 3 from micro */
PIN 3 = CS3_DELAYED;      /* Chip Select 3 from micro delayed*/
PIN 4 = A0_IN;      /* Address 0 */
PIN 5 = PWMA;      /* Boost converter clock */
PIN 6 = PWMB;      /* Buck converter clock */
PIN 7 = MOT;      /* Motoring signal from micro */
PIN 8 = BOOST_COMP;      /* Output of boost comparator */
PIN 9 = BUCK_COMP;      /* Output of buck comparator */
PIN 10 =  CMC;      /* Current mode control mode from micro */
PIN 11 = I_LB_IN_RANGE;      /* Boost current in range */
PIN 13 = I_PHASE_IN_RANGE;  /* Phase current in range */

/**  Outputs  **/
PIN 23 = LCD_ENABLE;      /* Chip select for LCD */
PIN 22 = LCD_ENABLE_BAR;      /* Inverted LCD enable to enable HC244 */
PIN 21 = R_W_OUT;      /* Buffered Read/Write signal to LCD  */
PIN 20 = A0_OUT;      /* Buffered A0 signal to LCD  */
PIN 19 = PWM_BOOST;      /* PWM signal for boost converter  */
PIN 18 = PWM_BUCK;      /* PWM signal for buck converter */
PIN 17 = BOOST_Q;      /* Output of Boost SR Latch */
```

```
PIN 16 = BUCK_Q;      /* Output of Buck SR Latch */
PIN 15 = I_PH_OVER_RANGE;    /* High when phase current exceeds range */
PIN 14 = I_LB_OVER_RANGE;    /* High when I_LB exceeds range */

/** Declarations and Intermediate Variable Definitions **/
I_LB_RESET =
(BOOST_COMP & !MOT) # (!BOOST_COMP & MOT) # !I_LB_IN_RANGE;

I_PHASE_RESET =
(BUCK_COMP & !MOT) # (!BUCK_COMP & MOT) # !I_PHASE_IN_RANGE;

BOOST_Q = !(PWMA # BOOST_QBAR);

BOOST_QBAR = !(BOOST_Q # I_LB_RESET);

BUCK_Q = !(PWMB # BUCK_QBAR);

BUCK_QBAR = !(BUCK_Q # I_PHASE_RESET);

/** Logic Equations **/
LCD_ENABLE = (!CS3 & !CS3_DELAYED);

LCD_ENABLE_BAR = !LCD_ENABLE;

PWM_BOOST = (!CMC & PWMA) # (CMC & BOOST_QBAR);

PWM_BUCK = (!CMC & PWMB) # (CMC & BUCK_QBAR);

A0_OUT = A0_IN;

R_W_OUT = R_W_IN;

I_PH_OVER_RANGE = !I_PHASE_IN_RANGE;

I_LB_OVER_RANGE = !I_LB_IN_RANGE;
```

```
============================================================
                  Chip Diagram
============================================================

                      _____________
                     |    misc_1   |
          R_W_IN x---|1           24|---x Vcc
             CS3 x---|2           23|---x LCD_ENABLE
     CS3_DELAYED x---|3           22|---x LCD_ENABLE_BAR
           A0_IN x---|4           21|---x R_W_OUT
            PWMA x---|5           20|---x A0_OUT
            PWMB x---|6           19|---x PWM_BOOST
             MOT x---|7           18|---x PWM_BUCK
      BOOST_COMP x---|8           17|---x BOOST_Q
       BUCK_COMP x---|9           16|---x BUCK_Q
             CMC x---|10          15|---x I_PH_OVER_RANGE
   I_LB_IN_RANGE x---|11          14|---x I_LB_OVER_RANGE
             GND x---|12          13|---x I_PHASE_IN_RANGE
                     |_____________|
```

B.4.2 Duty-Cycle Control of Boost Converter

```
Name      misc_2;
Partno    CA0006 ;
Date      11/28/95;
Revision  01;
Designer  ofori;
Company   MIT;
Assembly  None;
Location  None;
Device    P22V10;

/*************************************************************/
/* LCD enable pulse generator and Boost & Buck SR-Latches  */
/*                                                           */
/*************************************************************/

/**  Inputs  **/
PIN 1 = R_W_IN;      /* Read/Write signal from micro */
PIN 2 = CS3;      /* Chip Select 3 from micro */
PIN 3 = CS3_DELAYED;      /* Chip Select 3 from micro delayed*/
PIN 4 = A0_IN;      /* Address 0 */
PIN 5 = PWMA;      /* Boost converter clock */
PIN 6 = PWMB;      /* Buck converter clock */
PIN 7 = MOT;      /* Motoring signal from micro */
PIN 8 = BOOST_COMP;      /* Output of boost comparator */
PIN 9 = BUCK_COMP;      /* Output of buck comparator */
PIN 10 =  CMC;      /* Current mode control mode from micro */
```

```
PIN 11 = I_LB_IN_RANGE;      /* Boost current in range */
PIN 13 = I_PHASE_IN_RANGE;   /* Phase current in range */

/**  Outputs  **/
PIN 23 = LCD_ENABLE;      /* Chip select for LCD */
PIN 22 = LCD_ENABLE_BAR;     /* Inverted LCD enable to enable HC244 */
PIN 21 = R_W_OUT;      /* Buffered Read/Write signal to LCD  */
PIN 20 = A0_OUT;      /* Buffered A0 signal to LCD  */
PIN 19 = PWM_BOOST;      /* PWM signal for boost converter  */
PIN 18 = PWM_BUCK;      /* PWM signal for buck converter */
PIN 17 = BOOST_Q;      /* Output of Boost SR Latch */
PIN 16 = BUCK_Q;      /* Output of Buck SR Latch */
PIN 15 = I_PH_OVER_RANGE;    /* High when phase current exceeds range */
PIN 14 = I_LB_OVER_RANGE;    /* High when I_LB exceeds range */

/** Declarations and Intermediate Variable Definitions **/
I_LB_RESET =
(BOOST_COMP & !MOT) # (!BOOST_COMP & MOT) # !I_LB_IN_RANGE;

I_PHASE_RESET =
(BUCK_COMP & !MOT) # (!BUCK_COMP & MOT) # !I_PHASE_IN_RANGE;

BOOST_Q = !(PWMA # BOOST_QBAR);

BOOST_QBAR = !(BOOST_Q # I_LB_RESET);

BUCK_Q = !(PWMB # BUCK_QBAR);

BUCK_QBAR = !(BUCK_Q # I_PHASE_RESET);

/** Logic Equations **/
LCD_ENABLE = (!CS3 & !CS3_DELAYED);

LCD_ENABLE_BAR = !LCD_ENABLE;

PWM_BOOST = PWMA;

PWM_BUCK = PWMB;

A0_OUT = A0_IN;

R_W_OUT = R_W_IN;

I_PH_OVER_RANGE = !I_PHASE_IN_RANGE;

I_LB_OVER_RANGE = !I_LB_IN_RANGE;
```

Chip Diagram

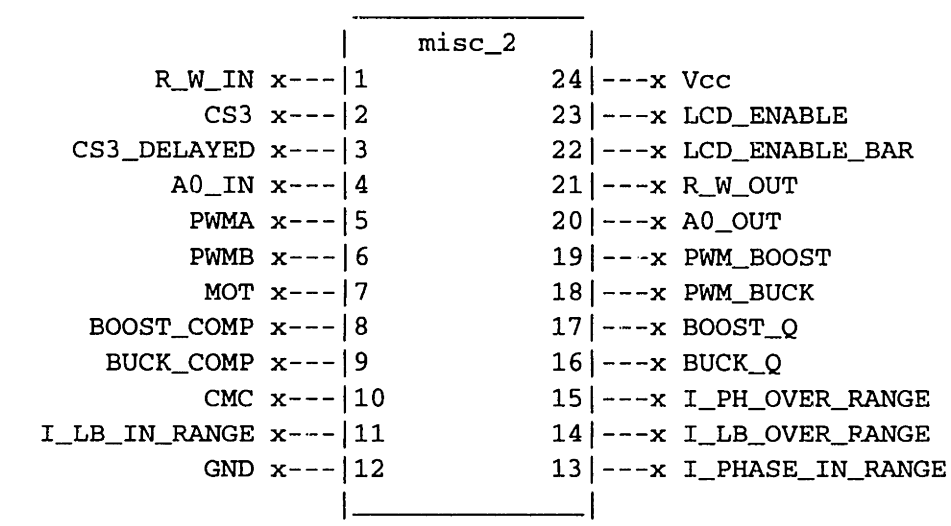

Appendix C

Determination of Feedback Gains

The feedback gains for the buck and boost converter control loops were determined with Matlab by using the scripts below the allow the closed loop poles to be placed anywhere in the z-plane as mentioned in Sections 5.3 and 6.4

C.1 Buck Converter Feedback Gains

```
% This file contains a Matlab script used in determining
% feedback gains for the buck and boost control loops


%  The buck control loop

%  Lm is the motor's synchronous inductance
%  Rm is the motor resistance
%  Ts is the switching frequency

Lm = 4e-3;
Rm = 0.47;
Ts = 244e-6;

%  Compute the continuous-time system and input coupling
%  matrices

A = [-Rm/Lm];
B = [1/Lm];

%  Compute discrete-time model of plant

I = [1];
```

```
F = expm(A*Ts);
G = inv(A)*((F-I)*B);

%  Form the discrete-time matrices that include the
%  integrator and one-sample delay

M = [F 0 G ; Ts 1 0 ; 0 0 0];
N = [0 ; 0 ; 1];


%  Find feedback gains using pole placement
%  [ki, kz, ku]
% ku = 0;
K = place(M,N,[0.4938 + 0.2447i 0.4938 - 0.2447i 0.9532 ])
```

C.2 Boost Converter Feedback Gains

```
%  The boost control loop

%  Cdc is the boost ouput capacitor + snubber capacitors
%  Lm is the motor's synchronous inductance
%  Rm is the motor resistance
%  Ts is the switching frequency

Cdc = 48e-6;
Lm = 4e-3;
Rm = 0.47;
Ts = 244e-6;

%  Compute the continuous-time system and input coupling
%  matrices

A = [0 -1/Cdc ; 1/Lm -Rm/Lm];
B = [1/Cdc ; 0];

%  Compute discrete-time model of plant

I = [1 0 ; 0 1];
F = expm(A*Ts);
G = inv(A)*((F-I)*B);

%  Form the discrete-time matrices that include the
%  integrator and one-sample delay

M = [F [0 ; 0] G ; 0 Ts 1 0 ; 0 0 0 0];
N = [0 ; 0 ; 0 ; 1];

%  Find feedback gains using pole placement
%  [kv, ki, kz, ku]
K = place(M,N,[0.2 0.4+0.2i 0.4-0.2i 0.9])
```

Appendix D

Maple Source Code

The magnetic circuit analyses and other analytic expressions that guided our study of Halbach and conventional arrays in Chapter 2, the design of the slotted wheel motor in Chapter 3, and and the inverter in Chapter 5 were done using the symbolic computations package Maple V. The source code included in this chapter show how the analytic expressions used in making design decisions and plotting selected graphs are computed.

D.1 Halbach vs. Conventional Torque Comparison

```
# This file contains the Maple code used to study the torque production
# characteristics of Halbach and conventional arrays.

# include libraries
readlib(optimize):
readlib(isolate):
with(plots):

# definitions of operators.  Laplacian, Divergence, Gradient & Curl
lap := proc(x) (1/r)*diff(r*diff(x,r),r)+(1/r^2)*diff(diff(x,phi),phi)
               + diff(diff(x,z),z) end;
div := proc(x) (1/r)*diff(r*x[1],r)+(1/r)*diff(x[2],phi)
               + diff(x[3],z) end;
grad := proc(x) [diff(x,r),(1/r)*diff(x,phi),diff(x,z)] end;
curl := proc(x) [simplify(diff(x[3],phi)/r - diff(x[2],z)),
                 simplify(diff(x[1],z) - diff(x[3],r)),
                 simplify((diff(r*x[2],r) - diff(x[1],phi))/r)] end;

# Solve general magnetic circuit with/without permeable rotor back-iron
```

```
print('Radial MAGNETS');
print('az => azimuthal, r => radial');

# Define magnetic scalar potentials for various regions
# Above magnets
psi_ar := C1r*((r/Rri)^(k*N) - (Rri/r)^(k*N))*sin(k*N*(phi-theta));
# Inside   magnets
psi_cr := (C2r*r^(k*N) - C3r*r^(-k*N))*sin(k*N*(phi-theta));
# Below magnets (in airgap and cu)
psi_dr := C4r * ((r/Rso)^(k*N) - (Rso/r)^(k*N))*sin(k*N*(phi-theta));

# Check if scalar potentials are Laplacian
print('Check if Laplace's equation is satisfied');
simplify(lap(psi_ar));
simplify(lap(psi_cr));
simplify(lap(psi_dr));
Har := grad(-psi_ar);
Hcr := grad(-psi_cr);
Hdr := grad(-psi_dr);
Bar_r := u0*Har[1];
Bcr_r := u0*(Hcr[1]+Mkr);
Bdr_r := u0*Hdr[1];
Baaz_r := u0*Har[2];
Bcaz_r := u0*Hcr[2];
Bdaz_r := u0*Hdr[2];

# Compute surface charges to be used for checks
sigma_smbr := u0*subs(r=R1,Mkr);
sigma_smcr := -u0*subs(r=Rm,Mkr);
Mkr := -Mr*(Rm/r)*sin(k*N*(phi-theta));

print('Check if divergence of M is zero');
divM := div([Mkr,0,0]);

# Set up equations to be solved.
print('Using the boundary conditions at r = Rm, scalar potential
      and normal B is continuous');
eqn1 := subs(r=R1,psi_ar)=subs(r=R1,psi_cr):
eqn2 := subs(r=Rm,psi_cr)=subs(r=Rm,psi_dr):
eqn3 := subs(r=R1,Bar_r)-subs(r=R1,Bcr_r)= 0:
eqn4 := subs(r=Rm,Bcr_r)-subs(r=Rm,Bdr_r)= 0:

# Solve for the unknown constants C1r,C2r,C3r,C4r
constants := solve({eqn1,eqn2,eqn3,eqn4},{C1r,C2r,C3r,C4r}):
assign(constants);

C1r := simplify(expand(C1r));
C2r := simplify(expand(C2r));
C3r := simplify(expand(C3r));
C4r := simplify(expand(C4r));
```

```
# Double check solutions
print(`Check that boundary conditions are satisfied`);
r := Rri;
`Potential` := simplify(psi_ar);
`Jump in tangential H` := simplify(-Har[2]);
r := R1;
`Jump in normal B` := simplify(expand(simplify(Bar_r - Bcr_r)));
`Jump in tangential H` := simplify(expand(simplify(Har[2]-Hcr[2])));
r := Rm;
`Jump in normal B` := simplify(Bcr_r - Bdr_r);
`Jump in tangential H` := simplify(Hcr[2]-Hdr[2]);
r := Rso;
`Potential` := simplify(psi_dr);
`Jump in tangential H` := simplify(Hdr[2]);

r := 'r';
print(` `);

# Now carry out the same procedure above for the azimuthal magnets
print(`Azimuthal MAGNETS`);

# Define magnetic scalar potentials for various regions
# Above magnets #
psi_aaz := C1az * ((r/Rri)^(k*N) - (Rri/r)^(k*N))*sin(k*N*(phi-theta));
# Inside magnets
psi_caz := (Rm*Maz/(k*N)+ C2az * r^(k*N) - C3az * r^(-k*N))
            *sin(k*N*(phi-theta));
# Below magnets (in airgap and cu
psi_daz := C4az * ((r/Rso)^(k*N) - (Rso/r)^(k*N))*sin(k*N*(phi-theta));

# Check if scalar potentials above and below magnets are Laplacian
print(`Check if Laplace's equation is satisfied`);
simplify(lap(psi_aaz));
simplify(lap(psi_daz));

# Check if potentials within magnets satisfy Poisson's equation
print(` `);
print(`Check if Poisson's equation is satisfied for region c`);
simplify(lap(psi_caz));
print(` `);

# Define the magnetic fields in the various regions
Haaz := grad(-psi_aaz);
Hcaz := grad(-psi_caz);
Hdaz := grad(-psi_daz);
Bar_az := u0*Haaz[1];
Bcr_az := u0*Hcaz[1];
Bdr_az := u0*Hdaz[1];
Baaz_az := u0*Haaz[2];
```

```
Ecaz_az := u0*(Hcaz[2]+Mkaz);
Bdaz_az := u0*Hdaz[2];

# Expression for the azimuthal magnetization
Mkaz := (Rm/r)*Maz*cos(k*N*(phi-theta));

# Expression for the volume charge in the azimuthal magnets
rho_m := -u0*div([0,Mkaz,0]);

# Set up the system of equations to be solved.
eqn1 := subs(r=R1,psi_caz)=subs(r=R1,psi_aaz);
eqn2 := subs(r=Rm,psi_caz)=subs(r=Rm,psi_daz);
eqn3 := subs(r=R1,Bcr_az)-subs(r=R1,Bar_az)= 0;
eqn4 := subs(r=Rm,Bcr_az)-subs(r=Rm,Bdr_az)= 0;

# Solve for the unknown arbitrary constants C1az,C3az,C4az,C2az.
constants := solve({eqn1,eqn2,eqn3,eqn4},{C1az,C3az,C4az,C2az});
assign(constants);
C1az := simplify(expand(C1az));
C2az := simplify(expand(C2az));
C3az := simplify(expand(C3az));
C4az := simplify(expand(C4az));
C5az := simplify(expand(C5az));

# Double check the solutions
print(`Check that boundary conditions are satisfied`);
r := Rri;
`Potential` := simplify(psi_aaz);
`Jump in tangential H` := simplify(expand(u0*Haaz[2]));
r := R1;
`Jump in normal B` := simplify(expand(simplify(expand(Bar_az -
                                                    Bcr_az))));
`Jump in tangential H` := simplify(expand(simplify(expand(u0*Haaz[2]-
                                                  u0*Hcaz[2])))));
r := Rm;
`Jump in normal B` := simplify(expand(simplify(expand(Bcr_az -
                                                     Bdr_az))));
`Jump in tangential H` := simplify(expand(simplify(expand(u0*Hcaz[2]-
                                                  u0*Hdaz[2])))));
r := Rso;
`Potential` := simplify(psi_daz);
`Jump in tangential H` := simplify(expand(simplify(expand(Hdaz[2])))));

r := 'r';
print(` `);

# Now add the radial and azimuthal potentials
print(`Now calculate the total fields`);
psia_radial := psi_ar;
psic_radial := psi_cr;
```

```
psid_radial := psi_dr;
psia_azi := psi_aaz;
psic_azi := psi_caz;
psid_azi := psi_daz;

#temporary constants
C1r1 := C1r:
C1r := 'C1r':
C2r1 := C2r:
C2r := 'C2r':
C3r1 := C3r:
C3r := 'C3r':
C4r1 := C4r:
C4r := 'C4r':

C1az1 := C1az:
C1az := 'C1az':
C2az1 := C2az:
C2az := 'C2az':
C3az1 := C3az:
C3az := 'C3az':
C4az1 := C4az:
C4az := 'C4az':
C5az1 := C5az:
C5az := 'C5az':

# Magnetic flux density in the air above the rotor steel
B_amag := [simplify(Bar_r + Bar_az),simplify(Baaz_r + Baaz_az)]:

# Magnetic flux density in the magnet
B_cmag := [simplify(Bcr_r + Bcr_az),simplify(Bcaz_r + Bcaz_az)]:
H_cmag := [simplify(Hcr[1]+Hcaz[1]),simplify(Hcr[2] + Hcaz[2])]:
# Magnetic flux density below the magnet
B_dmag := [simplify(Bdr_r + Bdr_az),simplify(Bdaz_r + Bdaz_az)]:

phi0 := Pi/(2*N);

# Now calculate the Torque integral
# Integral of the fundamental component of the torque contribution
# from the
# radial magnets
Bdr_norm_int := subs(cos(k*Pi/2)=0,pk_fac*simplify((-2*N*Weff*J0)
                *int(int(simplify(r*r*Bdr_r),phi= simplify(phi0-
                ((Pi/(2*N))*Gamma))
                ..simplify(phi0+((Pi/(2*N))*Gamma))),r=Rso..Rcu)));

# Commutation angle
theta_com := Pi/(N*Nphases);

# Integral of the fundamental component of the torque contribution
```

```
# from the
# azimuthal  magnets
Bdr_horz_int := subs(cos(k*Pi/2)=0,pk_fac*simplify((-2*N*Weff*J0)
                *int(int(simplify(r*r*Bdr_az),phi= simplify(phi0-
                ((Pi/(2*N))*Gamma))
                ..simplify(phi0+((Pi/(2*N))*Gamma))),r=Rso..Rcu)));

# Total fundamental component of torque
Bdr_tot_int := Bdr_norm_int + Bdr_horz_int;
Bdr_int := collect(simplify(Bdr_tot_int),[J0,N,Weff,pk_fac,u0],factor);

# average torque over commutation interval
ave_Bdr_int := int(Bdr_int,theta=evalf(-theta_com/2)..
               evalf(theta_com/2))/theta_com;

# This is the maximum current density under fixed power disspation
J0max := sqrt((Pohm*sigma)/(Pi*(Rcu^2-Rso^2)*pk_fac*w*Gamma));

# total axial length of motor
w := 0.1279;
# Inner radius of rotor steel
R1 := 0.196
# Outer radius of copper
Rcu := Rm-AG;
# NdFeB magnets will be used
# Magnet remanent flux density at 20 deg. C
Br0 := 1.2;
# Magnet coercive force at 20 deg. C
Hci0 := 700000;
t0 := 20;
# Temperature coefficient of magnet coercive force
Hc_coeff := -0.65;
# Temperature coefficent of magnet remanent flux density
Br_coeff := -0.11;
# Density of magnet
Denmag := 7500;
# Magnet temperature in deg. C
mag_temp := 110;
# Motor running clearance
AG := 0.000625;
# Inner radius of magnets
Rm := sqrt(R1^2 - (m_magnets/(Denmag*Pi*magnet_length *
      (beta+delta*(1-beta)))));
# Magnet thickness
tmag := R1-Rm;
# Fringing factor
fringe_fac := 0.1;
end_turn_length := Pi*((Rcu+Rso)/(2*N))* tan(Lambda);
Lambda := Pi/6;
magnet_length := (1+fringe_fac)*Weff;
```

```
Weff := 0.06:
total_axial_length := magnet_length + 2*end_turn_length:
# 2 out of 3 phases are on at a time
Gamma := 2/3;
# Number of phases
Nphases := 3;
# Resistivity of copper
restCu := (1/(5*10^7))*(234.5+temperature)/(234.5+20);
# Conductivity of copper
sigma := 1/restCu;
# Copper temperature
temperature := 110;
# Copper packing factor
pk_fac := 0.7;
# Ohmic power dissipation in windings
Pohm := 2500;
# Angle of alignment for peak torque within a communation period
phi0 := Pi/(2*N);
# Outside radius of stator steel
Rso := Rcu-tcu;
# Inner radius of stator steel
Rsi := Rso-tst;

# Include temperature dependence on magnetization
Mo := Br0*(1+(mag_temp-t0)*Br_coeff/100)/u0;
# Incluse temperature dependence on coercive force
Hc0 := Hci0*(1+(mag_temp-t0)*Hc_coeff/100);
# Permeability of free space
u0 := evalf(4*Pi*10^(-7));

# Fourier coefficinets of radial and azimuthal magnetizations
Mr := (-1)^((k-1)/2)*4*Mo*sin(k*beta*Pi/2)/(k*Pi);
Maz := delta *4*Mo*sin(k*alpha*Pi/2)/(k*Pi);

# add only odd harmonics
k := 2*n+1;
# Restore arbitrary constants
C1r := C1r1:
C2r := C2r1:
C3r := C3r1:
C4r := C4r1:
C5r := C5r1:
C1az := C1az1:
C2az := C2az1:
C3az := C3az1:
C4az := C4az1:
C5az := C5az1:

# Free up memory used for the temporary constants
C1r1 := 'C1r1':
```

```
C2r1 := 'C2r1':
C3r1 := 'C3r1':
C4r1 := 'C4r1':
C5r1 := 'C5r1':
C1az1 := 'C1az1':
C2az1 := 'C2az1':
C3az1 := 'C3az1':
C4az1 := 'C4az1':
C5az1 := 'C5az1':

# Compute total radial no load airgap magnetic flux from
# adding five harmonics

norm_noload_flux := evalf(subs(n=0,B_dmag[1])+subs(n=1,B_dmag[1])+
                    subs(n=2,B_dmag[1])+subs(n=3,B_dmag[1])+
                    subs(n=4,B_dmag[1])+subs(n=5,B_dmag[1])):

# Compute total azimuthal no load airgap magnetic flux from
# adding five harmonics
azim_noload_flux := evalf(subs(n=0,B_dmag[2])+subs(n=1,B_dmag[2])+
                    subs(n=2,B_dmag[2])+subs(n=3,B_dmag[2])+
                    subs(n=4,B_dmag[2])+subs(n=5,B_dmag[2])):

# Finish calculating the torque by adding five harmonics
tmp := evalf(Bdr_int):
Torque := evalf(subs(n=0,tmp)+subs(n=1,tmp)+subs(n=2,tmp)+
          subs(n=3,tmp)+subs(n=4,tmp)+subs(n=5,tmp)):
# Compute torque per current density
Torque_per_J := Torque/J0:

# Compute average torque over a commutation interval
tmp := evalf(ave_Bdr_int):
ave_Torque := evalf(subs(n=0,tmp)+subs(n=1,tmp)+subs(n=2,tmp)+
              subs(n=3,tmp)+subs(n=4,tmp)+subs(n=5,tmp)):
# Set the current density to maximum
J0 := evalf(J0max);
theta := 0;

break;

# Plot graphs
# 3d graph for peak Halbach torque with magnet mass and
# pole-arc to pole-pitch ratio (beta)
plot3d({evalf(subs({N=10,delta=1,Rri=evalf(R1)},Torque)),
      evalf(subs({N=10,delta=0,Rri=evalf(R1)},Torque))},
      beta=0.4..1,m_magnets=0.000001..17,labelfont=[TIMES,BOLD,16],
      axesfont=[TIMES,BOLD,16]);

# 3D graph for average Halbach torque with magnet mass and
# pole-arc to pole-pitch ratio (beta)
```

```
plot3d({evalf(subs({N=10,delta=1,Rri=10},ave_Torque)),
      evalf(subs({N=10,delta=0,Rri=10},ave_Torque))},
      beta=0.4..1,m_magnets=0.000001..17,
      labelfont=[TIMES,BOLD,16],axesfont=[TIMES,BOLD,16]);

# Graphs for conventional rotor magnet arrangement design
delta := 0;
Rri := evalf(R1);
m_magnets := 16;
N := 10;
beta := 0.75;
tcu := 0.02;

# Graph for variation of current density with copper thickness
plot(evalf(J0max),tcu=0.001..0.02,labelfont=[TIMES,BOLD,16],
     axesfont=[TIMES,BOLD,16]);

delta := 0;
Rri := evalf(R1);
m_magnets := 16;
N := 10;
beta := 0.75;
tcu := 0.02;
plot3d(evalf(norm_noload_flux),phi=0..evalf(2*Pi/N),
     r=evalf(Rso)..evalf(Rcu),labelfont=[TIMES,BOLD,16],
     axesfont=[TIMES,BOLD,16]);

delta := 0;
Rri := evalf(R1);
m_magnets := 16;
N := 10;
beta := 0.75;
tcu := 0.02;
plot3d(evalf(azim_noload_flux),phi=0..evalf(2*Pi/N),
    r=evalf(Rso)..evalf(Rcu),labelfont=[TIMES,BOLD,16],
    axesfont=[TIMES,BOLD,16]);

delta := 1;
Rri := evalf(R1);
m_magnets := 16;
N := 10;
beta := 0.75;
tcu := 0.02;
plot3d(evalf(norm_noload_flux),phi=0..evalf(2*Pi/N),
     r=evalf(Rso)..evalf(Rcu),labelfont=[TIMES,BOLD,16],
     axesfont=[TIMES,BOLD,16]);

# Graphs for Halbach no-load magnetic flux

delta := 1;
```

```
Rri := evalf(R1);
m_magnets := 16;
N := 10;
beta := 0.75;
tcu := 0.02;
plot3d(evalf(azim_noload_flux),phi=0..evalf(2*Pi/N),
       r=evalf(Rso)..evalf(Rcu),labelfont=[TIMES,BOLD,16],
       axesfont=[TIMES,BOLD,16]);
```

D.2 Slotted Motor Design

```
# This file contains the Maple code used to design the
# conventional slotted wheel motor in Chapter 3.

readlib(optimize):
readlib(piecewise):
readlib(optimize);
readlib(isolate);
readlib(unassign):
with(plots):
alias(I=I,j=sqrt(-1));

# definitions of operators.  Laplacian, Divergence, Gradient & Curl
lap := proc(x) (1/r)*diff(r*diff(x,r),r)+(1/r^2)*diff(diff(x,phi),phi)
               + diff(diff(x,z),z) end;
div := proc(x) (1/r)*diff(r*x[1],r)+(1/r)*diff(x[2],phi)
               + diff(x[3],z) end;
grad := proc(x) [diff(x,r),(1/r)*diff(x,phi),diff(x,z)] end;
curl := proc(x) [simplify(diff(x[3],phi)/r - diff(x[2],z)),
                 simplify(diff(x[1],z) - diff(x[3],r)),
                 simplify((diff(r*x[2],r) - diff(x[1],phi))/r)] end;

# Solve magnetic circuit.  Rotor and stator back iron are assumed
# to have infinite permeability.

print('Radial MAGNETS');
```

```
#inside   magnets
psia := C1 * ((r/Rri)^(k*N) - (Rri/r)^(k*N))*sin(k*N*(phi-theta));
#below magnets (in airgap )
psib := (C2*r^(k*N) - C3*r^(-k*N))*sin(k*N*(phi-theta));
# in the stator teeth
psic := C4 * ((r/Rso)^(k*N) - (Rso/r)^(k*N))*sin(k*N*(phi-theta));

print('Check if Laplace's equation is satisfied');
simplify(lap(psia));
simplify(lap(psib));
simplify(lap(psic));

# Define magnetic field intensities
Ha_mag := grad(-psia);
Hb_mag := grad(-psib);
Hc_mag := grad(-psic);

# Define magnetic flux densities
Ba_mag := [u0*(Ha_mag[1]+Mkr),u0*(Ha_mag[2])] ;
Bb_mag := [u0*Hb_mag[1],u0*Hb_mag[2]] ;
Bc_mag := [u_teeth*Hc_mag[1], u_teeth*Hc_mag[2]];

Mkr := -Mr*(Rm/r)*sin(k*N*(phi-theta));

# Harmonic contribution of magnet flux in stator steel
# assume no leakage across slots
Phi_stat_mag_k := subs({r=Rcu, theta=0},int(r*Bb_mag[1],
                          phi=0..Pi/(2*N)));

# Harmonic contribution of magnet flux in rotor steel
Phi_rot_mag_k := subs({r=Rri, theta=0},int(r*Ba_mag[1],
                          phi=0..Pi/(2*N)));

# Collect 1/3 of the flux from a magnet
Bteeth_mag_k :=evalf(int(subs({theta=0,r=Rcu},Bb_mag[1]),
phi=0..evalf(Pi/(3*N)))/evalf(Pi/(3*N)));
```

```
print('Check if divergence of M is zero');
divM := div([Mkr,0,0]);

print('Using the boundary conditions - psi and normal
      B is continuous');
eqn1 := subs(r=Rm,psia)=subs(r=Rm,psib):
eqn2 := subs(r=Rm,Ba_mag[1])-subs(r=Rm,Bb_mag[1])= 0:
eqn3 := subs(r=Rcu_cart,Bb_mag[1])-subs(r=Rcu_cart,Bc_mag[1])= 0:
eqn4 := subs(r=Rcu_cart,psib)-subs(r=Rcu_cart,psic)= 0:

constants := solve({eqn1,eqn2,eqn3,eqn4},{C1,C2,C3,C4}):

assign(constants);

C1 := simplify(C1);
#simplify(collect(expand(C1r),[Rcu,Rm],distributed));
C2 := simplify(C2);
C3 := simplify(C3);
#simplify(collect(expand(C3r),[Rri,Rm,Rri],distributed));
C4 := simplify(C4);

print('Check that boundary conditions are satisfied');

r := Rri;
'Potential' := simplify(psia);
'Jump in tangential H' := simplify(-Ha_mag[2]);
r := Rm;
'Jump in normal B' := simplify(Ba_mag[1] - Bb_mag[1]);
'Jump in tangential H' := simplify(Ha_mag[2]-Hb_mag[2]);
r := Rcu_cart;
'Jump in normal B' := simplify(Bb_mag[1] - Bc_mag[1]);
'Jump in tangential H' := simplify(Hb_mag[2]-Hc_mag[2]);
r := Rso;
'Potential' := simplify(psic);
'Jump in tangential H' := simplify(Hc_mag[2]);
```

```
#Airgap extended by 5% from Carter coefficient

Rcu_cart := Rcu*(1-0.05*AG);
r := 'r';

print(' ');

Mr := (-1)^((k-1)/2)*4*Mo*sin(k*beta*Pi/2)/(k*Pi);
k := 2*n+1;

Bteeth_mag := evalf(sum(Bteeth_mag_k,n=0..10) *
              (Rcu/(r- delta*Rso)));

# magnetic flux density in the stator steel due to magnets
Bstat_mag := evalf(sum(Phi_stat_mag_k,n=0..10)/t_stator);

# magnetic flux density in the rotor steel due to magnets
Brot_mag := evalf(sum(evalf(Phi_rot_mag_k),n=0..10)/t_rotor);

print('Armature reaction fields');

# in the magnet and airgap )
Hga := Hg_arm * Rcu/r;

# in the stator teeth;
Hta := Ht_arm * Rso/r;

# in the copper slot
Hcua := Hcu_arm * (r-Rso)/(tcu);

# in the slot opening
Hoa := Ho_arm ;

Bta := u_teeth*Hta;
Bga := u0*Hga;
```

```
eq1 :=  2*Ht_arm*Rso*ln(Rcu/Rso) + 2*Hg_arm*Rcu*ln(Rri/Rcu)
        = 2*J0*A_cu;
eq2 :=  2*Ht_arm*Rso*ln((Rso+tcu)/Rso) + 2*Hcu_arm*w_cu +
        2*u0*Hcu_arm*w_tt/(u_teeth) = 2*J0*A_cu;
eq3 :=  2*Ht_arm*Rso*ln(Rcu/Rso) + 2*Ho_arm*w_o +
        2*u0*Ho_arm*l_tp/u_teeth = 2*J0*A_cu;
eq4 := u0*Hcu_arm*tcu/2 + u0*Ho_arm*t_o+ u0*Hg_arm*l_tp_star
        = u_teeth*Ht_arm*w_tb;
#eq4 := u0*Hcu_arm*tcu/2 +u0*((Hcu_arm+Ho_arm)/2)*xi +
        u0*Ho_arm*t_o+ u0*Hg_arm*l_tp = u_teeth*Ht_arm*w_tb;

equations := {eq1,eq2,eq3,eq4}:
unknowns := {Ht_arm,Hg_arm,Hcu_arm,Ho_arm};
constants := solve(equations,unknowns):
assign(constants);

# approximate teeth flux with flux at 1/3 distance up base of slot
B_teeth := evalf(subs(r=(Rso+tcu/3),evalf(abs(Bteeth_mag)+ abs(Bta))));
#B_teeth := subs(r=Rcu,evalf(abs(Bteeth_mag)));

w_tb := (2*Pi*Rso/(2*N*3))*(1-delta);
w_cu := (2*Pi*Rso/(2*N*3))* delta;
l_tp := (2*Pi*Rcu/(2*N*3))- w_o;
l_tp_star := (2*Pi*Rcu/(2*N*3))- w_cu;
A_cu := w_cu * tcu * k_pf;
w_tt := (2*Pi*(Rso+tcu)/(2*N*3))-w_cu;
w_o := 0.00309;
xi := 0.577*(w_cu-w_o)/2;
t_o := 0.00266-xi;

rotor_length := (2*Pi*(Rri+(t_rotor/2)))/(2*N);
stator_length := (2*Pi*(Rso-(tst/2)))/(2*N);
mu_rotor := ur;
mu_stator := us;
Torque := evalf(2*N*u0*int(r*Hg_arm,r=Rm..Rri)*(2*Mo)*Weff):
```

```
#Torque := 2*N*u0*H_gap*Rcu*tmag*(2*Mo)*Weff:


#B_stator := evalf(sqrt((subs(r=Rcu,evalf(-Bgm*(beta*Pi*Rcu/(2*N))))^2
#             +  (u_teeth*Ht_arm*w_tb)^2))/t_stator);
#B_rotor := evalf(sqrt((subs(r=Rri,evalf(-Bmm*(beta*Pi*Rri/(2*N)))))^2
#             +  (u0*Hg_arm*l_tp)^2)/t_rotor);

#Eddy current and hysteresis losses in the steel.

#(1kg = 0.4536 lbs)
specific_stat_backiron_loss := (Ke*(N*f)^2*Bstat_mag^2 +
                                Kh*(N*f)*abs(Bstat_mag)^a)/0.4536:
specific_stat_teeth_loss := (Ke*(N*f)^2*B_teeth^2 +
                                Kh*(N*f)*abs(B_teeth)^a)/0.4536:
#specific_rot_steel_loss := (Ke*(N*f)^2*B_rotor^2 +
#                                 Kh*(N*f)*abs(B_rotor)^a)/0.4536:
f := omega/(2*Pi):
#Use M19, 29 Gage steel
Ke := 3.218274654*10^(-5);
Kh := 1.066431820363*10^(-2);
a := 1.7928;

stator_teeth_loss := mass_stator_teeth*specific_stat_teeth_loss:
stator_backiron_loss := mass_stator_backiron*specific_stat_backiron_loss:
stator_steel_loss := stator_teeth_loss + stator_backiron_loss:

#calculate motor efficiency
Ohmic_power := evalf((J0^2*(2*2*N*A_cu*
               (Wohm+2*ohmic_end_turn_length)))/sigma):
mech_power_out :=evalf(Torque*omega):
motor_losses := evalf(Ohmic_power+stator_steel_loss+ripple_power);
tot_power_in := mech_power_out + motor_losses;
motor_efficiency := evalf(mech_power_out/(mech_power_out+motor_losses)):

J0max := evalf(sqrt((Pohm_max*sigma)/(2*2*N*A_cu*
```

```
                    (Wohm+2*ohmic_end_turn_length))));
Rm := sqrt(Rri^2 - (m_magnets/(Denmag*beta*Pi*magnet_length)));
tmag := Rri-Rm;
end_turn_length := (Pi/(2*N))*((Rcu+Rso)/2)* (1-delta)/
                    (sqrt(1-(1-delta)^2));
ohmic_end_turn_length :=end_turn_length/delta;
magnet_length := Weff;
#Weff := w-2*end_turn_length:
total_axial_length := magnet_length + 2*end_turn_length;
Nphases := 3;
restCu := (1/(5*10^7))*(234.5+temperature)/(234.5+20);
sigma := 1/restCu;
temperature := 120;
k_pf := 0.7;
Rso := Rcu-t_o-xi-tcu;
Rsi := Rso-t_stator;

Rri := R0-t_rotor;
Rcu := Rm-AG;
skew_angle := arctan(evalf(((Rso+Rcu)/2)*tan(Pi/N/Nphases)/Weff));
Wohm := evalf(Weff/cos(skew_angle));

Mo := Br0*(1+(mag_temp-t0)*Br_coeff/100)/u0;
Hc0 := Hci0*(1+(mag_temp-t0)*Hc_coeff/100);
u0 := evalf(4*Pi*10^(-7));
ur := evalf(500*u0);
us := evalf(500*u0);
m_rotor_steel := Densteel*Pi*(R0^2-Rri^2)* Weff:
mass_stator_backiron := Densteel*Pi*(Rso^2-Rsi^2)*Weff:

mass_stator_teeth := evalf((Pi*(Rcu^2-Rso^2)-(2*N*3*(w_cu*tcu +
                    w_o*t_o + (w_cu+w_o)*xi/2)))*Weff*Densteel);

m_stator_steel := mass_stator_backiron+ mass_stator_teeth:
m_steel := m_stator_steel+m_rotor_steel:
m_Cu := evalf(3*2*N*A_cu*DenCu*(Wohm+2*(end_turn_length)));
```

```
Densteel :=7750;
DenCu:= 8650;
#M36 steel costs 0.67$/lb and 1lb=0.4526 kg
cost_steel := 0.67/0.4536;
cost_Cu := 20;
motor_mass := m_steel+m_magnets+m_Cu:
motor_cost := m_steel*cost_steel+m_magnets*cost_magnet+m_Cu*cost_Cu:
#Motor geometric parameters
#armature wire diameter
#d=0.0006;

Cslot := evalf(m_Cu/(60*2)* cu_spec_heat_cap);
Cpole := evalf(mass_stator_teeth/(60*2)*steel_spec_heat_cap);
Cback_iron := evalf(mass_stator_backiron/60*steel_spec_heat_cap);
cu_spec_heat_cap := 384;
steel_spec_heat_cap := 502;

#magnet parameters

Hci0 := 700000;
t0 := 20;
Hc_coeff := -0.65;
Br_coeff := -0.11;
Denmag := 7500;
mag_temp := 110;
cost_magnet := 200:

R0 := 0.206;
AG := 0.000625;
Pohm_max := 2700;
Br0 := 1.2;
beta := 0.9;
t_rotor := 0.01;
t_stator := 0.01;
m_magnets := 1.7;
Weff := 0.06;
```

```
N := 10;
tcu := 0.01984;
delta := 0.5;
#J0 := Nturns*I0/A_cu;
u_teeth := 50*u0;
Ri := 0.098;


#Enter B-H Curves

B_tol := 0.01;
u_tol := evalf(0.05*u0);
mu_tol := 0.01;

#B-H curve for M19-29
B_H := [[0,0],[0.6,0.77],[0.84,1.1],[0.9,1.2],[1.02,1.5],[1.14,2],
[1.21,2.5],[1.26,3],[1.3,3.5],[1.32,4],[1.36,5],[1.4,6],[1.42,7],
[1.44,8],[1.52,16],[1.54,20],[1.58,28],[1.6,32],[1.62,38],[1.66,52],
[1.7,70],[1.76,100],[1.84,170],[1.9,225],[1.95,300],[2.08,1000]]:

# array for storing torque profile with mu
torque_prof := array(1..100):

# array for storing mu
mu_prof := array(1..100):

# B-mu vectors
abs_Bmax := 100;
B_vec := array(1..nops(B_H)+1):
mu_vec := array(1..nops(B_H)+1):

#Now define a few proceedures

#Procedure to construct B-mu curve from B-H Curve
#puts results in B_vec[] and mu_vec[]
f_B_mu := proc(flux_vector)
```

```
local m,umax;
global B_vec,mu_vec;
B_vec[1] := 0;
mu_vec[1] := (flux_vector[2][1]/(flux_vector[2][2]*79.577472));
umax := mu_vec[1];
for m from 2 by 1 to nops(flux_vector) do
B_vec[m] := flux_vector[m][1];
mu_vec[m] := (flux_vector[m][1]/(flux_vector[m][2]*79.577472));
od;
B_vec[m] := 10;
mu_vec[m] := evalf(u0);
end:

#procedure to find the maximum mu
#result in answer

f_umax := proc(mu_vector)
local m, answer, size;
answer := 0;
size := nops([entries(eval(mu_vector))]);
for m from 1 by 1 to size do
if (mu_vector[m] > answer) then
answer := mu_vector[m];
fi;
answer;
od;
end:

#Procedure to find the correct mu given a B.

getmu := proc(B)
local x;
global mu_vec;
x := 1;
if (B >= abs_Bmax) then
u0;
```

```
else
while (B_vec[x]<= B) do
x := x+1;
od;
if (B_vec[x] = B) then
mu_vec[x];
else
mu_vec[x-1] + (B - B_vec[x-1])/(B_vec[x]-B_vec[x-1])
              *(mu_vec[x]-mu_vec[x-1])
fi;
fi;
end:

#Procedure to find the correct mu for teeth.

f_mu_teeth := proc()
global mu_tol,B_tol,B_teeth, u_teeth,u0,temp1,B_teeth_simp;
local B_calc,temp,temp_mu,mu_low,mu_high,B_low,B_high;
temp1 := evalf(u_teeth);
u_teeth := 'u_teeth';
B_teeth_simp := evalf(B_teeth);
u_teeth := temp1;
B_calc := evalf(B_teeth_simp);
temp_mu := evalf(u_teeth);
temp :=  500;
mu_low := evalf(u0);
mu_high := evalf(5000*u0);
if type(B_calc, numeric) then
while (temp > mu_tol or temp1 > B_tol) do
B_calc := evalf(B_teeth_simp);
temp_mu := getmu(B_calc);
if temp_mu < u_teeth then
mu_low := max(temp_mu,mu_low);
u_teeth := evalf((u_teeth+mu_low)/2);
if B_calc > 1.8 then
u_teeth := evalf(u_teeth-5*u0*rand()/999999999999);
```

```
fi;
else
mu_high := min(temp_mu,mu_high);
u_teeth := evalf((u_teeth+mu_high)/2);
if B_calc > 1.8 then
u_teeth := evalf(u_teeth+5*u0*rand()/999999999999);
fi;
fi;

temp := evalf(abs(evalf(u_teeth-temp_mu))
              /abs(evalf(u_teeth)));
temp1 := evalf(abs(evalf(B_calc-evalf(B_teeth_simp)))
              /abs(evalf(evalf(B_teeth_simp))));
evalf(u_teeth/u0);
od;
else
'f_mu_teeth'();
fi;
end;
#procedure to find motor torque for given mass of magnets
f_torque := proc(x)
global f_mu_teeth,Torque,m_magnets;
m_magnets := 'm_magnets';
m_magnets := x;
f_mu_teeth();
evalf(Torque);
end;
#plot(f_torque,0.5..3,numpoints=20);

#procedure to find teeth permeability for given mass of magnets
f_mu := proc(x)
global f_mu_teeth,Torque,m_magnets;
m_magnets := x;
f_mu_teeth();
end;
```

```
#procedure to find optimal torque per mass
f_opt_Weff := proc(x)
global f_mu_teeth,Torque,J0,J0max,Torque,Weff;
J0 := J0max;
Weff := x;
f_mu_teeth();
evalf(Torque);
end;

#procedure to find torque for a given thickness of copper
f_opt_tcu := proc(x)
global f_mu_teeth,Torque,tcu,J0,J0max,B_teeth;
tcu := 'tcu';
J0 := evalf(J0max);
tcu := evalf(x);
f_mu_teeth();
evalf(Torque);
end;

plot_tcu := proc()
global f_opt_tcu, J0, J0max,x1,y1,z1;
x1 := array(1..201);
y1 := array(1..201);
z1 := array(1..400);
J0 := evalf(J0max);
i := 0;
for t_cu from 0.005 by evalf((0.03-0.005)/200) to 0.03 do
i := i+1;
x1[i] := t_cu;
y1[i] := f_opt_tcu(t_cu);
od;
i := 'i';
for i from 1 to 200 do
z1[eval(2*i-1)] := x1[i];
z1[eval(2*i)] := y1[i];
od;
```

```
plot(eval(z1));
end;
#plot_tcu(eval(z1));
#plot(f_opt_tcu,0.01..0.03);

#procedure to find torque for a given number of pole pairs
f_opt_N := proc(x)
global f_mu_teeth,Torque,tcu,J0,J0max,N;
N := 'N';
J0 := J0max;
N := x;
f_mu_teeth();
evalf(Torque);
end;

#procedure to find how torque changes with ohmic power dissipation
f_torque_prof := proc(x)
global f_mu_teeth,Torque,J0,J0max,Pohm_max;
Pohm_max := 'Pohm_max';
J0 := J0max;
Pohm_max := x;
f_mu_teeth();
evalf(Torque);
end;
#plot(f_torque_prof,1..2500);

#procedure to find how torque changes with maximum radius
f_max_radius := proc(x)
global f_mu_teeth,Torque,J0,J0max,R0;
J0 := J0max;
R0 := x;
f_mu_teeth();
evalf(Torque);
end;
#plot(f_max_radius,0.15..0.19);
```

```
#Now construct B-mu curve and store max mu in umax

f_B_mu(B_H):
umax := f_umax(mu_vec):
#plot the B_H and B_mu curves
size := nops(B_H):
for j from 1 to (2*size) do
if type(j,odd) then
'B_H plot vector'[j] := B_H[(j+1)/2][2]*79.577472;
'B_mu plot vector'[j] := mu_vec[(j+1)/2]/u0;
'B_H log plot vector'[j] := B_H[(j+1)/2][1];
'B_mu log plot vector'[j] := B_H[(j+1)/2][1];
else
'B_H plot vector'[j] := B_H[j/2][1];
'B_mu plot vector'[j] := B_H[j/2][1];
'B_H log plot vector'[j] := B_H[j/2][2]*79.577472;
'B_mu log plot vector'[j] := mu_vec[j/2]/u0;
fi;
od;
'B_H plot vector' :=['B_H plot vector'[g] $
                    g=1..(2*size)]:
'B_mu plot vector' :=['B_mu plot vector'[g] $
                    g=1..(2*size)]:
'B_H log plot vector' :=['B_H log plot vector'[g] $
                    g=1..(2*size)]:
'B_mu log plot vector' :=['B_mu log plot vector'[g] $
                    g=1..(2*size)]:

#J0 := J0max;
min_N := 10:
max_N := 15:
r := 'r';
n := 'n';

#deg. C per minute
temp_rise_rate := evalf(60*Pohm_max/((m_steel+m_Cu)*Cp));
```

```
#Specific heat capacity of copper
Cp := 384;
max_profile := 0.21;
J0 := J0max;
f_mu_teeth();

readlib(piecewise):
readlib(optimize);
readlib(isolate);
readlib(unassign):
with(plots):
#alias(I=I,j=sqrt(-1));

ripple_power := 100;

#input fuds cycle [speed, torque,seconds]
fuds_cycle:= [[[0,-30,5],[0,-20,6],[0,-10,14],[0,0,256],[0,10,7],
[0,20,9],[0,30,6],[0,40,4],[0,50,6],[0,60,0]],
 [[1000,-30,23],[1000,-20,9],[1000,-10,7],[1000,0,3],[1000,10,1],
[1000,20,6],[1000,30,4],[1000,40,3],[1000,50,25],[1000,60,1]],
 [[2000,-30,16],[2000,-20,16],[2000,-10,4],[2000,0,9],[2000,10,5],
[2000,20,7],[2000,30,8],[2000,40,7],[2000,50,19],[2000,60,0]],
 [[3000,-30,16],[3000,-20,18],[3000,-10,15],[3000,0,26],[3000,10,15],
[3000,20,24],[3000,30,24],[3000,40,7],[3000,50,9],[3000,60,0]],
 [[4000,-30,8],[4000,-20,8],[4000,-10,34],[4000,0,104],[4000,10,113],
[4000,20,44],[4000,30,14],[4000,40,5],[4000,50,4],[4000,60,0]],
 [[5000,-30,3],[5000,-20,5],[5000,-10,8],[5000,0,104],[5000,10,67],
[5000,20,14],[5000,30,5],[5000,40,1],[5000,50,2],[5000,60,0]],
 [[6000,-30,0],[6000,-20,1],[6000,-10,7],[6000,0,29],[6000,10,35],
[6000,20,7],[6000,30,1],[6000,40,1],[6000,50,0],[6000,60,0]],
 [[7000,-30,0],[7000,-20,0],[7000,-10,4],[7000,0,0],[7000,10,0],
[7000,20,1],[7000,30,3],[7000,40,0],[7000,50,0],[7000,60,0]],
 [[8000,-30,0],[8000,-20,0],[8000,-10,3],[8000,0,6],[8000,10,13],
[8000,20,5],[8000,30,1],[8000,40,0],[8000,50,0],[8000,60,0]],
 [[9000,-30,0],[9000,-20,0],[9000,-10,0],[9000,0,19],[9000,10,29],
[9000,20,11],[9000,30,0],[9000,40,0],[9000,50,0],[9000,60,0]],
```

```
 [[10000,-30,0],[10000,-20,0],[10000,-10,0],[10000,0,2],[10000,10,16],
[10000,20,0],[10000,30,0],[10000,40,0],[10000,50,0],[10000,50,0]]]:

highway_cycle := [[[0,-30,0],[0,-20,0],[0,-10,2],[0,0,6],[0,10,0],
[0,20,0],[0,30,1],[0,40,0],[0,50,0],[0,60,0]],
 [[1000,-30,0],[1000,-20,2],[1000,-10,1],[1000,0,0],[1000,10,0],
[1000,20,0],[1000,30,0],[1000,40,0],[1000,50,2],[1000,60,0]],
 [[2000,-30,0],[2000,-20,2],[2000,-10,0],[2000,0,0],[2000,10,0],
[2000,20,0],[2000,30,0],[2000,40,0],[2000,50,2],[2000,60,0]],
 [[3000,-30,0],[3000,-20,2],[3000,-10,0],[3000,0,0],[3000,10,0],
[3000,20,0],[3000,30,0],[3000,40,2],[3000,50,0],[3000,60,0]],
 [[4000,-30,0],[4000,-20,3],[4000,-10,0],[4000,0,0],[4000,10,0],
[4000,20,0],[4000,30,1],[4000,40,2],[4000,50,0],[4000,60,0]],
 [[5000,-30,1],[5000,-20,1],[5000,-10,2],[5000,0,3],[5000,10,2],
[5000,20,7],[5000,30,1],[5000,40,0],[5000,50,0],[5000,60,0]],
 [[6000,-30,2],[6000,-20,0],[6000,-10,2],[6000,0,7],[6000,10,25],
[6000,20,1],[6000,30,2],[6000,40,1],[6000,50,0],[6000,60,0]],
 [[7000,-30,0],[7000,-20,1],[7000,-10,7],[7000,0,19],[7000,10,26],
[7000,20,20],[7000,30,1],[7000,40,0],[7000,50,0],[7000,60,0]],
 [[8000,-30,0],[8000,-20,1],[8000,-10,5],[8000,0,49],[8000,10,177],
[8000,20,14],[8000,30,0],[8000,40,0],[8000,50,0],[8000,60,0]],
 [[9000,-30,0],[9000,-20,1],[9000,-10,0],[9000,0,36],[9000,10,112],
[9000,20,21],[9000,30,0],[9000,40,0],[9000,50,0],[9000,60,0]],
 [[10000,-30,0],[10000,-20,0],[10000,-10,0],[10000,0,17],[10000,10,168],
[10000,20,6],[10000,30,0],[10000,40,0],[10000,50,0],[10000,50,0]]]:

#check if they add up right;
fuds_cycle_total := 0:
m := 'm':
n := 'n':
for m from 1 to nops(fuds_cycle) do
for n from 1 to nops(fuds_cycle[1]) do
fuds_cycle_total := fuds_cycle_total + fuds_cycle[m][n][3];
od:
od:
fuds_cycle_total;
```

```
highway_cycle_total := 0:
m := 'm';
n := 'n';
for m from 1 to nops(highway_cycle) do
for n from 1 to nops(highway_cycle[1]) do
highway_cycle_total := highway_cycle_total + highway_cycle[m][n][3];
od:
od:
highway_cycle_total;
#convert to SI unit & direct drive
m := 'm':
n := 'n':
for m from 1 to nops(fuds_cycle) do
for n from 1 to nops(fuds_cycle[1]) do
fuds_cycle_SI[m][n][1] := fuds_cycle[m][n][1]/12.18;
fuds_cycle_SI[m][n][2] := fuds_cycle[m][n][2]*16.51/4;
fuds_cycle_SI[m][n][3] := fuds_cycle[m][n][3]/fuds_cycle_total;
highway_cycle_SI[m][n][1] := highway_cycle[m][n][1]/12.18;
highway_cycle_SI[m][n][2] := highway_cycle[m][n][2]*16.51/4;
highway_cycle_SI[m][n][3] := highway_cycle[m][n][3]/highway_cycle_total;
od;
od;

J0 := 'J0';

max_Torque := evalf(subs({J0=J0max,theta=0},Torque));

#Calculate the Back emf per phase

Area_conductor := A_cu/Nturns;
I0 := simplify(J0max * Area_conductor):
omega := ((2*Pi)/60) * rpm;
max_omega := ((2*Pi)/60) * max_rpm;
max_rpm := 1300;
rpm_corner := evalf(max_rpm/4);
Bemf_const_JcrossB := ((subs(J0 = J0max,Torque)*
```

```
     subs(rpm=rpm_corner,omega))/(2*I0))/rpm_corner:
rpm := 'rpm';
voltage_per_phase_JcrossB := Bemf_const_JcrossB * rpm:
tim := 0;
peak_bemf := 0:
Nturns := 21:
rpm := 'rpm':
tim := 'tim':

Torque_per_J := evalf(Torque/J0);
Torque_per_amp := evalf(Torque/(J0*Area_conductor));
mech_power_out := evalf(subs(J0=peak_torque/
                  Torque_per_J,mech_power_out)):
tot_power_in := evalf(subs(J0=peak_torque/
                  Torque_per_J,tot_power_in)):
mot_power_diss := evalf(subs(J0=peak_torque/
                  Torque_per_J,motor_losses)):
fuds_pow_out := 0;
fuds_pow_in := 0;
highway_pow_out := 0;
highway_pow_in := 0;
m := 'm':
n := 'n':
for m from 1 to nops(fuds_cycle) do
for n from 1 to nops(fuds_cycle[1]) do
rpm := fuds_cycle_SI[m][n][1]:
#prevent division by zero
V_emf := max(1e-5,evalf(V_emf_base*rpm/rpm_corner));
peak_torque := max(1e-5,abs(fuds_cycle_SI[m][n][2])):
fuds_pow_out := evalf(fuds_pow_out +
                fuds_cycle_SI[m][n][3]*mech_power_out):
fuds_pow_in := evalf(fuds_pow_in +
                fuds_cycle_SI[m][n][3]*tot_power_in):
highway_pow_out := evalf(highway_pow_out +
                highway_cycle_SI[m][n][3]*mech_power_out):
highway_pow_in := evalf(highway_pow_in +
```

```
                highway_cycle_SI[m][n][3]*tot_power_in):
od:
od:
fuds_efficiency := evalf(fuds_pow_out/fuds_pow_in)*100;
highway_efficiency := evalf(highway_pow_out/highway_pow_in)*100;
rpm := 'rpm';
peak_torque := 'peak_torque';
m := 'm':
n := 'n':
V_emf := 'V_emf';
ef := evalf(subs(J0=peak_torque/Torque_per_J,100*motor_efficiency)):
Tqmax := evalf(J0max*Torque_per_J):
print('here');
Tq := Torque_per_J:
#FD := plot(subs({rpm=0,t=0},Torque),J0=0..evalf(J0max)
#       ,title = 'Peak Torque'):
#FE := plot3d(ef,peak_torque=0..Tqmax,rpm=0..max_rpm,
#       contours=[20,30,40,50,60,70,75,80,85,90,95],
#        view=0..400,labelfont=[HELVETICA,BOLD,10],
#        axesfont=[HELVETICA,BOLD,10],titlefont=[HELVETICA,BOLD,12],
#         labels=['Peak Torque (Nm)','Speed (rpm)','Eff'],
#         title='Efficiency Map of Motor'):

F40 := implicitplot(ef=40,rpm=0..max_rpm,peak_torque=0..Tqmax):
F50 := implicitplot(ef=50,rpm=0..max_rpm,peak_torque=0..Tqmax):
F60 := implicitplot(ef=60,rpm=0..max_rpm,peak_torque=0..Tqmax):
F70 := implicitplot(ef=70,rpm=0..max_rpm,peak_torque=0..Tqmax):
F75 := implicitplot(ef=75,rpm=0..max_rpm,peak_torque=0..Tqmax):
F80 := implicitplot(ef=80,rpm=0..max_rpm,peak_torque=0..Tqmax):
F85 := implicitplot(ef=85,rpm=0..max_rpm,peak_torque=0..Tqmax):
F90 := implicitplot(ef=90,rpm=0..max_rpm,peak_torque=0..Tqmax):
F95 := implicitplot(ef=95,rpm=0..max_rpm,peak_torque=0..Tqmax):
max_motor_power := 15000;
tspeed := proc(x)
if x <= rpm_corner then evalf(max_motor_power/(2*Pi*rpm_corner/60));
else
```

```
evalf(max_motor_power/(2*Pi*x/60));
fi;
end:
env := plot(tspeed,0..max_rpm,linestyle=2):
display({env,F40,F50,F60,F70,F75,F80,F85,F90,F95},
       labelfont=[HELVETICA,BOLD,10],axesfont=[HELVETICA,BOLD,15],
        titlefont=[HELVETICA,BOLD,15],labels=['Speed (rpm)',
        'Peak Torque (Nm)'],title='Efficiency Map of Motor'):

break;
#plotsetup(ps,plotoutput='efficiency_map.ps',
#           plotoptions='portrait,noborder'):
#plot({env,F20,F30,F40,F50,F60,F70,F75,F80,F85,F90,F95},
#      labelfont=[HELVETICA,BOLD,10],axesfont=[HELVETICA,BOLD,10],
#      titlefont=[HELVETICA,BOLD,12],
#      labels=['Speed (rpm)','Peak Torque (Nm)'],
#       title='Efficiency Map of Motor');

vol_frac := pk_fac;
kcu := 390;
kepox := 1.8;
kst := 20;
kmixl := kepox * ((kepox+kcu)*(kcu+av_sig)-phi1*ksi_2*(kcu-kepox)^2)/
         ((kepox+kcu)*(kepox+av_sig_bar)-phi1*ksi_2*(kcu-kepox)^2);
kmixu := kcu * ((kepox+kcu)*(kepox+av_sig)-phi2*ksi_1*(kcu-kepox)^2)/
         ((kepox+kcu)*(kcu+av_sig_bar)-phi2*ksi_1*(kcu-kepox)^2);
av_sig_bar := kcu*phi1 + kepox*phi2:
av_sig := kepox*phi1 + kcu*phi2:
ksi_2 := phi2/3 - 0.05707*phi2^2:
ksi_1 := 1-ksi_2:
phi2 := vol_frac:
phi1 := 1-phi2:
```

D.3 Inverter Design

The Maple source code in this section was used to design and analyze the inverter in Chapter 5.

```
readlib(piecewise):
readlib(optimize);
readlib(isolate);
readlib(unassign):
with(plots):
alias(I=I,j=sqrt(-1));

# Power electronics
# Battery has an open circuit voltage of 336 V
# with 0.3 ohms internal resistance
# Battery's allowable minimum output voltage
# is 255 V.

VB_full_load := 255;
VB_open_circuit := 336;
internal_resistance := 0.3;
#internal_resistance := 0.000000000003;
# 15 kW motor
max_motor_power := 15000;
# Assume 0.5 ohms motor resistance
R_motor := 0.5;
#R_motor := 0.0000000000001;
#Ohmic power dissipation in motor
Pohm_max := R_motor * I_corner^2;

# Compute maximum battery current allowed per wheelmotor
max_battery_current := evalf((VB_open_circuit -
               VB_full_load)/internal_resistance/4);
# Compute the maximum power that the inverter has to process
max_inverter_power := max_motor_power+Pohm_max+losses;
# Assume 1100 Watts of total inverter losses for now
losses := 1100;
#losses := 0;
# Make base voltage 200 Volts
V_emf_base := 200;
I_corner := evalf(max_motor_power/V_emf_base);
base_voltage := evalf(V_emf_base + R_motor*I_corner);
V_emf_max := 4*V_emf_base;
motor_current_at_max_rpm := max_motor_power/V_emf_max;
#R_motor := Pohm_max/(I_corner^2);
# Maximum steady-state inverter output voltage
V_out_max := V_emf_max + motor_current_at_max_rpm * R_motor;

# For the down converter the switching frequency
```

```
# in continuous conduction is related to the
#delta ripple in the inductor current by

f_cont_down := simplify(V_out*(1-V_out/V_in)/(Lm*delta_I_down));

delta_I_down_cont := simplify(solve(f_cont_down = fsw_max,delta_I_down));
I_peak_down_cont := simplify(I_out_ave+delta_I_down_cont/2);
I_valley_down_cont := simplify(I_out_ave-delta_I_down_cont/2);
I_peak_down_disc := evalf(2*I_out_ave*sqrt(subs(delta_I_down =
                    2*I_out_ave, f_cont_down)/fsw_max));
I_valley_down_disc := 0;

#continuous and discontinuous modes : 1 => continuous, 0 => discontinuous

mode_down := proc(v_emf,i_out_ave)
local temp, v_out;
v_out := v_emf+i_out_ave*R_motor;
temp := subs({I_out_ave=i_out_ave,V_out=v_out}, I_valley_down_cont);
if temp < 0 then
0
else
1
fi;
end;

I_Lm_down := proc(v_emf,i_out_ave)
local t2, ans1, ans2;
global V_emf,I_out_ave,t1,duty,duty_bar;
V_emf := v_emf;
I_out_ave := i_out_ave;
if evalf(I_valley_down_cont) < 0 then
t1 := evalf(Lm*I_peak_down_disc/(V_in-V_out));
duty := evalf(t1/T);
t2 := t1+evalf(Lm*I_peak_down_disc/(V_out));
duty_bar := evalf((t2-t1)/T);
ans1 := piecewise(t <= t1, evalf(I_valley_down_disc+
       (V_in-V_out)/Lm*t), t <= t2, evalf(I_peak_down_disc -
        (V_out)/Lm*(t-t1)),0);
ans1;
else
t1 := evalf(Lm*delta_I_down_cont/(V_in-V_out));
duty := evalf(t1/T);
t2 := evalf(1/fsw_max);
duty_bar := evalf((t2-t1)/T);
ans2 := piecewise(t <= t1, evalf(I_valley_down_cont +
        ((V_in-V_out)/Lm)*t),t <= t2, evalf(I_peak_down_cont -
        V_out/Lm*(t-t1)),0);
ans2;
fi;
end;
```

```
I_buscap_down := proc(v_emf,i_out_ave)
local t2, ans1, ans2;
global V_emf,I_out_ave,t1,duty,duty_bar,I_Lm_down;
V_emf := v_emf;
I_out_ave := i_out_ave;
I_Lm_down(V_emf,I_out_ave);
piecewise(t <= t1, evalf(I_in - I_Lm_down(V_emf,I_out_ave)),
         evalf(I_in));
end;

I_buscap_rms_down := proc(v_emf,i_out_ave)
global V_emf,I_out_ave,t1,duty,duty_bar,I_Lm_down,T;
V_emf := v_emf;
I_out_ave := i_out_ave;
I_Lm_down(V_emf,I_out_ave);
evalf(sqrt(int(simplify((I_in- evalf(I_valley_down_cont +
     ((V_in-V_out)/Lm)*t))^2),t=0..t1)/T +
     int(I_in^2,t=t1..T)/T));
end;

#plot3d('I_buscap_rms_down'(v_emf,i_out_ave),v_emf=1..200,
#i_out_ave=1..min(300,evalf(15000/v_emf)),
#labelfont=[HELVETICA,BOLD,16],axesfont=[HELVETICA,BOLD,16]);

I_Lm_ripple_rms_down := proc(v_emf,i_out_ave)
local t1,t2,T,ans1,ans2;
global V_emf,I_out_ave;
V_emf := v_emf;
I_out_ave := i_out_ave;
T := evalf(1/fsw_max);
if evalf(I_valley_down_cont) < 0 then
t1 := evalf(Lm*I_peak_down_disc/(V_in-V_out));
t2 := evalf(t1+evalf(Lm*I_peak_down_disc/(V_out)));
ans1 := sqrt((int(simplify((I_valley_down_disc+
        (V_in-V_out)/Lm*t - I_out_ave)^2),t=0..t1)+
        int(simplify((I_peak_down_disc - V_out/Lm*
        (t-t1)-I_out_ave)^2),t=t1..t2))/T);
#V_emf := 'V_emf';
#I_out_ave := 'I_out_ave';
ans1;
else
t1 := evalf(Lm*delta_I_down_cont/(V_in-V_out));
t2 := T;
ans2 := sqrt((int(simplify((I_valley_down_cont+(V_in-V_out)/
         Lm*t - I_out_ave)^2),t=0..t1)+
         int(simplify((I_peak_down_cont - (V_out)/
         Lm*(t-t1)-I_out_ave)^2),t=t1..t2))/T);
#V_emf := 'V_emf';
#I_out_ave := 'I_out_ave';
```

```
ans2;
fi;
end;

I_Lu_ripple_rms_down := proc(v_emf,i_out_ave)
local t1,t2,T,ans1,ans2;
global V_emf,I_out_ave;
V_emf := v_emf;
I_out_ave := i_out_ave;
T := evalf(1/fsw_max);
if evalf(I_valley_down_cont) < 0 then
t1 := evalf(Lm*I_peak_down_disc/(V_in-V_out));
#t2 := t1+evalf(Lm*I_peak_down_disc/(V_out));
ans1 := sqrt((int(simplify((I_valley_down_disc+
        (V_in-V_out)/Lm*t - I_in)^2),t=0..t1))/T);
#V_emf := 'V_emf';
#I_out_ave := 'I_out_ave';
ans1;
else
t1 := evalf(Lm*delta_I_down_cont/(V_in-V_out));
#t2 := T;
ans2 := sqrt((int(simplify((I_valley_down_cont+
        (V_in-V_out)/Lm*t - I_in)^2),t=0..t1))/T);
#V_emf := 'V_emf';
#I_out_ave := 'I_out_ave';
ans2;
fi;
end;

Motor_power_ripple_down := proc(v_emf,i_out_ave)
evalf(I_Lm_ripple_rms_down(v_emf,i_out_ave)^2*R_motor);
end;

Lu_power_ripple_down := proc(v_emf,i_out_ave)
evalf(I_Lu_ripple_rms_down(v_emf,i_out_ave)^2*R_Lu);
end;

fdown_sw := proc(v_emf,i_out_ave)
fsw_max;
end;

Ipk_down := proc(v_emf,i_out_ave)
local temp, v_out;
v_out := v_emf+i_out_ave*R_motor;
temp := subs({I_out_ave=i_out_ave,V_out=v_out},
        I_valley_down_cont);
if temp < 0 then
subs({I_out_ave=i_out_ave,V_emf = v_emf,V_out=v_out},
          I_peak_down_disc);
else
```

```
subs({I_out_ave=i_out_ave,V_emf = v_emf,V_out=v_out},
          I_peak_down_cont);
fi;
end;

Energy_pk_down := proc(v_emf,i_out_ave)
local temp, v_out;
v_out := v_emf+i_out_ave*R_motor;
temp := subs({I_out_ave=i_out_ave,V_out=v_out},
            I_valley_down_cont);
if temp < 0 then
subs({I_out_ave=i_out_ave,V_emf = v_emf,V_out=v_out},
            evalf(I_peak_down_disc^2*Lu/2));
else
subs({I_out_ave=i_out_ave,V_emf = v_emf,V_out=v_out},
            evalf(I_peak_down_cont^2*Lu/2));
fi;
end;

buck_boundary := proc(v_emf)
local temp;
temp := evalf(v_emf);
if type(temp,numeric) then
if temp <= VB_open_circuit then
evalf(min(I_corner,evalf(subs(V_emf=v_emf,max_curr_down)),
         evalf(max_motor_power/v_emf)));
else
0
fi;
else
'buck_boundary'(v_emf);
fi;
end;

clip := proc(x)
if type(x,numeric) then
if x < 0 then
0;
else
x;
fi;
else
'clip'(x);
fi;
end;

# the up converter

f_cont_up := V_in*(1-V_in/V_out)/(Lu*delta_I_up);
```

```
#a quadratic dependence of ripple on voltage leads
#to constant switching frequency:

delta_I_up_cont := simplify(solve(f_cont_up = fsw_max,delta_I_up));
I_peak_up_cont := simplify(I_in+delta_I_up_cont/2);
I_valley_up_cont := simplify(I_in-delta_I_up_cont/2);
I_peak_up_disc := evalf(2*I_in*sqrt(subs(delta_I_up =
                  2*I_in, f_cont_up)/fsw_max));
I_valley_up_disc := 0;

I_Lu_average_up := proc(v_emf,i_out_ave)
local t1,t2, ans1, ans2;
global V_emf,I_out_ave,duty,duty_bar;
V_emf := v_emf;
I_out_ave := i_out_ave;
if evalf(I_valley_up_cont) < 0 then
t1 := evalf(Lu*I_peak_up_disc/V_in);
duty := evalf(t1/T);
t2 := t1+evalf(Lu*I_peak_up_disc/(V_out-V_in));
duty_bar := evalf((t2-t1)/T);
ans1 := piecewise(t <= t1, evalf(I_valley_up_disc+(V_in)/Lu*t),
        t <= t2, evalf(I_peak_up_disc - (V_out-V_in)/Lu*(t-t1)),0);
#V_emf := 'V_emf';
#I_out_ave := 'I_out_ave';
ans1;
else
t1 := evalf(Lu*delta_I_up_cont/(V_in));
duty := evalf(t1/T);
t2 := evalf(1/fsw_max);
duty_bar := evalf((t2-t1)/T);
ans2 := piecewise(t <= t1, evalf(I_valley_up_cont +((V_in)/Lu)*t),
        t <= t2, evalf(I_peak_up_cont - (V_out-V_in)/Lu*(t-t1)),0);
#V_emf := 'V_emf';
#I_out_ave := 'I_out_ave';
ans2;
fi;
end;

# this assumes zero capacitor voltage and inductor current ripple.

I_Co_average_up := proc(v_emf,i_out_ave)
local t1,t2, ans1, ans2;
global V_emf,I_out_ave,duty,duty_bar;
V_emf := v_emf;
I_out_ave := i_out_ave;
if evalf(I_valley_up_cont) < 0 then
t1 := evalf(Lu*I_peak_up_disc/V_in);
duty := evalf(t1/T);
t2 := t1+evalf(Lu*I_peak_up_disc/(V_out-V_in));
duty_bar := evalf((t2-t1)/T);
```

```
ans1 := piecewise(t <= t1, I_out_ave, t <= t2, evalf(I_peak_up_disc
        - (V_out-V_in)/Lu*(t-t1)-I_out_ave),I_out_ave);
#V_emf := 'V_emf';
#I_out_ave := 'I_out_ave';
ans1;
else
t1 := evalf(Lu*delta_I_up_cont/(V_in));
duty := evalf(t1/T);
t2 := evalf(1/fsw_max);
duty_bar := evalf((t2-t1)/T);
ans2 := piecewise(t <= t1, -I_out_ave,t <= t2, evalf(I_peak_up_cont
       - (V_out-V_in)/Lu*(t-t1)-I_out_ave ),-I_out_ave);
ans2;
fi;
end;

I_Lu_average_ripple_rms_up := proc(v_emf,i_out_ave)
local t1,t2,T,ans1,ans2;
global V_emf,I_out_ave;
V_emf := v_emf;
I_out_ave := i_out_ave;
T := evalf(1/fsw_max);
if evalf(I_valley_up_cont) < 0 then
t1 := evalf(Lu*I_peak_up_disc/(V_in));
t2 := evalf(t1+evalf(Lu*I_peak_up_disc/(V_out-V_in)));
ans1 := sqrt((int(simplify((I_valley_up_disc+(V_in)/Lu*t - I_in)^2),
        t=0..t1)+ int(simplify((I_peak_up_disc - (V_out-V_in)/Lu*
        (t-t1)-I_in)^2),t=t1..t2))/T);
#V_emf := 'V_emf';
#I_out_ave := 'I_out_ave';
ans1;
else
t1 := evalf(Lu*delta_I_up_cont/(V_in));
t2 := T;
ans2 := sqrt((int(simplify((I_valley_up_cont+(V_in)/Lu*t - I_in)^2),
        t=0..t1)+ int(simplify((I_peak_up_cont - (V_out-V_in)/Lu*
        (t-t1)-I_in)^2),t=t1..t2))/T);
#V_emf := 'V_emf';
#I_out_ave := 'I_out_ave';
ans2;
fi;
end;

V_Co_average_ripple_up := proc(v_emf,i_out_ave)
local t1,t2,T,ans1,ans2,temp;
global V_emf,I_out_ave,Co;
V_emf := v_emf;
I_out_ave := i_out_ave;
T := evalf(1/fsw_max);
if evalf(I_valley_up_cont) < 0 then
```

```
t1 := evalf(Lu*I_peak_up_disc/(V_in));
t2 := evalf(t1+evalf(Lu*I_peak_up_disc/(V_out-V_in)));
temp := simplify(solve(I_peak_up_disc - (V_out-V_in)/
        Lu*(t-t1)-I_out_ave = 0,t));
ans1 := simplify((int(I_out_ave,t=0..t1)+ int(simplify(I_peak_up_disc
         - (V_out-V_in)/Lu*(t-t1)-I_out_ave),t=temp..t2) +
        int(I_out_ave,t=t2..T))/Co);
#V_emf := 'V_emf';
#I_out_ave := 'I_out_ave';
ans1;
else
t1 := evalf(Lu*delta_I_up_cont/(V_in));
t2 := T;
temp := simplify(solve(I_peak_up_cont -
        (V_out-V_in)/Lu*(t-t1)-I_out_ave=0,t));
ans2 := simplify((int(I_out_ave,t=0..t1)+ int(simplify((I_peak_up_cont -
        (V_out-V_in)/Lu*(t-t1)-I_out_ave)),t=temp..t2))/Co);
#V_emf := 'V_emf';
#I_out_ave := 'I_out_ave';
ans2;
fi;
end;

I_Co_average_rms_up := proc(v_emf,i_out_ave)
local t1,t2,T,ans1,ans2;
global V_emf,I_out_ave;
V_emf := v_emf;
I_out_ave := i_out_ave;
T := evalf(1/fsw_max);
if evalf(I_valley_up_cont) < 0 then
t1 := evalf(Lu*I_peak_up_disc/(V_in));
t2 := evalf(t1+evalf(Lu*I_peak_up_disc/(V_out-V_in)));
ans1 := sqrt((int(I_out_ave^2,t=0..t1)+ int(simplify((I_peak_up_disc -
        (V_out-V_in)/Lu*(t-t1)-I_out_ave)^2),t=t1..t2) +
        int(I_out_ave^2,t=t2..T))/T);
#V_emf := 'V_emf';
#I_out_ave := 'I_out_ave';
ans1;
else
t1 := evalf(Lu*delta_I_up_cont/(V_in));
t2 := T;
ans2 := sqrt((int(I_out_ave^2,t=0..t1)+ int(simplify((I_peak_up_cont -
        (V_out-V_in)/Lu*(t-t1)-I_out_ave)^2),t=t1..t2))/T);
#V_emf := 'V_emf';
#I_out_ave := 'I_out_ave';
ans2;
fi;
end;
Lu_power_ripple_up := proc(v_emf,i_out_ave)
evalf(I_Lu_ripple_rms_up(v_emf,i_out_ave)^2*R_Lu);
```

```
end;


fup_sw := proc(v_emf,i_out_ave)
fsw_max;
end;

mode_up := proc(v_emf,i_out_ave)
local temp, v_out;
v_out := v_emf+i_out_ave*R_motor;
temp := subs({I_out_ave=i_out_ave,V_out=v_out}, I_valley_up_cont);
if temp < 0 then
0
else
1
fi;
end;


Ipk_up := proc(v_emf,i_out_ave)
local temp, v_out;
v_out := v_emf+i_out_ave*R_motor;
temp := subs({I_out_ave=i_out_ave,V_out=v_out},
        I_valley_up_cont);
if temp < 0 then
subs({I_out_ave=i_out_ave,V_emf = v_emf,V_out=v_out},
        I_peak_up_disc);
else
subs({I_out_ave=i_out_ave,V_emf = v_emf,V_out=v_out},
        I_peak_up_cont);
fi;
end;

Energy_pk_up := proc(v_emf,i_out_ave)
local temp, v_out;
v_out := v_emf+i_out_ave*R_motor;
temp := subs({I_out_ave=i_out_ave,V_out=v_out},
        I_valley_up_cont);
if temp < 0 then
subs({I_out_ave=i_out_ave,V_emf = v_emf,V_out=v_out},
        evalf(I_peak_up_disc^2*Lu/2));
else
subs({I_out_ave=i_out_ave,V_emf = v_emf,V_out=v_out},
        evalf(I_peak_up_cont^2*Lu/2));
fi;
end;

fsw_max := 16440;
T := evalf(1/fsw_max);
#Lm :=evalf(268e-6 *(V_emf_max/894)^2);
```

```
Lm := 8e-3;
#internal_resistance := 1e-15;
Rs := 4*internal_resistance;
#V_out_max := 1000;
#Pohm := 2300;
max_motor_power := 15000;

V_out := V_emf+I_out_ave*R_motor;
V_emf_max := max(solve(subs(I_out_ave = (max_motor_power/V_emf),
             V_out)=V_out_max,V_emf));

V_in := VB_open_circuit - I_in*Rs;
I_in := VB_open_circuit/(2*Rs) - (VB_open_circuit^2 -
             4*Rs*V_out*I_out_ave)^(1/2)/(2*Rs);
#V_in := 250;
#I_in := V_out*I_out_ave/V_in;
#I_out_ave := I_corner;
#V_emf_down_ct_max := max(evalf(allvalues(solve(V_in=V_out,V_emf))));
#I_out_ave :=max_motor_power/V_emf;
#V_emf_down_cp_max := fsolve(V_in=V_out,V_emf=V_emf_base..V_emf_max);
I_out_ave := 'I_out_ave';
max_curr_down := max(evalf(allvalues(solve(V_in=V_out,I_out_ave))));
I_out_ave := 'I_out_ave';

#combined switching frequency

f_sw := proc(v_emf,i_ave)
local temp;
temp := buck_boundary(v_emf);
if v_emf <= VB_open_circuit and i_ave <= temp then
fdown_sw(v_emf,i_ave);
else
fup_sw(v_emf,i_ave);
fi;
end;
mode := proc(v_emf,i_ave)
local temp;
temp := buck_boundary(v_emf);
if v_emf <= VB_open_circuit and i_ave <= temp then
mode_down(v_emf,i_ave);
else
mode_up(v_emf,i_ave);
fi;
end;

I_Co_rms_ave := proc(v_emf,i_ave)
local temp;
temp := buck_boundary(v_emf);
if v_emf <= VB_open_circuit and i_ave <= temp then
0;
```

```
else
I_Co_average_rms_up(v_emf,i_ave);
fi;
end;

V_Co_ripple_ave := proc(v_emf,i_ave)
local temp;
temp := buck_boundary(v_emf);
if v_emf <= VB_open_circuit and i_ave <= temp then
0;
else
V_Co_average_ripple_up(v_emf,i_ave);
fi;
end;

I_Lu_pk := proc(v_emf,i_ave)
local temp;
temp := buck_boundary(v_emf);
if v_emf <= VB_open_circuit and i_ave <= temp then
Ipk_down(v_emf,i_ave);
else
Ipk_up(v_emf,i_ave);
fi;
end;

Energy_Lu_pk := proc(v_emf,i_ave)
local temp;
temp := buck_boundary(v_emf);
if v_emf <= VB_open_circuit and i_ave <= temp then
Energy_pk_down(v_emf,i_ave);
else
Energy_pk_up(v_emf,i_ave);
fi;
end;

Lu_power_ripple := proc(v_emf,i_ave)
local temp;
temp := buck_boundary(v_emf);
if v_emf <= VB_open_circuit and i_ave <= temp then
Lu_power_ripple_down(v_emf,i_ave);
else
Lu_power_ripple_up(v_emf,i_ave);
fi;
end;

Lu_energy_at_max_rpm := proc(inductance)
global Lu,V_emf,I_out_ave;
Lu := inductance;
V_emf := V_emf_max;
I_out_ave := max_motor_power/V_emf_max;
```

```
Energy_pk_up(V_emf,I_out_ave);
end;

Lu_power_ripple_at_max_rpm := proc(inductance)
global Lu,V_emf,I_out_ave;
Lu := inductance;
V_emf := V_emf_max;
I_out_ave := max_motor_power/V_emf_max;
Lu_power_ripple_up(V_emf,I_out_ave);
end;

#resistance of inductor; R proportional to N
R_Lu := 0.019;
max_core_loss := 170;
#:= 0.01*sqrt(Lu/30e-6);

#Critical maximum inductance for minimum energy
#storage at max. V_emf
V_emf_clip := 1200;
V_emf := V_emf_clip;
I_out_ave := max_motor_power/V_emf;
Lu_crit := V_in^2*(1-V_in/V_out)/(2*max_motor_power*fsw_max);
Lu := Lu_crit;
V_emf := 'V_emf';
I_out_ave := 'I_out_ave';

#Semiconductor parameters

V_d_on := 2.5;
t_on := 0.8e-6;
t_off := 1.5e-6;
tr :=0.6e-6;
tf := 0.5e-6;

# down conversion

P_s1_cond_down := 0;

P_s2_cond_down := proc()
local Vt2, a2, b2;
Vt2 := 0.4819;
a2 := 0.1196;
b2 := 0.4881;
evalf((Vt2+a2*I_in^b2)*I_in);
end;

P_s3_s8_cond_down := proc()
local Vt1,Vt2, a1,a2, b1,b2, I1, I2,
      E_trans,E_diode,E_trans1,E_trans2,t1;
Vt1 := 1.011;
```

```
a1 := 0.2324;
b1 := 0.5085;
Vt2 := 0.4819;
a2 := 0.1196;
b2 := 0.4881;
I1 := subs(t=0,I_Lm_down(V_emf,I_out_ave));
I2 := subs(t=duty*T,I_Lm_down(V_emf,I_out_ave));
E_trans := Vt1*(I1+I2)*duty*T/2+
           abs((I2^(b1+2)-I1^(b1+2))/(I2-I1))*
           (a1*duty*T)/(b1+2);
E_trans1 := E_trans;
I1 := I2;
I2 := subs(t=T,I_Lm_down(V_emf,I_out_ave));
E_diode := Vt2*(I1+I2)*duty_bar*T/2+
           abs((I2^(b2+2)-I1^(b2+2))/(I2-I1))*
           (a2*duty_bar*T)/(b2+2);
E_trans2 := E_diode*Vt1/Vt2;
evalf((E_trans+E_diode+E_trans1+E_trans2)/T);
end;

#2*V_ce_sat*I_out_ave*duty +2*V_d_on*I_out_ave*duty_bar;
P_RLu_cond_down := I_in^2*R_Lu;
#P_s3_s8_sw_down := 2*fsw_max*(E_on_down+E_off_down);

P_s3_s8_sw_down:= proc()
local Vt1,Vt2, a1,a2, b1,b2,
      I1,I2,E_trans_on,E_trans_off,E_sw,t1;
a2 := 0.0000294;
b2 := 1.3977682;
a1 := 0.0002064516;
b1 := 1;
I1 := subs(t=0,I_Lm_down(V_emf,I_out_ave));
I2 := subs(t=duty*T,I_Lm_down(V_emf,I_out_ave));
E_trans_on := V_in*a1*I1^b1/600;
E_trans_off := V_in*a2*I2^b2/600;
E_sw := E_trans_on +E_trans_off;
evalf(E_sw*fsw_max);
end;


P_RLu_cond_up := proc()
local I1, I2;
I1 := subs(t=0,I_Lu_average_up(V_emf,I_out_ave));
I2 := subs(t=duty*T,I_Lu_average_up(V_emf,I_out_ave));
evalf(R_Lu*(I1^2+I2^2+I1*I2)/3) +
evalf((V_emf*I_out_ave)*max_core_loss/max_motor_power);
end;

tot_pow_diss_down := proc(v_emf,i_ave)
global V_emf,I_out_ave;
```

```
local temp;
V_emf := v_emf;
I_out_ave := i_ave;
temp := evalf(P_s2_cond_down()+P_s3_s8_cond_down()+
        P_RLu_cond_down+P_s3_s8_sw_down());
end;

P_s1_s8_cond_up := proc()
local Vt1,Vt2, a1,a2, b1,b2, I1,I2,
      E_trans,E_diode,E_12,t1;
Vt1 := 1.011;
a1 := 0.2324;
b1 := 0.5085;
Vt2 := 0.4819;
a2 := 0.1196;
b2 := 0.4881;
I1 := subs(t=0,I_Lu_average_up(V_emf,I_out_ave));
I2 := subs(t=duty*T,I_Lu_average_up(V_emf,I_out_ave));
E_trans := Vt1*(I1+I2)*duty*T/2+abs((I2^(b1+2)-I1^(b1+2))
           /(I2-I1))*(a1*duty*T)/(b1+2);
I1 := subs(t=duty*T,I_Lu_average_up(V_emf,I_out_ave));
I2 := subs(t=(duty+duty_bar)*T,I_Lu_average_up(V_emf,I_out_ave));
E_diode := Vt2*(I1+I2)*duty_bar*T/2+
           abs((I2^(b2+2)-I1^(b2+2))/(I2-I1))*
           (a2*duty_bar*T)/(b2+2);
E_12 := evalf((E_trans+E_diode)/T);
evalf(E_12+2*2*Vt1*I_out_ave);
end;

P_s1_s2_sw_up := proc()
local Vt1,Vt2, a1,a2, b1,b2, I1,I2,E_trans_on,
      E_trans_off,E_sw,t1;
a2 := 0.0000294;
b2 := 1.3977682;
a1 := 0.0002064516;
b1 := 1;
I1 := subs(t=0,I_Lu_average_up(V_emf,I_out_ave));
I2 := subs(t=duty*T,I_Lu_average_up(V_emf,I_out_ave));
E_trans_on := V_out*a1*I1^b1/600;
E_trans_off := V_out*a2*I2^b2/600;
E_sw := E_trans_on +E_trans_off;
evalf(E_sw*fsw_max);
end;

P_s3_s8_sw_up := proc()
local Vt1,Vt2, a1,a2, b1,b2, I1,I2,E_trans_on,
      E_trans_off,E_sw,t1,fcom;
a2 := 0.0000294;
b2 := 1.3977682;
a1 := 0.0002064516;
```

```
b1 := 1;
I1 := I_out_ave;
I2 := I_out_ave;
fcom := (V_emf/V_emf_max)*6*max_rpm*N/60;
E_trans_on := V_out*a1*I1^b1/600;
E_trans_off := V_out*a2*I2^b2/600;
E_sw := E_trans_on +E_trans_off;
evalf(E_sw*fcom);
end;


tot_pow_diss_up := proc(v_emf,i_ave)
global V_emf,I_out_ave;
local E_on_up,E_off_up,temp;
V_emf := v_emf;
I_out_ave := i_ave;
temp := evalf(P_s1_s2_sw_up()+P_s1_s8_cond_up()
        +P_RLu_cond_up()+P_s3_s8_sw_up());
end;

tot_power_diss := proc(v_emf,i_ave)
global V_emf,I_out_ave;
local temp;
V_emf := v_emf;
I_out_ave := i_ave;
temp := buck_boundary(v_emf);
if v_emf <= VB_open_circuit and i_ave <= temp then
tot_pow_diss_down(v_emf,i_ave);
else
tot_pow_diss_up(v_emf,i_ave);
fi;
end;

switching_losses := proc(v_emf,i_ave)
global V_emf,I_out_ave;
local temp;
V_emf := v_emf;
I_out_ave := i_ave;
temp := buck_boundary(v_emf);
if v_emf <= VB_open_circuit and i_ave <= temp then
evalf(P_s3_s8_sw_down());
else
evalf(P_s1_s2_sw_up()+P_s3_s8_sw_up());
fi;
end;

conduction_losses := proc(v_emf,i_ave)
global V_emf,I_out_ave;
local temp;
V_emf := v_emf;
```

```
I_out_ave := i_ave;
temp := buck_boundary(v_emf);
if v_emf <= VB_open_circuit and i_ave <= temp then
evalf(P_s2_cond_down()+P_s3_s8_cond_down());
else
evalf(P_s1_s8_cond_up());
fi;
end;


inv_power_diss := proc()
local temp;
global I_out_ave;
I_out_ave := evalf(peak_torque/Torque_per_amp);
if type(I_out_ave,numeric) and type(V_emf,numeric) then
temp := buck_boundary(V_emf);
if V_emf <= VB_open_circuit and I_out_ave <= temp then
tot_pow_diss_down(V_emf,I_out_ave);
else
tot_pow_diss_up(V_emf,I_out_ave);
fi;
else
'inv_power_diss'();
fi;
end;


inv_efficiency := proc(v_emf,i_ave)
global V_emf, I_out_ave;
local temp,temp1,temp2,gdrive_power;
V_emf := v_emf;
I_out_ave := i_ave;
gdrive_power := 20;
temp := buck_boundary(v_emf);
if v_emf <= VB_open_circuit and i_ave <= temp then
temp1 := tot_pow_diss_down(v_emf,i_ave);
temp2 := evalf(100*V_out*I_out_ave/(V_in*
         I_in+temp1+gdrive_power));
V_emf := 'V_emf';
I_out_ave := 'I_out_ave';
temp2;
else
temp1 := tot_pow_diss_up(v_emf,i_ave);
temp2 := evalf(100*V_out*I_out_ave/
         (V_in*I_in+temp1+gdrive_power));
V_emf := 'V_emf';
I_out_ave := 'I_out_ave';
temp2;
fi;
end;
```

```
#plot3d('inv_efficiency'(vemf,iout),vemf=0.001..1000,
#iout=0.001..min(I_corner,evalf(max_motor_power/vemf)),
#contours=[10,20,30,40,50,60,70,80,90,95],
#labelfont=[HELVETICA,BOLD,16],axesfont=[HELVETICA,BOLD,16]);

power_elec_cost := proc()
local c_switch,c_cap_hv, c_cap_lv,c_ind,c_gdrives;
c_cap_hv := 20;
c_switch := 85.50;
c_gdrives := 5;
c_cap_lv := 50;
evalf(c_ind+4*c_switch+c_cap_lv+c_cap_hv+4*c_gdrives);
end;
break;

display({plot('conduction_losses'(vemf,40),
vemf = 0.1..min(V_emf_max,evalf(15000/40))),
plot('conduction_losses'(vemf,50),
vemf = 0.1..min(V_emf_max,evalf(15000/50))),
plot('conduction_losses'(vemf,18.75),
vemf = 0.1..min(V_emf_max,evalf(15000/18.75))),
plot('conduction_losses'(vemf,30),
vemf = 0.1..min(V_emf_max,evalf(15000/30))),
plot('conduction_losses'(vemf,10),
vemf = 0.1..min(V_emf_max,evalf(15000/10))),
plot('conduction_losses'(vemf,75),
vemf = 0.1..min(V_emf_max,evalf(15000/75))),
plot('conduction_losses'(vemf,60),
vemf = 0.1..min(V_emf_max,evalf(15000/60)))},
labelfont=[HELVETICA,BOLD,16],axesfont=[HELVETICA,BOLD,16]);

display({plot('switching_losses'(vemf,40),
vemf = 0.1..min(V_emf_max,evalf(15000/40))),
plot('switching_losses'(vemf,50),
vemf = 0.1..min(V_emf_max,evalf(15000/50))),
plot('switching_losses'(vemf,18.75),
vemf = 0.1..min(V_emf_max,evalf(15000/18.75)))},
plot('switching_losses'(vemf,30),
vemf = 0.1..min(V_emf_max,evalf(15000/30))),
plot('switching_losses'(vemf,10),
vemf = 0.1..min(V_emf_max,evalf(15000/10))),
plot('switching_losses'(vemf,75),
vemf = 0.1..min(V_emf_max,evalf(15000/75))),
plot('switching_losses'(vemf,60),
vemf = 0.1..min(V_emf_max,evalf(15000/60)))},
labelfont=[HELVETICA,BOLD,16],axesfont=[HELVETICA,BOLD,16]);

display({plot('tot_power_diss'(vemf,40),
vemf = 0.1..min(V_emf_max,evalf(15000/40))),
```

```
plot('tot_power_diss'(vemf,50),
vemf = 0.1..min(V_emf_max,evalf(15000/50))),
plot('tot_power_diss'(vemf,18.75),
vemf = 0.1..min(V_emf_max,evalf(15000/18.75))),
plot('tot_power_diss'(vemf,30),
vemf = 0.1..min(V_emf_max,evalf(15000/30))),
plot('tot_power_diss'(vemf,10),
vemf = 0.1..min(V_emf_max,evalf(15000/10))),
plot('tot_power_diss'(vemf,75),
vemf = 0.1..min(V_emf_max,evalf(15000/75))),
plot('tot_power_diss'(vemf,60),
vemf = 0.1..min(V_emf_max,evalf(15000/60)))},
labelfont=[HELVETICA,BOLD,16],axesfont=[HELVETICA,BOLD,16]);

FA := plot(min(75,evalf(max_motor_power/vemf)),
vemf=0.001..800,labelfont=[HELVETICA,BOLD,16],
axesfont=[HELVETICA,BOLD,16],linestyle=2):


display({FA,implicitplot('inv_efficiency'(vemf,iout)=90,
vemf=0.001..800,iout=0.001..75),
implicitplot('inv_efficiency'(vemf,iout)=93,
vemf=0.001..800,iout=0.001..75),
implicitplot('inv_efficiency'(vemf,iout)=95,
vemf=0.001..800,iout=0.001..75),
implicitplot('inv_efficiency'(vemf,iout)=96,
vemf=0.001..800,iout=0.001..75)},
labelfont=[HELVETICA,BOLD,16],axesfont=[HELVETICA,BOLD,16]);
```

Appendix E

Microcode

This appendix contains the assembly language code for prototype inverter and motor control, as described in Chapter 5. Detailed information on the MC68HC16Z1 processor and its intruction set can be found in [60] - [65].

```
*****************************************************************
*       Title : EQUATES                                         *
*       Description : This is a table of EQUates for all of the *
*                     registers in the HC16.                    *
*                                                               *
*       Note : This program is written for the M68HC16Z1EVB     *
*****************************************************************

************************************************
****   variables in ram                      ****
****   on chip 1k ram begins at f000h        ****
****   for words, high byte is stored first  ****
************************************************

$org     $f000              ; variable address start

***  periodic sampling clock is 244 us *****

ki_pll  equ  $27bd          ; pll int constant  (cutoff at 100 hz)
                            ; # = 2*pi*fc * ts * 2^16
ki_dc   equ  $7d8           ; dc filter (cutoff at 20 hz)
ki_low_cutoff equ $3ec      ; low cutoff frequency filter
ki_high_cutoff equ $27bd    ; high cutoff frequency filter

atod_midpoint     equ $1fa    ; (vrhp-vrlp)=5.12v, vref= ****
maxsteps          equ !20     ; number of steps in commutation period
torque_constant   equ !6      ; torque per amp (nm per amp)
corner_rpm        equ !325    ; corner rpm
max_const_torque  equ {(!61 * $1ff)/(!100 )} ; max average torque
                              ; (450 nm -- 0.61* $1ff)
max_bus_voltage   equ {(!400 * $7fe)/!400} ; max bus voltage
```

```
                                ; (400 v -- $7fe)
max_boost_voltage equ {(!1200 * $17fa)/!1200} ; max boost voltage
                                ; (1200 v -- $17fa)
max_phase_current equ {(!100 * $1ff)/!100} ; max phase current
                                ; (100 a -- $1ff)
max_boostdac_val  equ $2aa      ; maximum dac value 7ff
;max_boost_current equ {(!200 * $3ff)/!200} ; max boost inductor
                                ; current (200 a -- $3ff)
max_boost_current equ {(!200 * $2fe)/!200} ; max boost inductor
                                ; current (200 a -- $3ff)
max_temp equ {(!120 * $3ff)/!180} ; max winding (hot spot)  temperature
                                  ;(180 deg c -- $3ff)
max_rpm           equ !1300       ; maximum motor rpm
max_trq_rpm equ  {corner_rpm * max_const_torque} ; max product of
                                  ;torque * corner rpm
max_trpm_hi equ  max_trq_rpm/$10000  ; high byte
max_trpm_lo equ  max_trq_rpm%$10000  ; low byte

k_emf   equ   $18d     ; 0.777 volts/rpm
                       ; 0.777/200 * $3ff * 1000 (divide by 1000)
rpm_count   equ  !393185  ; divide this number by the number of
                          ;input capture
                          ;counts to get motor rpm
                          ; (60 sec/min)/(count * 10 counts/rev *
                          ; 15.26 us/count)
max_shp_rpm equ   !350  ; max rpm for torque shaping
min_shp_rpm equ   !7    ; min rpm for torque shaping since timer runs out
min_oc_rpm  equ   !30   ; frequency below which we disable hall effect
                        ; output comapares
soft_start_rpm equ !1300  ; above this speed we heavily filter
                          ;torque command
min_pav_rpm equ   !50     ; speed at which we start phase advance
max_filt_rpm equ   !1300  ; speed above which we filter the input
                          ;torque command
temp1     dw      $0000h    ; 2-byte storage for temporary variables
temp2     dw      $0000h    ; temporary storage of pc during display
temp3     dw      $0000     ; temporary storage for boost integrator
temp4     dw      $0000     ;temporary storage for boost integrator

temp_reg dw     0000        ; temp register.  delete later
                            ; contains full value of torque pot
max_perm_torque dw $000h    ; contains maximum permissible torque

mode      db      0c2h      ; control mode
                            ; start in torque,forward, coast, stop mode
                            ; need to push start and drive for action
mode_chg equ $02            ;

flags     db    %01001111   ; status flags

tof  equ   $01    ; timer overflow
```

```
ioca equ   $02     ; set when output compare on phase a is inhibited
iocb equ   $04     ; set when output compare on phase b is inhibited
iocc equ   $08     ; set when output compare on phase c is inhibited
fault  equ   $10   ; set when the current in the selected phase has
                   ; to be negated for servo
lds  equ   $20     ; leading zero flag.  used to display numbers
                   ; in decimal on lcd
soft_start equ $40   ; soft start flag
good_atod  equ $80   ; set if a/d value is good
leading_sign db $00  ; temporary storage for leading sign for
                     ; disnum subroutine

dec_places  db  $00  ; number of decimal places to be displayed by
                     ; disnum

old_tic1    dw  $0000    ; previous ic1 capture time
new_hea_period dw  $ffff ; new period of phase a hall effect sensor
hea_periodh  dw  $ffff   ; high byte of period of phase a hall effect
                         ; sensor signal
hea_periodl  dw  $ffff   ; low byte of period of phase a hall effect
                         ; sensor signal

old_tic2    dw  $0000    ; previous ic2 capture time
new_heb_period dw  $ffff ; new period of phase b hall effect sensor
heb_periodh  dw  $ffff   ; high byte of period of phase b hall effect
                         ; sensor signal
heb_periodl  dw  $ffff   ; low byte of period of phase b hall effect
                         ; sensor signal

old_tic3    dw  $0000    ; previous ic3 capture time
new_hec_period dw  $ffff ; new period of phase c hall effect sensor
hec_periodh  dw  $ffff   ; high byte of period of phase c hall effect
                         ; sensor signal
hec_periodl  dw  $ffff   ; low byte of period of phase c hall effect
                         ; sensor signal

heabc_period           ; average of hea_periodh, heb_periodh, and
                       ;hec_periodh
percent_adv dw  $0000  ; percent phase advance
to_count    db $02     ; number of times timer overflowed between
                       ;input capture interrupts
commcnt     db $00     ; torque ripple compensation pointer

motor_rpm   dw $0000   ; motor rpm
bemf        dw $0000   ; back emf
bemf_by_ffh dw $0000   ; back emf * ff (high byte)
bemf_by_ffl dw $0000   ; back emf * ff (low byte)

new_bus_volt     dw $0000 ; unfiltered bus voltage
dc_bus_volth     dw $0000 ; high byte of filtered dc bus voltage
dc_bus_voltl     dw $0000 ; low byte of filtered dc bus voltage
```

```
vbus_by_ffh      dw $0000 ; high byte of dc bus voltage multiplied by ff
vbus_by_ffl      dw $0000 ; low word of dc bus voltage multiplied by ff

new_boost_volt   dw $0000 ; unfiltered boost voltage
dc_boost_volth   dw $0000 ; high byte of filtered dc boost voltage
dc_boost_voltl   dw $0000 ; low  byte of filtered dc boost voltage
vboost_by_ffh    dw $0000 ; high byte of dc boost voltage multiplied by ff
vboost_by_ffl    dw $0000 ; low word of dc boost voltage multiplied by ff

new_phase_curr  dw $0000 ; unfiltered phase current
dc_phase_currh  dw $0000 ; high byte of filtered dc phase current
dc_phase_currl  dw $0000 ; low byte of filtered dc phase current
iphasea_zerop   dw $0200 ; offset on phasea current channel (non-inverted)
iphasea_zeron   dw $0200 ; offset on phasea current channel (inverted)
iphaseb_zerop   dw $0200 ; offset on phaseb current channel (non-inverted)
iphaseb_zeron   dw $0200 ; offset on phaseb current channel (inverted)
iphasec_zerop   dw $0200 ; offset on phasec current channel (non-inverted)
iphasec_zeron   dw $0200 ; offset on phasec current channel (inverted)
iphase_zero     dw $01f3 ; temporary
new_boost_curr  dw $0000 ; unfiltered boost current
dc_boost_currh  dw $0000 ; high byte of filtered dc boost current
dc_boost_currl  dw $0000 ; low byte of filtered dc boost current
ilb_zero        dw $0200 ; offset on boost current channel

new_torque_cmd   dw $0000 ; instantaneous torque command
fil_torque_cmdh  dw $0000 ; high byte of filtered commanded torque
fil_torque_cmdl  dw $0000 ; low byte of filtered commanded torque
comp_torque_cmd  dw $0000 ; commanded torque, compensated for
                          ; commutation torque ripple
                             ; torque servo is closed around this number
phase_curr_err   dw $0000 ; phase current error for torque loop

new_brake_cmd    dw $0000 ; instantaneous brake command
fil_brake_cmdh   dw $0000 ; high byte of filtered brake command
fil_brake_cmdl   dw $0000 ; low byte of filtered brake command
comp_brake_cmd   dw $0000 ;

winding_temp     dw $0000 ; winding temperature
endturn_temp     dw $0000 ; end turn temperature
commtime         dw $0000 ; time of last commutaiont

;* control variables  (buck, motor)

buckm_interrh   dw  $0000 ; high byte of integrator error
buckm_interrl   dw  $0000 ; low byte of integrator error
kp_buck_mot     equ $5fa  ; proportional gain
;kp_buck_mot equ $4fb
ki_buck_mot      equ $38   ; integral gain
ku_buck_mot_sat  equ $ffff ; (-4 * 0.266)  multiplier of old command in
                           ;buck, motor, saturation mode
ki_buck_mot_sat  equ $04   ; (4 * 2 * 0.5267) multiplier of phase current
```

```
kv_buck_mot_sat  equ $28f5 ; (4 * 0.08 * 7fff) multiplier of boost voltage

;*  control variables - boost motor
mult_fac       dw   $0000 ; contains 2*ts*(vout-vin)/lu
boost_cmd_data dw  $0000  ; storage for computed boost dac data
boost_ipk      dw  $0000  ; peak boost current
ki_boost_mot   equ $6500  ; integral gain (0.6344* $8000)
max_voltage    dw  $0000  ; max boost volage
kp_boost_mot   equ $1     ;
;ku_boost_mot  equ $01    ; command gain
kv_boost_mot    equ $e1aa ; voltage gain (-0.237 * $8000)
boostm_interrh  dw  $0000 ; high byte of integrator error
boostm_interrl  dw  $0000 ; low byte of integrator error


boost_volt_cmd  dw  $0000 ; commanded boost voltage from buck controller
pwmdata         dw  $0000 ; where newly computed pwm data is stored
boostdac_data   dw  $0000 ; newly computed datat for boost dac

motor_resistance  dw  $3c28 ;0.47 * $8000
                            ;
proftab          dw $0000   ;

*****  sim module registers  *****

simmcr  equ     $fa00    ;sim module configuration register
simtr   equ     $fa02    ;system integration test register
syncr   equ     $fa04    ;clock synthesizer control register
rsr     equ     $fa07    ;reset status register
simtre  equ     $fa08    ;system integration test register (e clock)
porte0  equ     $fa11    ;port e data register (same data as porte1)
boostled equ    $80
buckled  equ    $40
init     equ    $20
* neg    equ    $10      ; has been defined in flags
porte1  equ     $fa13    ;port e data register (same data as porte0)
porte   equ     porte0   ;port e data register (same data as porte0)
ddre    equ     $fa15    ;port e data direction register
pepar   equ     $fa17    ;port e pin assignment register
portf0  equ     $fa19    ;port f data register (same data as portf1)
strt    equ     $10
driv    equ     $20
forw    equ     $40
torq    equ     $80

portf1  equ     $fa1b    ;port f data register (same data as portf0)
portf   equ     portf0   ;port f data register (same data as portf0)
ddrf    equ     $fa1d    ;port f data direction register
pfpar   equ     $fa1f    ;port f pin assignment register
sypcr   equ     $fa21    ;system protection control register
picr    equ     $fa22    ;periodic interrupt control register
```

```
pitr    equ     $fa24    ;periodic interrupt timing register
swsr    equ     $fa27    ;software service register
tstmsra equ     $fa30    ;master shift register a
tstmsrb equ     $fa32    ;master shift register b
tstsc   equ     $fa34    ;test module shift count
tstrc   equ     $fa36    ;test module repetition count
creg    equ     $fa38    ;test submodule control register
dreg    equ     $fa3a    ;distributed register
cspdr   equ     $fa41    ;port c data register
portc   equ     $fa41    ;port c data register (same as cspdr)
buck    equ  $40
mot     equ  $20
*for    equ  $10
lock    equ  $08
inh     equ  $04
cmc     equ  $02

cspar0  equ     $fa44      ;chip-select pin assignment register 0
cspar1  equ     $fa46      ;chip-select pin assignment register 1
csbarbt equ     $fa48      ;chip-select boot base address register
csorbt  equ     $fa4a      ;chip-select boot option register
csbar0  equ     $fa4c      ;chip-select 0 base address register
csor0   equ     $fa4e      ;chip select 0 option register
csbar1  equ     $fa50      ;chip-select 1 base address register
csor1   equ     $fa52      ;chip-select 1 option register
csbar2  equ     $fa54      ;chip-select 2 base address register
csor2   equ     $fa56      ;chip-select 2 option register
csbar3  equ     $fa58      ;chip-select 3 base address register
csor3   equ     $fa5a      ;chip-select 3 option register
csbar4  equ     $fa5c      ;chip-select 4 base address register
csor4   equ     $fa5e      ;chip-select 4 option register
csbar5  equ     $fa60      ;chip-select 5 base address register
csor5   equ     $fa62      ;chip-select 5 option register
csbar6  equ     $fa64      ;chip-select 6 base address register
csor6   equ     $fa66      ;chip-select 6 option register
csbar7  equ     $fa68      ;chip-select 7 base address register
csor7   equ     $fa6a      ;chip-select 7 option register
csbar8  equ     $fa6c      ;chip-select 8 base address register
csor8   equ     $fa6e      ;chip-select 8 option register
csbar9  equ     $fa70      ;chip-select 9 base address register
csor9   equ     $fa72      ;chip-select 9 option register
csbar10 equ     $fa74      ;chip-select 10 base address register
csor10  equ     $fa76      ;chip-select 10 option register


*****  sram module registers  *****

rammcr  equ     $fb00      ;ram module configuration register
ramtst  equ     $fb02      ;ram test register
rambah  equ     $fb04      ;ram base address high register
rambal  equ     $fb06      ;ram base address low register
```

```
*****  qsm address map *****

qmcr    equ     $fc00       ;qsm module configuration register
qtest   equ     $fc02       ;qsm test register
qilr    equ     $fc04       ;qsm interrupt levels register
qivr    equ     $fc05       ;qsm interrupt vector register
sccr0   equ     $fc08       ;sci control register 0
sccr1   equ     $fc0a       ;sci control register 1
scsr    equ     $fc0c       ;sci status register
scdr    equ     $fc0e       ;sci data register
qpdr    equ     $fc15       ;qsm port data register
qpar    equ     $fc16       ;qsm pin assignment register
qddr    equ     $fc17       ;qsm data direction register
spcr0   equ     $fc18       ;qspi control register 0
spcr1   equ     $fc1a       ;qspi control register 1
spcr2   equ     $fc1c       ;qspi control register 2
spcr3   equ     $fc1e       ;qspi control register 3
spsr    equ     $fc1f       ;qspi status register
rr0     equ     $fd00       ;spi rec.ram 0
rr1     equ     $fd02       ;spi rec.ram 1
rr2     equ     $fd04       ;spi rec.ram 2
rr3     equ     $fd06       ;spi rec.ram 3
rr4     equ     $fd08       ;spi rec.ram 4
rr5     equ     $fd0a       ;spi rec.ram 5
rr6     equ     $fd0c       ;spi rec.ram 6
rr7     equ     $fd0e       ;spi rec.ram 7
rr8     equ     $fd00       ;spi rec.ram 8
rr9     equ     $fd02       ;spi rec.ram 9
rra     equ     $fd04       ;spi rec.ram a
rrb     equ     $fd06       ;spi rec.ram b
rrc     equ     $fd08       ;spi rec.ram c
rrd     equ     $fd0a       ;spi rec.ram d
rre     equ     $fd0c       ;spi rec.ram e
rrf     equ     $fd0e       ;spi rec.ram f
tr0     equ     $fd20       ;spi txd.ram 0
tr1     equ     $fd22       ;spi txd.ram 1
tr2     equ     $fd24       ;spi txd.ram 2
tr3     equ     $fd26       ;spi txd.ram 3
tr4     equ     $fd28       ;spi txd.ram 4
tr5     equ     $fd2a       ;spi txd.ram 5
tr6     equ     $fd2c       ;spi txd.ram 6
tr7     equ     $fd2e       ;spi txd.ram 7
tr8     equ     $fd30       ;spi txd.ram 8
tr9     equ     $fd32       ;spi txd.ram 9
tra     equ     $fd34       ;spi txd.ram a
trb     equ     $fd36       ;spi txd.ram b
trc     equ     $fd38       ;spi txd.ram c
trd     equ     $fd3a       ;spi txd.ram d
tre     equ     $fd3c       ;spi txd.ram e
```

```
trf     equ     $fd3e       ;spi txd.ram f
cr0     equ     $fd40       ;spi cmd.ram 0
cr1     equ     $fd41       ;spi cmd.ram 1
cr2     equ     $fd42       ;spi cmd.ram 2
cr3     equ     $fd43       ;spi cmd.ram 3
cr4     equ     $fd44       ;spi cmd.ram 4
cr5     equ     $fd45       ;spi cmd.ram 5
cr6     equ     $fd46       ;spi cmd.ram 6
cr7     equ     $fd47       ;spi cmd.ram 7
cr8     equ     $fd48       ;spi cmd.ram 8
cr9     equ     $fd49       ;spi cmd.ram 9
cra     equ     $fd4a       ;spi cmd.ram a
crb     equ     $fd4b       ;spi cmd.ram b
crc     equ     $fd4c       ;spi cmd.ram c
crd     equ     $fd4d       ;spi cmd.ram d
cre     equ     $fd4e       ;spi cmd.ram e
crf     equ     $fd4f       ;spi cmd.ram f


*****  gpt module registers  *****

gptmcr  equ     $f900       ;gpt module configuration register
gptmtr  equ     $f902       ;gpt module test register (reserved)
gpticr  equ     $f904       ;gpt interrupt configuration register
gptpddr equ     $f906       ;parallel data direction register
gptpdr  equ     $f907       ;parallel data register

hea     equ  $01
heb     equ  $02
hec     equ  $04
; pgp3 not used
heapl   equ  $10
hebpl   equ  $20
hecpl   equ  $40

oc1m    equ     $f908       ;oc1 action mask register
oc1d    equ     $f909       ;oc1 action data register
tcnt    equ     $f90a       ;timer counter register
pactl   equ     $f90c       ;pulse accumulator control register
pacnt   equ     $f90d       ;pulse accumulator counter
tic1    equ     $f90e       ;input capture register 1
tic2    equ     $f910       ;input capture register 2
tic3    equ     $f912       ;input capture register 3
toc1    equ     $f914       ;output compare register 1
toc2    equ     $f916       ;output compare register 2
toc3    equ     $f918       ;output compare register 3
toc4    equ     $f91a       ;output compare register 4
ti4o5   equ     $f91c       ;input capture 4 or output compare 5
tctl1   equ     $f91e       ;timer control register 1
tctl2   equ     $f91f       ;timer control register 2
tmsk1   equ     $f920       ;timer interrupt mask register 1
```

```
tmsk2   equ     $f921       ;timer interrupt mask register 2
tflg1   equ     $f922       ;timer interrupt flag register 1
tflg2   equ     $f923       ;timer interrupt flag register 2
cforc   equ     $f924       ;compare force register
pwmc    equ     $f925       ;pwm control register
pwma    equ     $f926       ;pwm register a
pwmb    equ     $f927       ;pwm register b
pwmregs equ     pwma        ; so that word storage can be done
pwmcnt  equ     $f928       ;pwm counter register
pwmbufa equ     $f92a       ;pwm buffer register a
pwmbufb equ     $f92b       ;pwm buffer register b
prescl  equ     $f92c       ;gpt prescaler


*****  adc module registers  *****

adcmcr  equ     $f700       ;adc module configuration register
adtest  equ     $f702       ;adc test register
adcpdr  equ     $f706       ;adc port data register
adctl0  equ     $f70a       ;a/d control register 0
adctl1  equ     $f70c       ;a/d control register 1
adstat  equ     $f70e       ;adc status register
adstatccf equ   adstat+1    ;adc conversion complete flags
iph_f   equ     $01         ; phase current flag
ilb_f   equ     $02         ; boost inductor current flag
vbst_f  equ     $04         ; bus voltage flag
vbus_f  equ     $08         ; boost voltage flag
torq_f   equ     $10         ; torque command flag
brk_f   equ     $20         ; brake command flag
wtemp_f equ     $40         ; winding temperature flag
etemp_f equ     $80         ; endturn temperature flag
rjurr0  equ     $f710       ;right justified unsigned result register 0
rjurr1  equ     $f712       ;right justified unsigned result register 1
rjurr2  equ     $f714       ;right justified unsigned result register 2
rjurr3  equ     $f716       ;right justified unsigned result register 3
rjurr4  equ     $f718       ;right justified unsigned result register 4
rjurr5  equ     $f71a       ;right justified unsigned result register 5
rjurr6  equ     $f71c       ;right justified unsigned result register 6
rjurr7  equ     $f71e       ;right justified unsigned result register 7
ljsrr0  equ     $f720       ;left justified signed result register 0
ljsrr1  equ     $f722       ;left justified signed result register 1
ljsrr2  equ     $f724       ;left justified signed result register 2
ljsrr3  equ     $f726       ;left justified signed result register 3
ljsrr4  equ     $f728       ;left justified signed result register 4
ljsrr5  equ     $f72a       ;left justified signed result register 5
ljsrr6  equ     $f72c       ;left justified signed result register 6
ljsrr7  equ     $f72e       ;left justified signed result register 7
ljurr0  equ     $f730       ;left justified unsigned result register 0
ljurr1  equ     $f732       ;left justified unsigned result register 1
ljurr2  equ     $f734       ;left justified unsigned result register 2
ljurr3  equ     $f736       ;left justified unsigned result register 3
```

```
ljurr4  equ     $f738       ;left justified unsigned result register 4
ljurr5  equ     $f73a       ;left justified unsigned result register 5
ljurr6  equ     $f73c       ;left justified unsigned result register 6
ljurr7  equ     $f73e       ;left justified unsigned result register 7

*****  (external) lcd registers  *****
instr_reg  equ     $f800       ;lcd instruction register
data_reg  equ     $f804       ;lcd data register

*********************************************************************
*   Title : ORG00008
*   Description : This file initializes the interrupt/
*                 exception vectors ($0008 - $01fe).
*                 If an interrupt occurs requiring the use of
*                 any of these vectors, program flow will
*                 continue at the label "bdm" which must be
*                 added by the programmer to his/her code to
*                 put the program into background debug mode
*                 or some other appropriate routine.
*
*********************************************************************

        org $0008       ;put the following code in memory
                        ;starting at address $0008 of the map
                        ;(after the reset vector).
                        ;there is a total of 252 of these
                        ;"dw bdm" lines
                        ;vector number (in base 10)
                        ;and vector description

        dw  bdm     ;4    breakpoint (bkpt)
        dw  bdm     ;5    bus error (berr)
        dw  bdm     ;6    software interrupt (swi)
        dw  bdm     ;7    illegal instruction
        dw  bdm     ;8    divide by zero
        dw  bdm     ;9    (unassigned reserved)
        dw  bdm     ;10   (unassigned reserved)
        dw  bdm     ;11   (unassigned reserved)
        dw  bdm     ;12   (unassigned reserved)
        dw  bdm     ;13   (unassigned reserved)
        dw  bdm     ;14   (unassigned reserved)
        dw  bdm     ;15   uninitialized interrupt
        dw  bdm     ;16   (unassigned reserved)
        dw  bdm     ;17   level 1 interrupt autovector
        dw  bdm     ;18   level 2 interrupt autovector
        dw  bdm     ;19   level 3 interrupt autovector
        dw  bdm     ;20   level 4 interrupt autovector
        dw  bdm     ;21   level 5 interrupt autovector
        dw  bdm     ;22   level 6 interrupt autovector
        dw  bdm     ;23   level 7 interrupt autovector
        dw  bdm     ;24   spurious interrupt
```

```
dw  bdm     ;25   (unassigned reserved)
dw  bdm     ;26   (unassigned reserved)
dw  bdm     ;27   (unassigned reserved)
dw  bdm     ;28   (unassigned reserved)
dw  bdm     ;29   (unassigned reserved)
dw  bdm     ;30   (unassigned reserved)
dw  bdm     ;31   (unassigned reserved)
dw  bdm     ;32   (unassigned reserved)
dw  bdm     ;33   (unassigned reserved)
dw  bdm     ;34   (unassigned reserved)
dw  bdm     ;35   (unassigned reserved)
dw  bdm     ;36   (unassigned reserved)
dw  bdm     ;37   (unassigned reserved)
dw  bdm     ;38   (unassigned reserved)
dw  bdm     ;39   (unassigned reserved)
dw  bdm     ;40   (unassigned reserved)
dw  bdm     ;41   (unassigned reserved)
dw  bdm     ;42   (unassigned reserved)
dw  bdm     ;43   (unassigned reserved)
dw  bdm     ;44   (unassigned reserved)
dw  bdm     ;45   (unassigned reserved)
dw  bdm     ;46   (unassigned reserved)
dw  bdm     ;47   (unassigned reserved)
dw  bdm     ;48   (unassigned reserved)
dw  bdm     ;49   (unassigned reserved)
dw  bdm     ;50   (unassigned reserved)
dw  bdm     ;51   (unassigned reserved)
dw  bdm     ;52   (unassigned reserved)
dw  bdm     ;53   (unassigned reserved)
dw  bdm     ;54   (unassigned reserved)
dw  bdm     ;55   (unassigned reserved)
dw  bdm     ;56   user defined interrupt vector 1
dw  bdm     ;57   user defined interrupt vector 2
dw  bdm     ;58   user defined interrupt vector 3
dw  bdm     ;59   user defined interrupt vector 4
dw  bdm     ;60   user defined interrupt vector 5
dw  bdm     ;61   user defined interrupt vector 6
dw  bdm     ;62   user defined interrupt vector 7
dw  bdm     ;63   user defined interrupt vector 8
dw  bdm     ;64   user defined interrupt vector 9
dw  bdm     ;65   user defined interrupt vector 10
dw  bdm     ;66   user defined interrupt vector 11
dw  bdm     ;67   user defined interrupt vector 12
dw  bdm     ;68   user defined interrupt vector 13
dw  bdm     ;69   user defined interrupt vector 14
dw  bdm     ;70   user defined interrupt vector 15
dw  bdm     ;71   user defined interrupt vector 16
dw  bdm     ;72   user defined interrupt vector 17
dw  bdm     ;73   user defined interrupt vector 18
dw  bdm     ;74   user defined interrupt vector 19
dw  bdm     ;75   user defined interrupt vector 20
```

```
dw  bdm     ;76   user defined interrupt vector 21
dw  bdm     ;77   user defined interrupt vector 22
dw  bdm     ;78   user defined interrupt vector 23
dw  bdm     ;79   user defined interrupt vector 24
dw  bdm     ;80   user defined interrupt vector 25
dw  bdm     ;81   user defined interrupt vector 26
dw  bdm     ;82   user defined interrupt vector 27
dw  bdm     ;83   user defined interrupt vector 28
dw  bdm     ;84   user defined interrupt vector 29
dw  bdm     ;85   user defined interrupt vector 30
dw  bdm     ;86   user defined interrupt vector 31
dw  bdm     ;87   user defined interrupt vector 32
dw  bdm     ;88   user defined interrupt vector 33
dw  bdm     ;89   user defined interrupt vector 34
dw  bdm     ;90   user defined interrupt vector 35
dw  bdm     ;91   user defined interrupt vector 36
dw  bdm     ;92   user defined interrupt vector 37
dw  bdm     ;93   user defined interrupt vector 38
dw  bdm     ;94   user defined interrupt vector 39
dw  bdm     ;95   user defined interrupt vector 40
dw  bdm     ;96   user defined interrupt vector 41
dw  bdm     ;97   user defined interrupt vector 42
dw  bdm     ;98   user defined interrupt vector 43
dw  bdm     ;99   user defined interrupt vector 44
dw  bdm     ;100  user defined interrupt vector 45
dw  bdm     ;101  user defined interrupt vector 46
dw  bdm     ;102  user defined interrupt vector 47
dw  bdm     ;103  user defined interrupt vector 48
dw  bdm     ;104  user defined interrupt vector 49
dw  bdm     ;105  user defined interrupt vector 50
dw  bdm     ;106  user defined interrupt vector 51
dw  bdm     ;107  user defined interrupt vector 52
dw  bdm     ;108  user defined interrupt vector 53
dw  bdm     ;109  user defined interrupt vector 54
dw  bdm     ;100  user defined interrupt vector 55
dw  bdm     ;111  user defined interrupt vector 56
dw  bdm     ;112  user defined interrupt vector 57
dw  bdm     ;113  user defined interrupt vector 58
dw  bdm     ;114  user defined interrupt vector 59
dw  bdm     ;115  user defined interrupt vector 60
dw  bdm     ;116  user defined interrupt vector 61
dw  bdm     ;117  user defined interrupt vector 62
dw  bdm     ;118  user defined interrupt vector 63
dw  bdm     ;119  user defined interrupt vector 64
dw  bdm     ;120  user defined interrupt vector 65
dw  bdm     ;121  user defined interrupt vector 66
dw  bdm     ;122  user defined interrupt vector 67
dw  bdm     ;123  user defined interrupt vector 68
dw  bdm     ;124  user defined interrupt vector 69
dw  bdm     ;125  user defined interrupt vector 70
dw  bdm     ;126  user defined interrupt vector 71
```

```
dw  bdm     ;127  user defined interrupt vector 72
dw  bdm     ;128  user defined interrupt vector 73
dw  bdm     ;129  user defined interrupt vector 74
dw  bdm     ;130  user defined interrupt vector 75
dw  bdm     ;131  user defined interrupt vector 76
dw  bdm     ;132  user defined interrupt vector 77
dw  bdm     ;133  user defined interrupt vector 78
dw  bdm     ;134  user defined interrupt vector 79
dw  bdm     ;135  user defined interrupt vector 80
dw  bdm     ;136  user defined interrupt vector 81
dw  bdm     ;137  user defined interrupt vector 82
dw  bdm     ;138  user defined interrupt vector 83
dw  bdm     ;139  user defined interrupt vector 84
dw  bdm     ;140  user defined interrupt vector 85
dw  bdm     ;141  user defined interrupt vector 86
dw  bdm     ;142  user defined interrupt vector 87
dw  bdm     ;143  user defined interrupt vector 88
dw  bdm     ;144  user defined interrupt vector 89
dw  bdm     ;145  user defined interrupt vector 90
dw  bdm     ;146  user defined interrupt vector 91
dw  bdm     ;147  user defined interrupt vector 92
dw  bdm     ;148  user defined interrupt vector 93
dw  bdm     ;149  user defined interrupt vector 94
dw  bdm     ;150  user defined interrupt vector 95
dw  bdm     ;151  user defined interrupt vector 96
dw  bdm     ;152  user defined interrupt vector 97
dw  bdm     ;153  user defined interrupt vector 98
dw  bdm     ;154  user defined interrupt vector 99
dw  bdm     ;155  user defined interrupt vector 100
dw  bdm     ;156  user defined interrupt vector 101
dw  bdm     ;157  user defined interrupt vector 102
dw  bdm     ;158  user defined interrupt vector 103
dw  bdm     ;159  user defined interrupt vector 104
dw  bdm     ;160  user defined interrupt vector 105
dw  bdm     ;161  user defined interrupt vector 106
dw  bdm     ;162  user defined interrupt vector 107
dw  bdm     ;163  user defined interrupt vector 108
dw  bdm     ;164  user defined interrupt vector 109
dw  bdm     ;165  user defined interrupt vector 110
dw  bdm     ;166  user defined interrupt vector 111
dw  bdm     ;167  user defined interrupt vector 112
dw  bdm     ;168  user defined interrupt vector 113
dw  bdm     ;169  user defined interrupt vector 114
dw  bdm     ;170  user defined interrupt vector 115
dw  bdm     ;171  user defined interrupt vector 116
dw  bdm     ;172  user defined interrupt vector 117
dw  bdm     ;173  user defined interrupt vector 118
dw  bdm     ;174  user defined interrupt vector 119
dw  bdm     ;175  user defined interrupt vector 120
dw  bdm     ;176  user defined interrupt vector 121
dw  bdm     ;177  user defined interrupt vector 122
```

```
dw  bdm     ;178  user defined interrupt vector 123
dw  bdm     ;179  user defined interrupt vector 124
dw  bdm     ;180  user defined interrupt vector 125
dw  bdm     ;181  user defined interrupt vector 126
dw  bdm     ;182  user defined interrupt vector 127
dw  bdm     ;183  user defined interrupt vector 128
dw  bdm     ;184  user defined interrupt vector 129
dw  bdm     ;185  user defined interrupt vector 130
dw  bdm     ;186  user defined interrupt vector 131
dw  bdm     ;187  user defined interrupt vector 132
dw  bdm     ;188  user defined interrupt vector 133
dw  bdm     ;189  user defined interrupt vector 134
dw  bdm     ;190  user defined interrupt vector 135
dw  bdm     ;191  user defined interrupt vector 136
dw  bdm     ;192  user defined interrupt vector 137
dw  bdm     ;193  user defined interrupt vector 138
dw  bdm     ;194  user defined interrupt vector 139
dw  bdm     ;195  user defined interrupt vector 140
dw  bdm     ;196  user defined interrupt vector 141
dw  bdm     ;197  user defined interrupt vector 142
dw  bdm     ;198  user defined interrupt vector 143
dw  bdm     ;199  user defined interrupt vector 144
dw  bdm     ;200  user defined interrupt vector 145
dw  bdm     ;201  user defined interrupt vector 146
dw  bdm     ;202  user defined interrupt vector 147
dw  bdm     ;203  user defined interrupt vector 148
dw  bdm     ;204  user defined interrupt vector 149
dw  bdm     ;205  user defined interrupt vector 150
dw  bdm     ;206  user defined interrupt vector 151
dw  bdm     ;207  user defined interrupt vector 152
dw  bdm     ;208  user defined interrupt vector 153
dw  bdm     ;209  user defined interrupt vector 154
dw  bdm     ;210  user defined interrupt vector 155
dw  bdm     ;211  user defined interrupt vector 156
dw  bdm     ;212  user defined interrupt vector 157
dw  bdm     ;213  user defined interrupt vector 158
dw  bdm     ;214  user defined interrupt vector 159
dw  bdm     ;215  user defined interrupt vector 160
dw  bdm     ;216  user defined interrupt vector 161
dw  bdm     ;217  user defined interrupt vector 162
dw  bdm     ;218  user defined interrupt vector 163
dw  bdm     ;219  user defined interrupt vector 164
dw  bdm     ;220  user defined interrupt vector 165
dw  bdm     ;221  user defined interrupt vector 166
dw  bdm     ;222  user defined interrupt vector 167
dw  bdm     ;223  user defined interrupt vector 168
dw  bdm     ;224  user defined interrupt vector 169
dw  bdm     ;225  user defined interrupt vector 170
dw  bdm     ;226  user defined interrupt vector 171
dw  bdm     ;227  user defined interrupt vector 172
dw  bdm     ;228  user defined interrupt vector 173
```

```
        dw  bdm     ;229  user defined interrupt vector 174
        dw  bdm     ;230  user defined interrupt vector 175
        dw  bdm     ;231  user defined interrupt vector 176
        dw  bdm     ;232  user defined interrupt vector 177
        dw  bdm     ;233  user defined interrupt vector 178
        dw  bdm     ;234  user defined interrupt vector 179
        dw  bdm     ;235  user defined interrupt vector 180
        dw  bdm     ;236  user defined interrupt vector 181
        dw  bdm     ;237  user defined interrupt vector 182
        dw  bdm     ;238  user defined interrupt vector 183
        dw  bdm     ;239  user defined interrupt vector 184
        dw  bdm     ;240  user defined interrupt vector 185
        dw  bdm     ;241  user defined interrupt vector 186
        dw  bdm     ;242  user defined interrupt vector 187
        dw  bdm     ;243  user defined interrupt vector 188
        dw  bdm     ;244  user defined interrupt vector 189
        dw  bdm     ;245  user defined interrupt vector 190
        dw  bdm     ;246  user defined interrupt vector 191
        dw  bdm     ;247  user defined interrupt vector 192
        dw  bdm     ;248  user defined interrupt vector 193
        dw  bdm     ;249  user defined interrupt vector 194
        dw  bdm     ;250  user defined interrupt vector 195
        dw  bdm     ;251  user defined interrupt vector 196
        dw  bdm     ;252  user defined interrupt vector 197
        dw  bdm     ;253  user defined interrupt vector 198
        dw  bdm     ;254  user defined interrupt vector 199
        dw  bdm     ;255  user defined interrupt vector 200

*********************************************************************
*   This is the end of the org00008.asm file.
*
*       Title : InitVec.ASM
*       Description : This file is included to set up the reset
*                     vector ($00000 - $00006), and the GPT module
*                     IC1 interrupt vector ($0082,$0083)
*
*********************************************************************

initvec:  org    $0000     ; put the following reset vector information
                           ;at address $00000 of the memory map
          dw   $00f0        ; zk=0, sk=f, pk=0
          dw   $0200        ; pc=200 -- initial program counter
          dw   $f3fe        ; sp=f3fe -- initial stack pointer
          dw   $0000        ; iz=0 -- direct page pointer

         org    $000c
swi_vec: dw   oc1int       ;

         org    $0080
tof_vec: dw   tofint       ; jump vector for tof interrupt handler
ic1_vec: dw   ic1int       ; jump vector for ic1 interrupt handler
```

```
ic2_vec: dw   ic2int      ; jump vector for ic2 interrupt handler
ic3_vec: dw   ic3int      ; jump vector for ic3 interrupt handler
oc1_vec: dw   oc1int      ; jump vector for oc1 interrupt handler
oc2_vec: dw   oc2int      ; no interrupt for oc2
oc3_vec: dw   oc3int      ; no interrupt for oc3
oc4_vec: dw   oc4int      ; no interrupt for oc4
ic4_oc5_vec: dw bdm       ; no interrupt for ic4/oc4
tof_dvec: dw  bdm         ; no interrupt for tof here since it
                          ;has been promoted
paovf_vec: dw bdm         ; no interrupt for pulse accumulator overflow
paif_vec: dw bdm          ; no interrupt for pulse accumulator input flag
pit_vec:  dw pitint       ; jump vector for periodic interrupt handler


*************************************************************************
*       Title : initsys
*       Description : initialize & configure system including
*                     the software watchdog and system clock.
*************************************************************************

initsys:                  ; give initial values for extension registers
                          ;and initialize system clock and cop

        ldab   #$0f
        tbek              ; point ek to bank f for register access
        tbyk              ; point yk to bank f
        ldab   #$00
        tbxk              ; point xk to bank 0
        ldab   #$01
        tbzk              ; point zk to bank 1

; ldd    #$00cf    ; make imb available to cpu
; std    simmcr    ; (for some reason this statement crashes the debugger)
        bclr    sypcr,$80  ; turn cop (software watchdog) off,
                           ; since cop is on after reset
        ldaa   #$7f        ; w=0, x=1, y=111111
        staa   syncr       ; set system clock to 16.78 mhz
        ldd    #$0003      ; at reset, the csboot block size is 512k.
        std    csbarbt     ; this line sets the block size to 64k since
                           ; that is what physically comes with the evb16
        ldd    #$0103
        std    csbar0      ; set up 64k ram in page 1 of address space
        std    csbar1
        std    csbar2
        ldd    #$fff8
        std    csbar3      ; set up 2k block for external duart
                           ; (lcd uses first 2 bytes of this block)

        ldd    #$7830      ; no wait states for the pseudo-rom
        std    csorbt
        ldd    #$5030
```

```
        std     csor0           ; cs0 -> upper byte, write only
        ldd     #$3030
        std     csor1           ; cs1 -> lower byte, write only
        ldd     #$7830
        std     csor2           ; cs2 -> both bytes, read and write
;        ldd    #$38f0
;        std    csor3            ; cs3 -> 3 wait states, read and write
        ldd     #$3b70          ;
        std     csor3    ; cs3 -> lower byte, read and write, 13 wait states

        ldd     #$02ff          ; csboot chip select for 16-bit port
                                ; evb board also requires cs0,cs1 & cs2
                                ; to be configured as chip selects
                                ; cs3 is chip select for lcd (8-bit port)
                                ; addr23/cs10 is set for eclk output
        std     cspar0          ;
        ldd     #$0000          ;
        std     portc           ; make the pins on portc that will be
                                ; configured as output ports low
        ldd     #$0000          ; pc1,pc2,pc3,pc4,pc5,pc6,pc7 configured
                                ; as output ports instead of chip selects
        std     cspar1          ;
        bclr    pepar,#$ff      ; configure porte as i/o port
        bset    porte0,#$ff     ;
        bset    ddre,#$ef       ; configure porte as i/o output port
                                ; except pe4 (the negate phase bit)

        bclr    pfpar,#$ff      ; configure portf as i/o port
        bclr    portf,#$ff      ; make the pins on portf that will be
                                ; configured as outputs low
        bclr    ddrf,#$ff       ; configure portf as input port
        ldd     #$064c          ; periodic interrupt request level 6
        std     picr            ; periodic interrupt vector is $0c
        ldd     #$0002          ; periodic timer clock not prescaled (122 us per count)
        std     pitr            ; periodic timer modulus is 2 (i.e. 4.098 khz)


*************************************************************************
*       Title : initram
*       Description : initialize the hc16's 1k internal sram
*                     (put sram in memory map at $fff000 to fff3ff)
*                     and set the stack inside it.
*************************************************************************

initram:                        ;initialize internal sram and stack
        ldd     #$00ff
        std     rambah          ; store high ram array, bank f
        ldd     #$f000
        std     rambal          ; store low ram array
        clr     rammcr          ; enable ram
```

```
        ldab    #$0f
        tbsk                    ; set sk to bank f for system stack
        lds     #$f3fe          ; put sp at top of 1k internal sram

        ldx     #$f000          ; initialize ram contents...
        ldy     #$f000
ramloop:ldd     0,x
        std     0,y
        aix     #2
        aiy     #2
        cpx     #$f3fe
        bne     ramloop

*************************************************************************
*   Title : InitADC.ASM
*   Description :  Initializes the A/D module for 10-bit conversions
*                  with a 9 uSecond conversion time.
*
*************************************************************************

InitADC:
        LDD     #$0000
        STD     ADCMCR          ; enable A/D module
        LDD     #$0083
        STD     ADCTL0          ; configure A/D for 10-bit, 9 uSec conversions
                                ; write to ADCTL1 to start a conversion


*************************************************************************
*       Title : InitQSM.ASM
*       Description : Initializes the Queued Serial Module for operation
*                     with the MAX537 12-bit serial DAC.
*************************************************************************

InitQSM:
*        ldaa   #$80             ; qsm disabled
*        staa   qmcr             ; don't set iarb
        ldaa    #$0f            ;
        staa    qilr            ; disable interrupts
        ldaa    #$08
        staa    qpdr            ; sck inactive low, pcs0 inactive high
        ldaa    #$0a
        staa    qpar            ; assign pcs0 & mosi pins to qsp module
        ldaa    #$ff
        staa    qddr            ; configure qspi pins as outputs
        ldd     #$8002
        std     spcr0           ; master, cpol=cpha=0, 4.19 mhz, 16-bit transfer
        ldd     #$0000
        std     spcr2           ; newqp=0, endqp=0; 1 word sent
;fill command ram:
        ldaa    #$40
```

```
        staa   cr0        ; cont=0, bitse=1, pcs2,1,0 = 000, assert cs0
                           ; don't use spcr1 delay to sck, no delay between
                           ; (16 bit transfer to dac1)
        staa   cr1         ;
        staa   cr2
        staa   cr3         ; only 4 command registers may be used
;
;fill transmit ram (addresses and zeroes):
        ldd    #$1000
        std    boostdac    ; load dac1 with zeros
        ldd    #$5000      ;
        staa   buckdac     ; load dac2 with zeros
        ldd    #$9000      ;
        staa   tr2         ; load dac3 with zeros
        ldd    #$d000      ;
        staa   tr3         ; load dac4 with zeros

boostdac  equ     tr0      ; -> boost current control dac (12 bits)
buckdac   equ     tr1      ; -> phase current control dac (12 bits)
torquedac equ     tr2      ; -> set torque echo dac (12 bits)
brakedac  equ     tr3      ; -> set brake echo dac (12 bits)

*************************************************************************
*       Title : InitGPT.ASM
*       Description :  configure input capture and output compares
*                       for phase locking hall effect sensor signals.
*                      and interrupt processing
*
*************************************************************************
InitGPT:
        ldaa   #$00        ;
        staa   gptpdr      ; write low to gpt output port
        ldaa   #$78        ;
        staa   gptpddr     ; make output compare pins outputs

        ldd    #$0081
        std    gptmcr      ;iarb=1 for gpt module
        ldd    #$9240
        std    gpticr      ;int. request level =2, int. vector base =40h
                           ;(ic1 vector is 41h, or address 82 & 83h)
                           ;oc1 is promoted to highest priority
                           ;(oc1 vector address is 80 & 81)
input_capture:
; input capture channel 4 function enabled.

    ldaa  pactl
    anda  #$fb
    oraa  #$04
    staa  pactl
; input capture channel 1 both edges.
; input capture channel 2 both edges.
```

```
; input capture channel 3 both edges.
; input capture channel 4 is disable.
    ldaa  #$3f
    staa  tctl2
; input capture channel 1 interrupt enable.
; input capture channel 2 interrupt enable.
; input capture channel 3 interrupt enable.
; input capture channel 4 interrupt disable.
    ldaa  tmsk1
    anda  #$78
    oraa  #$07
    staa  tmsk1
; system clock divide by 256.
; timer overflow interrupt is enabled.
    ldaa  tmsk2
    anda  #$f8
    oraa  #$86
    staa  tmsk2
output_compare:
; output compare 5 function enabled.
    ldaa  pactl
    anda  #$fb
    staa  pactl
; oc2..0c4 connected to timer logic
    ldaa  #$3f
    staa  tctl1
; all output compare interrupts are disabled
    ldaa  tmsk1
    anda  #$07
    oraa  #$70
    staa  tmsk1
; reset oc1m7.
    ldaa  #$00
    staa  oc1m
; all force compare bits are off.
    ldaa  cforc
    anda  #$07
    staa  cforc
; timer output compare register 5 is set to $ffff
    ldd   #$ffff
    std   ti4o5
; timer output compare resister 1 is set to $0f
    ldd   #$0f
    std   toc1
pwm:
; disable discrete output from f1a bit, driven out on the pwma pin.
; disable discrete output from f1b bit, driven out on the pwmb pin.
    ldaa  cforc
    anda  #$fc
    staa  cforc
; system clock divide by 4
```

```
; normal pwm operation on pwma.
; the higher speed of pwma is selected
; normal pwm operation on pwmb.
; the higher speed of pwmb is selected
    ldaa  #$10
    staa  pwmc
; duty cycle for channel a is set to 5%
    ldaa  #$0d
    staa  pwma
; duty cycle for channel b is set to 5%
    ldaa  #$0d
    staa  pwmb
pam_gated:
; pulse accumulator overflow interrupts disabled.
; pulse accumulator interrupts disabled.
    ldaa  tmsk2
    anda  #$af
    staa  tmsk2
; gated time accumulation mode is set.
; pulse accumulator is enabled.
; a zero on pai inhibits counting.
; system clock divided by 512.
    ldaa  pactl
    anda  #$04
    oraa  #$60
    staa  pactl
; pulse accumulator counter is set to $00
    ldaa  #$00
    staa  pacnt

*****************************************************************
*       File Name : MACROS.ASM
*       Description : This file contains all macros used in this thesis
*       Note : This program is written for the M68HC16Z1EVB.
*****************************************************************

$macro write_boostdac   ; transmit serial data to boostdac (takes
                        ; about 4 us for 1 transmission)
       ldd   #$0000     ; endqp=0, newqp=0
       std   spcr2      ;
       ldd   #$8000     ; start transmission
       std   spcr1      ;
$macroend
$macro write_buckdac    ; transmit serial data to buckdac (takes about
                        ; 4 us for 1 transmission)
       ldd   #$0101     ; endqp=1, newqp=1
       std   spcr2      ;
       ldd   #$8000     ; start transmission
       std   spcr1      ;
$macroend
$macro write_torquedac  ; transmit serial data to torquedac (takes
```

```
                        ; about 4 us for 1 transmission)
        ldd   #$0202    ; endqp=2, newqp=2
        std   spcr2     ;
        ldd   #$8000    ; start transmission
        std   spcr1     ;
$macroend
$macro write_brakedac   ; transmit serial data to brakedac (takes
                        ; about 4 us for 1 transmission)
        ldd   #$0303    ; endqp=3, newqp=3
        std   spcr2     ;
        ldd   #$8000    ; start transmission
        std   spcr1     ;
$macroend
$macro rupdx            ; round result of division up and exchange the
                        ; contents of ix and d
        bcc rdx         ; if no carry, just exchange result
        aix #$01        ; increment the quotient by one
rdx:  xgdx              ; put quotient in d
$macroend
$macro ton_hea
        bset gptpdr,#heapl ; take oc2 pin high
        psha               ;
        ldaa tctl1         ;
        bclr tctl1,#$03    ; disconnect oc_pin from timer
        staa tctl1         ;
        pula
$macroend
$macro toff_hea        ;
        bclr gptpdr,#heapl ; take oc2 pin low
        psha               ;
        ldaa tctl1         ;
        bclr tctl1,#$03    ;  disconnect oc_pin from timer
        staa tctl1         ;
        pula
$macroend                  ;
$macro ton_heb         ;
        bset gptpdr,#hebpl ;  take oc3 pin high
        psha
        ldaa tctl1         ;
        bclr tctl1,#$0c ;  disconnect oc_pin from timer
        staa tctl1
        pula
$macroend
$macro toff_heb        ;  take oc3 pin low
        bclr gptpdr,#hebpl ;
        psha
        ldaa  tctl1
        bclr tctl1,#$0c ;  disconnect oc_pin from timer
        staa tctl1
        pula
$macroend
```

```
$macro ton_hec          ; take oc4 pin high
       bset gptpdr,#hecpl ;
       psha
       ldaa  tctl1
       bclr tctl1,#$30 ;  disconnect oc_pin from timer
       staa  tctl1
       pula
$macroend
$macro toff_hec         ;
       bclr gptpdr,#hecpl ;
       psha
       ldaa tctl1
       bclr tctl1,#$30 ;  disconnect oc_pin from timer
       staa tctl1
       pula
$macroend
$macro ton_buck_led
       bset porte0,#buckled;
$macroend
$macro toff_buck_led
       bclr porte0,#buckled  ;
$macroend
$macro ton_boost_led
       bset porte0,#boostled  ;
$macroend
$macro toff_boost_led
       bclr porte0,#boostled
$macroend
$macro set_init_pin
       bset porte0,#init
$macroend
$macro clr_init_pin
       bclr porte0,#init
$macroend
$macro rdbf_and_address
       ldd       #instr_reg      ; result in accum a, bit7 is busy flag
                                 ; the rest is contents of address counter
$macroend
$macro pushab
       psha
       pshb
$macroend
$macro pushba
       pshb
       psha
$macroend
$macro pullab
       pulb
       pula
$macroend
$macro pullba
```

```
       pula
       pulb
$macroend
$macro toff_gate_drives  ; disable motor drive
       bset portc,#$04 ;
$macroend
$macro ton_gate_drives   ; engage motor drive
       bclr portc,#$04 ;
$macroend
$macro lock_motor        ; lock motor on phase a-b
       bset portc,#$08 ;
$macroend
$macro unlock_motor      ; unlock motor
       bclr portc,#08  ;
$macroend
$macro forward_rotation  ; motor should rotate in the forward direction
       bset portc,#$10  ;
$macroend
$macro reverse_rotation ; motor should rotate in the reverse direction
       bclr portc,#$10   ;
$macroend
$macro motor_mode        ;  motor - as opposed to regenerate
       bset portc,#$20 ;
$macroend
$macro regen_mode        ; regeneration mode
       bclr portc,#$20 ;
$macroend
$macro buck_mode         ; chop battery voltage
       bset portc,#$40  ;
$macroend
$macro boost_mode        ; boost battery voltage
       bclr portc,#$40  ;
$macroend
$macro curr_mode_cont  ; implement current mode control
       ldd  #$0707     ;
       std  pwmregs
       bset portc,#$02  ;
$macroend
$macro duty_cycle_cont  ; implement duty-cycle control
       bclr portc,#$02   ;
$macroend

*****************************************************************
*       Title : InitMOTOR.ASM
*       Description :  Initialize MOTOR DRIVE AND CONTROL SETTINGS
*
*****************************************************************
InitMOTOR:                  ;Initialize MOTOR DRIVE AND CONTROL SETTINGS
        ldaa   gptpdr       ;load the state of the hall effect sensors
        anda   #$07         ;
        asla                ; shift left until bit one becomes bit 5
```

```
        asla                ;
        asla                ;
        asla                ; bit 1 is now bit 5
        staa  gptpdr        ;
        ldaa  tctl1         ;
        bclr  tctl1,#$3f    ; disconnect oc2,oc3&oc4 from timer output
                            ; and output what is in gptpdr
        staa  tctl1         ;
        bclr  flags,#fault  ;
initmot1:
        clr   commcnt      ; clear the torque ripple compensation pointer

        toff_gate_drives    ;
        forward_rotation    ;
        duty_cycle_cont     ;
        motor_mode          ;
        unlock_motor        ;
        buck_mode           ;

*************************************************************************
*       Title : INITKEYPAD
*       Description : Initialize the keypad and store mode settings in
*                     FLAGS
*************************************************************************
INITKEYPAD:               ;* Initialize Keypad
        set_init_pin      ;
        brn initkeypad    ;
        brn initkeypad    ;
        clr_init_pin      ;
        jsr read_keypad   ; store initial keypad setting in flags

*************************************************************************
*       Title : InitLCD.ASM
*       Description :  Initialize the LCD Display
*
*************************************************************************
InitLCD:                  ;Initialize LCD
        ldd     #$ffff    ;
ilcd0:  subd    #$0001    ;
        bne     ilcd0     ;
        ldaa    #$38        ;
        staa    instr_reg     ; function set (8 bit interface)
        ldd     #$ffff    ;
ilcd1:  subd    #$0001    ;
        bne     ilcd1     ;
        ldaa   #38h         ;
        staa   instr_reg    ;
        ldd     #$ffff    ;
ilcd2:  subd    #$0001    ;
        bne     ilcd2     ;
        ldaa   #38h         ;
```

```
        staa    instr_reg       ; repeat function set (8 bit interface)
        jsr     wait_busy_flag ;
        ldaa     #38h           ;
        staa    instr_reg       ; 2 lines, 5x7 font
        jsr     wait_busy_flag ;
        ldaa    #08h            ;
        staa    instr_reg       ; turn display off
        jsr     wait_busy_flag ;
        ldaa    #0eh            ;
        staa    instr_reg       ; display on, cursor on, don't blink
        jsr     wait_busy_flag ;
        ldaa    #01h            ;
        staa    instr_reg       ; clear display and return the cursor home


*************************************************************************
*  File Name : DISPLAY.ASM
*
*  Description : This is the main program.
*                Initializes peripherals
*                Reads buttons and execute button commands
*                Process Hall Effect (Input Capture) and
*                control (Periodic Timer) interrupts.
*       Note : This program is written for the M68HC16Z1EVB.
*************************************************************************

$include "..\equates.asm"   ;table of equates for register addresses
$include "..\init\org00008.asm" ; point all unused interrupts to bdm
$include "..\init\vec.asm"  ;initialize reset and interrupt vectors
        org     $0200       ;start program after interrupt vectors
*****   initialization routines *****
$include "..\init\sys.asm"  ;initially set ek=f, xk=0, yk=f, zk=1
                            ;set sys clock at 16.78 mhz, disable cop
$include "..\init\ram.asm"  ;initialize and turn on sram
                            ;set stack (sk=f, sp=f3fe)
$include "..\init\adc.asm"  ;configure a/d for 10-bit, 9 usec conversion
$include "..\init\qsm.asm"  ;configure qspi to interface with
                            ;power electronics module and display
$include "..\init\gpt.asm"  ;configure ic1 interrupt
****    include macros *****
$include "..\macros\macros.asm" ; lcd macros and other stuff
$include "..\init\motor.asm"  ; motor drive and control settings
$include "..\init\keypad.asm" ; initialize keypad
****    lcd initialization routine  ****
$include "..\init\lcd.asm"  ; initialize lcd
*****   start of user program area  *****
$set  left_justified   ; if this conditional assembly variable is
                       ; set, all numbers on lcd display are
                       ; left-justified.  if not, the numbers will
                       ; be right-justfied, i.e. numbers on lcd may
                       ; have leading spaces
```

```
        jsr clear_display
        jsr cursor_off
        ton_gate_drives
        duty_cycle_cont
        buck_mode
        jsr  offset_null      ; go null all analog current channels
        ldd    #$8000
        tdp                   ; allow interrupts
start:
        jsr carriage_return
        ldaa  #2
        staa  dec_places
        ldd   fil_brake_cmdh
        lde   #!50            ; max pot location is 50% phase advance
        emul
        ldx   #$3ff
        ediv
        xgdx
; brake pot controls phase advance
        std percent_adv

        ldd temp_reg         ;
        lde   #!1000
        emul
        ldx  #!2002
        ediv
        xgdx
        jsr   disnumu
        jsr   message0
        db    ' v   \'
        ldaa  #2
        staa  dec_places
        ldd   fil_brake_cmdh
        lde   #!1000
        emul
        ldx #!2002
        ediv
        xgdx
        jsr   disnumu
        jsr   message0
        db    ' v \'

        jsr   goto_line2
        ldd   fil_torque_cmdh
        lde   #!450
        ldx   #max_const_torque
        emuls
        edivs
        rupdx
        clr   dec_places
```

```
        jsr    disnums
        jsr   message0
        db    ' nm  \'
        ldd   new_torque_cmd
        lde   #!450
        ldx   #max_const_torque
        emul
        ediv
        rupdx
        clr   dec_places
        jsr    disnums
        jsr   message0
        db    ' nm      \'
        jsr   goto_line3
        ldd   dc_bus_volth
        lde   #!400             ; 100 v --> 1ff
        ldx   #$7fe
        emul
        ediv
        rupdx
        clr   dec_places
        jsr   disnums
        jsr   message0
        db    ' v   \'
        ldd   dc_boost_volth
        lde   #!400
        ldx   #$7fe             ; 100 v --> 1ff
        emul
        ediv
        rupdx
        clr   dec_places
        jsr   disnums
        jsr   message0
        db    ' v     \'

        jsr   goto_line4
testb:  ldd   dc_phase_currh
        lde   #!100
        ldx   #$1ff             ; 100 a --> 1ff
        emuls
        edivs
        xgdx
        clr   dec_places
        jsr   disnums
        jsr   message0
        db    ' \'
        ldd   dc_boost_currh
        lde   #!100           ; 100 a --> 1ff
        ldx   #$1ff           ; current multiplied by 2 after a/d
        emuls
        edivs
```

```
        xgdx
        clr dec_places
        jsr   disnums
        jsr   message0
        db    ' \'
        ldd   motor_rpm
        clr   dec_places
        jsr  disnumu
        jsr   message0
        db    ' rpm       \'

        jsr   set_drive_mode
         brclr flags,#fault,mlcont
         jsr  clear_display
         jsr  message0
         db   '   !! fault !!   \'
         jmp  bdm
mlcont:  jmp   start



ic1int:    pshm d,e,x       ; save registers
           brset gptpdr,#$01,ic1_high ; test if ic1 is set since
                                      ;we interrupt on both edges
           jmp  ic1_low     ;
ic1_high:  ton_hea
           ldaa to_count    ; determine if timer has overflowed twice
           clr  to_count    ; reset the timer overflow counter
           cmpa #$01        ;
           blt  ic1_tok     ; timer is ok
           beq  ic1_ckof    ; check overflow
ic1_ovf:   ton_hea          ;
           bset flags,#tof  ; set the timer overflow flag for
                            ;use by the other two hall effect channels
           ldd  #$ffff      ;
           std  new_hea_period ;
           movw tic1,old_tic1 ; store the rising edges
           jmp  ic1_chk_comm ; go do commutation stuff

ic1_ckof:  ldd  tic1        ; check if counter has overrun
           subd old_tic1    ;
           bcc  ic1_ovf     ; counter overrun

ic1_tok:   ldd  tic1        ;
           subd old_tic1    ;
           std  new_hea_period ;
           movw tic1,old_tic1  ; store the rising edges
           bclr flags,#tof  ;
           ldd  motor_rpm     ;
           cpd  #min_pav_rpm  ; minimum rpm above which we do
                              ; phase advance
```

```
          bgt  ic1_phase_adv ; do phase advance
          ldd  hea_periodh    ; period of hall effect a from pll
          jmp  ic1_pav_skip  ; skip phase advance
ic1_phase_adv:
          ldd  hea_periodh  ;
          jsr  calc_pav_deltat ; calculate phase advance delta t
ic1_pav_skip:
          addd tic1        ; adjust tic1 with the amount of phase advance
          std  toc2        ; load toc2 for output compare
          jmp  ic1_chk_comm ;

ic1_low:  toff_hea         ; take hea pin low

ic1_chk_comm:
          lde   tic1        ;
;          jsr  torque_shp_sync ; go sync the torque shaping interrupts

reset_ic1: bclr tflg1,#$01  ;
          pulm d,e,x       ; restore accumulator d,e&x
          rti              ; return from interrrupt


ic2int:   pshm    d,e,x                ; save registers
          brset   gptpdr,#$02,ic2_high ; test if ic2 is set since
                                       ; we interrupt on both edges
          jmp     ic2_low              ;
ic2_high: ton_heb
          brset   flags,#tof,ic2_ovf   ; if timer overflow flag set
                                      ;then turn on the output compare pin
          jmp     ic2_tok              ; timer ok
ic2_ovf:  ton_heb            ; timer overflow, or speed below
                             ;min_oc_rpm so turn on the oc pin
          ldd     #$ffff           ;
          std     new_heb_period   ;
          movw    tic2,old_tic2    ;
          jmp  ic2_chk_comm        ; go do commutation stuff
ic2_tok:  ldd     tic2                ;
          subd    old_tic2            ;
          std     new_heb_period      ;
          movw tic2,old_tic2 ;
          ldd  motor_rpm     ;
          cpd  #min_pav_rpm  ; minimum rpm above which we do
                             ; phase advance
          bgt  ic2_phase_adv ; do phase advance
          ldd  heb_periodh   ; period of hall effect b from pll
          jmp  ic2_pav_skip  ; skip phase advance
ic2_phase_adv:
          ldd  heb_periodh  ;
          jsr  calc_pav_deltat ; calculate phase advance delta t
ic2_pav_skip:
          addd tic2        ; adjust tic2 with the amount of phase advance
```

```
            std  toc3         ; load toc3 for output compare
            jmp ic2_chk_comm ;

ic2_low:    toff_heb          ; take heb pin low

ic2_chk_comm:
            lde  tic2             ;
;            jsr  torque_shp_sync ; go sync the torque shaping interrupts
reset_ic2: bclr tflg1,#$02   ;
            pulm d,e,x        ; restore accumulator d,e&x
            rti               ; return from interrrupt


ic3int:     pshm d,e,x      ; save registers
            brset gptpdr,#$04,ic3_high ; test if ic3 is set since
                                       ;we interrupt on both edges
            jmp  ic3_low    ;
ic3_high:ton_hec
            brset   flags,#tof,ic3_ovf   ; if timer overflow flag set
                                       ;then turn on the output compare pin
            jmp     ic3_tok             ; timer ok
ic3_ovf:    ton_hec             ; timer overflow, or speed below
                                ;min_oc_rpm so turn on the oc pin
            ldd     #$ffff      ;
            std     new_hec_period ;
            movw tic3,old_tic3 ;
            jmp  ic3_chk_comm  ; go do commutation stuff
ic3_tok:    ldd  tic3           ;
            subd old_tic3       ;
            std  new_hec_period ;
            movw tic3,old_tic3 ;
            ldd  motor_rpm      ;
            cpd  #min_pav_rpm   ; minimum rpm above which we do phase
                                ;advance
            bgt  ic3_phase_adv ; do phase advance
            ldd  hec_periodh    ; period of hall effect c from pll
            jmp  ic3_pav_skip   ; skip phase advance
ic3_phase_adv:
            ldd  hec_periodh  ;
            jsr  calc_pav_deltat ; calculate phase advance delta t
ic3_pav_skip:
            addd tic3         ; adjust tic3 with the amount of phase advance
            std  toc4         ; load toc4 for output compare
            jmp ic3_chk_comm ;

ic3_low:    toff_hec          ; take hec pin low

ic3_chk_comm:
            lde  tic3         ; tic3
;            jsr  torque_shp_sync ; go sync the torque shaping interrupts
reset_ic3: bclr tflg1,#$04   ;
```

```
          pulm d,e,x        ; restore accumulator d,e&x
          rti               ; return from interrrupt



oc1int:   rti

          pshm d,e,x,y;
          brset  gptpdr,#$08,clear
          bset  gptpdr,#$08
          jmp   comm1
clear:    bclr  gptpdr,#$08
comm1:    clre              ;
          ldd   heabc_period ;
          ldx   #{maxsteps * !6}   ;
          ediv              ; interrupt #maxsteps times within a
                            ;commutation interval
          rupdx             ; round up result and exchange d and ix
          tst commcnt       ;
          beq   new_comm    ;
          addd  toc1        ; add the time interval till next interrupt
          jmp   sto_next    ;
new_comm: addd  commtime    ; sync to hall effect sensors
          bset  tmsk1,#$08   ; enable oc1 interrupts for torque shaping
sto_next: std   toc1        ; store in toc1 for next output compare
          clra
          ldab  commcnt     ;
          aslb              ; two bytes per entry
          tde
          ldx   #trcomp_tab ; modify comand torque
          ldd   e,x         ; get the percent fraction torque ripple boost
          lde   fil_torque_cmdh  ; get the commanded torque
          asle
          fmuls             ;
          adce  fil_torque_cmdh  ;
          ste  comp_torque_cmd ; this is the compensated torque command
                            ; for this interval
;* diagnostic
          ldy   #buckdac
          jsr   setup_dac
          write_buckdac

          ldaa commcnt      ; advance the current profile counter
          inca
          cmpa #maxsteps     ; check if we have exceeded the limit
          bls  sto_cnt       ; store the count
          movw fil_torque_cmdh,comp_torque_cmd ; if we ever exceed
                            ;this, then don't do
                                    ; any torque shaping
          ldaa #maxsteps     ; if so then fix it at maximum
sto_cnt:  staa commcnt       ;
```

```
oc1_reset: bclr tflg1,#$08   ;
           pulm d,e,x,y        ; restore registers
           rti               ;

oc2int:
;          pshm d
;          ldd    hea_periodh
;          addd   old_tic1
;          std    toc2
          bclr  tflg1,#$10   ;
;          pulm  d
          rti

oc3int:
;          pshm d
;          ldd   heb_periodh
;          addd   old_tic2
;          std   toc3
          bclr  tflg1,#$20   ;
;          pulm  d
          rti

oc4int:
;      pshm d
;          ldd   hec_periodh
;          addd   old_tic3
;          std   toc4
          bclr  tflg1,#$40   ;
;          pulm  d
          rti
tofint:    pshm  d          ;
           ldaa   to_count  ;
           inca
           staa   to_count
           cmpa   #$02      ; permissible maximum count
           blt    tof_reset ; timer has not overflowed more than
                            ;once so exit
           ldaa  #$02
           staa  to_count
           bset  flags,#tof ;
tof_reset: bclr  tflg2,#$80 ; clear the timer overflow flag
           pulm  d          ;
           rti              ; return from interrpt


;***********************************************
;* modify this routine to sequentially null all
;* three channels.  store a lookup table of commutation
;* pattern in code space with pointer to the appropriate
;* offsets, and use the appropriate offsets in computation
;* whenever needed
```

```
;* disable all interrupts when entering this routine
;*******************************************************
offset_null: pshm d,e,x,y,z ; save registers
           clrd
           std   pwmdata              ;
           std   pwmregs              ;  turn off phases
           jsr   clear_display
           jsr   message0
           db    '  calibration    \'
           jsr   goto_line2
           jsr   message0
           db    ' in progress ... \'
           jsr   goto_line3
           jsr   message0
           db    '.. one moment .. \'
           jsr   goto_line4
           jsr   message0
           db    'nulling phase a\'
           ldaa  portc          ; save the state of portc pins (these
                                ; have been set by initmotor)
           psha                 ;
           ldaa  tctl1          ; save the oc control settings
           psha
           ldaa  gptpdr         ; save the hall effect settings
           psha
           forward_rotation     ;
           clr  pwma
           clr  pwmb            ; make pwm channels quiet
           bclr tctl1,#$3f      ; disconnect output compare pins from timer
check:     bset gptpdr,#heapl ; take oc2 high
           bclr gptpdr,#hebpl ; take oc3 low
           bset gptpdr,#hecpl ; take oc4 high , 101 selects phase a (no
                              ; negation)
           ldy   #iphasea_zerop ; where phase a (non-inverted) offset
                                ; should be stored
           brset porte0,#$10,null_error ; neg_phase signal should be clear
           jsr   null_channel ; go compute channel a offset
           bclr gptpdr,#heapl ;
           bset gptpdr,#hebpl ;
           bclr gptpdr,#hecpl ; 010 selects phase a (negated)
           ldy  #iphasea_zeron; where the phase a (inverted) offset
                              ; should be stored
           brclr porte0,#$10,null_error ; neg_phase signal should be high
           jsr   null_channel ; go compute channel a inverted offset
           jsr   goto_line4
           jsr   message0
           db    'nulling phase b\'
           bset gptpdr,#heapl ; take oc2 high
           bset gptpdr,#hebpl ; take oc3 high
           bclr gptpdr,#hecpl ; take oc4 low , 110 selects phase b
           ldy   #iphaseb_zerop ; where phase b offset should be stored
```

```
            brset porte0,#$10,null_error ; neg_phase signal should be clear
            jsr   null_channel ; go compute channel b offset
            bclr gptpdr,#heapl ; take oc2 low
            bclr gptpdr,#hebpl ; take oc3 low
            bset gptpdr,#hecpl ; take oc4 high , 001 selects phase b
                               ; inverted
            ldy   #iphaseb_zeron ; where phase b offset should be stored
            brclr porte0,#$10,null_error ; neg_phase signal should be set
            jsr   null_channel ; go compute channel b offset
            jsr   goto_line4   ;
            jsr   message0
            db    'nulling phase c\'
            bset gptpdr,#heapl ; take oc2 high
            bclr gptpdr,#hebpl ; take oc3 low
            bclr gptpdr,#hecpl ; take oc4 low , 100 selects phase c
                               ; (negated)
            ldy  #iphasec_zeron ; where phase c negated offset should
                                ; be stored
            brclr porte0,#$10,null_error ; neg_phase signal should be set
            jsr   null_channel ; go compute channel c offset
            bclr gptpdr,#heapl ; take oc2 high
            bset gptpdr,#hebpl ; take oc3 low
            bset gptpdr,#hecpl ; take oc4 low , 011 selects phase c
            ldy  #iphasec_zerop ; where phase c offset should be stored
            brset porte0,#$10,null_error ; neg_phase signal should be clear
            jsr   null_channel ; go compute channel c offset
            pula               ; the hall effect input settings
            staa  gptpdr       ;
            pula               ; the timer control settings
            bclr  tctl1,#$3f   ; disconnect oc2, oc3 & oc4 from timer
                               ; output
            staa  tctl1        ;
            pula
            staa  portc
            jsr   clear_display ;
            pulm  d,e,x,y,z    ; restore the resgisters
            rts
null_error:
            jsr  clear_display
            jsr  message0
            db   '  !! error !!  \'
            jsr  goto_line2
            jsr  message0
            db   ' in commutation\'
            jsr  goto_line3
            jsr  message0
            db   '       pal     \'
            jmp  bdm

null_channel:
            pshm  y          ; save the result pointer
```

```
            ldz   #$0fff      ; output should settle $fff of times
osn0:       ldd   #$0030      ;
            std   adctl1      ; scan 4 channels (an0 - an3) but we are
                              ; only interested in phase current
                              ; and boost inductor current
osn1:       brclr adstatccf,#$01,osn1  ; wait for data
            ldd   rjurr0      ; the phase current
            std   new_phase_curr ;
            lde   #$7d9           ; filter cutoff frequency parameter
            ldy   #dc_phase_currh ;
            jsr   lowpass_filter
osn2:       brclr adstatccf,#$02,osn2  ; wait for data
            ldd   rjurr1      ; the boost inductor current
            std   new_boost_curr ;
            lde   #$7d9          ; filter cutoff frequency parameter
            ldy   #dc_boost_currh ;
            jsr   lowpass_filter  ;
            ldd   dc_phase_currh  ;
            cpd   new_phase_curr  ;
            bne   osn0            ;
            ldd   dc_boost_currh  ;
            cpd   new_boost_curr  ;
            bne   osn0            ;
            aiz   #$-1            ;
            bne   osn0            ;
            ldd   dc_phase_currh  ; the result
            pulm  y               ; the destination pointer
            std   0,y             ; store the result
            movw  dc_boost_currh,ilb_zero ;
            rts

pitint:     pshm  d,e,x,y,z

atod:       ldd #$0030
            std adctl1        ; single conversion on all 8 channels
                              ; do some computations before the the
                              ;atod conversion is done (10 us)
            ldab  gptpdr      ; get the position of the motor from
                              ; hall effect signals
            andb  #$70        ; save only the 0c4..0c2 bits
            stab  temp1       ; temporary store it
            asrb
            asrb
            asrb              ; shift only 3 times because we have
                              ; 2 bytes per entry
            cmpb  #$00
            beq  bad_atod       ; multiplexer error (bail out for now)
            cmpb  #$0e
            beq  bad_atod       ; multiplexer error (bail out for now)
            ldaa  gptpdr      ;
            anda  #$70        ; save only the oc4..oc2 bits
```

```
            cmpa  temp1
            bne   bad_atod    ; commutation occured so bail out
            bset  flags,#good_atod  ; a/d value is good
            clra
            brclr portc,#forw,atod1 ;
            orab  #$10        ; if forw bit is set then set the
                              ; msnibble (remember x2)
atod1:      tde
            ldx   #pho_adj_tab ; phase offset adjust table
            ldd   e,x          ; get the pointer to the offset
            xgdy               ; the pointer should point to data space
wait_atod: brclr adstatccf,#$01,wait_atod ; if phase current
                              ; conversion not done, then wait
            ldd   rjurr0       ; get the a/d phase current
;            brclr flags,#good_atod,atod2 ; if value not good then don't
                              ;store
            subd  0,y          ; subtract the offset
            std   new_phase_curr ; this is the new phase current
atod2:      bset  flags,#good_atod ; set flag for the case of two bad a/d
                                  ;in a row
            brset portc,#inh,no_loop ; if for any reason we have
                                 ;disengaged the drive disengage control loop
            ldd   dc_boost_volth   ;
            lbeq   no_input       ;  if bus voltage is zero then do nothing
             jmp   buck_loop
bad_atod:  brclr flags,#good_atod,atod2 ; exit a/d conversion
                                  ;if we've been here before
            bclr  flags,#good_atod   ; set a flag to indicate one
                                  ;unsucessful a/d
            jmp   atod               ; go try one more conversion
no_loop:
          clrw  buckm_interrl
          clrw  buckm_interrh
          clrw  boostm_interrl
          clrw  boostm_interrh
          toff_buck_led
          toff_boost_led
          jmp     phase_lock

buck_loop:    buck_mode
              duty_cycle_cont      ;
             movw  pwmdata,pwmregs           ; write the pwm data from previous comput
new_buck_calc:
            ldd    dc_boost_volth     ; check for bus overvoltage
            lde    bemf
            adde   #$3ff
            cpe    #$ff8             ; 800 v for now
            ble    maxv_ok
            lde    #$ff8
maxv_ok:     ste    max_voltage        ;
            cpd    #$ff8              ; 800 v for now
```

```
            cpd     max_voltage
            bgt     no_boost            ; turn off boost converter
            ldd     bemf                ; get the back emf voltage
            addd    #$1ff               ; 100 v over the back emf
            xgdx                        ; desired boost voltage in x
            ldd     dc_bus_volth        ; the bus voltage
            lde     #$ff                ; unity duty cycle
            emul
            ediv
            xgdx                       ; vin/vout_desired is in d
            lde   #$ff                 ;
            sde                        ;  e contains ff-(vin*ff)/vout_desired
            bcs   no_boost            ; if vin > vout_desired, then no_boost
            beq   no_boost
            cpe   #$b2                  ; 0.7 max duty cycle
            ble   duty_ok               ;
            lde   #$b2                  ; set to max duty cycle
            jmp   duty_ok               ;
no_boost:   clre                        ; zero duty cycle
            ton_buck_led
            toff_boost_led              ;
            jmp  duty_ok1
duty_ok:    ton_boost_led
            toff_buck_led
duty_ok1:   ted                         ;
            stab  pwmdata               ; store the boost duty cycle
new_loop:   ldd  buckm_interrl
            lde  buckm_interrh
            pshm d,e                    ; save the integrator state
;       ldd  comp_torque_cmd      ;  does not work unless we have interrupts
            ldd  fil_torque_cmdh        ; do no torque ripple compensation
            subd new_phase_curr
            std   phase_curr_err        ; the phase current error
            lde   #ki_buck_mot          ; the chopper integrator constant
            emuls                      ; comupte ki * error
            addd  buckm_interrl        ; add to low word of buck,motor,
                                       ;integrator error
            adce  buckm_interrh        ; add to the high word
            sted  buckm_interrh        ; store the integrator error
                                       ; (number stored it actual
            ldd   phase_curr_err       ;
            lde   #kp_buck_mot         ;
            emuls
            addd  buckm_interrl        ;
            adce  buckm_interrh        ; output of controller is
                                       ; (d*vin-vemf) * 255
            addd  bemf_by_ffl          ; add low word of back_emf*ff
            adce  bemf_by_ffh          ; add high byte
            jsr   limited              ;
;           ldx   new_boost_volt       ; get the bus voltage from the output filter
               ldx   dc_boost_volth ;
               /
```

```
                edivs                   ; could round result
                bmi    tbm_neg_sat      ; torque, buck, motor, negative
                                        ; saturation  (** go do regen)
                cpx    #$ff             ; max duty cycle
                bgt    tbm_pos_sat      ;  positive saturation
                pulm   d,e              ; restore the stack
                xgdx                    ; answer in b
                std  pwmdata            ; answer --> pwmb, to be loaded
                                        ; on next interrupt
                jmp     phase_lock      ;
tbm_neg_sat:
                clrw    pwmdata         ; 0 -> pwmb ; to be loaded on
                                        ; next interrupt
                pulm   d,e              ; get the pushed integrator state
                sted   buckm_interrh    ; don't update the integrator
                jmp    phase_lock       ;
tbm_pos_sat:
                ldd   #$ff              ;
                std    pwmdata          ; ff-> pwmb , to be loaded on next
                                        ;interrupt
                pulm   d,e              ; get the pushed integrator state
                sted   buckm_interrh    ; don't update the integrator
no_input:       jmp    phase_lock       ;

speed_loop:
              jmp  phase_lock           ;


phase_lock:
              ldd  new_phase_curr
              jsr   pll                 ; phase lock the hall-effect signals
reset_pitr:
              pulm  d,e,x,y,z
               rti
mux_error:    ton_boost_led
               jmp  atod

bdm:      ton_buck_led
          jmp bdm
          rti

;*********************************************************
;* phase current offset adjust table
;*********************************************************

pho_adj_tab:
;* reverse (i.e. msb = 0)
        dw     $0000            ; 000 never happens (but keep here to
     ; keep indexing simple)
        dw     iphaseb_zerop    ; 001 phase b
        dw     iphasea_zerop    ; 010 phase a
```

```
        dw    iphasec_zeron  ; 011 phase c negated
        dw    iphasec_zerop  ; 100 phase c
        dw    iphasea_zeron  ; 101 phase a negated
        dw    iphaseb_zeron  ; 110 phase b negated
        dw    $0000          ; 111 never happens (but keep here to
                             ; keep indexing simple)
;* forward (i.e. msb=1)
        dw    $0000          ; 000 never happens (but keep here to
                             ; keep indexing simple)
        dw    iphaseb_zeron  ; 001 phase b negated
        dw    iphasea_zeron  ; 010 phase a negated
        dw    iphasec_zerop  ; 011 phase c
        dw    iphasec_zeron  ; 100 phase c negated
        dw    iphasea_zerop  ; 101 phase a
        dw    iphaseb_zerop  ; 110 phase b
        dw    $0000          ; 111 never happens (but keep here to
                             ; keep indexing simple)

;*********************************************************************
;* torque ripple compensation table.  entry is the signed percent    *
;* fraction  by which torque should be increased                     *
;*********************************************************************

trcomp_tab:                  ; torque ripple compensation table
        dw    !0 ;{(!90 * $8000)/!100}  ; i.e. 90 %
        dw    !0 ;{(!70 * $8000)/!100}  ; i.e. 70 %
        dw    !0 ;{(!40 * $8000)/!100}  ; i.e. 40 %
        dw    !0 ;{(!20 * $8000)/!100}  ; i.e. 20 %
        dw    !0 ;{(!10 * $8000)/!100}  ; i.e. 10 %
        dw    !0 ;{(!5  * $8000)/!100}  ; i.e. 5 %
        dw    !0
        dw    !0
        dw    !0
        dw    !0
        dw    !0
        dw    !0
        dw    !0
        dw    !0
        dw    !0 ;{(!5  * $8000)/!100}  ; i.e. 5 %
        dw    !0 ;{(!10 * $8000)/!100}  ; i.e. 10 %
        dw    !0 ;{(!20 * $8000)/!100}  ; i.e. 20 %
        dw    !0 ;{(!40 * $8000)/!100}  ; i.e. 40 %
        dw    !0 ;{(!70 * $8000)/!100}  ; i.e. 70 %
        dw    !0 ;{(!90 * $8000)/!100}  ; i.e. 90 %

*        dw    {0 - ((!20  * $8000)/!100)}  ; i.e. -5 %
*        dw    {0 - ((!50  * $8000)/!100)}  ; i.e. -10 %
*        dw    {0 - ((!80  * $8000)/!100)}  ; i.e. -20 %
$include "..\sbrts\subs.asm"

*********************************************************************
```

```
*       File Name : SUBS.ASM
*       Description : This file contains all subroutines
*       Note : This program is written for the M68HC16Z1EVB.
*****************************************************************



;*********************************************************;
;*  this subroutine is used for lcd display operations   *;
;*  it saves accumulator a and waits until lcd busy flag *;
;*  is cleared.                                          *;
;*********************************************************;

wait_busy_flag:
        psha            ; save accum a on stack
wbf0:   brclr instr_reg,#80h,rtn_bf ; if bit 7 clear, then exit loop
        ldaa  #$ff      ;
wbf1:   deca
        bne wbf1        ;
        bra wbf0        ;
rtn_bf: pula            ; pop a from the stack
        rts             ;


;*************************************************************
;* this subroutine displays in-line messages written         *
;* in code space on the lcd display.  end of message         *
;* is indicated by the '\' character.  values in             *
;* registers ix,iy,d,e are clobbered, along with values      *
;* in temp1, and temp2   if you need any of these, then      *
;* save them before entering this subroutine.                *
;*************************************************************

message0: pullba                ; pop the condition code
          tde                   ; put condition code in register e
          pullba                ; pop the return pc address
          subd  #0002h          ; popped address is to bytes higher
          xgde                  ; exchange d and e, cc in d, pc-2 in e
          std   temp1           ; store  cc in temporary register 1
          ste   temp2           ; store  pc-2 in temporary register 2
          xgex                  ; pc-2 in ix
          lde   #0000h          ;
message1: ldaa  e,x             ; get first character
          adde   #01h            ; increment pointer
          cmpa  #'\'            ; check if terminator
          beq   message2        ; if yes, skip down
          jsr   write_character  ; takes an ascii in accum a
          bra   message1        ; loop for next character
message2: adde  #02h             ; add the two we subtracted
          adde  temp2            ; add the pc-2
          xgde                   ; put the new pc in ab
```

```
        pushba                  ; put it on the stack
        ldd temp1               ; get the condition codes
        pushba                  ; put it on the stack
        rts


;*************************************************************
;* this subroutine returns the cursor home.  the contents    *
;* display is cleared of data display ram remains unchanged *
;*************************************************************

cursor_home:
        jsr       wait_busy_flag ; wait until busy flag is clear
        ldaa      #02h           ; return cursor home
        staa      instr_reg      ; does not erase contents of ddram
        rts

;*********************************************************************
;* this subroutine clears the display and returns the cursor home.  *
;* display is cleared of data display ram remains unchanged          *
;*********************************************************************

clear_display:
      jsr        wait_busy_flag  ; wait until busy flag is clear
      ldaa       #01h            ; clear the display
      staa       instr_reg       ;
      rts                        ;

;*********************************************************************
;* this subroutine shifts the cursor one character to the left       *
;*********************************************************************

shift_cursor_left:
      psha                       ; push data to be written on stack
      jsr        wait_busy_flag  ; wait until busy flag is clear
      ldaa      #10h             ; shift cursor to the left
      staa      instr_reg        ;
      pula                       ; restore data to be written
      rts

;*********************************************************************
;* this subroutine turns the cursor on and blinks the cursor         *
;*********************************************************************

cursor_on_blink:
      jsr        wait_busy_flag ; wait until busy flag is clear
      ldaa      #0fh            ; turn on cursor and blink
      staa      instr_reg       ;
      rts

;*********************************************************************
```

```
;* this subroutine turns the cursor on but does not blink the cursor *
;*********************************************************************

cursor_on_noblink:
       jsr       wait_busy_flag   ; wait until busy flag is clear
       ldaa      #0eh             ; turn on cursor and blink
       staa      instr_reg        ;
       rts

;****************************************
;* this subroutine turns the cursor off *
;****************************************

cursor_off:
       jsr        wait_busy_flag ; wait until busy flag is clear
       ldaa      #0ch            ; turn on cursor off
       staa      instr_reg       ;
       rts

;*****************************************************
;* this subroutine shifts the display to the left     *
;*****************************************************

shift_display_left:
       jsr        wait_busy_flag ; wait until busy flag is clear
       ldaa      #18h            ; shift display to the left
       staa      instr_reg
       rts

;*************************************************************
;* this subroutine sets the character gernerator ram address *
;* 6-bit address is assumed to be in accumulator a           *
;*************************************************************

set_cgram_address:
       jsr        wait_busy_flag ; wait until busy flag is clear
       anda      #3fh            ; clobber 2 msbs
       oraa       #40h           ; set the function code: 01xxxxxx
       staa      instr_reg       ; set cgram address to xxxxxx
       rts                      ;

;*****************************************************
;* this subroutine sets the data display ram address *
;* 6-bit address is assumed to be in accumulator a   *
;*****************************************************

set_ddram_address:
       jsr       wait_busy_flag ; wait until busy flag is clear
       anda      #7fh          ; clobber 2 msbs
       oraa      #80h          ; set the function code: 1xxxxxxx
       staa      instr_reg     ; set ddram address to xxxxxxx
```

```
        rts

;*************************************************************
;* this subroutine positions the cursor at the begining of   *
;* the first line.                                           *
;*************************************************************

carriage_return:                ; position cursor at begining of 1st line
        jsr     wait_busy_flag ; wait until busy flag is clear
        ldaa    #00h            ; takes the 6-bit address
        anda    #7fh            ; clobber 2 msbs
        oraa    #80h           ; set the function code: 1xxxxxxx
        staa    instr_reg       ; set ddram address to xxxxxxx
        rts

;*************************************************************
;* this subroutine positions the cursor at the begining of   *
;* the second line.                                          *
;*************************************************************

goto_line2:
        jsr     wait_busy_flag ; wait until busy flag is clear
        ldaa    #40h          ; takes the 6-bit address
        anda    #7fh          ; clobber 2 msbs
        oraa    #80h          ; set the function code: 1xxxxxxx
        staa    instr_reg     ; set ddram address to xxxxxxx
        rts

;*************************************************************
;* this subroutine positions the cursor at the begining of   *
;* the third line.                                           *
;*************************************************************

goto_line3:
        jsr     wait_busy_flag ; wait until busy flag is clear
        ldaa    #10h          ; takes the 6-bit address
        anda    #7fh          ; clobber 2 msbs
        oraa    #80h          ; set the function code: 1xxxxxxx
        staa    instr_reg     ; set ddram address to xxxxxxx
        rts

;*************************************************************
;* this subroutine positions the cursor at the begining of   *
;* the fourth line.                                          *
;*************************************************************

goto_line4:
        jsr     wait_busy_flag ; wait until busy flag is clear
        ldaa    #50h          ; takes the 6-bit address
        anda    #7fh          ; clobber 2 msbs
        oraa    #80h          ; set the function code: 1xxxxxxx
```

```
        staa      instr_reg    ; set ddram address to xxxxxxx
        rts

;*************************************************************
;* this subroutine writes an ascii character in accumulator  *
;* a to the current cursor position                          *
;*************************************************************

write_character:
        jsr      wait_busy_flag  ; wait until busy flag is clear
        staa     data_reg        ; write data in data register
wc1:    rts

;*************************************************************
;* this subroutine reads what ascii character is written at  *
;* the current cursor position.  result is in accumulator a  *
;*************************************************************

read_character:
        jsr      wait_busy_flag ; wait until busy flag is clear
        ldaa      data_reg      ; read ascii data, data is in accum a
        rts ;

*****************************************************************
* this subroutine displays the keypad settings mode on the lcd   *
* display                                                       *
*****************************************************************
disp_mode:    jsr carriage_return          ; carriage return
              brset flags,#$80,torque_mode ; if torque bit set
                                           ; goto torque_mode
              jsr message0                 ; write "speed" message
              db  '  [m]  speed     \'            ;
              bra disp_mode2               ; skip next two lines
torque_mode:  jsr message0                 ; write "torque" message
              db  '  [m]  torque    \'             ;
disp_mode2:   jsr goto_line2               ; position cursor on line 2
              brset flags,#$40,forw_mode ; if forward bit set
                                           ; goto forw_mode
              jsr message0                 ; write "reverse" message
              db  '  [o]  reverse   \'      ;
              bra disp_mode3               ; skip next two lines
forw_mode:    jsr message0                 ;
              db  '  [o]  forward   \'      ; write "forward" message
disp_mode3:   jsr goto_line3               ; position cursor on line 3
              brset flags,#$20,drive_mode ; if drive bit set
                                           ; goto drive_mode
              jsr  message0                ; write "coast" message
              db  '  [d]  coast     \'       ;
              bra disp_mode4               ; skip next two lines
drive_mode:   jsr message0                 ;
              db  '  [d]  drive     \'        ; write "drive" message
```

```
disp_mode4:   jsr goto_line4            ; position cursor on line 4
              brset flags,#$1.,start_mode ; if start_bit set
                                        ; goto start_mode
              jsr message0              ; write "stop" message
              db  '  [e]  stop     \'       ;
              bra dm_exit               ; skip next two lines
start_mode:   jsr message0              ; write "start" message
              db  '  [e]  start    \'       ;
dm_exit:      rts                       ; return from subroutine

;*****************************************************************
;* this subroutine delays the for a period indicated by contents  *
;* of accumulator d                                               *
;*****************************************************************

delay:   lde    #000fh          ;
loop0:   jsr    read_keypad     ; read keypad while you wait
         brset  flags,#mode_chg,dl_exit; if mode changes, the exit
         sube   #0001h          ;
         bne    loop0           ;
         subd   #0001h          ;
         bne    delay           ;
dl_exit: rts


;*****************************************************************
;*  this subroutine displays which control loop is currently active *
;*****************************************************************

loop_msg: jsr carriage_return ;
          brset flags,#$80,tlmsg1
          jsr message0
          db  '[* speed loop *] \'
          bra lpmsg1
tlmsg1:   jsr message0
          db  '[ torque  loop ] \'
lpmsg1:   jsr goto_line2
          jsr message0
          db  '[*** active ***] \'
          jsr goto_line3
          jsr message0
          db  'torque: 450 nm   \'
          jsr goto_line4
          jsr message0
          db  'speed : 1100 rpm \'
          rts

;*****************************************************************
;*  this subroutine displays inverter's input and outpud dc voltage *
;*  and current.                                                   *
;*****************************************************************
```

```
vi_msg:   jsr carriage_return
          jsr message0
          db  'v_in  = 255 v    \'
          jsr goto_line2
          jsr message0
          db  'i_in  = 39.6 a   \'
          jsr goto_line3
          jsr message0
          db  'v_out = 877 v    \'
          jsr goto_line4
          jsr message0
          db  'i_out = 14.8 a   \'
          rts

;*************************************************************************
;* this subroutine displays the inverters input and ouput powers        *
;* and the boost converter's efficiency                                 *
;*************************************************************************

pow_msg:  jsr carriage_return
          jsr message0
          db  ' inverter power  \'
          jsr goto_line2
          jsr message0
          db  'p_in   = 12.7 kw \'
          jsr goto_line3
          jsr message0
          db  'p_out  = 11.5 kw \'
          jsr goto_line4
          jsr message0
          db  'bc_eff = 94.5 %  \'
          rts

;*************************************************************************
;*  this subroutine reads the keypad settings and updates the mode     *
;*  status in the upper nibble of flags                                 *
;*************************************************************************

read_keypad:
          pushab          ; push accumulator ab on stack
          ldaa  portf   ; read keypad
          anda  #$f0    ; only upper nibble is used
          ldab  flags   ;
          andb  #$f0    ; get rid of the other status bits
          cba           ; see if there is change
          beq   rkexit  ; it is the same so quit
          ldab  flags   ; get the flags again
          andb  #$0f    ; clobber upper nibble
          aba           ; add b to a
          staa  flags   ; store keypad in upper nibble of flags
```

```
          bset  flags,#mode_chg ; set the mode change flag
rkexit:   pullab          ; restore accumulator ab
          rts

;*********************************************************************
;* this subroutine to display 2's complement number in accumulator d *
;* with sign, leading zero blanking, and decimal point. number       *
;* of digits after decimal point is stored in memory location        *
;* dec_places. allow for a total of six characters                   *
;*********************************************************************

disnums:
          tstd                ; test whether number is negative
          bpl  disnums0        ; if positive number, skip down
          negd                ; if negative, make it a positive number
          tde                 ; put the number in accumulator e
          ldaa #'-'           ; initial sign
          bra  disnums1        ; skip down
disnums0:  tde                 ; put the number in accumulator e
          ldaa #' '           ; put a space
disnums1:  ldab #$6            ; 6 digits total
          subb dec_places     ;
          stab dec_places     ;
          staa leading_sign   ;
          ted                 ; put number to be displayed back in d
          bset flags,#$04     ; set the leading zero flag
          ldx  #!10000        ; display ten thoudands digit
          jsr  disnums2        ;
          ldx  #!1000         ; display one thousands digit
          jsr  disnums2        ;
          ldx  #!100          ; display one hundreds digit
          jsr  disnums2        ;
          ldx  #!10           ; display tens digit
          jsr  disnums2        ;
          ldx  #!1            ; display units digit
          jsr  disnums2        ;
          rts                 ; return
disnums2:  pushab              ; save the number
          ldab dec_places     ;
          decb
          stab dec_places     ; store back the decimal place counter
          bne  disnums3        ; if not zero, skip down
          ldaa #'.'           ; if zero, display decimal point
          bclr flags,#$04     ; clear leading sign flag
          jsr write_character  ;
disnums3:  pullab              ; restore the number
                              ; leading sign still in a
          idiv                ; quotient in ix, remainder in d
          aix #'0'            ; add the ascii zero offset
          xgdx                ; remainder in ix, ascii number in b
          brclr flags,#$04,disnums7 ; if leading zero flag is
```

```
                                ;cleared, skip down
          cmpb #'0'             ;
          bne disnums5          ; if no, skip down
          ldaa dec_places
          cmpa #$1              ; check decimal point after next digit
          beq  disnums5         ; if yes, skip down
$if  left_justified
          xgdx                 ;  {assemble for left justified number
                               ;  display}
          rts                   ; {assemble for left justified number
                                ; displays}
$endif
          ldab #' '             ; if no, init for space
          bra  disnums7         ; display it
disnums5:   ldaa leading_sign   ;
$if  left_justified
          cmpa #' '       ;{assemble for left justified number displays}
          beq  disnums6   ; {assemble for left justified number displays}
$endif
          jsr  write_character ;
disnums6:   bclr flags,#$04     ; clear leading zero flag
disnums7:   tba
          jsr  write_character;
          xgdx
          rts


;*************************************************************************
;* this displays an unsigned binary number in accumulator d             *
;* with leading zero blanking, and decimal point.       number           *
;* of digits after decimal point is stored in memory location            *
;* dec_places. allow for a total of six characters                       *
;*************************************************************************

disnumu:    tde
          ldaa #' '             ; put a space
          ldab #$6              ; 6 digits total
          subb dec_places       ;
          stab dec_places       ;
          staa leading_sign     ;
          ted                   ; put number to be displayed back in d
          bset flags,#$04       ; set the leading zero flag
          ldx  #!10000          ; display ten thoudands digit
          jsr  disnumu2         ;
          ldx  #!1000           ; display one thousands digit
          jsr  disnumu2         ;
          ldx  #!100            ; display one hundreds digit
          jsr  disnumu2         ;
          ldx  #!10             ; display tens digit
          jsr  disnumu2         ;
          ldx  #!1              ; display units digit
```

```
            jsr  disnumu2          ;
            rts                   ; return
disnumu2:    pushab               ; save the number
            ldab dec_places       ;
            decb
            stab dec_places       ; store back the decimal place counter
            bne  disnumu3         ; if not zero, skip down
            ldaa #'.'             ; if zero, display decimal point
            bclr flags,#$04       ; clear leading sign flag
            jsr write_character   ;
disnumu3:    pullab               ; restore the number
                                  ; leading sign still in a
            idiv                  ; quotient in ix, remainder in d
            aix #'0'              ; add the ascii zero offset
            xgdx                  ; remainder in ix, ascii number in b
            brclr flags,#$04,disnumu7 ; if leading zero flag is
                                  ;cleared, skip down
            cmpb #'0'             ;
            bne disnumu5          ; if no, skip down
            ldaa dec_places
            cmpa #$1              ; check decimal point after next digit
            beq  disnumu5         ; if yes, skip down
$if  left_justified
            xgdx      ;  {assemble for left justified number displays}
            rts       ; {assemble for left justified number displays}
$endif
            ldab #' '             ; if no, init for space
            bra  disnumu7         ; display it
disnumu5:    ldaa leading_sign    ;
$if  left_justified
            cmpa #' '     ;{assemble for left justified number displays}
            beq  disnumu6 ; {assemble for left justified number displays}
$endif
            jsr  write_character ;
disnumu6:    bclr flags,#$04      ; clear leading zero flag
disnumu7:    tba
            jsr  write_character;
            xgdx
            rts



limite:                   ; correct over/under flow of adde instruction
        bvc    eok        ; if no over/under flow, jump to return
        bpl    eunder     ; v=1 and n=0 => underflow
        lde    #$7fff     ; v=1 and n=1 => overflow, set e at maximum
        rts               ; return from subroutine
eunder: lde    #$8000     ; set e at minimum
eok:    rts               ; return from subroutine

limitd:                   ; correct over/under flow of addd instruction
```

```
        bvc     dok          ; if no over/under flow, jump to return
        bpl     dunder       ; v=1 and n=0 => underflow
        ldd     #$7fff       ; v=1 and n=1 => overflow, set d at maximum
        rts                  ; return from subroutine
dunder: ldd     #$8000       ; set d at minimum
dok:    rts                  ; return from subroutine

limited:                    ; correct over/under flow of addd/e instructions
        bvc     edok         ; if no over/under flow, jump to return
        bpl     edunder      ; v=1 and n=0 => underflow
        lde     #$7fff       ; v=1 and n=1 => overflow, set ed at maximum...
        ldd     #$ffff
        rts                  ; return from subroutine
edunder:lde     #$8000       ; set ed at minimum...
        ldd     #$0000
edok:   rts                  ; return from subroutine

tedwsx:                      ; transfer e to d with sign extend
        ted                  ; move e contents to d
        bmi     negsgn       ; see if lsword is negative
        clre                 ; if lsword is not negative, extend plus
        rts                  ; return from subroutine
negsgn: lde     #$ffff       ; if lsword is negative, extend minus
        rts                  ; return from subroutine


;*************************************************************
;* this subroutine reads the keypad and sets the appropriate *
;* drive mode, filters all a/d data and computes motor speed *
;*************************************************************

set_drive_mode:
       jsr  calc_motor_rpm ; compute the motor rpm
       ldd  motor_rpm      ;
check_out_comp:
       cpd  #min_oc_rpm    ; below this speed we don't do output compares
       bge  set_direction  ; check keypad settings
       ldd  tcnt
       addd #$ffff       ; advance output compare timer with maximum count
       std  toc2           ;
       std  toc3           ;
       std  toc4           ;
set_direction:
       brset portf,#forw,forward_dir ;
       reverse_rotation    ;   motor reverse
       jmp chk_fault       ;
forward_dir:
       forward_rotation    ;   motor forward
chk_fault:
       jmp   no_fault      ;  diagnostic **
       ldaa  portf         ;
```

```
       anda  #$0e          ;  keep the fault bits
       beq   no_fault      ;
       bset  flags,#fault
gates_off:
       toff_gate_drives    ;
     jmp   filter_signals ; fault condition so don't bother to check drive
no_fault:
       bclr  flags,#fault  ;
       brclr portf,#driv,gates_off ; if coast then turn gates off
       brclr portf,#strt,gates_off ; if stop then turn gates off for now
       ldd   winding_temp          ;
       cpd   #max_temp             ;
;       bge   gates_off            ;
       ldd   endturn_temp          ;
       cpd   #max_temp             ;
;       bge   gates_off            ;
drive:
       unlock_motor         ;
       ton_gate_drives    ;
filter_signals:  brclr adstatccf,ilb_f,filter_vboost ; go filter vboost
filter_iphase:
       ldd   new_phase_curr   ; get the selected phase current.
                              ; appropriately negated in control routine
       lde   #ki_dc           ; the filter parameter
       ldy   #dc_phase_currh  ;  pointer to high byte of where the
                              ;  output is stored
       jsr   lowpass_filter ;  go find dc component
filter_ilboost:
       ldd   rjurr1          ; get the a/d value of the boost current
       subd  ilb_zero        ; subtract the offset
       asld                  ; multiply by 2 so that 100a --> 1ff
       std   new_boost_curr  ;
       lde   #ki_dc          ;
       ldy   #dc_boost_currh ; pointer to high byte of filtered boost
                             ; current
       jsr   lowpass_filter  ; go find dc component
filter_vboost: brclr  adstatccf,#vbst_f,filter_vbus
       ldd   rjurr2         ; get the a/d value of the boost voltage
       lde   #$6            ;
       emul                 ; multiply by 6 to make 100v -> 1ff
       std   new_boost_volt  ; store the result
       lde   #ki_dc          ; load filter constant
       ldy   #dc_boost_volth  ; load pointer to high byte of output
       jsr   lowpass_filter   ; go find dc component
       ldd   dc_boost_volth  ;
;       ldd   new_boost_volt
       lde   #$ff             ;
       emul
       sted  vboost_by_ffh    ; store vboost*ff for control
filter_vbus: brclr adstatccf,#vbus_f,filter_torque
       ldd   rjurr3         ; get the a/d value of the boost voltage
```

```
        asld                    ; multiply by 2 to make 400v --> 7fe
        std   new_bus_volt      ; store the result
        lde   #ki_dc            ; load filter constant
        ldy   #dc_bus_volth     ; load pointer to high byte of output
        jsr   lowpass_filter    ; go find dc component
        ldd   dc_bus_volth      ;
        lde   #$ff              ;
        emul
        sted  vbus_by_ffh       ; store bus voltage * ff for control
filter_torque: brclr adstatccf,#torq_f,filter_brake
        ldd   rjurr4            ; get the a/d value of the torque command
        std   temp_reg          ;
        lde   #$1ff             ; scale potentiometer reading to 1ff (max)
        emul
        ldx   #$3fc             ; $3fc instead of 3ff to allow some
                                ; headroom for pot
        ediv
        rupdx
        pshm  d                 ; potential new torque command is pushed
                                ; on stack
                                ; pot has been scaled to max
                                ; torque. 100a --> 3ff
        ldd   motor_rpm         ;
        cpd   #corner_rpm       ;
        bgt   tspeed            ;
        lde   #max_const_torque ; below base speed, so limit commanded
                                ; torque to maximum constant torque
        ste    max_perm_torque  ; maximum permissible torque
        jmp    ft2              ;
tspeed:
        lde   #max_trpm_hi      ;
        ldd   #max_trpm_lo      ;
        ldx   motor_rpm         ;
        ediv                    ;
        rupdx                   ;
        std   max_perm_torque   ;  maximum constant power permissible torque
        ble    ft3              ;

ft2:    pulm  d                 ; the potential new torque command
        cpd  max_perm_torque    ;  compare potential torque to
                                ; max permissible torque
        bls   ft3               ; torque not exceeded so potential
                                ; torque is fine
        ldd   max_perm_torque   ;  clamp at maximum permissible torque
ft3:    std   new_torque_cmd    ;
        lde   #ki_dc            ;
        ldy   #fil_torque_cmdh  ;
        jsr   lowpass_filter    ;

filter_brake: brclr adstatccf,#brk_f,filter_wind_temp
        ldd   rjurr5            ;
```

```
       std   new_brake_cmd   ;
       lde   #ki_dc
       ldy   #fil_brake_cmdh ;
       jsr   lowpass_filter  ;
filter_wind_temp: brclr adstatccf,#wtemp_f,filter_endt_temp ;
       ldd   rjurr6          ;
       std   winding_temp    ;
filter_endt_temp: brclr adstatccf,#etemp_f,sdm_rtn
       ldd   rjurr7          ;
       std   endturn_temp    ;
;now compute boost mulitplication factor
       ldd   dc_boost_volth
       subd  dc_bus_volth
       bpl   boostok         ; output volts < input volts
       clrw  mult_fac        ; zero multiplication factor
       rts
boostok:
       lde   #!5      ; 2*244e-6s/100uh
       emul                  ;
       std   mult_fac        ; this number is used by boost controller
sdm_rtn:  rts


;*****************************************************************
;*   data to be filtered in d.  filter ki in e.  pointer to where
;*     data is stored in iy

lowpass_filter:
       subd   0,y          ; xh[n]-yh[n-1]
       emuls               ; error * ki
       addd   2,y          ; add in yl[n-1]
       adce   0,y          ; add in yh[n-1]
       ste    0,y          ; store high byte
       std    2,y          ; store low byte
       rts



calc_motor_rpm:
       brclr  flags,#tof,cmrpm
       ldd    #$ffff       ;
       std    hea_periodh
       std    heb_periodh
       std    hec_periodh
       std    new_hea_period
       std    new_heb_period
       std    new_hec_period
zero_rpm:
       clrd
       std    bemf
       std    bemf_by_ffh
```

```
        std     bemf_by_ffl
        std     motor_rpm
        rts
cmrpm:  clre                    ; calculate motor speed
        ldd     hea_periodh     ;
        addd    heb_periodh     ;
        adce    #0              ;
        addd    hec_periodh     ;
        adce    #0              ;
        ldx     #$03            ;
        ediv
        bcc     cmrpm1          ;
        aix     #$01            ;
cmrpm1:
        stx     heabc_period
        lde     #{rpm_count/$10000}  ;
        ldd     #{rpm_count%$10000}  ;
        ediv
        rupdx                   ;
        cpd     #!7             ;
        bhs     good_rpm        ;
        jmp     zero_rpm        ;
good_rpm:
        std     motor_rpm       ;
        lde     #k_emf          ; back emf per rpm contant
        emul
        ldx   #!100           ; bemf constant had a factor of 100 in it
        ediv
        xgdx                    ; answer in d
        std     bemf
        lde     #$ff            ;
        emul                    ;
        sted  bemf_by_ffh     ; back emf * ff
        rts


;*************************************************************
;* this subroutine loads up data in accumulator e into the   *
;* dac pointed to by iy.                                     *
;*************************************************************

setup_dac:
        cpe     #$07ff          ; maximum positive number
        bgt     sdac1           ;
        cpe     #$f800          ; minimum negative value
        blt     sdac2           ;
sdac3:  ldd     #$0800          ; the 12-bit dac offset
        ade                     ; add an offset
        ldd     0,y             ; get the current dac address & data
        andd    #$f000          ; save the address bits
        ade                     ;
```

```
       ste    0,y          ; put the new data & address back
       rts
sdac1: lde    #$07ff       ; upper limit
       jmp    sdac3        ;
sdac2: lde    #$f800       ; lower limit
       jmp    sdac3        ;


;*************************************************************
;* this subroutine calculates the time between the input     *
;* capture and rising edge under phase advance               *
;* the hex_period is passed in d
;*************************************************************

calc_pav_deltat:
        lde   percent_adv   ;
        nege                ;
        adde  #!100         ;
        emul                ;
        ldx   #!100         ;
        ediv                ;
        rupdx               ; round up result and exchange d and ix
        rts

;*************************************************************
;* this subroutine updates commtime with ticx. it disables *
;* oc1 interrupts if speed is too high or timer has          *
;* overflowed.  it calls a software interrupt to sync oc1    *
;* interrupts to motor commutation. ticx is passed in e      *
;*************************************************************
torque_shp_sync:
          brset flags,#tof,doc1 ; if timer has overflown,
                                ; disable torque shaping
          ldd   motor_rpm   ;
          cpd #max_shp_rpm  ;
          bgt  doc1         ;
          clr  commcnt      ; we commutate on each edge
          ste  commtime     ; ticx --> commtime
          swi
          rts               ;
doc1:  bclr tmsk1,#$08      ; disable oc1 interrupts
       movw fil_torque_cmdh,comp_torque_cmd ; no torque shaping
       rts                ;


;*********************************************************************
;* this subroutine phase locks the period of the hall-effect       *
;* sensors                                                         *
;*********************************************************************

pll:     ldy     #new_hea_period  ;
```

```
          jsr     pl_loop          ;
          ldy     #new_heb_period  ;
          jsr     pl_loop          ;
          ldy     #new_hec_period  ;
          jsr     pl_loop          ;
          rts

pl_loop:  ldd     0,y              ; new hall effect period
          cpd     2,y              ; hex_periodh
          bhi     pll_pos_err
          beq     pll_zero_error   ;
pll_neg_err:
          ldd     2,y              ; hex_periodh
          subd    0,y              ;
          lde     #ki_pll          ;
          emul                     ;
          pshm    e
          lde     4,y              ; hex_periodl
          sde                      ;
          ste     4,y              ;
          pulm    d                ;
          lde     2,y              ;
          sbce    #0
          sde
          ste     2,y
;          bcc    pll_rtn
;          clre
;          clrd
          jmp    pll_rtn
pll_zero_error:
          rts

pll_pos_err:
          subd   2,y               ; hex_periodh
          lde     #ki_pll
          emul
          addd   4,y               ; hex_periodl
          adce   2,y               ; hex_periodh
;          bcc     pll_rtn         ;
;          ldd     #$ffff
;          tde
pll_rtn:  ste    2,y               ; hex_periodh
          std    4,y               ; hex_periodl
          rts
```

References

[1] "Modern Transportation", *Encyclopaedia Britannica*, Vol. 28, p. 775.

[2] BATES, B., "Electric vehicles: A decade of transition", *SAE Pt. 40*

[3] FURUTANI, M., YOKOTA, M., OKAWA, M., "Development of the Toyota EV-30 Passenger Car", *Electric Vehicle Developments*, Vol. 8, No. 3, July 1989, pp. 82-83, p. 106.

[4] CHAN, C. C., LEUNG, W. S., WILLIAMS, B., W., "An AC Drive System for Electrical Vehicles", *Proceedings of the International Conference on Electrical Machines*, Lausanne, Switzerland, p. 3 Vol. 1226, 1984, pp. 831-834.

[5] DVORAK, P., "The Shocking Truth About Electric Vehicles", *Machine Design*, Vol. 8, No. 1, September 1989, pp. 86-94.

[6] BRAHAM, R., "Prolog to: An overview of electric vehicle technology", *Proceedings of the IEEE*, Vol. 81, No. 9, September 1993, p. 1201.

[7] RIEZENMAN, M. J., "California considers hybrid EVs...", *IEEE Spectrum*, September, 1995, p. 72.

[8] BRAHAM, R., "PNGV Program Plan",Released on July 27, 1994.

[9] RIEZENMAN, M. J., "Special Report/Electric Vehicles: Architechting the system", *IEEE Spectrum*, November, 1992, p. 94.

[10] RILEY, R. Q., "Alternative cars in the 21st century: A personal transportation paradigm", *SAE*, 1994.

[11] CHAN, C. C., " An overview of electric vehicle technology", *Proceedings of the IEEE*, Vol. 81, No. 9, September 1993, p. 1202-1213.

[12] WOUK, V., "Hybrids: Then and now", *IEEE Spectrum*, July, 1995, pp. 16-21.

[13] RIEZENMAN, M. J., "Special Report/Electric Vehicles: The great battery barrier", *IEEE Spectrum*, November, 1992, p. 101.

[14] CHAN, C. C. ET AL, " A novel polyphase multipole square-wave permanent magnet motor drive for electric vehicles", *IEEE Transactions on industry applications*, Vol. 30, No. 5, September/October 1994, p. 1258-1266.

[15] CHAN, C. C. ET AL, " A novel permanent magnet hybrid motor for electric vehicles", *International conference on electrical machines*, Paris, 1995.

[16] Private correspondence with Dr. Hitoshi Yamamoto, Sumitomo Special Metals America, Inc., 23326 Hawthorne Blvd., Suite 360, Skypark 10, Torrance, CA 90505. October 18, 1994

[17] YAMAMOTO, H.," NEOMAX Update", *NdFeB, ReCo and ReFeN Permanent Magnets Conference*, February 16, 17 and 18, 1992, Orlando, Florida, USA.

[18] Private conversation with Prof. C. C. Chan. For more information, contact: The General Manager (Mr. Zhang Xin Yu), Tsinghua University, Yin-na High Tech Company, P. O. Box 1021, Beijing 102201. Phone: 86 10 255-3731, ext. 279 or 86 10 977-1350, ext. 331. Fax: 86 10 977-1874.

[19] YAMAMOTO, H.," NEOMAX Update", *NdFeB, ReCo and ReFeN Permanent Magnets Conference*, February 16, 17 and 18, 1992, Orlando, Florida, USA.

[20] *Powerex IGBT and Intellimod^{TM} Applications and Technical Data Book*,1st edition, Powerex Inc, October, 1991.

[21] Private conversation with Mr. Allan Gale, Ford Motor Company. May 1995.

[22] ALASUVANTO, T., JOKINEN, T., "Comparison of four different permanent magnet rotor constructions", *Proceedings of the International Conference on Electrical Machines*, Cambridge, MA, pp. 1034-1039, August 1994.

[23] RUSSENSCHUCK, S., ANDRESEN, E. CH., "Comparison of different magnet configurations in the rotor of synchronous machines using numerical field calculation and vector-optimization methods", *Proceedings of the International Conference on Electrical Machines*, Cambridge, MA, pp. 1027-1033, August 1994. Sept./Oct. 1980.

[24] KUMADA, M., ET. AL, "3-D analysis of a rare earth linear wiggler for a free electron laser", *IEEE Transactions on Magnetics*, vol. 24, no.2, pt.1, pp. 982-985.

[25] HALBACH, K., "Design of permanent multipole magnets with oriented rare earth cobalt materials", *Nuclear Instruments and Methods*, vol. 169 (1980), pp. 1-10, North Holland Publishing Company.

[26] POOLE, M. W., WALKER, R. P., "Periodic magnets for undulators and free electron Lasers - A review of performance features", *IEEE Transactions on Magnetics*, vol. MAG 17, no.5, pp. 1978-1981, September, 1981.

[27] HALBACH, K., "Applications of Permanent Magnets in Accelerators and Electron Storage Rings", *Journal of Applied Physics*, vol. 57, no.8, pt. IIA, pp. 3605-3608.

[28] HALBACH, K., "Perturbation effects in segmented rare earth cobalt multipole magnets", *Nuclear Instruments and Methods*, vol. 198 (1982), pp. 213-215, North Holland Publishing Company.

[29] TRUMPER, D. L., WILLIAMS, M. E., NGUYEN, T. H., "Magnet arrays for synchronous machines", *Proceedings of the IEEE IAS 28th Annual Meeting*, pp. 9-18, Toronto, Ont., Canada; October 2-8, 1993.

[30] POST, R. F, FOWLER, T. K., POST, S. F., "A high-efficiency electromechanical battery", *Proceedings of the IEEE*, vol. 81, no. 3, pp. 462-474, March 1993.

[31] OFORI-TENKORANG, J., LANG, J. H., "Halbach permanent magnet motors: a candidate for direct-drive wheel motors", *29th Universities Power Engineering Conference*, Galway, Ireland, pp. 17-20, Sept. 1994.

[32] MARINESCU, M., MARINESCU, N.,"New concept of permanent magnet excitation for electrical machines. Analytical and numerical computation", *IEEE Transactions on Magnetics*, vol. 28, no. 2, pp. 1390-1393, March, 1992.

[33] KIRTLEY, J. L.,"Design and construction of an armature for an alternator with a superconducting field winding", Ph.D Thesis (Electrical Engineering), Massachusetts Institute of Technology, Cambridge, MA, 1971.

[34] ARKADAN, A. A., VYAS, R., VAIDYA, J. G., SHAH, M. J.,"Effect of toothless stator design on core and stator conductors eddy current losses in permanent magnet generators", *IEEE Transactions on Energy Conversion*, vol. 7, no. 1, pp. 231-237, March, 1992.

[35] KADDOURI, A., LE-HUY, H.,"Analysis and design of a slotless NdFeB permanent-magnet synchronous motor for direct drive", *Proceedings of the IEEE IAS Annual Meeting*, vol. 1, pp. 271-278, Houston, TX, Oct. 4-9, 1992.

[36] SPOONER, E.,"DC traction motor with slotless armature", *IEE Proceedings*, vol. 132, Pt. B, No. 2, pp. 61-71, March 1985.

[37] JUFER, M., RADULESCU, M. M.,"Comparative study of slotted and slotless electronically-commutated permanent-magnet DC servomotors", *Fifth International Conference on Electrical Machines and Drives*, pp. 131-135.

[38] BATES, B., "Private correspondence" Aug. 5th, 1992.

[39] BOULES, N.,"Prediction of no-load flux density distribution in permanent magnet machines", *IEEE Transactions on Industry Applications*, vol. 21, no. 4, pp. 633-643, May/June, 1985.

[40] TRUMPER, D.L., WON-JONG KIM, WILLIAMS, M.E.,"Design and analysis framework for linear permanent-magnet machines", *IEEE Transactions on Industry Applications*, vol. 32, no. 2, pp. 371-379, March-April 1996.

[41] JACK, A. G., MECROW, B. C., "Design and Initial Test Results from a Permanent Magnet Synchronous Motor for a Vehicle Drive", *Proceedings. International Conference on Electrical Machines*, Manchester, UK. Vol. 2, pp. 751-755, Sept. 1992.

[42] GALE, ALLAN R., "Private telephone conversation" March, 1995.

[43] MILLER, T. J. E, *Brushless Permanent-Magnet and Reluctance Motor Drives* Oxford University Press, 1993.

[44] DEODHAR, R.P., STATON, D.A., JAHNS, T.M., MILLER, T.J.E., " Prediction of cogging torque using the flux-MMF diagram" *IAS '95. Conference Record of the 1995 IEEE Industry Applications Society. Thirtieth IAS Annual Meeting*,vol. 1, pp. 693-700, Orlando, FL, USA; 8-12 Oct. 1995.

[45] *Nonoriented sheet steel for magnetic applications*, United States Steel International Inc., 600 Grand Street, Pittsburgh, PA 15230, USA.

[46] SEBASTIAN, T., VINEETA, G., "Analysis of Induced EMF Waveforms and Torque Ripple in a Brushless Permanent Magnet Machine" *IEEE Transactions on Industry Applications*,vol. 32, no. 1, Jan./Feb. 1996.

[47] "STYCAST 2850FT Epoxy Encapsulant" *Technical Data Sheet*, Emerson & Cumming, Inc., 77 Dragon Court, Woburn, MA 01888.

[48] TORQUATO, S., LADO, F., "Bounds on the Conductivity of a Random Array of Cylinders", *Proceedings of the Royal Society of London, Series A (Mathematical and Physical Sciences)*, Vol. 417, No. 1852, May, 1988, pp. 59-80.

[49] JAHNS, T. M., KLIMAN, G. B., NEUMANN, T. W., "Interior Permanent-Magnet Synchronous Motors for Adjustable-Speed Drives", *IEEE Transactions on Industry Applications*, Vol. IA-22, No. 4, July, 1986, pp. 738-747.

[50] JAHNS, T. M., "Flux-Weakening Regime Operation of an Interior Permanent Magnet Synchronous Motor Drive", *IEEE Transactions on Industry Applications*, Vol. IA-23, No. 4, July, 1987, pp. p. 681-689.

[51] CARICCHI, F., CRESCIMBINI, F., FEDELI, E., NOIA, G., "Design and Construction of a Wheel-Directly-Coupled Axial-Flux PM Motor Prototype for EVs", *Proceedings of the IEEE IAS 29th Annual Meeting*, pp. 254-261, Denver October, 1994.

[52] CARICCHI, F., CRESCIMBINI, F., NOIA, G., PIROLO, D., "Experimental Study of a Bidirictional DC-DC Converter for the DC Link Voltage Control and the Regenerative Braking in PM Motor Drives Devoted to Electrical Vehicles", *Proceedings of 1994 IEEE Applied Power Electronics Conference and Exposition - APEC'94*, pt. 2, pp. 381-386. Orlando, FL, USA; 13-17 Feb. 1994

[53] SLEMON, G. R.,"Achieving a Constant Power Speed Range for PM Drives", *Proceedings of the IEEE IAS 28th Annual Meeting*, Toronto, Ont., Canada; vol. 1, pp. 43-48, 2-8 Oct. 1993.

[54] *Electronic Components Catalog*, North American Capacitor Company, Indianapolis, 1992.

[55] *Capacitors for High Current, Power Semiconductor, and D-C Applications*, GE Capacitor and Power Protection, Publication no. CPD 513, 10/20/92.

[56] *PC-146B Hi-Flux^{TM} Powder Cores*, The Arnold Engineering Company, Marengo, IL. USA.

[57] BOZIC, S. M., *Digital and Kalman filtering : An Introduction to Discrete-Time Filtering and Optimum Linear Estimation*, 2nd ed.,Edward Arnold, 1994

[58] *Solid State Sensors*, Catalog 20, Micro Switch Sensing and Control, October 1994.

[59] DEISCH, C. W., "Simple Switching Control Method Changes Power Converter into a Current Source", *PECC '78 Record* pp. 300-306.

[60] *MC68HC16Z1, User's Manual*, Motorola Literature Distribution; Phoenix, AZ.

[61] *MC68HC16Z1, System Integration Module Reference Manual*, Motorola Literature Distribution; Phoenix, AZ.

[62] *MC68HC16Z1, Analog-to-Digital Converter Reference Manual*, Motorola Literature Distribution; Phoenix, AZ.

[63] *MC68HC16Z1, CPU16 Reference Manual*, Motorola Literature Distribution; Phoenix, AZ.

[64] *MC68HC16Z1, Queued Serial Module Reference Manual*, Motorola Literature Distribution; Phoenix, AZ.

[65] *MC68HC16Z1, General Purpose Timer Reference Manual* , Motorola Literature Distribution; Phoenix, AZ.